UNIVERSITY OF WOLVERHAMPTON
School of Applied Sciences

DOCTORAL THESIS

Synthesis of zeolites from geological materials and industrial wastes for potential application in environmental problems

Carlos Alberto Ríos Reyes

The Graduate School

Synthesis of zeolites from geological materials and industrial wastes for potential application in environmental problems

A thesis submitted to the Graduate School of the University of Wolverhampton

By

Carlos Alberto Ríos Reyes

In partial fulfilment of the requirements for the degree of Doctor in Philosophy in the School of Applied Sciences

2008

Table of Contents

Declaration

I declare that this PhD thesis presents work carried out by myself and does not incorporate without acknowledgements and references cited in the work any material previously submitted in any form to any university, and that to the best of my knowledge it does not contain any material previously published or written by another person except where due reference is made in the text. I confirm that the intellectual content of this work is the result of my own efforts and of no other person.

The right of Carlos Alberto Ríos Reyes to be identified as author of this work is asserted in accordance with ss.77 and 78 of the Copyright, Designs and Patents Act 1988. At this date copyright is owned by the author.

Signature of Candidate:  Date: August 25, 2008

Abstract

Zeolites are among the least-known products for environmental pollution control, separation science and technology. Due to their unique porous properties, they are used in various applications in petrochemical cracking, ion-exchange and separation and removal of gases and solvents. The preparation of synthetic zeolites from chemical reagents is expensive. Therefore, in order to reduce costs, zeolite researchers are seeking cheaper aluminosilicate bearing raw materials, such as clay minerals, to produce synthetic zeolites.

This research concerns the synthesis of zeolites and zeotypes derived from low-cost materials like kaolinite (KAO), natural clinker (NC) and fly ash (FA). The motivation for using these sources as the starting materials in zeolite synthesis is driven by factors, such as they are cheap and available in bulk quantities, are currently under-utilized, have high workability, and require less water (or solution) for activation. The raw materials were activated by two different routes: (1) classic alkaline hydrothermal synthesis and (2) alkaline fusion prior to hydrothermal synthesis. In the first method, the synthesis of zeolitic materials was carried out generally in alkaline media, although KAO or its calcination product, metakaolinite (MTK), was also activated in the presence or absence of structure directing agents (SDAs) and additional silica (precipitated SiO_2), with the last one determining the SiO_2/Al_2O_3 ratio of the reaction mixture and the time given for zeolitization. Synthesis in fluoride- and calcium-bearing media was also used to activate kaolinite. The process of synthesis was optimized by applying a wide range of experimental conditions with a wide range of reaction temperature, time, mineralizer concentration and solid/solution ratio. In the second approach, an alkaline fusion step was conducted prior to hydrothermal treatment, because it plays an important role in enhancing the hydrothermal conditions for zeolite synthesis. On the other hand, this approach was adopted because it can dissolve more aluminosilicates.

The main synthesis products obtained after activation of KAO in NaOH solutions included zeolite LTA (LTA), sodalite (SOD), cancrinite (CAN), faujasite (FAU), zeolite Na-P1 (GIS), JBW-type zeolite (JBW), analcime (ANA), whereas the activation of KAO in KOH solutions produced chabazite (CHA), zeolite Barrer-KF, phillipsite (PHI) and K-feldspar. The hydrothermal conversion of kaolinite in fluoride media did not produce successful results, although traces of FAU, GIS, CHA, SOD and CAN crystallized. The activation of KAO in the system $CaO\text{-}SiO_2\text{-}Al_2O_3\text{-}H_2O$ promoted the formation of different calcium silicate hydrate (C-S-H) phases, including hydrogarnet (HYD) and tobermorite (TOB). Following the fusion approach, the main zeolitic

phases obtained using NaOH as mineralizer were LTA and CAN.

The main as-synthesized zeolites obtained from NC by the conventional hydrothermal treatment method include PHI, SOD and CAN. Using the fusion approach, FAU and LTA were obtained with NaOH as an activator, whereas non-zeolitic material crystallized when KOH was used.

The main as-synthesized zeolitic materials obtained by hydrothermal reaction of FA include PHI, zeolite Barrer-KF, CHA and SOD with traces of TOB, ANA, zeolite LTF (LTF) and herschelite (HER), appearing occasionally. By the fusion approach, FAU was obtained with NaOH as activator, whereas no zeolitic material crystallized using KOH.

Experimental results indicate that the method, mineralizer, concentration and time have strong effects on the type and degree of crystallinity of the synthesis products. On the other hand, the type and chemical composition of the as-synthesized products are strongly dependent on the chemical composition of the starting material. The chemistry of zeolite synthesis was subject to perturbations caused by the presence of impurities in the raw materials, which may remain insoluble during crystallization and cause undesired species to nucleate, developing mixtures of different types of zeolites. However, other physicochemical factors may play a very important role in the thermodynamics and kinetics of zeolite formation. The raw materials have very high contents of SiO_2 and Al_2O_3, with SiO_2/Al_2O_3 ratios appropriate for the synthesis of low-Si zeolitic materials with high crystallinity and cation exchange capacity (CEC). However, although zeolites' CEC represents a very important characteristic quality in the removal of undesired species from polluted effluents, it is not the deciding factor in determining zeolite performance during ion exchange processes, since numerous other factors also need to be considered.

Finally, the potential application of the raw materials and their as-synthesized products as low-cost sorbents in the remediation of metal ions and ammonium from wastewater effluents was investigated. PHI showed a lower efficiency than FAU. Selectivity of FAU for metal removal was, in decreasing order, Fe>As>Pb>Zn>Cu>Ni>Cr. Based on these results, the use of these materials has the potential to provide improved methods for the treatment of contaminated effluents.

Acknowledgments

This project would not have been successful without the strength, grace and ability that come from the Lord.

I would like to express my heartfelt gratitude to my research advisor, Prof. Craig D. Williams for agreeing to supervise this PhD project, for all his guidance and advice, for the large amount of time that he has devoted to discussions of my research, as well as providing me with the opportunity to work in the Zeolite Research Group. I would also like to thank my other supervisors, Prof. Michael A. Fullen and Dr Clive L. Roberts, for their support and advice throughout my project and their hospitality and sympathy. Special thanks go to every one of my supervisors for their patience and care and for all things I have learnt from them over the past three years, for the freedom granted during the research, as well as letting me to enjoy our research meetings. I would not have been able to pull this through without your help and understanding.

Likewise, I am deeply grateful to Dr Martin Maple for introducing me into the field of zeolite science and training me on different techniques of characterization, for helping me both with useful comments and suggestions and assistance with the analytical data acquisition, and for always having answers to my questions, no matter whether scientific or personal aspects. I am indebted to Dave, Barbara and Diane for their help and co-operation with the collection of XRD, SEM and ICP-EAS data, respectively. I am thankful to Dr. David C. Apperley of the Department of Chemistry of the University of Durham for the acquisition of Solid-state Nuclear Magnetic Resonance data and their interpretation, and Dr. Jose A. Henao and co-workers (Monica, Angelica, Miguel and Andelfo) of the School of Chemistry of the Universidad Industrial de Santander (Colombia) for their useful comments and suggestions on XRD analysis.

I really appreciate to the administrative staff of the Graduate School and the School of Applied Sciences of the University of Wolverhampton for all their help. Thanks to the IT Service and the Library staff for their advice and support.

I am also grateful to all members of the Zeolite Research Group for contributing to the very friendly working environment and for their constant willingness to participate in discussions, and those who used to work here, specially to Rob for his friendship, ideas and help, but specially for sharing with me enjoyable moments playing football indoors along with other friends.

This research was supported by the Programme Alban, the European Union Programme of High Level Scholarships for Latin America, Scholarship No. E05D060429CO, and the Universidad Industrial de Santander (a remunerated commission) for funding me and has benefited from research facilities provided by the School of Applied Sciences at the University of Wolverhampton.

I must acknowledge to Dr. Catherine V. Duke (School of Applied Sciences of the University of Wolverhampton) and Dr. Paul A Wright (School of Chemistry of the University of St Andrews) for their constructive comments and suggestions during my 'viva' and constant patience in correcting and proof-reading the entire manuscript of this research.

The author is most grateful to the above-named people and institutions for support.

Furthermore, I want to express my sincere thanks to my friends Juan and Lorena, as well as Beck and his family for their invaluable friendship and support during my stay at Wolverhampton, as well as to Glyn and Ana for their kindness and sympathy to involve me along with my family in a cultural exchange.

This thesis is dedicated to my lovely spouse (Norma) and daughters (Maria Paula and Luciana), for their love and comprehension, for being close to me all the time, and because your are my life, to my parents (Salomon and Ines) for giving their very best to make me what I am, to Martha and Cesar for their company during my single day life, and in general to my extended family for all of their love and support throughout my years of study.

List of Tables

List of Figures

List of Abbreviations

Abbreviation	Meaning
4-1	Complex 4-1
4-4-1	Complex 4-4-1
5-1	Complex 5-1
Å	Angstrom
AMD	Acid mine drainage
ANA	Analcime
ATR	Attenuated Total Reflectance
Ats	Anatase
C	Celsius
$Ca(OH)_2$	Calcium hydroxide or portlandite
CAN	Cancrinite
CEC	Cation exchange capacity
CHA	Chabazite
cm	Centimetre
C-S-H	Calcium silicate hydrate
D4R	Double four ring
D6R	Double six ring
DTG	First derivative of thermogravimetry
EC	Electrical conductivity
EDX	Electron dispersive X-ray
FA	Fly ash
FA-CAN	Fly ash-based cancrinite
FA-CHA	Fly ash-based chabazite
FA-FAU	Fly ash-based faujasite
FA-GIS	Fly ash-based zeolite Na-P1
FA-HER	Fly ash-based herschelite
FA-PHI	Fly ash-based phillipsite
FA-SOD	Fly ash-based sodalite
FA-TOB	Fly ash-based tobermorite
FAU	Faujasite
FAZs	Fly ash-based zeolitic materials
FT-IR	Fourier transform infrared spectroscopy
g	Gram
GIS	GIS-type zeolite
h	Hour
HA-EM	High acid, extreme metal
HA-HM	High acid, high metal
HA-LM	High acid, low metal

Hal	Halloysite
Hem	Hematite
HER	Herschelite
HEU	Heulandite-type zeolite
HGT	Hydrogarnet
ICDD	International Centre for Diffraction Data
ICP-AES	Inductively coupled plasma atomic emission spectroscopy
Ili	Illite
IZA	International Zeolite Association
JWB	JBW-type zeolite
KAO	Kaolinite
KAO-ANA	Kaolinite-based analcime
KAO-CAN	Kaolinite-based cancrinite
KAO-CHA	Kaolinite-based chabazite
KAO-FAU	Kaolinite-based faujasite
KAO-GIS	Kaolinite-based zeolite Na-P1
KAO-HYD	Kaolinite-based hydrogarnet
KAO-JBW	Kaolinite-based JBW-type zeolite
KAO-LTA	Kaolinite-based zeolite LTA
KAO-PHI	Kaolinite-based phillipsite
KAO-SOD	Kaolinite-based sodalite
KAO-TOB	Kaolinite-based tobermorite
KAOZs	Kaolinite-based zeolitic materials
KF	Zeolite Barrer-KF
Kfs	K-feldspar
KH	Zeolite KH
kV	Kilovolt
l	Litre
LOI	Loss on ignition
LSZ	Low-silica zeolite
m	Metre
M	Molarity
µm	Micrometre
mA	Milliampere
MA-EM	Moderate acid, extreme metal
MA-HM	Moderate acid, high metal
MA-LM	Moderate acid, low metal
MAS-NMR	Magic Angle Spinning Nuclear Magnetic Resonance
MeAPO	Metalloaluminophosphate
mg	Milligram
mg l^{-1}	Milligram per litre

min	Minute
ml	Millilitre
mm	Millimetre
Ms	Muscovite
mS cm^{-1}	MicroSiemens per centimetre
mS m^{-1}	MicroSiemens per metre
MTK	Metakaolinite
MTK-ANA	Metakaolinite-based analcime
MTK-CAN	Metakaolinite-based cancrinite
MTK-CHA	Metakaolinite-based chabazite
MTK-FAU	Metakaolinite-based faujasite
MTK-GIS	Metakaolinite-based zeolite Na-P1
MTK-HYD	Metakaolinite-based hydrogarnet
MTK-LTA	Metakaolinite-based zeolite LTA
MTK-SOD	Metakaolinite-based sodalite
MTK-TOB	Metakaolinite-based tobermorite
MTKZs	Metakaolinite-based zeolitic materials
Mul	Mullite
mV	Millivolt
N	Nitrogen
NC	Natural clinker
NC-CAN	Natural clinker-based cancrinite
NC-FAU	Natural clinker-based faujasite
NC-HEU	Natural clinker-based heulandite-type zeolite
NC-LTA	Natural clinker-based zeolite LTA
NC-PHI	Natural clinker-based phillipsite
NC-SOD	Natural clinker-based sodalite
NCZs	Natural clinker-based zeolitic materials
NN-EM	Near neutral, extreme metal
NN-HM	Near neutral, high metal
NN-LM	Near neutral, low metal
PHI	Phillipsite
ppm	Parts per million
PTFE	Polytetrafluoroethylene
Qtz	Quartz
S4R	Single four ring
S6R	Single six ring
S8R	Single eight ring
SAPO	Siliconaluminophosphate
SBU	Secondary building unit
SDA	Structure directing agent

SE1	Forward-scattered primary electron
SEM	Scanning electron microscopy
SOD	Sodalite
TEA	Triethylamine
TEDA	Triethylene diamine
TLAM	Triethanolamine
TG	Thermogravimetry
TGA	Thermogravimetric analysis
TMS	Tetramethylsilane
TPAB	Tetrapropylammonium bromide
TOR	Tobermorite
VMS	Volcanogenic Massive Sulphide
XRD	X-ray diffraction analysis
μm	Micrometre

Publications: Journals and Conferences

Parts of the work presented in this thesis have been published in international or national journals and the proceedings of international and national conferences. Publications relating to this work are listed below.

Refereed international journal papers

Ríos, C.A. and Williams, C.D., Synthesis of zeolitic materials from natural clinker: A new alternative for recycling coal combustion by-products, Fuel 87 (2008) 2482–2492.

Ríos, C.A., Williams, C.D. and Roberts, C.L., Removal of heavy metals from acid mine drainage (AMD) using fly ash, natural clinker and synthetic zeolites, Journal of Hazardous Materials 156 (2008) 23–35.

Ríos, C.A., Williams, C.D. and Fullen, M.A., Nucleation and growth history of zeolite LTA as-synthesized from kaolinite by two different methods, Applied Clay Science (2008), doi:10.1016/j.clay.2008.05.006.

Ríos, C.A., Williams, C.D., Fullen, M.A. and Roberts, C.L., A comparative study of two methods for the synthesis of fly ash-based sodium and potassium type zeolites with potential use in the purification of wastewaters, Fuel, submitted 18 April, 2008.

Ríos, C.A., Williams, C.D. and Fullen, M.A., Hydrothermal synthesis of hydrogarnet and tobermorite at 175 ^{o}C from kaolinite and metakaolinite in the CaO-Al_2O_3-SiO_2-H_2O system: A comparative study, Applied Clay Science, submitted 28 May, 2008.

Sandoval, M.V., Henao, J.A., Ríos, C.A., Williams, C.D. and Apperley, D.C., Synthesis and characterization of zeotype ANA framework by hydrothermal reaction of natural clinker, Fuel, submitted 23 June, 2008.

Refereed international conference and symposium papers or posters

Ríos, C.A., Williams, C.D., Roberts, C.L. and Fullen, M.A., Synthetic faujasite based on coal by-products for the treatment of acid mine drainage (AMD). Abstract accepted as a poster and published at the Proceedings of the 2nd International Conference on Engineering for Waste Valorization, Patras, Greece, 3-5 June 2008.

Refereed national journal papers

Ríos, C.A., Williams, C.D. and Castellanos, O.M., Synthesis and characterization of zeolites by alkaline activation of kaolinite and industrial by-products (fly ash and natural clinker), Bistua 4 2006, 60-71.

Ríos, C.A., Williams, C.D. and Maple, M.J., Synthesis of zeolites and zeotypes by hydrothermal transformation of kaolinite and metakaolinite, Bistua 5 2007, 15-26.

Henao, J.A., Carreño, A.M., Ramos, M.A., Quintero, J.A., Candela S.A., and Ríos, C.A., Petrography and application of the Rietveld method to quantitative phase analysis of minerals in clinker generated by the autocombustion of coal, Bulletin of Geology – Universidad Industrial de Santander, submitted 2 January 2008.

Refereed national conference and symposium papers or posters

Ríos, C.A., Maple, M.J., Williams, C.D., Roberts, C.L., and Fullen, M.A., Synthesis and characterization of cancrinite (CAN), sodalite (SOD) and Linde Type A (LTA) zeolites from kaolinite clay, Presented as a poster and published as an Abstract at the XXIX Annual British Zeolite Association Conference, Ambleside (England), 31 July - 4 August 2006.

Ríos, C.A., Williams, C.D., Roberts, C.L. and Fullen, M.A., Alkali hydrothermal conversion of coal fly ash (CFA) into zeolites, Presented as a poster and published as an Abstract at the XXX Annual British Zeolite Association Conference, York (England), 26-28 March 2007.

Ríos, C.A., Williams, C.D., Fullen, M.A., and Roberts, C.L., Synthesis of zeolites and zeotypes from geological materials, Presented as a poster and published as an Abstract at the XXX Annual British Zeolite Association Conference, York (England), 26-28 March 2007.

Ríos, C.A., Williams, C.D., Roberts, C.L. and Fullen, M.A., Potential contribution of zeolites in clean technology, Presented as a poster at the Regional Poster Competition and Networking Event for PhD Researchers, Coventry, 11 July 2007.

Ríos, C.A., Williams, C.D., Roberts, C.L. and Fullen, M.A., Treatment of acid mine drainage (AMD) using natural clinker-based zeolites, Presented as a poster and published as an Abstract at the XXXI Annual British Zeolite Association Conference, Keele (England), 31 March - 2 April 2008.

Chapter 1

Chapter 1. Introduction

1.1. Background

This introductory section describes general aspects of the major challenges and serious environmental problems caused by the disposal of waste materials and the use of zeolitic materials for environmental protection. An explanatory multidisciplinary review of zeolite science is presented, focusing on zeolite structures and properties. This includes their industrial applications and role in solving environmental problems. The scope of the thesis is then defined.

Globally, millions of tonnes of miscellaneous solid, liquid and gaseous waste materials, such as household, commercial, industrial, agricultural, radioactive and clinical wastes, are generated annually. The disposal of waste materials poses major challenges and can cause serious hazards to human health and the environment, if they are handled incorrectly. Furthermore, the amount of discharged material is expected to increase dramatically in the future.

As a part of sustainable development, waste management should attempt to reduce waste materials' effect on human health and the environment and to convert them into useful products by recycling. This can be beneficial in many ways, such as reducing the amount of raw materials used and/or operating costs, reducing the volume of waste materials and reducing their environmental impact.

Mining industry is of importance around the world. However, it presents several environmental problems, such as soil erosion, impacts on local biodiversity and water pollution. The quality of life in many countries around the world is strongly affected by the products and processes of mining industries.

Coal mining includes the production of fly ash (FA) and acid mine drainage (AMD). Globally, over 500 million tonnes of FA are generated annually from coal combustion by thermal power plants and its disposal poses major challenges and serious environmental and economic problems. The disposal of FA in dams or heaps presents an immense problem due to its alkalinity (pH >12) and chemical characteristics. AMD is a widespread environmental problem associated with both working and abandoned mining operations, resulting from the microbial oxidation of pyrite in the presence of water and air, affording an acidic solution that contains

toxic metal ions. The generation of AMD and release of dissolved heavy metals is an important concern facing the mining industry. Therefore, due to the shortage of landfill sites and stricter environmental regulations, it is very important to promote the effective recycling of these waste materials into products of greater value and thus mitigate the depletion of resources and environmental impacts. These objectives can be achieved through their zeolitization.

Zeolite synthesis is conventionally developed by hydrothermal crystallization under alkaline conditions, which has been reported by several patents and technical articles. Recently, the classic alkaline hydrothermal synthesis has been improved by using more sophisticated treatments, which include an alkaline fusion step followed by hydrothermal treatment, the application of microwave-assisted zeolite synthesis and a method for synthesizing zeolites under molten conditions without any addition of water. Zeolites are industrially important, being used widely in catalysis, ion exchange and adsorption. Their use is becoming increasingly important in several environmental applications and thus is of increasing interest in water purification, particularly for the removal of ammonia, heavy metals, radioactive species and organic substances.

The preparation of zeolites is generally expensive and, therefore, their use in environmental remediation is restricted due to prohibitive costs. Cost limitations can be overcome by using low-cost materials for zeolite synthesis, such as kaolinite (KAO), natural clinker (NC) and FA. The use of these materials in the zeolite synthesis is evaluated, discussing their potential application in the remediation of polluted water. This experimental work in zeolite synthesis is particularly important in understanding and predicting applications of the raw materials under real-world conditions, because many applications are used under conditions quite distinct from typical laboratory conditions. To draw attention to unresolved or unaddressed issues that deserve experimental attention, it is particularly interesting to study the synthesis of zeolites under a wide range of experimental conditions. These studies should enable investigations of the types of zeolites that form from specific raw materials under different conditions, the interacting influence of different factors, the genesis of the alteration process, the succession of zeolite formation and the nucleation and growth kinetics of zeolites.

Laboratory experiments were conducted to evaluate metal ion and ammonium removal during the treatment of polluted solutions to compare the capacity and selectivity of different sorbents during the treatment process and to confirm that zeolites have an advantage over other ion exchangers. These experiments took into account their lower cost and high ion selectivity. Important parameters, such as sorbent dose (g) per effluent volume unit (ml), reaction time and

metal concentration were examined, in order to understand the removal mechanisms involved and to optimize the overall removal efficiency of the system. On the basis of this information, which includes the synthesis of zeolites from KAO, NC and FA and the use of potentially cost-effective ion exchange materials in water treatment, the reported research project was thus developed.

1.2. Environmental impact

Hazardous wastes are generated annually throughout the world by all industries and their disposal poses major challenges and serious environmental problems. In turn, these cause serious health risks, taking into account that the amount of discharged material is expected to increase in the future. Recently, due to the shortage of landfill sites and stricter environmental regulations, there has been a shift in societal attitudes, resulting in strong interest in developing beneficial recycling of industrial by-products, which is now permissible in various applications, which include zeolitization. The ‘Green highways concept’ aims at encouraging and accelerating the widespread use of recycled materials. In fact, FA and other industrial by-products have been or are in the process of being beneficially used in several applications. The use of waste materials in zeolite synthesis both contributes to the mitigation of environmental problems, generally in the field of water purification, removing heavy metals or ammonium, and turns them into attractive and useful products.

1.3. Water treatment technology

Water is the source of life and is a basic pre-requisite for human survival. However, severe water contamination and insufficient water source are two difficult and ubiquitous problems. Municipal, industrial and agricultural wastewater pollutants include suspended solids and dissolved species. Wastewater has the potential to harm life forms and the environment. There are huge challenges all over the world regarding the handling of wastewater for a sustainable future. If not carefully managed, however, wastewater may produce both short- and long-term negative impacts on human health and ecological systems. In many developing countries, there are deadly consequences associated with exposure to contaminated water, as many developing countries have increasing population densities, increasingly scarce water resources and

inadequate water treatment utilities. Wastewater treatment is the last line of defence against water pollution.

Research in the field of wastewater purification is very important. Processes commonly used for wastewater treatment can be improved and innovative technologies, especially energy-saving processes, should be developed. Wastewater management focuses on the development and testing of processes for advanced wastewater treatment. Most technologies using zeolites for water purification are based on their unique cation-exchange behaviour, through which dissolved cations can be removed from water by exchanging with cations on the exchangeable sites of those industrial materials. These technologies are emerging to improve existing operations and industrial mineral technology, representing a simple and inexpensive solution. Zeolites can provide dramatic results for wastewater treatment. Recent methods to remove pollutants from contaminated water have involved physicochemical methods, such as precipitation, activated carbon adsorption, ion exchange, reverse osmosis, flotation techniques and cementation.

1.4. Zeolites and the environment

There are three main uses of zeolites: catalysts, gas separation and ion exchange. However, they have been increasingly used in various application areas, such as industry, agriculture, environmental protection and medicine.

Different research groups give particular attention to the properties of zeolites, which have been driven by environmental concerns or play significant roles in preserving and improving the environment. The use of zeolitic materials for environmental protection is based on their chemical structure and physicochemical properties. Zeolites protect the environment in many ways.

Synthetic zeolites can be used as adsorbents or substitute for sodium tri-polyphosphate, the traditional water-softening agent in detergents (Rege and Yang, 1997; Eken-Saraçoğlu and Çulfaz, 1999). However, their preparation from chemical sources of silica and alumina is expensive and, therefore, their use in environmental remediation is restricted due to prohibitive costs, which can be overcome by seeking cheaper raw materials for zeolite synthesis. These include clay minerals, natural zeolites, volcanic glasses, diatomite, high silica bauxite and oil shale. Low-cost raw materials, such as KAO, NC and FA have been used in this study as

starting materials in zeolite synthesis. NC was used for the first time as starting material in zeolite synthesis because: (1) it is a coal by-product, thus it adds value, reduces cost and enhances the environment, (2) its potential application in zeolite synthesis and water technology is not utilized and (3) it is very resistant to weathering and erosion and highly workable. In this study, the use of several sorbents (raw materials and as-synthesized products) in laboratory-scale experiments was investigated in the purification of polluted effluents.

1.5. Scope and objectives of this research

The scope of this work was to conduct the synthesis and characterization of zeolites based on geological materials and industrial by-products, using both existing and novel methods, enhancing their potential application to environmental problems related to water contamination. Zeolite synthesis has largely been a non-systematic field, with many experiments based on variations in the basic parameters.

The hydrothermal transformation of KAO (or MTK), NC and FA mainly in alkaline solutions or alkali-fused products in aqueous media was investigated. Moreover, a modification of the classic hydrothermal synthesis was achieved by adjusting the SiO_2/Al_2O_3 ratio at representative compositions with precipitated SiO_2 or introducing a 'structure directing agent' (SDA). During classic hydrothermal synthesis, several variables were considered: mineralizer type and concentration, reaction time, temperature and solution/raw material ratio. Using the alkaline fusion approach, alkaline activator/raw material ratio for fusion, H_2O/alkali fused product ratio, reaction time and temperature were the considered parameters. NaOH and KOH were used to activate KAO and MTK, although the transformation of these raw materials was also investigated using fluoride- and calcium-bearing media.

This study investigates whether the use of geological sources and industrial by-products as low-cost materials is suitable for zeolite synthesis and future applications. Evaluated applications include the efficiency of both raw materials and their synthesis products for removal of heavy metals and ammonium from artificial or natural polluted effluents as a potential remediation alternative for the purification of wastewaters.

In order to satisfy the above aims, the following objectives must be fulfilled:

(1) To investigate the transformation of geological materials (KAO), mining by-products (NC) and industrial solid wastes (FA) via: (1) conventional hydrothermal treatment with alkaline solutions and (2) alkaline fusion prior to hydrothermal reaction.

(2) To characterize both the raw materials and their synthesis products by X-Ray Diffraction (XRD) Analysis, Fourier Transform Infrared (FT-IR) Spectroscopy, Scanning Electron Microscopy (SEM) and Thermogravimetric analysis (TGA), as well as by more sophisticated analytical techniques, such as ^{29}Si and ^{27}Al Magic Angle Spinning Nuclear Magnetic Resonance (MAS NMR).

(3) To evaluate several sorbents in water purification processes and to develop a laboratory-scale experimental model (batch reaction) at room temperature.

(4) To monitor the pH and electrical conductivity (EC) and determine the metal ion and ammonium concentrations using Inductively Coupled Plasma Atomic Emission Spectroscopy (ICP-AES) and photometry, respectively.

(5) To examine the effectiveness of the raw materials and their synthetic zeolites as sorbents in removing heavy metals and ammonium from artificial and naturally-polluted effluents.

(6) To contribute understanding of the conditions under which zeolites form in the natural environment, by using the knowledge and techniques gained during the study of the hydrothermal synthesis of zeolites.

1.6. Structure of the thesis

In this thesis, Chapter 1 presents a brief overview of salient aspects of the proposed study. These include the impact of waste materials, water treatment technology and the importance of alternative materials for wastewater treatment. Chapter 2 is a literature survey of zeolite science and technology, the use of KAO, NC and FA in zeolite synthesis and the potential application of the raw materials and as-synthesized products in the treatment of wastewater effluents. Chapter 3 presents the materials and methods used in this work. Its purpose is to provide background information on the raw materials used in the synthesis process and the experimental methods of investigation. These investigative methods include synthesis, application of inorganic exchangers in batch reaction tests and fundamental techniques of characterization, including X-

ray diffraction (XRD) analysis, Fourier transform infrared (FT-IR) spectroscopy, scanning electron microscopy (SEM) and thermogravimetric (TG) analysis. More sophisticated analytical techniques are also discussed, including magic angle spinning nuclear magnetic resonance (MAS NMR) and inductively coupled plasma atomic emission spectroscopy (ICP-AES). The detailed experimental protocol for the batch reaction tests are also concisely described, including all necessary calculations. Chapter 4 examines the characterization of the raw materials, providing useful information on their appropriate mineralogical and chemical composition for their application in zeolite synthesis, taking into account that the chemical composition has an important influence on both the potential application of the raw materials and the environmental impact of their subsequent use. Chapters 5, 6 and 7 discuss the results of the synthesis and characterization of zeolitic materials based on KAO, NC and FA, respectively, which is very important to establish their potential applications. Chapter 8 presents the functional application of low-cost sorbents (raw materials and their derivate synthetic zeolites) in batch reaction experiments to clean-up wastewater effluents, particularly to remove heavy metals and ammonium. Chapter 9 summarizes the contributions that can be drawn from the results presented in this thesis and suggests directions for future research.

Chapter 2

Chapter 2. Literature survey

2.1. Historical remarks

The Swedish mineralogist A. F. Cronstedt introduced the term ‘zeolite’ in 1756 for certain silicate minerals in allusion to their behaviour on being heated in a blowpipe flame. This result led to all other minerals that showed this property to be called zeolites, which is derived from the Greek words ‘zeo’ meaning ‘to boil’ and ‘lithos’ meaning ‘stone’. Since then, zeolites have been recognized as a separate group of minerals, one of the most abundant on earth. The first attempt artificially to synthesize zeolitic materials was by St. Claire-Deville in 1862, simulating the geological conditions under which zeolites were believed to form in nature. However, it was only until 1948 that Barrer reported the first definitive synthesis of an analogue of a natural zeolite.

In the late 1940s and early 1950s Milton and co-workers at the Union Carbide Corporation carried out hydrothermal zeolite syntheses at low temperature (~100 ^{o}C) and low pressure (autogenous) using alkali metal aluminosilicate gels. They prepared a series of synthetic zeolites, including the zeolites A, X, and Y that the company commercialized in 1954 as a new class of industrial materials for separation and purification. In 1956, Linde Type A, the first commercial zeolite was synthesized (Breck, 1974). Today, at least 150 synthetic zeolites are known. Some of the earlier synthetic zeolites include zeolites A, X, Y, L, ZSM-5 and omega (Meier and Olson, 1987).

In the early 1960s Barrer and Denny (1961) were the first to carry out synthesis of zeolites using organic alkylammonium cations instead of alkali metal cations. In 1962, Mobil Oil introduced the use of synthetic zeolite X as a cracking catalyst, followed by the synthesis of the high silica zeolites beta and ZSM-5. The introduction of organic cations resulted in an increase in the Si/Al ratio and the discovery of ZSM-5, being the most important new structure (Argauer and Landolt, 1972). Flanigen *et al*. (1978) reported the synthesis of silicalite (the all-silica counterpart of ZSM-5), with higher Si/Al ratios, based on the patent of Grose and Flanigen (1977). This material shows remarkable properties because of its hydrophobic and organophilic character. Other molecular sieves such as the porous aluminophosphates (AlPOs), VPI-5 molecular sieves and their derivatives have been discovered (Flanigen *et al*., 1986). The most recently synthesized

molecular sieves are the nanostructured MCM-41 and silica aerogel. Mesoporous MCM-41 and aerogels are nanostructured materials with great potential as catalyst and nanocomposites (Hamdan *et al*., 2001). The most noteworthy advance in crystalline microporous solids has recently been the synthesis of extra large pore zeolites with more than 12-ring apertures (Freyhardt *et al*., 1996; Yoshikawa *et al*., 1998; Zhou *et al*., 2001; Lin *et al*., 2001).

At present, synthetic zeolites are used commercially more often than natural zeolites due to the purity of crystalline products and the uniformity of particle sizes (Breck, 1974). However, the preparation of synthetic zeolites from chemical sources of silica and alumina is expensive. Such costs may be reduced by the use of various geomaterials like clays or industrial wastes as starting materials. Zeolite synthesis has been also developed by the transformation of one zeolite type into others. The major discoveries and advances in synthetic zeolites are summarized in Table 2.1.

Table 2.1. Evolution of synthetic zeolites (Hamdan, 2003).

Late 1940s to Early 1950s	Low Si/Al ratio zeolites
Mid to Late 1960s	High Si/Al ratio zeolites
Early 1970s	SiO_2 molecular sieves
Late 1970s	$AlPO_4$ molecular sieves
Early 1980s	SAPO and MeAPO molecular sieves
Mid 1980s	$AlPO_4$ based molecular sieves
Late 1980s	Metallo-silicates, aluminosilicates
Early 1990s	Mesoporous molecular sieves
Late 1990s	Large pore zeolites

2.2. Zeolite framework structure and properties

Zeolites are crystalline, porous, hydrated aluminosilicates of alkaline or alkaline earth metals. The frameworks are composed of $[SiO_4]^{4-}$ and $[AlO_4]^{5-}$ tetrahedra, which corner-share to form different open structures with an overall negative charge, which is balanced by the cations which move freely in and out of its framework. A representative empirical formula for a zeolite would be:

$$\mathbf{M_{2/n}O:Al_2O_3:xSiO_2:yH_2O}$$

where M represents the charge-balance cation, n the charge of the cation, x is generally ≥ 2, and y the water contained in the voids of the zeolite (McCusker and Baerlocher, 2001). It is generally accepted that no two AlO_4 can be linked directly by sharing their corner in the zeolite framework.

The fascinating properties of zeolitic materials essentially originate from their structures. The topology of zeolite frameworks is given by a code consisting of three capital letters assigned by the 'Structure Commission of the International Zeolite Association' (IZA). The codes are generally derived from the names of the type material, which is the species first used to establish the structure type. The IZA Structure Commission provides up-to-date classification by framework type, which is available on the internet site of the IZA (http: //www.iza-online.org) or in the Atlas of Zeolite Framework Types (Baerlocher *et al.*, 2001). Currently, three classification schemes are widely used for zeolite structures. Two of these are based upon specifically defined aspects of crystal structure, whereas the third has a more historical basis, placing zeolites with similar properties into the same group (Armbruster and Gunter, 2001).

The first structural classification is based upon the framework topology, with distinct frameworks receiving a three-letter code (Meier *et al.*, 1996). The frameworks for zeolites with the same code are identical. A 3-letter framework type code is assigned to zeolites and the priority in the naming of zeolites depends on the first mineral discovered in the group. This classification is useful for zeolite researchers whose major interests are in cation exchange and synthetic zeolites, but does not assist geologists attempting to name zeolite minerals (Armbruster and Gunter, 2001).

The second structural method for the classification of zeolites is described by Meier (1968) based on a concept termed 'secondary building unit' (SBU) as shown in Figure 2.1. The primary building unit for zeolites is the tetrahedron and the SBUs are the geometric arrangements of tetrahedra (Breck, 1974; Armbruster and Gunter, 2001). Quite often, these SBUs tend to control zeolite morphology.

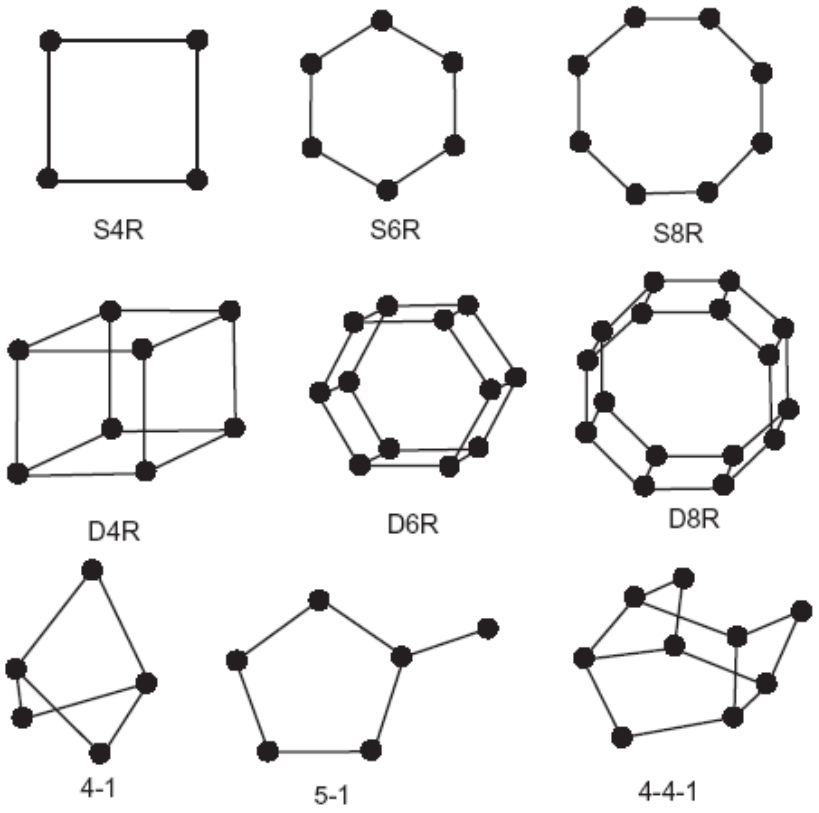

Figure 2.1. Secondary building units in zeolites (Meier, 1968). The oxygen atoms in between those of silicon and aluminium are omitted for simplicity.

In these SBUs only the position of tetrahedral (T) Si and Al are shown. Oxygen atoms lie near the connecting solid lines, which are not intended to mean bonds. The classification used by Breck (1974) is based of the framework topology of the zeolites for which the structures are known, and it consists on seven groups (Table 2.2), within which zeolites have a common subunit of structure that is a specific array of $(Al,Si)O_4$ tetrahedra. In the classification, the Si-Al distribution is neglected. These subunits have been called SBUs by Meier (1968). The primary building unit for zeolites is the tetrahedron.

There are many possible zeolite structures due to the large number of ways in which the SBU can be linked to form various polyhedra which when combined create networks of regular channels and cavities (Barrer, 1978; Sulikowski *et al.*, 1987).

Gottardi and Galli (1985) proposed a classification scheme, which is similar to the SBU classification of Breck (1974), except that it includes some historical context of how the zeolites

were discovered and named (Figure 2.2). This scheme uses a combination of zeolite group names which have specific SBUs and is widely used by geologists, and consists of some complex structural units of tetrahedron, whether finite or infinite, which are: (a) the chain of fibrous zeolites; (b) the single connected 4-ring chain; (c) the double connected 4-ring chain; (d) the 6-ring, single or double; (e) the hexagonal sheet with handles; (f) the heulandite unit. These complex units mostly are simply connected to form the actual frameworks, but in some cases vertices, edges or also faces shared with nearby units.

Table 2.2. Classification of zeolite structures (Breck, 1974).

Group	Secondary Building Unit (SBU)
1	Single 4-ring, S4R
2	Single 6-ring, S6R
3	Double 4-ring, D4R
4	Double 6-ring, D6R
5	Complex 4-1, T_5O_{10} unit
6	Complex 5-1, T_8O_{16} unit
7	Complex 4-4-1, $T_{10}O_{20}$ unit

Zeolite pores consists of 6, 8, 10, 12 and 14 membered of oxygen ring systems to form tube-like structure and pores that interconnected to each other (Bahruji, 2005). However, other factors such as the location, size and coordination of the extra-framework cations are also influencing pore size (Gualtieri, 2006). The fascinating properties of zeolites, such as ion exchange, separation, catalysis and their role are essentially determined by their unique structural characteristics such as the interconnected regular three-dimensional network of micropores, the Si/Al ratio and the nature and content of the extra-framework cations. The well-defined micropores give the zeolites molecular sieving properties. As the Si/Al ratio decreases, the surface becomes more hydrophilic and more cations are needed to compensate the negative charges introduced by aluminum (Gualtieri, 2006). Another property of zeolite is possessed acid sites (Brønsted acid and Lewis acid) that results from the net negative framework charges, making it as a great heterogenic catalyst (Govind *et al*., 2002; Gualtieri, 2006). Brønsted acid sites associated with the protons attached to framework oxygen which is connected to the framework aluminium, whereas Lewis acid sites are provided by the non-framework aluminium (Gualtieri, 2006).

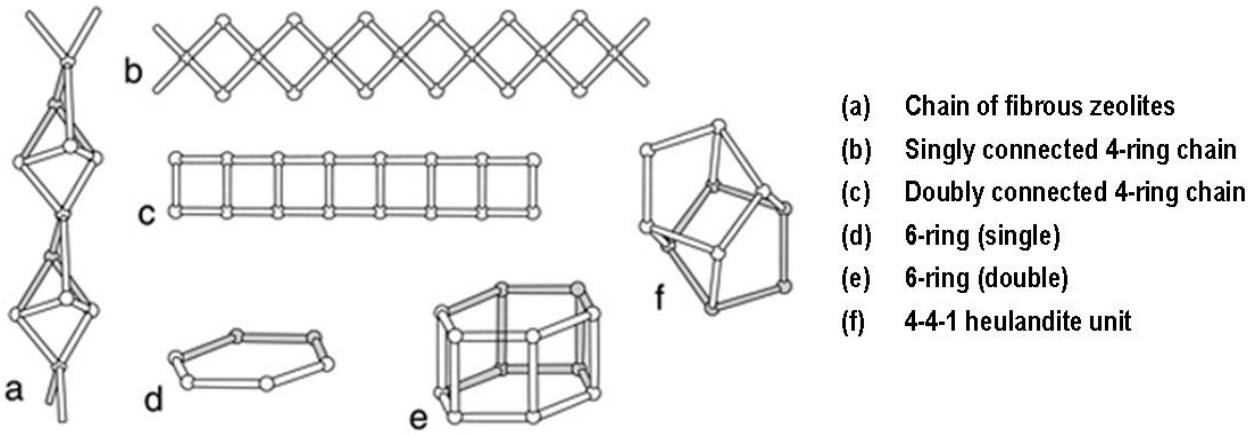

Figure 2.2. The structural units, finite or infinite, which may be used to assemble the frameworks of zeolites (Breck, 1974; Gottardi and Galli, 1985). The balls represent tetrahedra ($SiO4^{4-}$ or $AlO4^{5-}$) and the bars represent oxygens shared by the tetrahedra.

2.3. Environmental applications

Zeolites have found widespread environmental applications, which are gaining new research interests mainly due their value to one or more of three properties: adsorption, ion exchange and catalysis. Major uses of zeolitic materials include petrochemical cracking, ion-exchange (water softening and purification), and gas and solvent separations and removal, agriculture, mining, paper products, animal husbandry and construction, among others. However, the main environmental applications of zeolites are particularly concern in wastewater treatment. Many industrial processing and wastewater streams, such as waters from leaching, mining, rinsing, etc., contain rare and/or toxic heavy metals mixed with other pollutants, frequently organic substances and ammonium (Šiška, 2005). Zeolites are of interest by different research groups for environmental pollution control, separation science and technology, particularly cleaning up wastewaters. The main advantages of synthetic zeolites when compared with naturally-occurring zeolites are that they can be engineered with a wide variety of chemical properties and pore sizes and that they have greater thermal stability. They are known excellent adsorbents that can readily adsorb and exchange several toxic substances in their framework. The presence of heavy metals in the environment is an issue of great concern because of growing discharge, toxicity and other adverse effects of heavy metals on the receiving waters and/or soils (Stathi *et al*., 2007). The excessive presence of ammonia in water streams and effluents is a problem of great concern for the environment and industrial water systems, mainly due to eutrophication

and corrosion/biological fouling problems, respectively (Rozic *et al*., 2000). Removal of the pollutants from aqueous media, therefore, has received a considerable amount of attention (Table 2.3).

Table 2.3. Environmental applications of zeolites in wastewater treatment.

Wastewater treatment	References
Ammonia removal	Mercer *et al*. (1970), Hlavay *et al*. (1982), Baykal (1998), Langella et al. (2000), Cincotti *et al*. (2001), Jorgensen and Weatherley (2003), Meininghaus and Prins (2000), Rozic *et al*. (2000), Marañón et al. (2006), Saltalı *et al*. (2007), Lei et al. (2008)
Heavy metals removal	Kesraoui-Ouki *et al*. (1994), Mondale *et al*. (1995), Kesraoui-Ouki and Kavannagh (1997), Cincotti *et al*. (2001), Langella *et al*. (2000), Moreno *et al*. (2001a, 2001b), Panayotova (2001), Inglezakis *et al*. (2001, 2003), Wingenfelder *et al*. (2005)
Organic compounds removal	García *et al*. (1993), Li *et al*. (2000), Schüth *et al*. (2004), Altare *et al*. (2007)
Radioactive elements removal	Dyer and Zubair (1998), Abusafa and Yucel (2002), Marinin and Brown (2002)

2.4. Zeolite synthesis

2.4.1. Background

Since the pioneering work of Barrer in the 1950s the conditions for zeolite synthesis have changed little. Zeolite synthesis has been extensively reviewed in several books and literature on this subject is abundant (Breck, 1974; Barrer, 1982; Jacobs and Martens, 1987; Szoztak, 1998). The general method of zeolite production involves dissolving an aluminium source (metal or oxide) into an alkaline solution. Once this solution has cooled the silica source (and organic template, if required) is added in the form of aqueous slurry and the resulting gel stirred until homogenous. The gel is then transferred to a reaction autoclave and aged at temperatures of between 80-200 ^{o}C for time periods ranging from hours to days, depending on the zeolite required. Most aluminosilicate zeolites probably could be obtained at temperatures <100 °C in alkaline solutions. This is generally the case for zeolites with a low Si/Al ratio. However, in order to reduce reaction times (especially for zeolites with a high Si/Al ratio) and to control crystallite sizes, morphologies and compositions, some syntheses are performed at temperatures >100 °C under autogeneous pressure in autoclaves. The initial reaction gel composition has little resemblance to the chemical stoichiometry of the final zeolitic product and the nature and

properties of starting materials used in the reaction mixture are very important parameters that determine the properties of the resulting material. Typical precursor materials include: SiO_2 and Al_2O_3 sources, mineralizer and organic molecules. The synthetic zeolitic product depends not only on the chemical composition, temperature and pressure, but most important, on the nature of the chemical sources needed, as listed in Table 2.4.

Table 2.4. Chemical sources and their function in zeolite synthesis.

Sources	**Functions**
SiO_2	Primary building unit(s) of the framework
AlO_2^-	Origin of framework charge
OH^-	Mineralizer, guest molecule
Alkali cation, template	Counterion of framework charge, guest molecule
H_2O	Solvent, guest molecule

The discovery of SDAs, sometimes called 'templates', resulted in the preparation of nearly 100 different silicate frameworks (International Zeolite Association, www.iza-structure.org). The mode of action of these SDAs has been extensively investigated by Davies and Zones (1997) and this has led to some empirical rules, without the absolute ability to design new solids (Lobo *et al*., 1995). However, the role of the SDA during crystallization is not totally clear and several possible mechanisms for its interaction with the forming zeolite are: (1) the true template effect, where the zeolite is formed around the SDA which determines the pore topology due to its own shape; (2) a pore filling effect, where the template stabilizes the micropores of the zeolite by filling them and, thus, preventing pore collapse and (3) a pH-stabilizing effect, due to the functionality of the organic molecules. Other synthetic variables including the source of the inorganic precursors, the mineralizing agent (OH^- or F^-) and the reactant concentrations have also resulted in new crystalline materials. The use of fluoride as a mineralizer in zeolite synthesis was developed by Flanigen (1973) and has resulted in zeolites being prepared with fewer defect sites and higher silica contents. There are many other crucial synthesis parameters which are often well known, especially for industrially-important materials. If SDAs are used during synthesis, a calcination process must follow synthesis. By that step, the SDA is removed from the zeolite micropores which make them accessible. Usually, temperatures between 450-600 °C are applied to remove the SDA, which is not critical for the stability of the zeolites, since they are

usually stable in much higher temperatures. Depending on the purpose of zeolite production, further post-synthetic transformation is applied to modify the properties of the as-synthesized products.

In spite of vigorous research efforts for over three decades few, if any, hard empirical rules have been established that explain the wealth of synthetic results. In fact recent experimental results leave us to ponder over how little is known about zeolite nucleation and growth (e.g. possible at room temperature, at atmospheric pressure, in non-aqueous environments and accelerated by acidic anions).

2.4.2. Zeolite synthesis from kaolinite, natural clinker and fly ash

The preparation of synthetic zeolites from chemical sources of silica and alumina is expensive. Therefore, in order to reduce costs, zeolite researchers are seeking cheaper raw materials for zeolite synthesis, which include geological materials, such as clay minerals, natural zeolites, volcanic glasses, diatomite, high silica bauxite or oil shale and combustion residues, such as coal ashes, municipal solid waste incineration ashes and industrial slags. However, in this study the focus of interest is on the use of KAO, NC and FA as starting materials in zeolite synthesis.

2.4.2.1. Kaolinite-based zeolitic materials

The synthesis of crystalline aluminosilicate zeolites can be carried out from clay minerals, such as KAO (Breck, 1974; Barrer *et al.*, 1974; Boukadir *et al.*, 2002), halloysite (Klimkiewicz and Drąg, 2004), illite, smectite, interstratified illite-smectite (Baccouche *et al.*, 1998), montmorillonite (Cañizares *et al.*, 2000) and bentonite (Ruiz *et al.*, 1997; Boukadir *et al.*, 2002). Previous work has shown that the improvement of the properties of the KAO by chemical methods is difficult due to its low reactivity. This clay mineral is not significantly affected by acid or alkaline treatments, even under strong conditions (Lussier, 1991; Murat *et al*., 1992; Akolekar *et al*., 1997; Perissinotto *et al*., 1997; Chandrasekhar and Pramada, 1999; Demortier *et al*. 1999; Xu *et al*., 1999). Therefore, KAO is usually used after calcination at temperatures between 550-950 °C (Mackenzie, 1970) to obtain a more reactive phase (MTK) under chemical treatments, with the

loss of structural water with reorganization of the structure. Only a small part of AlO_6 octahedra is maintained, while the rest are transformed into much more reactive tetra- and penta-coordinated units (Lambert, 1989). The conditions of the kaolin calcination strongly influence the reactivity of the obtained solids. The best conditions for obtaining a very reactive MTK have been discussed by several authors who reported values between 600-800 °C (Lussier, 1991; Murat *et al*., 1992; Akolekar *et al*., 1997; Perissinotto *et al*., 1997; Chandrasekhar and Pramada, 1999; Demortier *et al*. 1999; Xu *et al*., 1999). Calcination at higher temperatures leads to the formation of mullite and cristobalite (Mackenzie, 1970).

Several authors have reported the synthesis of KAO-based zeolitic materials (KAOZs) and MTK-based zeolitic materials (MTKZs), including the following zeolitic products: LTA (Rocha *et al.*, 1991; Gualtieri *et al*., 1997; Sanhueza *et al.*, 1999; Zhao *et al.*, 2004; Covarrubias *et al.*, 2006); FAU (Dudzik and Kowalak, 1974; Basaldella *et al*.,1993; Basaldella and Tara, 1995; Basaldella *et al.*,1995; Akolekar *et al.*, 1997; Liu *et al*., 2003; Covarrubias *et al.*, 2006); GIS (Covarrubias *et al.*, 2006); CAN (Buhl, 1991b; Buhl *et al*., 2000a; Chorover *et al.*, 2003; Zhao *et al.*, 2004); SOD (Buhl and Löns, 1996; Buhl *et al*., 2000a; Chorover *et al.*, 2003 ; Zhao *et al.*, 2004); JBW (Healey *et al*., 2000a; Lin *et al*., 2004; Ríos *et al*., 2007). Numerous investigations have been conducted on the stability of KAO in high pH conditions (Carroll and Walther, 1988, 1990; Huang, 1993; Bauer and Berger, 1998; Bauer *et al*., 1998; Cama *et al*., 2000). Rees and Chandrasekhar (1993) have converted KAO into zeolites by hydrothermal reaction in fluoride media. Zeolite production from waste kaolin was performed by Alberti *et al.* (1994). The benefits of using kaolin as an aluminosilicate source in zeolite synthesis to obtain low-cost catalysts, adsorbents or ion exchangers are widely known (Breck, 1964, 1974; Howell and Acara, 1964; Haden and Dzierzanowski, 1968, 1972; Basaldella *et al*., 1993, 1995; Basaldella and Tara, 1995). Unfortunately, it is difficult to find pure natural kaolins. LTA is largely utilized as an adsorbent. For this reason, the concentration of impurities in raw kaolins used to synthesize LTA was limited in order to fulfil the established specifications in detergent formulation (such as crystallinity, particle size distribution, exchange capacity and whiteness (Llenado, 1983). Murat *et al*. (1992) suggested that the kinetics of zeolite crystallization from KAO were affected by Fe impurities present in the clay. Nevertheless, other authors (Hamilton *et al*., 1993), using sodium aluminate and sodium silicate as raw materials, found that the Fe influence in zeolite synthesis was the same as that produced by other solid impurities, independent of its nature. Additionally, studies performed by Madani *et al*. (1990) indicated that the Al co-ordination number in the raw material played an important role in zeolite conversion from kaolins.

2.4.2.2. Natural clinker-based zeolitic materials

Coal geologists refer to thermally (fused or partly fused) altered sedimentary rocks associated with spontaneous combustion of coal seams during the recent geologic past (since early Pliocene time) as NC. These rocks are common geologic features that have been reported throughout the world (Ellyett and Fleming, 1974; Heffern *et al*., 1983; Lindqvist *et al*., 1985; Foit *et al*., 1987; Cosca *et al*., 1989; Heffern and Coates, 1997; Prakash *et al*., 1997; Zhang, 1998; Râdan and Râdan, 1998; Lyman and Volkmer, 2001; de Boer *et al*., 2001). The (partially) fused and often highly vesicular rocks resemble blast furnace slags to a large extent, both in appearance and mineralogy (de Boer *et al*., 2001). NC is used as road base where there is no other suitable material and NC deposits are nearby, and for mine roads, reclamation and stabilization purposes (Hoffman, 1996). It is also crushed and screened for roofing granules or walkways or used as a building and ornamental stone (U.S. Geological Survey and U.S. Bureau of Mines, 1975). As construction aggregate for concrete, it have not the required strength for permanent structures (Hoffman, 1996). The use of NC is dependent on the availability and cost of other aggregates. Fredlund (1976) and Le Blanc (1991) reported the discovery of 75 archaeological sites in the Cape Bathurst Peninsula (Canada) representing occupations spanning more than 3.000 years, characterized by the predominant use of NC. The fact that NC beds are extensive both on and off the reservation, plus the lack of local markets, restricts their economic development for other than local usage. However, taking into account the chemical similarity of NC with the volcanic parent material, from which natural zeolites originated by post-magmatic hydrothermal activity, it is possible to use it as starting material in zeolite synthesis.

Henao *et al*. (2005) carried out the characterization of the NC used in this study to synthesize NC-based zeolitic materials (NCZs), by X-ray diffraction analysis using the Rietveld method. Recently, Henao and co-workers determined that NC is mainly composed by several crystalline polymorphs of SiO_2. However, this coal by-product contains other crystalline phases like hematite, spinel, mullite, cordierite, anatasa, montmorillonite, rutile, kaolinite, calcite and orthoclase. In addition, NC presents an amorphous phase in the range 48-55%. NC has very high contents of SiO_2 (45.18-60.63%) and Al_2O_3 (15.87-20.81%) with SiO_2/Al_2O_3 ratios = 2.3-3.5 appropriate for the synthesis of low-Si zeolitic materials with high crystallinity and cation exchange capacity. This has motivated attempts to make zeolites from this material, justifying the development of future investigations in the field of the synthesis of new materials with potential industrial applications. To our knowledge, no previous effort has been made to use NC as a SiO_2 and Al_2O_3 source in zeolite synthesis, except by recent studies carried out by Ríos *et*

al. (2006, 2008a, b) and Ríos and Williams (2008). Actually, Henao and co-workers (personal communication) are conducting the synthesis and characterization of ANA-type framework by hydrothermal reaction of NC. According with them, highly crystalline analcime (with traces of hematite and other minor phases) can be successfully synthesized from NC by hydrothermal treatment under the selected experimental conditions (3M NaOH, solution/NC ratio = 8 ml/g, 150^{o}C and 24 h), demonstrating that this coal by-product is suitable for zeolite synthesis. Regardless of the starting material, the synthesis products synthesized were zeolite Na-P1, analcime and cancrinite, and their formation and amount mainly depends on mineralizer concentration, reaction temperature and reaction time.

Although its potential application could consume only a small part of NC generated by the combustion of coal, the as-synthesised zeolites could reach an added value much higher than at present. NC was used in this study because: (1) it is a coal-by product thus it adds value, reduces cost and enhances the environment, (2) its potential application in zeolite synthesis and water technology is under-utilized and (3) it is very resistant to weathering and erosion and highly workable. Therefore, attempts were made to investigate the potential of NC as a novel raw material for the production of NCZs.

2.4.2.3. Fly ash-based zeolitic materials

Waste products are generated annually in the world by all industries, and their disposal poses a major challenge and a serious environmental problem, taking into account that the amount of discharged material is expected to increase in future. Globally, over 500 million tonnes of FA are generated annually from coal combustion by thermal power plants and has been used for reclamation, asphalt shingle production, quarry-fill and sludge stabilization, but most is disposed as landfill. Due to the shortage of landfill sites and stricter environmental regulation, new ways to recycle FA should be quickly developed, and one new way is through zeolitization. The classic hydrothermal synthesis of FA-based zeolites (FAZs) has been reported by several patents and research articles (Höller and Barth-Wirsching, 1985; Kato *et al*., 1986; Yoshida and Inoue, 1986; Yoshida and Inoue, 1986; Bergk *et al*., 1987; Henmi, 1987; Mondragón *et al*., 1990; La Rosa *et al.*, 1992; Lin and Hsi, 1995; Park and Choi, 1995; Singer and Berkgaut, 1995; Querol *et al*., 1995, 1197b, 1999, 2001, 2002a; Shih *et al.*, 1995; Shih and Chang, 1996; Amrhein *et al.*, 1996; Catalfamo *et al.*, 1997; Kolousek *et al*., 1997; Hollman *et al.*, 1999; Maruyama *et al.*, 2002; Mouhtaris *et al.*, 2003; Molina and Poole, 2004; Ojha *et al.*, 2004; Inada *et al.*, 2005). The FAZs

cover a wide range of known zeolite frameworks and have been reviewed (Querol *et al.*, 2002a). Recently, more sophisticated treatments have been reported. An alkaline fusion step followed by hydrothermal treatment (Shigemoto *et al.*, 1992, 1993; Berkgaut and Singer, 1996; Chang and Shih, 1998) facilitated the formation of highly active Na aluminosilicate salts readily soluble in water and promoted zeolite formation. However, the alkaline fusion procedure has been modified to obtain high porous size and cation exchange capacity (CEC) zeolitic material (Rayalu *et al*., 2000, 2001). The application of microwave radiation to the conventional synthesis parameters at a laboratory scale (Querol *et al.*, 1997b) resulted in a drastically decrease in reaction time. A new method for synthesizing zeolite under molten conditions without any addition of water has been developed (Park *et al.*, 2000a, 2000b), although complete zeolitization of FA could not be accomplished by this method. A two step procedure has been developed consisting of an initial Si-extraction from FA using a light alkaline treatment of FA, followed by a synthesis of pure zeolites by adding an Al-bearing residue solution obtained from Al-anodizing industry (Hollman *et al.*, 1999). Moreno *et al*. (2001a, 2002) has optimized this method to obtain zeolites with high purity from SiO_2 extracts and another zeolitic product (the solid residue from SiO_2 extracts). Apart from the formation of zeolites, the hydrothermal conversion of FA can also produce amorphous form aluminosilicate, referred to geopolymers (Davidovits, 1991). Several researchers have also investigated geopolymer synthesis from FA in hydrothermal conversion and could only achieve partial conversion of FA (Swanepoel and Strydom, 2002; van Jaarsveld *et al*., 2003; Steveson and Sagoe-Crentsil, 2005). Therefore, the alkaline fusion method can be applied to transform the crystalline phases in FA to amorphous geopolymer (Li *et al*., 2006). Geopolymers can be viewed as the amorphous equivalent of certain synthetic zeolites and would have more or less the same chemical composition although the absence of the distinctive long-range zeolite structure makes them amorphous to X-rays (van Jaarsveld *et al*., 1997).

The type and yield of synthesized zeolite strongly depended on alkaline condition and SiO_2/Al_2O_3 ratio of the starting FA, although the Si and Al concentrations are determined by the starting FA composition, alkaline concentration and liquid/solid ratio. The SiO_2/Al_2O_3 ratio is important to predict whether the FA could successfully be converted into a specific zeolitic material by the adopted synthesis procedures (Somerset *et al*., 2005c). On the other hand, in order to synthesize a specific zeolite from any FA source, it is necessary to clarify the influence of the silica–alumina composition for the zeolite formation because the FA composition seriously changes depending on the origin of coal sources (Inada *et al*., 2005). The glass phase of FA plays an important role during the zeolitization process because it easily dissolves into the

alkaline solution compared to crystalline phases like quartz and mullite, which generally persist in the synthesis products. Therefore, the Si/Al molar ratio of the glass phase has a large influence on the type of synthesized zeolite (Inada *et al*., 2005). Querol *et,al*. (1997a) have highlighted the importance of the mineralogical composition of FA; similar SiO_2/Al_2O_3 ratios in this coal by-product can promote the synthesis of different zeolites under the same experimental conditions and these differences could be attributed to different SiO_2/Al_2O_3 ratios of the glass phase inferred from the differences in mineralogy at the same bulk chemical composition.

Intense research on the potential industrial applications of FAZs has be developed mainly in the removal of heavy metals and ammonium from wastewater (Catalfano *et al*., 1993; Lin and Hsi, 1995; Park and Choi, 1995; Singer and Berkgaut, 1995; Amrhein *et al.*, 1996; Berkgaut and Singer, 1996; Catalfamo *et al.*, 1997; Querol *et al.*, 1997b; Kolousek *et al*., 1997; Moreno *et al*., 2001a; 2001b; Querol *et al*., 2002b; 2006).

Chapter 3

Chapter 3. Materials and experimental methods

3.1. Raw materials

The synthesis of zeolites was carried out from raw materials that can be classified as chemical reagents and natural sources. Three different aluminosilicate sources such as KAO (clay mineral) or its calcined product, NC (coal mining by-product) and FA (industrial waste solid material) were used as starting materials. To modify the SiO_2/Al_2O_3 ratio, precipitated SiO_2 was used. Natural raw materials and commercial chemical reagents with their suppliers, purity and chemical formula are listed in Table 3.1.

Table 3.1. Raw materials used for the synthesis of zeolitic materials.

Raw material	Supplier	Purity	General aspects	Chemical formula
Aluminosilicate source				
Kaolinite (supreme powder)	ECC International			$Al_2Si_2O_5(OH)_4$
Metakaolinite			by calcination of kaolinite	$Al_2Si_2O_7$
Natural clinker	Late Paleocene Cerrejón Formation, Cerrejón Coal Deposit, Colombia		by autocombustion of coal	
Fly ash	Rugeley Power Station, West Midlands, England		by combustion of coal	
Mineralizer				
Sodium hydroxide (pellets)	Aldrich Chemical Company, Inc	99.99%		NaOH
Sodium hydroxide (powder)	BDH Laboratory Supplies	96%		NaOH
Potassium hydroxide (pellets)	Aldrich Chemical Company, Inc	>85%		KOH
Potassium hydroxide (powder)	Fluka	≥85%		KOH
Ammonium fluoride	Aldrich Chemical Company, Inc	98+% A.C.S.		NH_4F
Sodium fluoride	Fluka	99%		NaF
Silica source				
Precipitated silica	BDH Laboratory Supplies	98%		SiO_2
Structure directing agent				
Triethylamine (TEA)	BDH Laboratory Supplies	99%		$(C_2H_5)_3N$
Triethylene diamine (TEDA)	Aldrich Chemical Company, Inc	98%		$C_6H_{12}N_2$
Triethanolamine (TLAM)	BDH Laboratory Supplies	99%		$(CH_2CH_2OH)_3N$
Tetrapropylammonium bromide (TPAB)	Aldrich Chemical Company, Inc	98%		$(CH_3CH_2CH_2)_4NBr$
Solvent				
Distilled water	Standard purification method			H_2O

3.2. Zeolite synthesis

The aluminosilicate sources were prepared prior to the synthesis process as follows. Powder preparation techniques included both a SpectroMill Ball Pestle Impact grinder and a mortar and

pestle. After grinding, samples were sieved under dry conditions and the size fraction of 200 mesh collected and particles of < 75 μm selected for zeolite synthesis. The dried powder samples were then ground as fine as possible, using a mortar and pestle, for further characterization. The conversion of the raw materials into zeolitic materials was conducted by two routes: (1) conventional hydrothermal synthesis and (2) alkaline fusion prior to hydrothermal synthesis, taking into account that the direct treatment of the raw materials using alkaline solutions could be quite time consuming, energy intensive and/or environmentally unfriendly, which can be overcome by using the alkaline fusion approach. Figure 3.1 illustrates the conversion of raw materials into zeolitic materials by the routes used in this study. A complete set of the experimental conditions for zeolite synthesis will be present in Tables 5.1-5.2, 6.1-6.2 and 7.1-7.2.

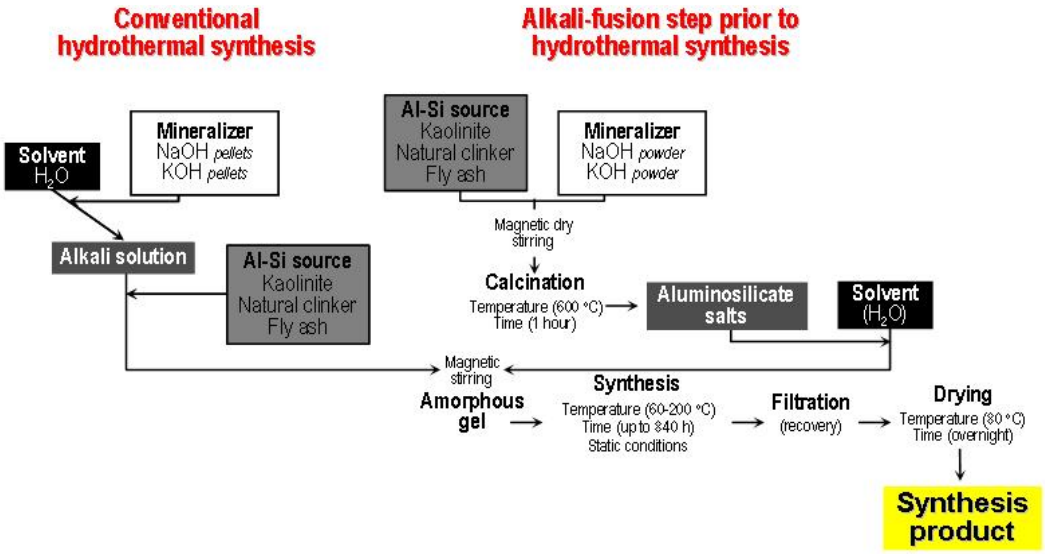

Figure 3.1. Flowchart showing the activation of raw materials.

3.2.1. Classic hydrothermal synthesis

In the classic hydrothermal synthesis, 0.96 or 2.87 g of NaOH and 1.35 or 4.03 g of KOH in pellets were added to distilled water (18 ml) to prepare alkaline solutions 1.33 or 3.99M in reaction plastic beakers (150-250 ml), and then 3.10 or 6.20 g of the raw materials were added to the alkaline solutions. The progressive addition of reagents was carried out with stirring until they dissolved to homogenize the reaction gel. Table 3.2 shows typical examples of the calculation of the molar gel compositions used for the synthesis of zeolites using KAO and MTK

as starting materials. For the calculation of the molar gel composition, NaOH and the chemical compositions of KAO and MTK were expressed in terms of molar oxide.

Table 3.2. Calculation of the molar gel composition using KAO and MTK as starting materials.

CLASSIC HYDROTHERMAL METHOD

	Substance	Molecular Weight (g/mol)	Mass used (g)	Partial # moles	Molar oxide	Total # moles
Solvent	H_2O	18.00	18.00	1.000		1.000
Activator	NaOH	40.00	0.96	0.024	$0.5Na_2O$	0.012
					$0.5H_2O$	0.012
KAO	$Al_2Si_2O_5(OH)_4$	258.16	3.10	0.012	$2SiO_2$	0.024
					Al_2O_3	0.012
					$2H_2O$	0.024
Molar gel composition	$Na_2O:Al_2O_3:2SiO_2:86.3H_2O$					

	Substance	Molecular Weight (g/mol)	Mass used (g)	Partial # moles	Molar oxide	Total # moles
Solvent	H_2O	18.00	18.00	1.000		1.000
Activator	NaOH	40.00	0.96	0.024	$0.5Na_2O$	0.012
					$0.5H_2O$	0.012
MTK	$Al_2Si_2O_7$	222.13	2.67	0.012	$2SiO_2$	0.024
					Al_2O_3	0.012
Molar gel composition	$Na_2O:Al_2O_3:2SiO_2:84.2H_2O$					

ALKALINE FUSION METHOD

	Substance	Molecular Weight (g/mol)	Mass used (g)	Partial # moles	Molar oxide	Total # moles
Solvent	H_2O	18.00	65.65	3.647		3.647
Activator	NaOH	40.00	7.44	0.186	$0.5Na_2O$	0.093
					$0.5H_2O$	0.093
KAO	$Al_2Si_2O_5(OH)_4$	258.16	6.20	0.024	$2SiO_2$	0.048
					Al_2O_3	0.024
					$2H_2O$	0.048
Molar gel composition	$3.9Na_2O:Al_2O_3:2SiO_2:153.9H_2O$					

	Substance	Molecular Weight (g/mol)	Mass used (g)	Partial # moles	Molar oxide	Total # moles
Solvent	H_2O	18.00	65.65	3.647		3.647
Activator	NaOH	40.00	7.44	0.186	$0.5Na_2O$	0.093
					$0.5H_2O$	0.093
MTK	$Al_2Si_2O_7$	222.13	6.20	0.028	$2SiO_2$	0.056
					Al_2O_3	0.028
Molar gel composition	$3.3Na_2O:Al_2O_3:2SiO_2:134H_2O$					

To evaluate the influence of additives, additional hydrothermal treatments were performed reacting KAO or MTK in NaOH solutions, followed by the addition of 0.24 g of precipitated SiO_2 to adjust the SiO_2/Al_2O_3 ratio or by the addition of SDAs (0.92 g of TPAB, 0.61 or 1.22 g of TEA, 0.67 g of TEDA and 0.90 g of TLAM) to explore the chance to obtain different zeolitic products. These raw materials were also activated in fluoride media, using 1.01 g of NaF and 0.89 or 2.66 g of NH_4F, with or without the addition of SDAs to investigate the formation of silica-rich zeolites in slight acidic media. The use of several mineralizers is justified by the fact that it is interesting to compare their effect and efficiency in the synthesis process. The hydrothermal transformation of KAO and MTK in the system $CaO\text{-}SiO_2\text{-}Al_2O_3\text{-}H_2O$ was also carried out. A calcination process was carried out in order to obtain amorphous phases required in some experiments as follows: MTK was prepared by calcining KAO at 600 °C in air for 2 h; $Al(OH)_3$ and $CaCO_3$ were calcined at 550 and 1000 °C, respectively, for 1 h to obtain Al_2O_3 and CaO, respectively. Calculated amounts of CaO (4.90 or 5.20 g) were added to distilled water (18 ml), and finally 3.00 g of MTK or 3.40 g of KAO was added to the CaO solutions. An additional test was conducted dissolving

5.40 g of precipitated SiO_2 and then 1.00 g of Al_2O_3 (amorphous) in the CaO solutions.

The efficiency of this method is affected by some crystalline aluminosilicate phases that remain inert in the raw materials, particularly using NC and FA as starting materials. Table 3.3 shows typical examples of the calculation of the molar gel compositions used for the synthesis of zeolites from coal by-products (NC and FA). For the calculation of the molar gel composition, NaOH was expressed in terms of molar oxide and the chemical compositions of NC and FA were converted to ratio mass per mass used of these raw materials.

Table 3.3. Calculation of the molar gel composition using NC and FA as starting materials.

CLASSIC HYDROTHERMAL METHOD

	Substance	Weight% (EDX)	Molecular Weight (g/mol)	Mass used (g)	Partial # moles	Molar oxide	Partial # moles	Ratio mass per 3.10 g of NC	Total # moles
Solvent	H_2O		18.00	18.00	1.000		1.000		1.000
Activator	NaOH		40.00	0.96	0.024	$0.5Na_2O$	0.012		0.012
						$0.5H_2O$	0.012		0.012
Natural Clinker	SiO_2	56.60	60.08					1.75	0.029
	Al_2O_3	23.61	102.00					0.73	0.007
	TiO_2	1.10	79.87					0.03	0.000
	Fe_2O_3	9.41	159.69					0.29	0.002
	MgO	3.94	40.30					0.12	0.003
	Na_2O	1.41	61.98					0.04	0.001
	K_2O	1.95	94.20					0.06	0.001
	SO_3	1.11	80.06					0.03	0.000
	CaO	0.53	56.08					0.02	0.000
	MnO	0.35	70.94					0.01	0.000
Molar gel composition	$1.8Na_2O:0.1K_2O:0.4MgO:0.3Fe_2O_3:Al_2O_3:4.1SiO_2:141H_2O$								

	Substance	Weight% (EDX)	Molecular Weight (g/mol)	Mass used (g)	Partial # moles	Molar oxide	Partial # moles	Ratio mass per 3.10 g of FA	Total # moles
Solvent	H_2O		18.00	18.00	1.000		1.000		1.000
Activator	NaOH		40.00	0.96	0.024	$0.5Na_2O$	0.012		0.012
						$0.5H_2O$	0.012		0.012
Fly Ash	SiO_2	52.96	60.08					1.64	0.027
	Al_2O_3	43.60	102.00					1.35	0.013
	TiO_2	0.14	79.87					0.00	0.000
	Fe_2O_3	0.41	159.69					0.01	0.000
	MgO	0.33	40.30					0.01	0.000
	Na_2O	0.33	61.98					0.01	0.000
	K_2O	1.30	94.20					0.04	0.000
	SO_3	0.45	80.06					0.01	0.000
	CaO	0.48	56.08					0.01	0.000
	MnO	0.00	70.94					0.00	0.000
Molar gel composition	$0.9Na_2O:Al_2O_3:2.1SiO_2:76.4H_2O$								

	Substance	Weight% (EDX)	Molecular Weight (g/mol)	Mass used (g)	Partial # moles	Molar oxide	Partial # moles	Ratio mass per 3.10 g of NC	Total # moles
Solvent	H_2O		18.00	18.00	1.000		1.000		1.000
Activator	KOH		56.11	1.35	0.024	$0.5K_2O$	0.012		0.012
						$0.5H_2O$	0.012		0.012
Natural Clinker	SiO_2	56.60	60.08					1.75	0.029
	Al_2O_3	23.61	102.00					0.73	0.007
	TiO_2	1.10	79.87					0.03	0.000
	Fe_2O_3	9.41	159.69					0.29	0.002
	MgO	3.94	40.30					0.12	0.003
	Na_2O	1.41	61.98					0.04	0.001
	K_2O	1.95	94.20					0.06	0.001
	SO_3	1.11	80.06					0.03	0.000
	CaO	0.53	56.08					0.02	0.000
	MnO	0.35	70.94					0.01	0.000
Molar gel composition	$0.1Na_2O:1.8K_2O:0.4MgO:0.3Fe_2O_3:Al_2O_3:4.1SiO_2:141H_2O$								

	Substance	Weight% (EDX)	Molecular Weight (g/mol)	Mass used (g)	Partial # moles	Molar oxide	Partial # moles	Ratio mass per 3.10 g of FA	Total # moles
Solvent	H_2O		18.00	18.00	1.000		1.000		1.000
Activator	KOH		56.11	1.35	0.024	$0.5K_2O$	0.012		0.012
						$0.5H_2O$	0.012		0.012
Fly Ash	SiO_2	52.96	60.08					1.64	0.027
	Al_2O_3	43.60	102.00					1.35	0.013
	TiO_2	0.14	79.87					0.00	0.000
	Fe_2O_3	0.41	159.69					0.01	0.000
	MgO	0.33	40.30					0.01	0.000
	Na_2O	0.33	61.98					0.01	0.000
	K_2O	1.30	94.20					0.04	0.000
	SO_3	0.45	80.06					0.01	0.000
	CaO	0.48	56.08					0.01	0.000
	MnO	0.00	70.94					0.00	0.000
Molar gel composition	$0.9K_2O:Al_2O_3:2.1SiO_2:76.4H_2O$								

ALKALINE FUSION METHOD

	Substance	Weight% (EDX)	Molecular Weight (g/mol)	Mass used (g)	Partial # moles	Molar oxide	Partial # moles	Ratio mass per 6.20 g of NC	Total # moles
Solvent	H_2O		18.00	66.65	3.703		3.703		3.703
Activator	NaOH		40.00	7.44	0.186	$0.5Na_2O$	0.093		0.093
						$0.5H_2O$	0.093		0.093
Fly Ash	SiO_2	56.60	60.08					3.51	0.058
	Al_2O_3	23.61	102.00					1.46	0.014
	TiO_2	1.10	79.87					0.07	0.001
	Fe_2O_3	9.41	159.69					0.58	0.004
	MgO	3.94	40.30					0.24	0.006
	Na_2O	1.41	61.98					0.09	0.001
	K_2O	1.95	94.20					0.12	0.001
	SO_3	1.11	80.06					0.07	0.001
	CaO	0.53	56.08					0.03	0.001
	MnO	0.35	70.94					0.02	0.000
Molar gel composition	$6.6Na_2O:0.1K_2O:0.4MgO:0.3Fe_2O_3:Al_2O_3:4.1SiO_2:264.5H_2O$								

	Substance	Weight% (EDX)	Molecular Weight (g/mol)	Mass used (g)	Partial # moles	Molar oxide	Partial # moles	Ratio mass per 6.20 g of FA	Total # moles
Solvent	H_2O		18.00	65.65	3.647		3.647		3.647
Activator	NaOH		40.00	7.44	0.186	$0.5Na_2O$	0.093		0.093
						$0.5H_2O$	0.093		0.093
Fly Ash	SiO_2	52.96	60.08					3.28	0.055
	Al_2O_3	43.60	102.00					2.70	0.027
	TiO_2	0.14	79.87					0.01	0.000
	Fe_2O_3	0.41	159.69					0.03	0.000
	MgO	0.33	40.30					0.02	0.001
	Na_2O	0.33	61.98					0.02	0.000
	K_2O	1.30	94.20					0.08	0.001
	SO_3	0.45	80.06					0.03	0.000
	CaO	0.48	56.08					0.03	0.001
	MnO	0.00	70.94					0.00	0.000
Molar gel composition	$3.5Na_2O:Al_2O_3:2.1SiO_2:141.1H_2O$								

3.2.2. Alkaline fusion followed by hydrothermal reaction

In the second method**,** an alkaline fusion step was introduced prior to the hydrothermal treatment, because it plays an important role in enhancing the hydrothermal conditions for zeolite synthesis. On the other hand, this approach was adopted in this study because larger amounts of aluminosilicates can be dissolved employing this method. In a typical synthesis process, 6.20 g of raw material (KAO, NC or FA) were dry mixed with 7.44 g of NaOH or KOH powder (raw material/alkaline activator = 1/1.2 in weight) for 30 min and the resultant mixture was fused at 600 °C for 1 h. The alkaline reagent added to the starting material acts as an activator agent during fusion. The product yield from the fusion can be as high as 100%. Some of the inert crystalline phases in the raw materials can be fully reacted. The fused product was ground in a mortar and then 4.40 g of this was dissolved in 21.50 ml of distilled water (ratio = 1/4.9) under stirring conditions to form the amorphous precursors. In special cases, the fused product was dissolved in distilled water under static conditions. However, in some cases the alkaline-fused products were dissolved in water with or without stirring for different reaction times. Tables 3.2 and 3.3 show typical examples of the calculation of the molar gel compositions used for the synthesis of zeolites using the alkaline fusion method.

The amount of reagents used for the preparation of the hydrogels was based on previous literature search. In both synthesis procedures, the raw materials were activated by magnetic stirring to produce a reaction gel with a specific molar composition. The hydrothermal reaction was carried out under static conditions, transferring the hydrogels to PTFE (polytetrafluoroethylene = Teflon) bottles (Cowie Technology Ltd) of 65 ml for preparations heated < 100 °C or PTFE-lined stainless steel autoclaves for preparations heated > 100 °C. The reactors were removed from the oven at the scheduled times and were quenched in cold water to stop the reaction. Hydrogel pH was measured before and after hydrothermal treatment. Then, the reaction mixtures were filtered and washed with distilled water to remove excess alkali. Finally, the samples were oven dried at 80 °C overnight. The dried samples were weighed and kept in plastic bags for characterization.

3.3. Preparation of synthetic solutions and sampling of acid mine drainage

Synthetic solutions were prepared as shown in Table 3.4. A weighed amount of each nitrate salt, ammonium chloride and other compounds, which include CH_3COOH, $C_6H_{12}O_6$, $CaCl_2$, KCl, NH_4Cl, KH_2PO_4 and $MgSO_4$, were dissolved in distilled water to formulate the artificially polluted stock solutions (1000 mg l^{-1}) used to make up SS1, SS2 and SS3 solutions containing the selected metals.

Table 3.4. Composition of synthetic solutions used for sorption experiments.

Chemical reagent	Supplier	Purity	Component (mg l^{-1})		
			SS1	SS2	SS3
$Cu(NO_3)_2.3H_2O$	Scientific & Chemical Supplies Ltd	General purpose	25	25	50
$Pb(NO_3)_2$	BDH Laboratories Supplies	General purpose, 99%	25	25	50
$Zn(NO_3)_2.6H_2O$	Hopkins & Williams AnalaR	Laboratory reagent	25	25	50
$Cr(NO_3)_3.9H_2O$	Hopkins & Williams AnalaR	Laboratory reagent	25	25	50
$Ni(NO_3)_2.6H_2O$	Hopkins & Williams AnalaR	98%	25	25	50
CH_3COOH			250	250	
$C_6H_{12}O_6$			50	25	
$CaCl_2$	Fisher Scientific	Fused	5	25	
KCl	Fisher Scientific	99.79%	25	25	
NH_4Cl	Scientific & Chemical Supplies Ltd	General purpose	20	25	25
KH_2PO_4	BDH Laboratories Supplies		20	25	
$MgSO_4$	Fisher Scientific	70%	10	10	

SS1, SS2 and SS3, synthetic solutions 1, 2 and 3

The Parys Mountain copper-lead-zinc deposit of Anglesey (North Wales), Figure 3.2, represents a volcanogenic massive sulphide (VMS) district of major metallogenic importance, which is characterized by the occurrence of concordant massive to banded sulphide lens formed by volcanic processes normally on the sea-floor. However, mining activities at this deposit have generated AMD (a by-product of the mining industry), producing a strong environment impact. AMD samples were collected at this mining site to perform an experimental work using natural polluted sources.

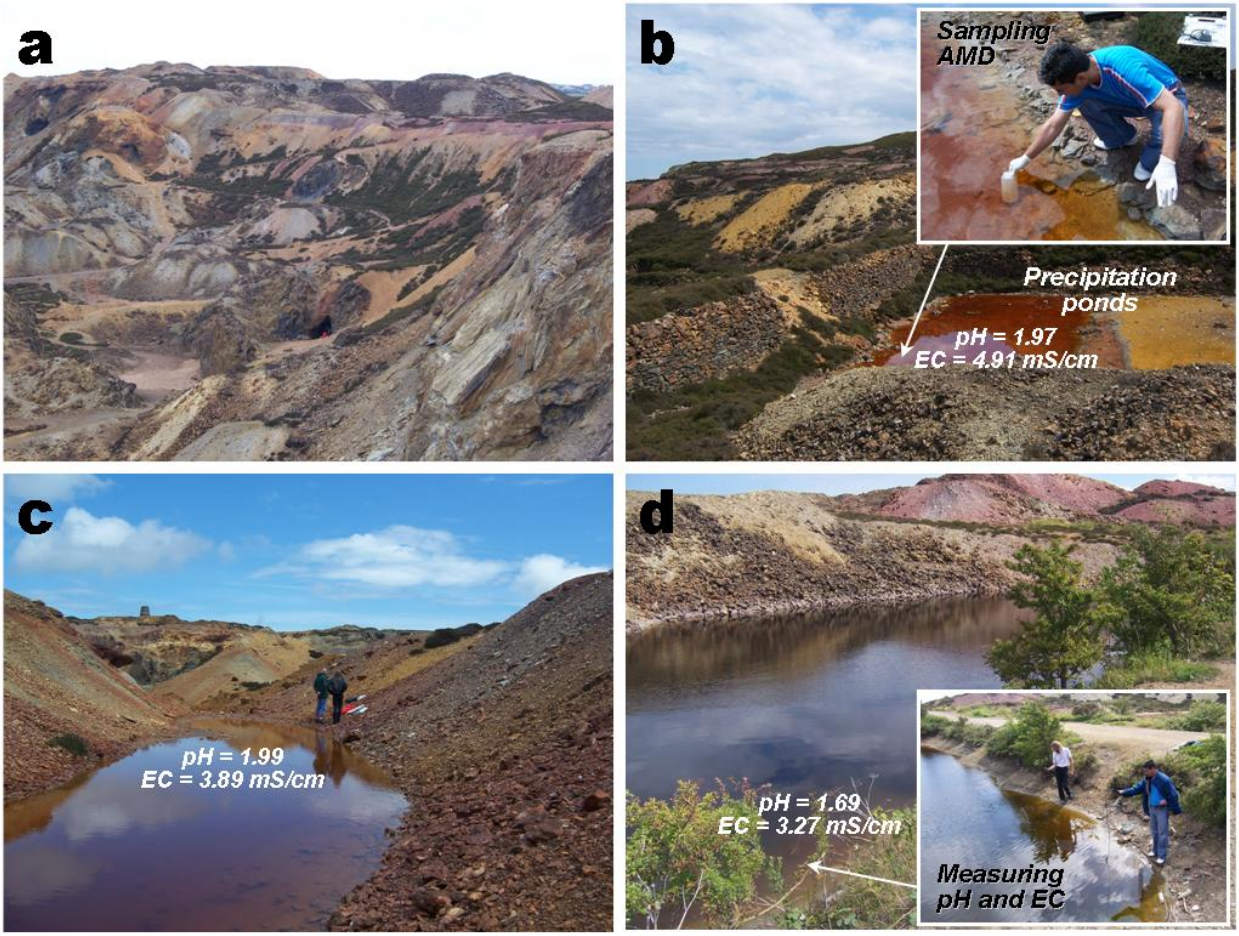

Figure 3.2. General aspects of the Parys Mountain copper-lead-zinc deposit, Anglesey (North Wales): (a) a panoramic view of the Great Opencast from the viewing platform; (b) brick-lined precipitation ponds used to extract copper; (c) and (d) shallow and deep transient ponds from rainfall between spoil heaps near the top of the mountain and by the entry road of the copper mine, respectively.

The Great Opencast (Figure 3.2a) forms part of the geological heritage of Parys Mountain, being a focus of tourist attraction for visitors due to its similarity with a lunar landscape, and was opened up at an early stage of mining. However, AMD is a natural consequence of mining activity. AMDs were collected in three major locations and sealed in high-density polyethylene bottles (upper right side photograph in Figure 3.2b). Brick-lined precipitation ponds (Figure 3.2b) have been used to extract copper from water which was pumped up to the mountain top and allowed to drain down through the spoil and underground workings, dissolving copper from the rocks. The copper precipitation is carried out by the accumulation of copper-rich water in these ponds and then adding scrap iron, which results in dissolution of iron and precipitation of copper as a black powder, which can be removed for processing. This process has been very efficient

to recover small amounts of relatively pure copper. Figure 3.2c illustrates a shallow transient pond from rainfall occurring between spoil heaps near the top of the mountain. Figure 3.2d shows a deeper transient pond located by the entry road of the copper mine, where the lowest pH (1.69) was obtained. On-site analyses of the pH and EC were performed in different surface drainage waters, as illustrated in the lower right side photograph in Figure 3.2d.

3.4. Batch experiments

The sorption of metal ions and ammonium onto different inorganic exchangers (raw materials or synthesis products) were conducted to investigate their efficiency to clean-up wastewater effluents. Sorption tests were carried out in high density plastic polyethylene containers with a volume capacity of 100 ml through batch type reactions at room temperature, by using a given sorbent dose (sorbent:solution mixture of 0.25, 0.5 and 1 g / 20 ml or 1 g / 50 ml) and the suspension was kept in a rotary shaker with a constant agitation speed of 150 rpm for a given time interval. In these experiments the sorbent:liquid ratio was varied to investigate the effects of variation of sorbent dose on the metal retention of selected metals with the sorbent. Each sorbent/solution sample was individually placed in separate containers and at the scheduled times each container was removed from the shaker and the filtrate collected by filtering the suspension with a 0.45 μm membrane filter, and finally the pH and EC measured. The resultant leachates were kept in a refrigerator at 4 ^{o}C for ICP-AES. General aspects concerning this experimental work are illustrated in Figure 3.3.

The application of the sorbents needs to consider specific variables, particularly with respect to the qualitative assessment of parameters associated with the decontamination of polluted aqueous media. The process of ion exchange is defined as the reversible interchange of a charged ion for a similarly charged ion between a solid material (the ion exchanger) and the surrounding liquid, in which there is no permanent change in the structure of the solid (Kitchener, 1957). According to Hendricks (2005), this process resembles sorption, in that in both cases, a dissolved species is taken up by a solid. However, the characteristic difference between the two phenomena is that ion exchange is a stoichiometric process where every ion which is removed from the solution is replaced by an equivalent amount of another species of the same sign, whereas sorption indicates that a solute is taken up without being replaced by another species. On the other hand, the distinction between the two phenomena seems clear-

cut, virtually every ion-exchange process is accompanied by electrolyte sorption or desorption and most of the common sorbents can act, in turn, as ion exchangers.

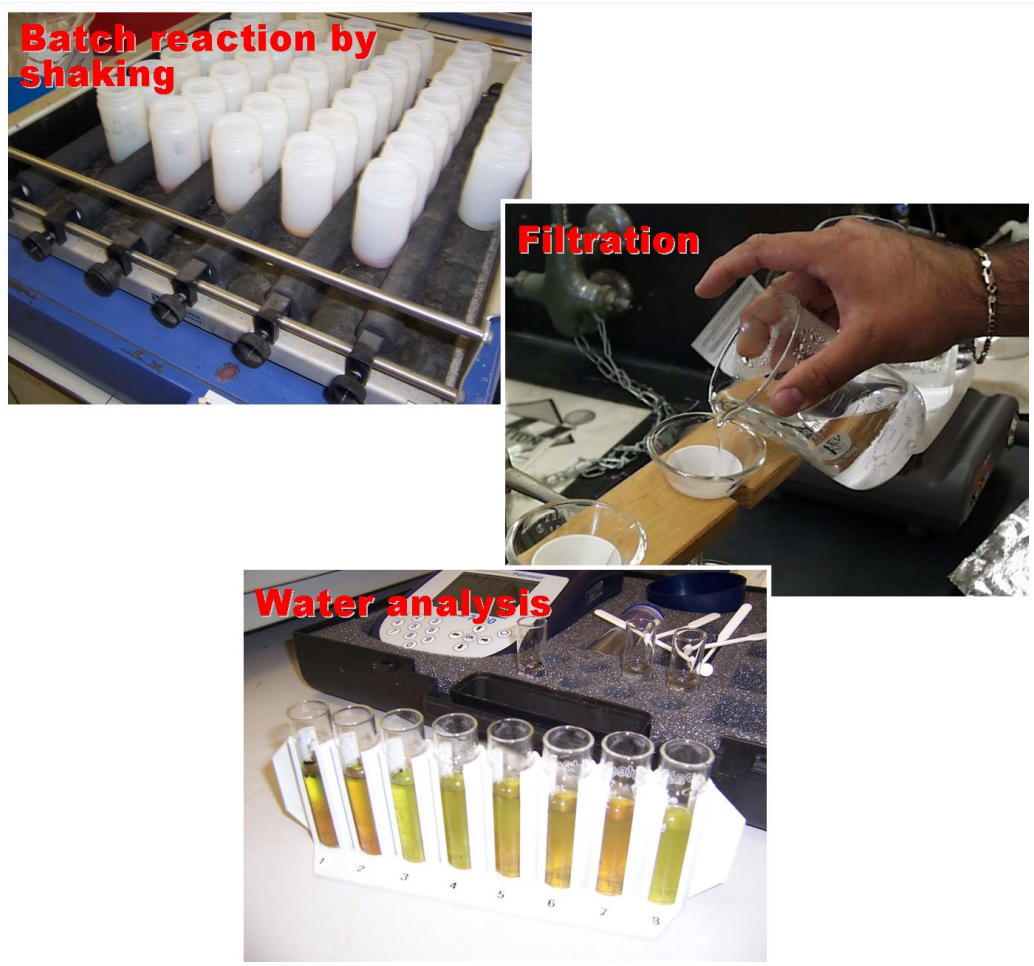

Figure 3.3. Experimental work for the sorption study.

3.5. Techniques of characterization

Table 3.5 depicts the analytical facilities (and their placement) used in this study to carry out the characterization of raw materials and synthesis products. Each analysis technique typically probes only a particular aspect of the material and, therefore, a combination of methods is necessary to obtain a complete description of the starting materials as well as the frequently complex zeolitic products. This is very important to use and improve a zeolitic material for a

specific application. Generally, the characterization of a zeolite has to provide information on: (1) its structure and morphology; (2) its chemical composition; (3) its ability to sorb and retain molecules; and (4) its ability to chemically convert those molecules.

Table 3.5. Analytical techniques and instruments.

Analytical Technique	Instrument	Place
XRD	Phillips PW 1710 X-ray diffractometer	University of Wolverhampton
TGA/DTA	Mettler Toledo TG 50 thermobalance	
SEM/EDX	ZEISS EVO50 scanning electron microscope	
FT-IR	Mattson Genesis II FT-IR spectrometer	
ICP-AES	Thermo Jarrell-Ash ICAP-9000 ICP-AE Spectrometer	
pH	pH 211 Auto-calibration bench pH/mV meter - Hanna instruments	
EC	Conductivity meter - version Cond 315i - WTW	
NH_4^+	Photometer 7100 - Palintest	
MAS-NMR	Varian Unity Inova Spectrometer	University of Durham

3.5.1. X-Ray Diffraction (XRD) Analysis

The raw materials and synthesis products were identified by XRD on a Phillips PW 1710 X-ray powder diffractometer operating in Bragg-Brentano geometry with Cu-Kα radiation at 40 mA and 40 kV and secondary monochromation. Data collection was carried out in the 2θ range 3-50°, with a scanning step of 0.02°. Raw materials and zeolitic products were crushed with agate mortar and pestle, ground to powder form (< 5 μm) and mounted in aluminium plate sample holders with a volume of 0.1 cm^3. The crystalline patterns were compared with the standard line patterns from the powder diffraction file database supplied by International Centre for Diffraction Data (ICDD).

3.5.2. Fourier Transform Infrared (FT-IR) Spectroscopy

FT-IR spectra of the raw and zeolitic materials were recorded in the range 4000-400 cm^{-1} using a Mattson Genesis II FT-IR spectrometer in a transmission mode, used in conjunction with a diamond attenuated total reflectance (ATR) accessory. However, only the 1200-400 cm^{-1} region

was investigated, taking into account that it is where the spectra showed remarkable changes. ATR analysis is less complicated than using KBr pellets, is fast and a very small amount of the sample is needed. Powdered samples were sieved to give a particle size < 5 μm and then placed onto the diamond ATR crystal surface. Finally, a force was applied to the sample for spectrum collection. The sample was then removed from the crystal surface in order to prepare the accessory to collect additional spectra.

3.5.3. Scanning Electron Microscopy (SEM)

The morphology of the raw and zeolitic materials was investigated by SEM on a ZEISS EVO50 scanning electron microscope under the following analytical conditions: EHT = 20.00 kV, Signal A = SE1, WD = 4.0mm. Specimens were prepared by spraying dried raw material or zeolite powder onto aluminium stubs using double-sided adhesive carbon discs and sputter coated with gold to reduce static charging and then observing under SEM conditions. For EDX analysis the samples were prepared in a similar way to SEM. However, to avoid errors in the aluminium content, a carbon sample holder was used instead of aluminium stud and gold was not coated on the samples.

3.5.4. Thermogravimetric Analysis (TGA)

The starting materials and as-synthesized products were analyzed by thermogravimetry on a Mettler Toledo TG 50 thermobalance between 25-700 °C for raw materials and zeolitic products, using a heating rate of 10 °C min^{-1} under flowing air (200 cm^3 min^{-1}). The ground sample can be directly filled into the crucible for TG testing. The amount was normally 15-20 mg to minimize background noise. This analytical technique was very useful to estimate the thermal stability of the synthesis products.

3.5.5. ^{29}Si and ^{27}Al Magic Angle Spinning Nuclear Magnetic Resonance (MAS NMR)

Solid-state ^{29}Si and ^{27}Al MAS NMR spectra were recorded at room temperature on a Varian Unity INOVA or VNMRS spectrometer. Spectra were obtained using a direct-polarisation pulse sequence under the conditions given in Table 3.6. The chemical shifts were referenced to tetramethylsilane (TMS) for ^{29}Si and 1 M $AlCl_3$ aqueous solution for ^{27}Al. The Si/Al ratios of the zeolitic phases were calculated on basis of ^{29}Si MAS NMR data according to the equation 3.1 of Engelhardt and Michel (1987). A deconvolution of these spectra reveals that these peaks have similar relative intensities due to similar Si/Al ratios of the samples.

$$Si/Al = \Sigma_n I_n / (I_4 + 0.75\, I_3 + 0.5\, I_2 + 0.25 I_1) \quad (3.1)$$

(I_n = intensity of Q^4/nAl signals in ^{29}Si MAS NMR spectra, n = 0–4 without consideration of the signals of the non-zeolitic admixtures).

Table 3.6. Recording conditions of the MAS NMR spectra.

	^{29}Si	^{27}Al
MAS probe (mm)	7.5	4.0
Frequency (MHz)	59.6	78.1
Spectral width (Hz)	29996.3	100000.0
Acquisition time (ms)	30	10
Recycle delay (s)	120	0.5
Number of repetitions	15	2200
Spinning rate (Hz)	5040	14000
Pulse angle (radians)	$\pi/2$	$\pi/10$

3.5.6. Standard Methods for the Examination of Water and Wastewater

All measurements were performed adopting the 'Standard Methods for the Examination of Water and Wastewater' (American Public Health Association, 2005). The samples were stored in a refrigerator before the analyses were carried out. Analysis of synthetic or natural wastewaters

and leachates was initially performed monitoring pH (pH 211 Auto-calibration bench pH/mV meter - Hanna instruments) and EC (Conductivity meter - version Cond 315i - WTW). Dilutions were made using distilled water, depending on the original EC of each sample. The filtered supernants were analysed for the major cations (Al^{3+}, Si^{4+}, Na^{+}, K^{+}, Ca^{2+}, Mg^{2+}) and heavy metals by inductively coupled plasma atomic emission spectroscopy (ICP-AES), using a Spectro Ciros ICP-AES spectrometer. A Photometer 7100 fully integrated with the Palintest water test system was used to measure ammonia over the range 0-1.0 mg l^{-1} N. Dilutions of 1:10 ml were made to obtain appropriate ammonium concentrations.

Chapter 4

Chapter 4. Characterization of the raw materials

Knowledge of the characteristics of the raw materials is very important in both zeolite synthesis and application of sorbents in water treatment. Their detailed characterization of them may be very difficult, due to the complexity of their chemical structures. However, by combining the results of different methods, a thorough insight into their structure can be obtained. Technological properties of zeolitic products depend on the physical, chemical and mineralogical characteristics of the starting materials, which also control the overall processing of treatment of polluted effluents.

This chapter describes the characterization of the raw materials used in this study, which can be divided in three types according to their origin: geological materials (KAO), mining by-products (NC) and industrial solid wastes (FA). The chemical composition of these materials and their loss on ignition (LOI) values are indicated in Table 4.1.

Table 4.1. Chemical composition (in weight %) and LOI of the raw materials used for zeolite synthesis.

Raw material	SiO_2	Al_2O_3	TiO_2	Fe_2O_3	MgO	Na_2O	K_2O	SO_3	CaO	MnO	LOI
KAO	46.44	38.80	0.03	0.52	<0.08	<0.33	0.69	---	---	---	15.35
NC	56.60	23.61	1.10	9.41	3.94	1.41	1.95	1.11	0.53	0.35	3.40
FA	52.96	43.60	0.14	0.41	0.33	0.33	1.30	0.45	0.48	---	8.65

The similar chemical composition of the raw materials and some volcanic rocks from which zeolites form has prompted several research groups to test the potential for zeolite synthesis from clay minerals like KAO and industrial solid wastes like FA. However, the chemical composition of NC also justifies its use as starting material for the synthesis of zeolites. The $Si0_2$/ Al_2O_3 ratios of the starting materials used in this study are suitable for the synthesis of low-Si zeolites, which have a high ion exchange capacity, a high selectivity for polar molecules and a large pore volume, having important industrial applications, particularly as sorbents for removal of heavy metals and ammonium from contaminated wastewaters.

4.1. Raw kaolinite

4.1.1. Introduction

KAO is a white non-swelling clay which has been formed typically by intense weathering which has leached the source rocks leaving predominantly relatively pure white KAO. Its structure can be depicted as SiO_4 tetrahedral sheets joined to $Al(O,OH)_6$ octahedral sheets through shared oxygens, as shown in Figure 4.1. In nature these plates occur in stacks or 'books' that exhibit varying degrees of stacking regularity. Because an individual KAO particle has an oxygen surface on one side and a hydroxyl surface on the other, it is strongly hydrogen bonded to the plates above and below it. It is a very important raw material having widespread applications, such as ceramics, manufacture of paper, ink and paints, as additive in the production of rubber and polymers and as adsorbent in the retention of radionuclides and heavy metals.

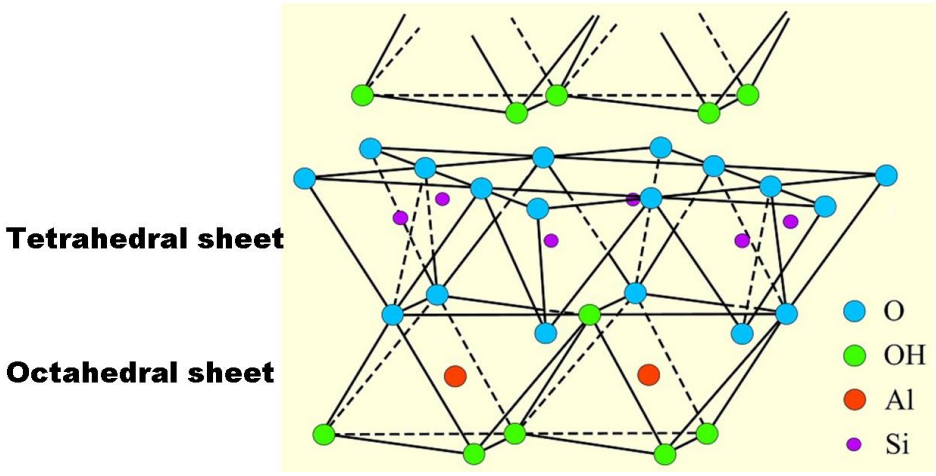

Figure 4.1. Diagrammatic sketch of the KAO structure (modified after Grim, 1968).

4.1.2. Chemical and mineralogical analyses

As shown in the XRD pattern (Figure 4.2), KAO is the predominant mineral phase, which can be identified by its characteristic XRD peaks at 12.34° and 24.64° 2θ as reported by Zhao *et al*.

(2004). However, minor impurities, such as illite, muscovite and halloysite, also occur. KAO can be recognized by its platy morphology and hexagonal outlines (Figure 4.2), with small well-formed hexagonal plates loosely packed, defining an orientation. The chemical composition of KAO used in this study is listed in Table 4.1.

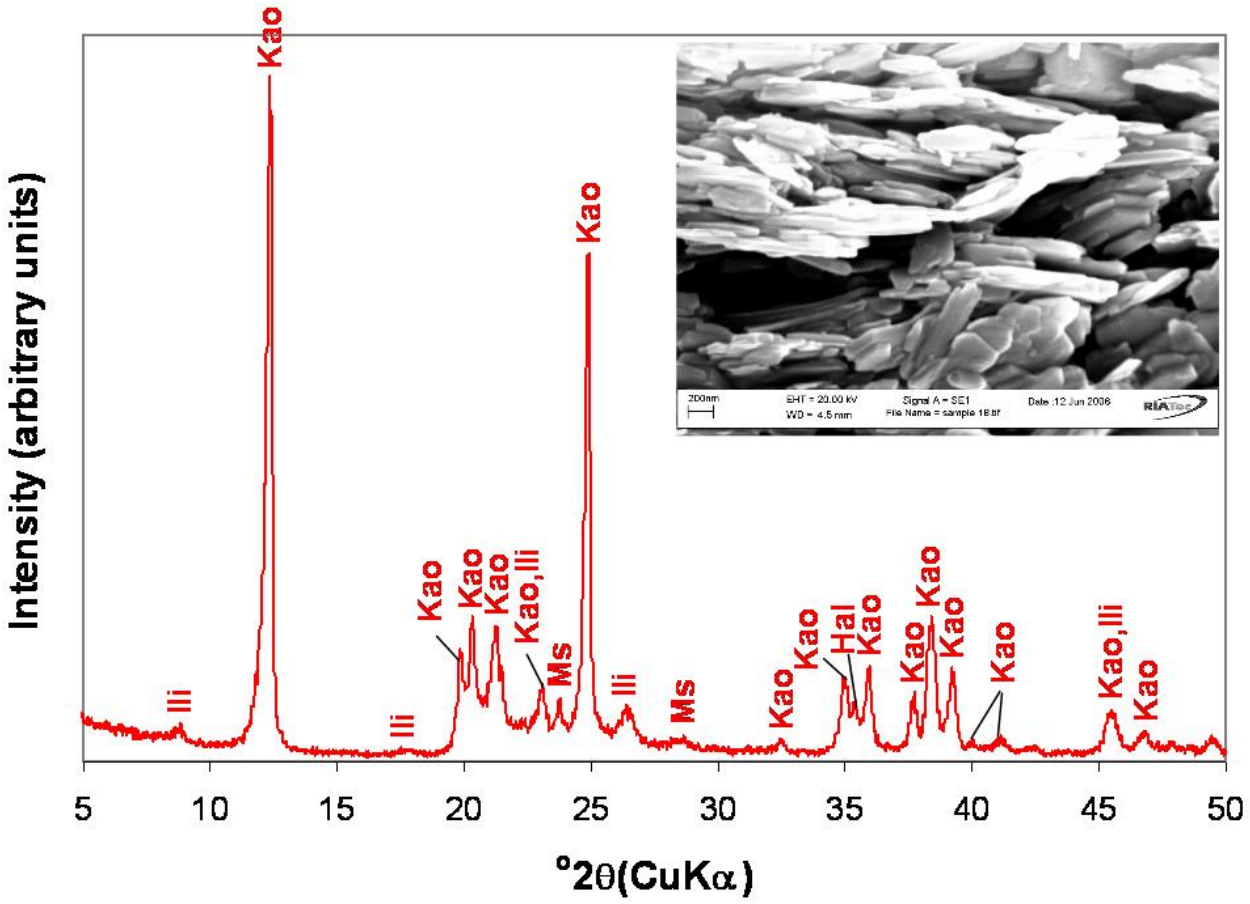

Figure 4.2. XRD pattern of KAO and its SEM image. Kao, Kaolinite; Ili, illite; Ms, muscovite; Hal, halloysite.

4.1.3. Dehydroxylation of kaolinite

It is well known that the improvement of the properties of KAO by chemical methods is difficult due to its low reactivity. Although the thermal transformation of KAO has been investigated for many years, controversy about the process of dehydroxylation (elimination of the OH groups

from the KAO structure) remains. The thermal decomposition of KAO is illustrated in the TG and its first derivative (DTG) curves on Figure 4.3 and can be summarized by a sequence of reactions.

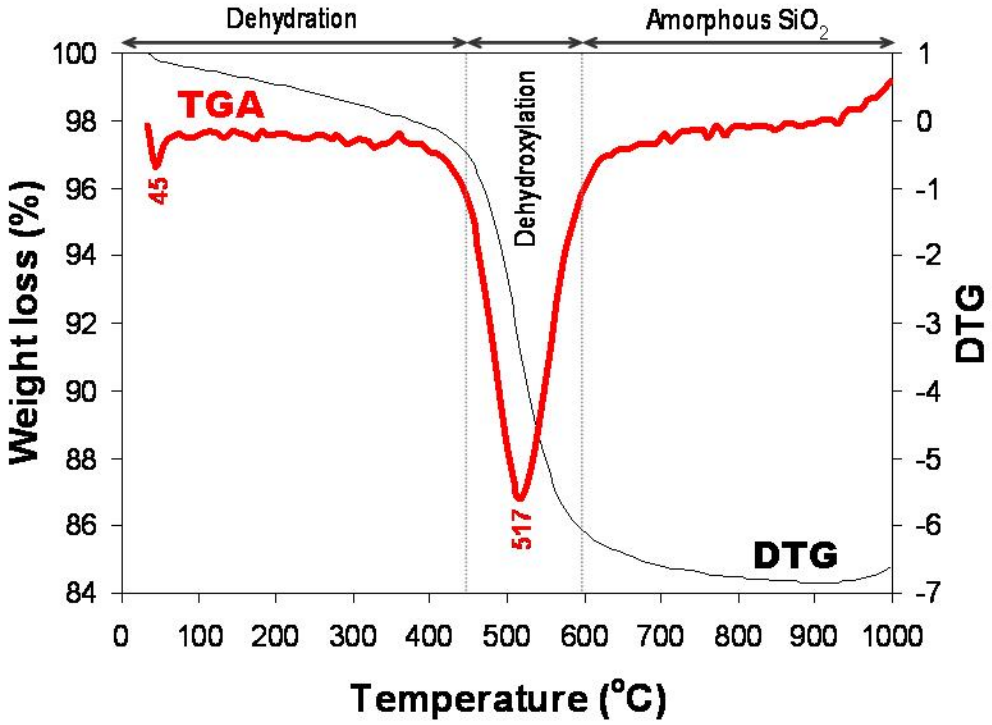

Figure 4.3. TG/DTG curves between 25-1000ºC for KAO.

At < 100 ºC, low temperature release of absorbed water in pores, on the surfaces, etc (water desorption), which depends on the nature of the KAO and the degree of disorder of stacking (Frost *et al*., 2003). Between ~100–400 °C, a weight loss that can be correlated with a pre-dehydration process takes place as a result of the reorganization in the octahedral layer, first occurring at the OH of the surface (Balek and Murat, 1996). After dehydration, KAO goes through a pre-dehydroxylation state (Frost *et al*., 2003).

According to Kakali *et al*. (2001), between ~400–650 °C, the KAO dehydroxylation occurs, with the transformation to a non-crystalline phase, metakaolinite (MTK). On the other hand, Frost *et al*. (2003) considered that this process occurred between 450-550 ºC. However, in this study a

dehydroxylation process occurring between 450-600 °C is suggested, which indicates that the starting temperature of dehydroxylation (at 450 °C) is higher than that reported by Kakali *et al*. (2001) and the finishing temperature of this process (at 600 °C) is higher and lower than those reported by Frost *et al*. (2003) and Kakali *et al*. (2001), respectively, which indicates a more perfect structure of KAO. The following reaction may be envisaged:

$$Al_2Si_2O_5(OH)_{4\ (KAO)} \rightarrow Al_2Si_2O_{7\ (MTK)} + 2H_2O \qquad (4.1)$$

A progressive decomposition of KAO occurs up to 900 °C. An exothermic peak at ~1000 °C reveals the breakdown of the MTK structure and the formation of mullite by the following reaction:

$$3Al_2Si_2O_{7\ (MTK)} \rightarrow Si_2Al_6O_{13\ (mullite)} + 4SiO_{2\ (crystalline)} \qquad (4.2)$$

The exothermic peak observed at ~1000 °C can be also attributed to the formation of Si-Al spinel with mullite-like composition, as reported by Chakravorty and Ghosh (1991).

Breck (1974) consider the decomposition of MTK and the formation of mullite as the result of two stages according to the reactions:

$$2Al_2Si_2O_{7\ (MTK)} \rightarrow Si_3Al_4O_{12\ (spinel)} + SiO_{2\ (amorphous)} \qquad (4.3)$$

$$Si_3Al_4O_{12\ (spinel)} \rightarrow 2Si_2Al_6O_{13\ (mullite)} + 5SiO_{2\ (cristobalite)} \qquad (4.4)$$

According to several researchers (e.g. Breck, 1974; Kakali *et al*., 2001), reaction (4.3) occurs in the temperature range of 900-950 °C and indicates that MTK decomposes into non-equilibrium spinel-type phases with the liberation of amorphous silica, whereas reaction (4.4) proceeds between 1000-1100 °C and explains the transformation of spinel into mullite and cristobalite.

4.1.4. Characterization of the unreacted and thermally treated kaolinite

XRD patterns of the untreated and thermally treated KAO at 600, 950 and 1000 °C are shown in Figure 4.4. MTK is characterized by the disappearance of all the XRD peaks of KAO, accompanied by the appearance of an amorphous aluminosilicate (see the broad hump at 2θ = 13-33°, having a maximum at 2θ = ~22°), which persists between 600 (MTK600) and 950 °C

(MTK950). The best conditions for obtaining a very reactive MTK have been discussed by several authors, who reported values between 600-800 °C (Lussier, 1991; Murat *et al*., 1992; Akolekar *et al*., 1997; Perissinotto *et a*l., 1997; Chandrasekhar and Pramada, 1999; Demortier *et al*. 1999; Xu *et al*., 1999).

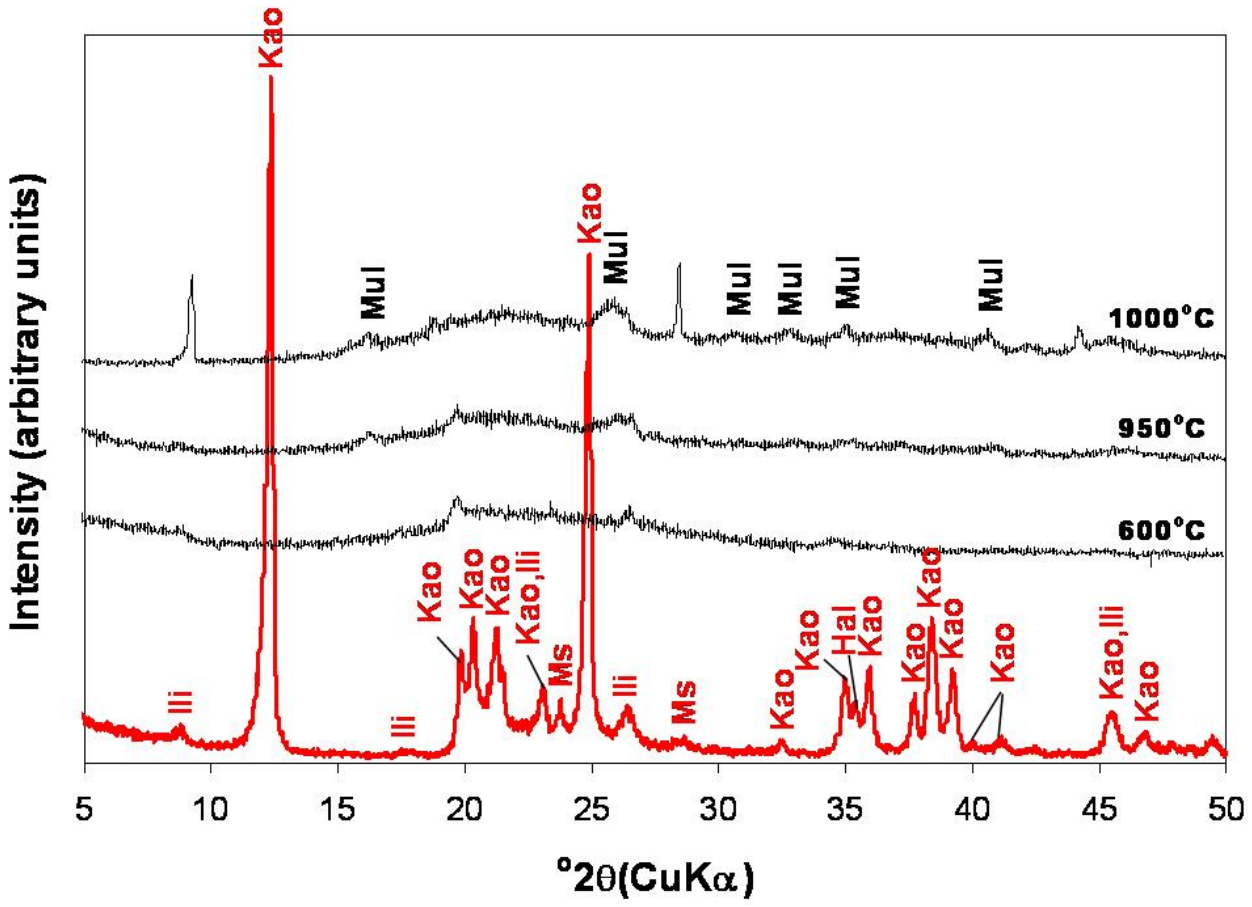

Figure 4.4. XRD patterns of uncalcined (in red) and calcined KAO at different temperatures. Ili, illite; Kao, Kaolinite; Ms, muscovite; Hal, halloysite; Mul, mullite.

Therefore, MTK600 was used as starting material in zeolite synthesis. However, MTK contains mullite as the main crystalline phase at 1000 °C (MTK1000). Similar results have reported by Mackenzie (1970) for calcination at higher temperatures, which leads to the formation of mullite and cristobalite.

After the decomposition of KAO, the higher-order reflections of this mineral lost their intensity and merged into the XRD background, as shown by MTK600, MTK950 and MTK1000, which led to the opinion that MTK can be amorphous, although actually a conception of the short-range order crystalline structure of MTK predominates (Brindley and Nakahira, 1959a, b; Chen and Tuan, 2002; Lee *et al*., 2003). The first attempt to compile a crystallographic model of MTK was made by Brindley and Nakahira (1959a, b). Therefore, the activation of KAO produces structural changes of this mineral, promoting its reactivity during zeolite synthesis.

Figure 4.5 illustrates the FT-IR spectra over the range 400–4000 cm^{-1}, corresponding to the transformation of KAO to MTK. The bands at 3692 and 3619 cm^{-1} have been assigned to the stretching vibration of hydroxyl groups in the KAO structure (Liu *et al*., 2001; Saikia *et al*., 2003; Zhao *et al*., 2004; Alkan *et al*., 2005) which are not present in the MTK spectra. However, the bands at 3669 and 3652 cm cm^{-1} reported by Zhao *et al*. (2004) and Hoch and Bandara (2005) were not observed. According to Kristof *et al*. (1993), the band at 3692 cm^{-1} represents the stretching vibration modes of 'inner surface hydroxyls' that are located at the surface of octahedral sheets opposite to the tetrahedral oxygens of the adjacent KAO layer, whereas the band at 3619 cm^{-1} is related to the stretching vibration modes of 'Inner hydroxyls' and refer to OH groups located in the plane common to octahedral and tetrahedral sheets. The band at 1119 cm^{-1} is referred to Si-O stretching vibrations, while the bands at 1034 and 1012 cm^{-1} are rather caused by Si-O-Si and Si-O-Al lattice vibrations (van der Marel and Beutelspacher, 1976). The OH bending vibrations at 942 and 916 cm^{-1} can be referred to the 'surface OH bending' and 'inner OH bending' (Frost *et al*., 2002). According to Marel and Beutelspacher (1976), these bands are mainly caused by Al-OH groups. Further, bands in low range of frequency (762, 696 and 539 cm^{-1}) can be largely attributed to different Si-O and Al-O vibrations; the first two of them can be attributed to the distortion of the tetrahedral and octahedral layers (Hoch and Bandara, 2005). The conversion of KAO to MTK is revealed by the disappearance of these characteristic bands. These changes are similar to those reported in other studies (Akolekar *et al*., 1997; Zhao *et al*., 2004; Covarruvias *et al*., 2006). The characteristic bands observed in the MTK were 1049, 802, 642, 571 and 434 cm^{-1}, with three broad bands centred at 1049, 802 and 434 cm^{-1}. A significant shift of the Si-O vibration bands at 1034 and 1012 cm^{-1} in KAO to a higher frequency band at 1049 cm^{-1} in MTK was observed, which has been assigned to amorphous SiO_2, as reported by some authors (Sinha *et al*., 1995; Valcke *et al*., 1997; Qiu *et al*., 2004). The stretching vibration of Al $(O,OH)_6$ octahedra in the KAO (Lambert *et al*., 1989) is observed at 539 cm^{-1}, but is substituted by a peak at 802 cm^{-1} corresponding to the vibration band of AlO_4 tetrahedron in MTK; these peaks indicate the formation of the disordered MTK phase. The

splitting of the 802 cm^{-1} band into two separate modes at 784 and 811 cm^{-1} with increasing temperature, which can be attributed to the formation of mullite from Al–Si-spinel. These FT-IR results are in good agreement with those obtained from the XRD data.

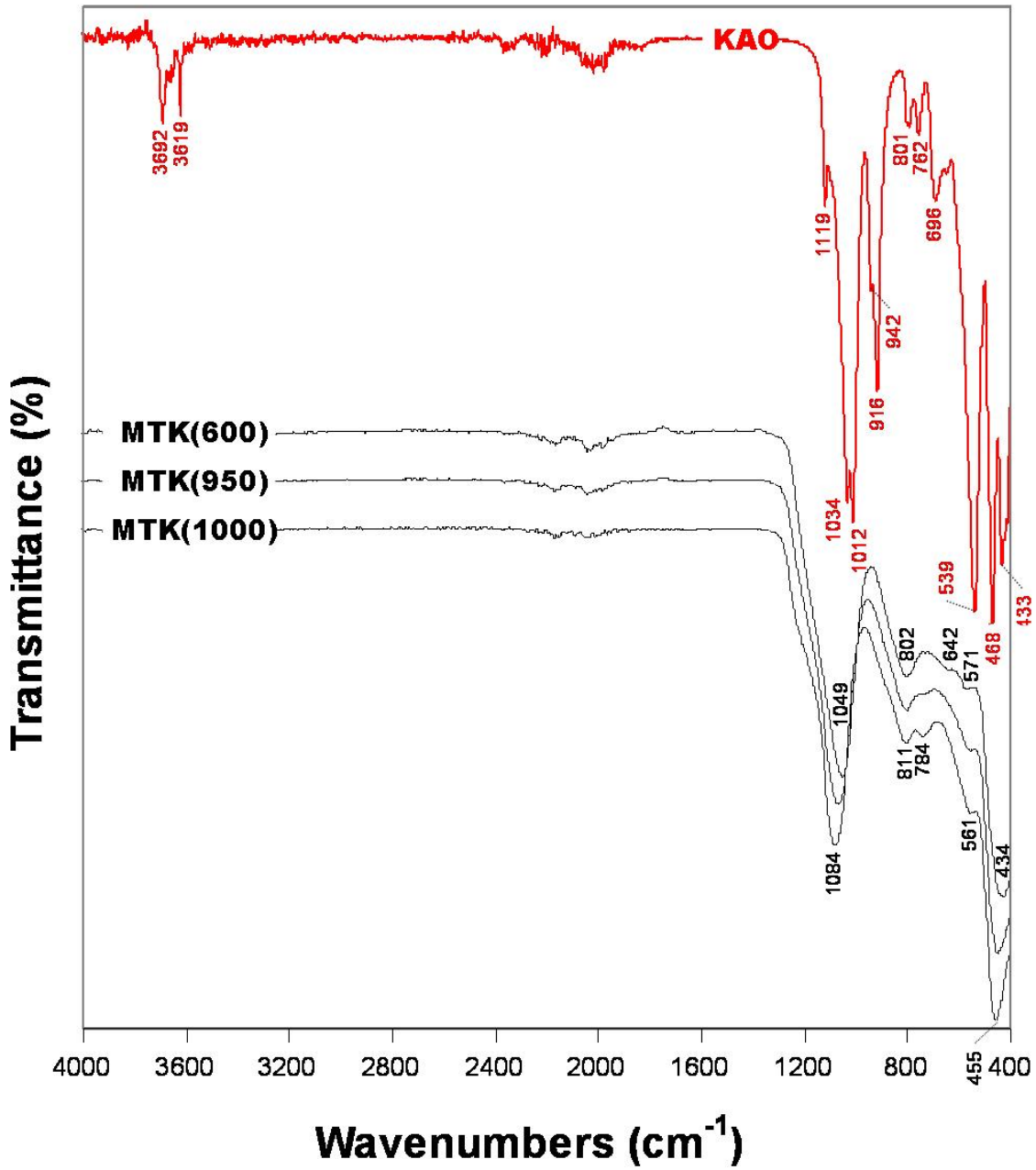

Figure 4.5. FT-IR spectra of KAO (in red) and MTK (black) obtained after calcination of KAO at 600, 950 and 1000 ^{o}C.

KAO is a hydrous layer silicate clay mineral and its structural unit of KAO consists of a Si-O tetrahedral sheet and an Al-O(OH) octahedral sheet. The ^{29}Si and ^{27}Al MAS NMR spectra of KAO and its calcined product are given in Figure 4.6.

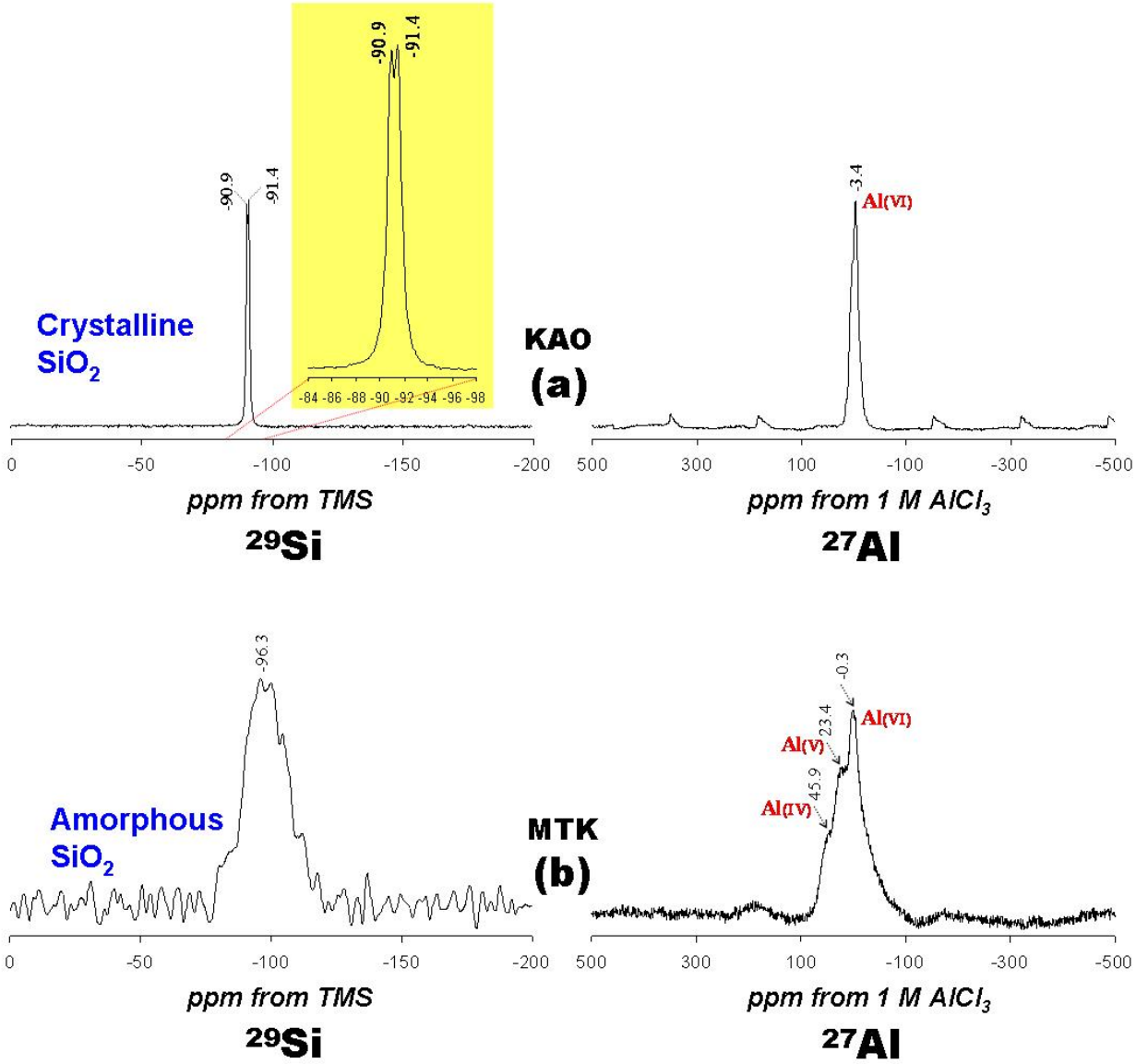

Figure 4.6. ^{29}Si and ^{27}Al MAS NMR spectra of (a) KAO and (b) MTK.

The ^{29}Si MAS NMR spectrum of KAO is given in Figure 4.6a. It displays two well resolved signals at -90.9 and -91.4 ppm (see detail in yellow rectangle in Figure 4.6a) attributed to the existence

of two different but equally populated silicon sites. The observation of these different ^{29}Si NMR signals for KAO was reported previously (e.g. Barron *et a*l., 1983; Thompson and Barron, 1987; Hayashi *et al*., 1992; Letaief *et al*., 2006). It was proposed that interlayer hydrogen bonding resulting in two different silicon environments is the main reason for the ^{29}Si NMR signal splitting in KAO (Thompson and Barron, 1987). The ^{29}Si MAS NMR spectrum of MTK (Figure 4.6b) displays a broad signal around -96.3 ppm, indicating the heterogeneity of the calcined KAO, with Si linked to four other Si atoms in silica polymorphs (Smith and Blackwell, 1983), and the presence of amorphous silica (Rocha and Klinowski, 1990). Previous studies have examined these signals in detail (Madani *et al*., 1990; Palomo *et al*., 2004). According to Mackenzie *et al*. (1985), when KAO is dehydroxylated, the Si atoms undergo a range of environments of different distortion and the broadness of the MTK line is attributed to these variations in the Si-O-Si(Al) bond angles. The ^{27}Al MAS NMR spectrum of KAO (Figure 4.6a) consists of a single resonance at -3.4 ppm that is assigned to 6-coordinated Al. The dehydroxylation of KAO brings about major changes, especially in the octahedral Al–O layers which are most closely associated with the structural hydroxyl groups (Mackenzie *et al*., 1985). This is graphically illustrated by the change in the ^{27}Al MAS NMR spectrum from a sharp octahedral Al–O resonance in KAO to a spectrum containing broad overlapping resonances at -0.3, 23.4 and 45.9 ppm (Figure 4.6b) that can be attributed to 6-, 5- and 4-coordinated Al local environments, in agreement with triple-quantum ^{27}Al MAS NMR data reported by Rocha (1999), although different compared with those reported by several authors (Rocha and Klinowski, 1990; Guo *et al*., 1997; Liu *et al*., 2001). The broader and asymmetrical peak shapes of MTK show its disordered structure (Liu *et al*., 2001). The results from MAS NMR are consistent with those from XRD and FT-IR analysis.

4.2. Raw natural clinker

4.2.1. Geological setting

NC outcrops cover extensive areas of sedimentary basins and represent natural burning of tens of billions of tones of coal throughout the past few million years. The degree of thermal alteration produced by burning coal beds is variable and a single outcrop may contain altered rock ranging from slightly baked (NC) to entirely fused (paralava) (Heffern, 2006). According to Heffern (2006), rock types in the NC reflect the rock types in the overburden and have varying degrees

of hardness, depending on the degree of heating. For instances, baked sandstone retains its grain structure but hardens to a brick-like texture, while baked shale layers may weld together to form a ceramic rock called porcellanite. Paralava forms where rocks were heated enough to melt. Candela and Quintero (2004) carried out the first detailed geologic cartography of NC in all the area of the mining concession of the Cerrejón coal site (Colombia), the world's largest export open pit coal mining operation, which in addition included its modelling and structural control in depth. A typical outcrop of NC interlayered within different coal seams is illustrated in Figure 4.7.

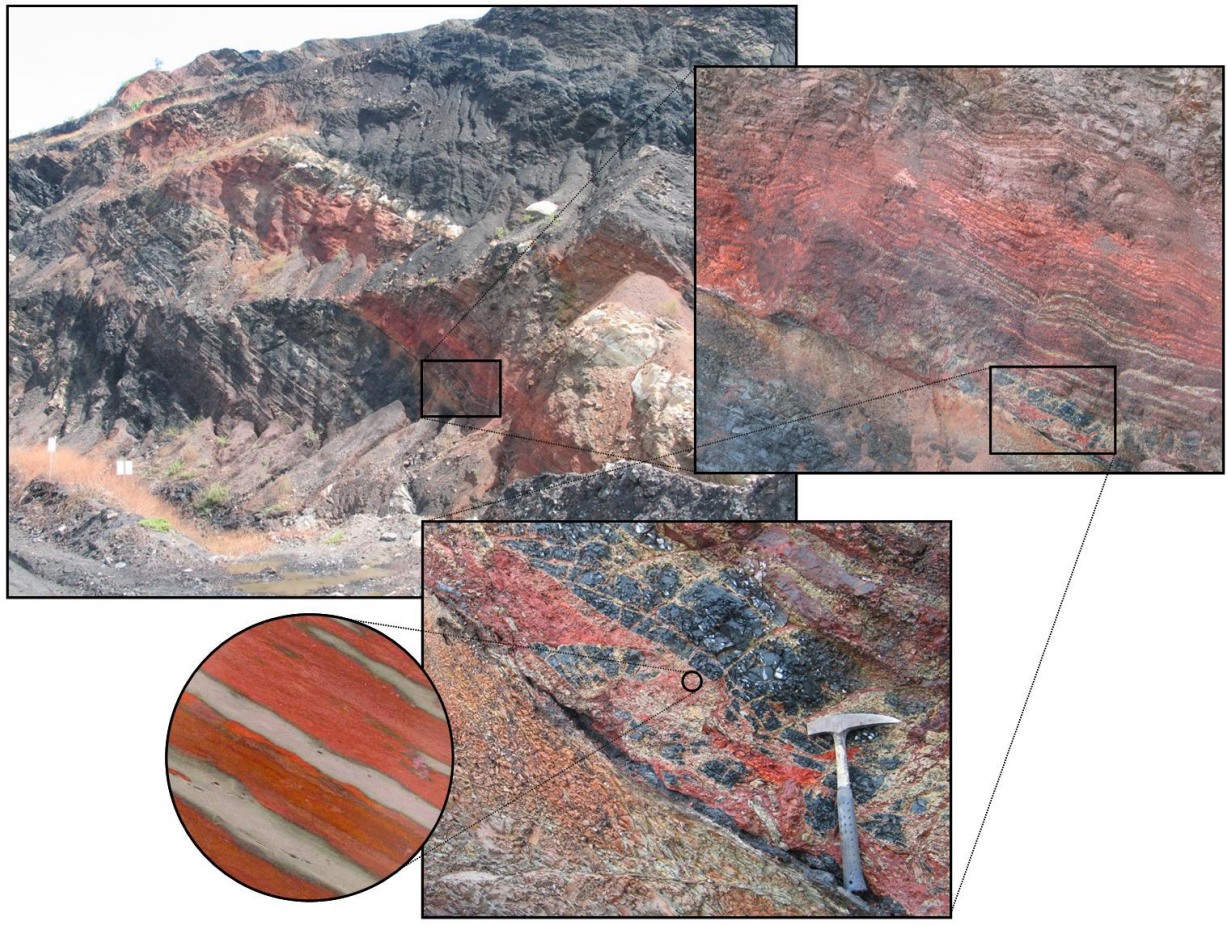

Figure 4.7. Geological aspects of the NC occurring at the Cerrejón coal deposit, La Guajira (Colombia) (courtesy of J.A. Quintero).

NC is characterized to be a very fine-grained, compact and highly fractured rock, mainly reddish brown to red in colour, due to the presence of hematite. However, it can exhibit various shades

of yellow, green, red, purple, black, grey and white, depending on the composition, texture and other characteristics of the original sediment and degree of oxidation or reduction achieved during burning. It is essentially a complex mixture of various amorphous and crystalline inorganic constituents and contains remaining inorganic materials derived from claystones originally associated with the coal. On the left side of Figure 4.7 is shown a photograph of a hand-specimen of NC used as raw material in zeolite synthesis with a 'tigerstripe' appearance in colour, from reddish-brown and red colour, due to the presence of hematite to grey colour (non-thermally affected rock, corresponding to the original protolith). Relict bedding is generally preserved, although local heating and melting may obscure or totally obliterate original structures.

4.2.2. Chemical and mineralogical analyses

The mineral phases in NC are dependent on many physical and chemical variables including the original sediment bulk composition, temperature, degree of melting, and degree of oxidation or reduction achieved during burning (Cosca *et al*., 1989). The XRD pattern of the unreacted NC (Figure 4.8) shows that the major crystalline phases are quartz, hematite and muscovite. However, it represents a geomaterial with a complex mineralogy, with overlapping of peaks corresponding to different mineral phases, which makes it difficult to perform quantitative analysis by conventional XRD analysis. Recently, Henao *et al*. (2005), using XRD data recorded from the raw NC used in this work, established the mineralogy and crystal structure of the mineral phases and the final model was refined by the Rietveld method. According to them, NC is mainly composed by quartz and hematite, with traces of muscovite, anatase, illite, kaolinite, montmorillonite and spinel group phases. NC can be considered as an aluminosilicate and therefore can be used like other geomaterials in zeolite synthesis, which is very versatile since the glassy phase both reacts and also goes into solution before the crystalline phase. The SEM image (Figure 4.8) reveals that NC consists of irregular particles of various sizes, showing a blocky-like shape. The elemental composition of NC calculated from the quantitative analysis of the EDX spectra and expressed as weight percentages is shown in Table 4.1. It is different (low SiO_2/Al_2O_3 ratio and Fe_2O_3 and CaO contents) to that reported by Cosca *et al*. (1989) at the Powder River Basin, Wyoming (USA), where NC displays variations of up to 15 wt% among its major oxides (SiO_2, Al_2O_3, K_2O and CaO). This probably reflects local heterogeneity related to small changes in the original sedimentary rock.

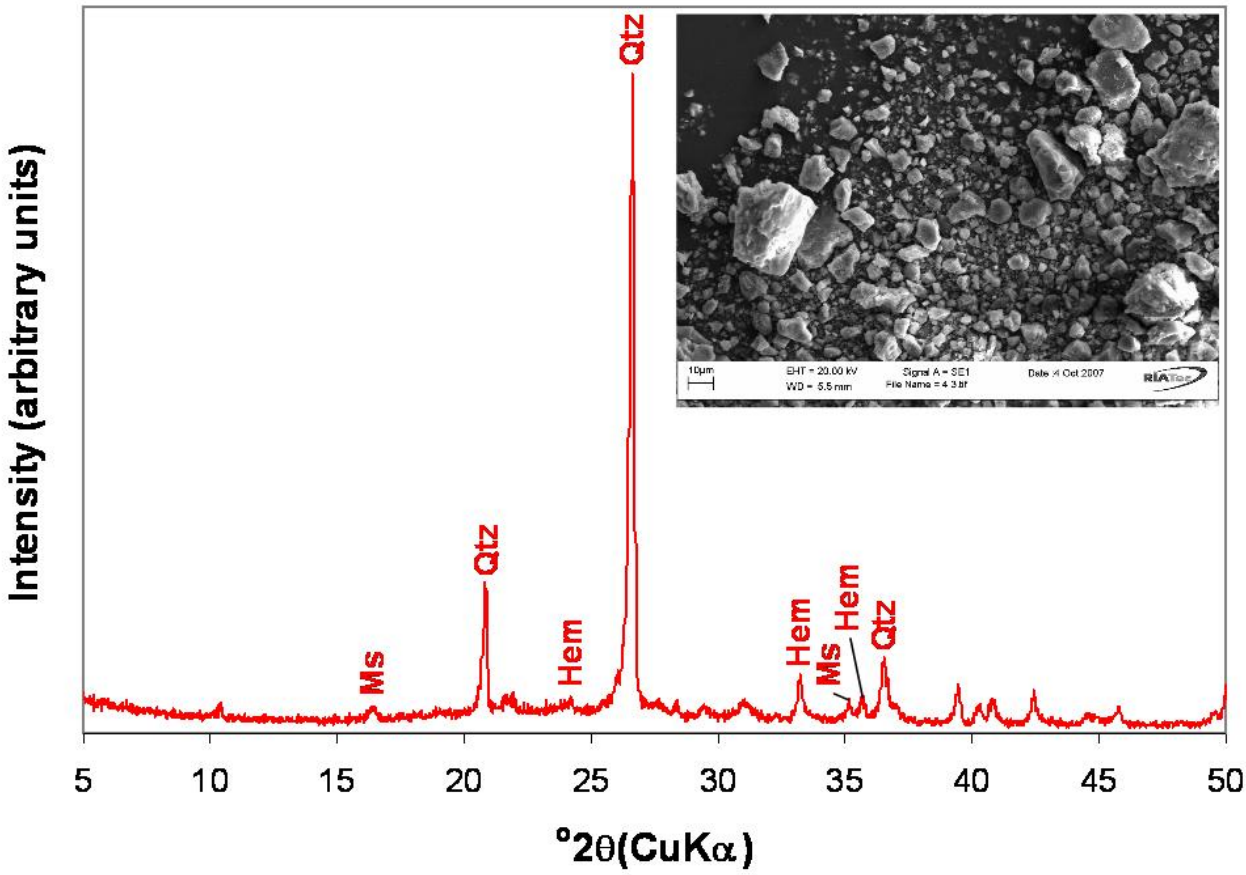

Figure 4.8. XRD pattern of NC and its SEM image. Qtz, quartz; Hem, hematite; Ms, muscovite.

NC contains very high contents of SiO_2 and Al_2O_3, with a SiO_2/Al_2O_3 ratio = 2.4, comparable to ratios of 2.05-2.28 reported by Gitari *et al*. (2003) in FA, and appropriate for the synthesis of low-Si zeolitic materials with high crystallinity and CEC. However, Rayalu *et al*. (2000) reports that if this ratio is > 1.5, the formation of faujasite as zeolitic product is favoured. The SiO_2/Al_2O_3 ratio was determined in order to predict the success in the process of zeolite synthesis, although it is also important to consider the occurrence of impurities in the starting material. NC shows very low contents of Ca and S, and a high content of Fe associated with the presence of hematite. This is very important taking into account that Fe-bearing minerals, mainly hematite, can show an inert behaviour and Ca-bearing phases can act as a zeolite synthesis inhibitors through the formation of C-S-H phases (Juan *et al*., 2007).

The FT-IR spectrum for NC (Figure 4.9a) shows the three wide bands characteristic of aluminosilicates: the band at 447 cm^{-1} is associated with T–O bending vibrations; the bands appearing at 700, 781 and 798 cm^{-1} are associated with T–O (T = Al, Si) symmetric stretching

vibrations and correspond to quartz. The band appearing at 1061 cm^{-1} is associated with T–O (T = Al, Si) asymmetric stretching vibrations. Figure 4.9b shows the ^{29}Si and ^{27}Al MAS NMR spectra of NC. The most intense peak in the ^{29}Si MAS NMR spectrum of NC centred at -107.6 ppm can be assigned to highly polymerized Q^4 Si sites [Si(4Si)] and attributed to quartz. The ^{27}Al MAS NMR spectrum of NC consists of a single resonance at 50.3 ppm and is largely tetrahedral Al. The intense spinning sidebands result from a relatively high level of paramagnetic impurities in NC. The intensity in the sidebands at the edges of the ^{29}Si and ^{27}Al MAS NMR spectra corresponding to NC confirms the occurrence of some paramagnetic impurities (hematite), which provide it with a high-intensity thermoremanent magnetization that appears to faithfully record the ambient geomagnetic field, allowing mapping of burn zones and tracing of magnetic reversals in ancient burns (Jones *et al*., 1984). A similar behaviour of the ^{29}Si and ^{27}Al MAS NMR has been observed for FA due to the occurrence of Fe-bearing phases as described in the next section. Figure 4.9c illustrates the TG and its first derivative (DTG) curves for NC, with a weight loss (LOI, loss of ignition = 3.40%); a first dehydration step at 39 ^{o}C associated with surface water; and a weight loss between 100-400 °C, which can be related to decomposition of Fe-bearing phases or relict organic matter. However, it is probable that the maximum weight loss occurred at >700 ^{o}C, which is relatively higher than that for KAO and FA, taking into account that NC had already been associated with the coal combustion process. This is similar to evidence reported by Chou *et al*. (2006), where most weakly bonded, highly volatile organic materials present in FA have either been burned off or converted to tightly bonded organic materials. These were retained in the ash particles and then released at a higher temperature during heating.

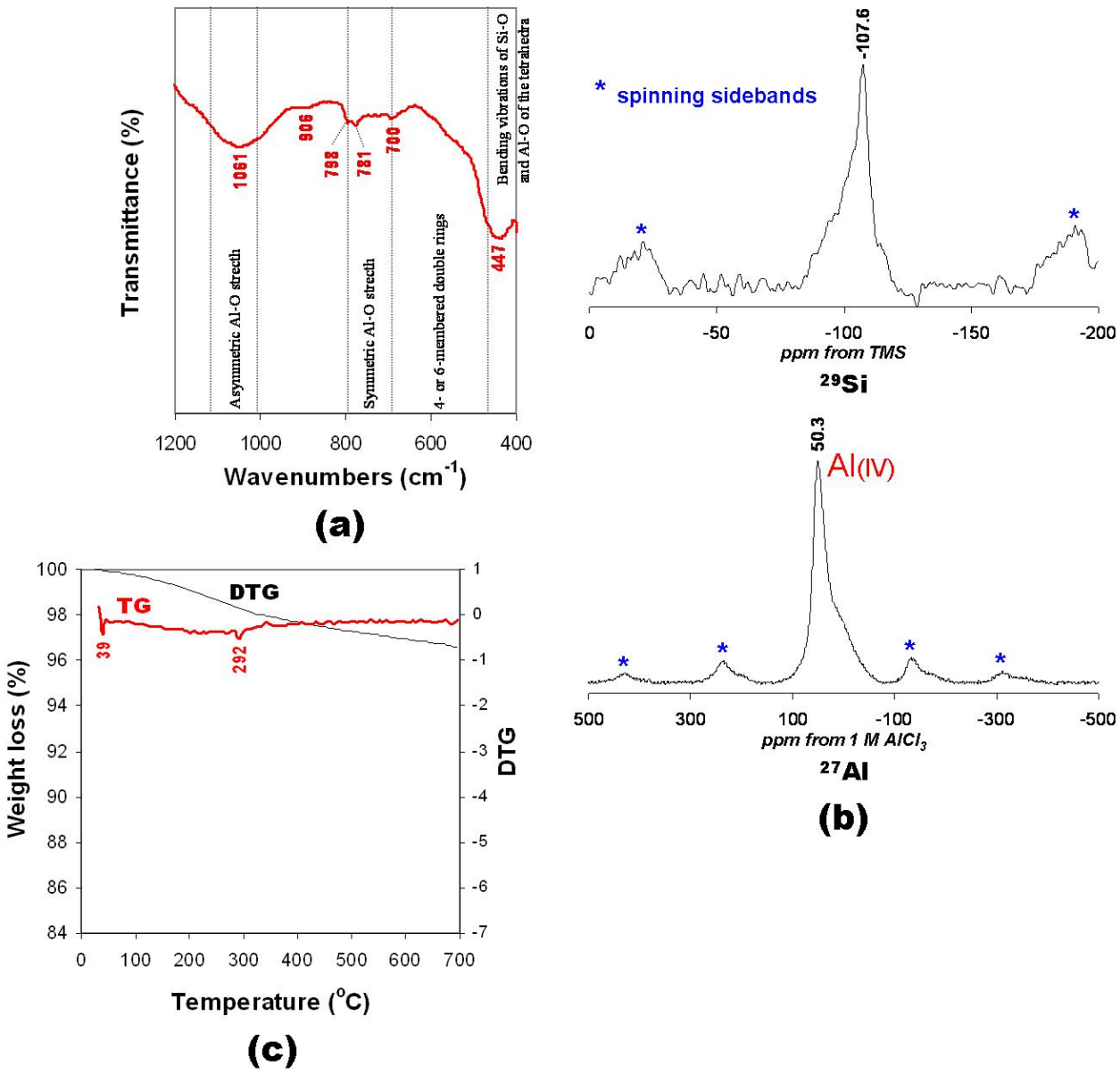

Figure 4.9. (a) FT-IR spectrum, (b) ^{29}Si and ^{27}Al MAS NMR spectra and (c) TG/DTG curves between 25-700 °C for NC.

4.3. Raw fly ash

4.3.1. Industrial context

FA can be defined as a finely divided and predominantly inorganic residue resulting from the combustion of coal in electricity generating plants. Since the particles solidify while suspended in the exhaust gases, FA particles are generally spherical in shape and range in size from 0.5 to 100 μm. They consist mostly of SiO_2, Al_2O_3 and Fe_2O_3. When processed to the correct surface area (particle size), they can be also pozzolanic in nature and react with $Ca(OH)_2$ and alkali to form C-S-H phases. Chemical composition has an important influence both on the potential application of FA and on the environmental impact of its subsequent use (Juan *et al*., 2007). Although FA does not exhibit hazardous characteristics, specially designed landfills are required to prevent the possible leaching of trace elements from this waste material that can reach drinking water sources (Maroto-Valer *et al*., 1999). Worldwide, the cement industry has almost reached its maximum consumption level of FA, so too its use as landfill. Rugeley Power Station in the West Midlands (England) aims to extend the market for this waste solid material and is committed to the generation of low cost electricity in a safe and environmentally-responsible manner.

4.3.2. Chemical and mineralogical analyses

Figure 4.10 shows the XRD pattern of the raw FA, which mainly consists of an amorphous phase giving rise to the broad hump in the 2θ range of 20-35°. There are a few weak peaks indicating the occurrence of quartz (SiO_2) and mullite ($Al_6Si_2O_{13}$) as crystalline phases, with the first one from melting and the second one formed at high temperature during coal combustion. The SEM image (Figure 4.10) reveals the typical morphology of the FA particles.

FAs are classified globally into two chemical types (Class F and Class C) for their industrial application. The elemental composition of FA used in this study is shown in Table 4.1, being similar to that reported from a wide range of European FAs (Singh and Kolay, 2002; Petrik *et al*., 2003; Moreno *et al*., 2005; Somerset *et al*., 2005a, b, c; Wingenfelder *et al*., 2005; Brindle and McCarthy, 2006; Gitari *et al*., 2006; Juan *et al*., 2007). The raw FA has $\geq$70%

SiO_2+Al_2O_3+Fe_2O_3, with a SiO_2/Al_2O_3 ratio = 1.2, and very low contents of major impurities, such as Fe, Ca and S. Therefore, it can be classified as a low-calcium Class F FA (Vassilev and Vassileva, 2007) or as a Sialic FA type (Roy and Griffin, 1982; Vassilev and Vassileva, 2007). According to Vassilev and Vassileva (2007), it is generally produced from the burning of highest-rank bituminous coals and anthracites, and, to a lesser extent, sub-bituminous coals, which are highly enriched in detrital mineralization; this FA is pozzolanic in nature (hardening when reacted with $Ca(OH)_2$ and water). The properties and chemical composition of FA vary according to coal source and power plant operation, which makes this waste solid material even more versatile.

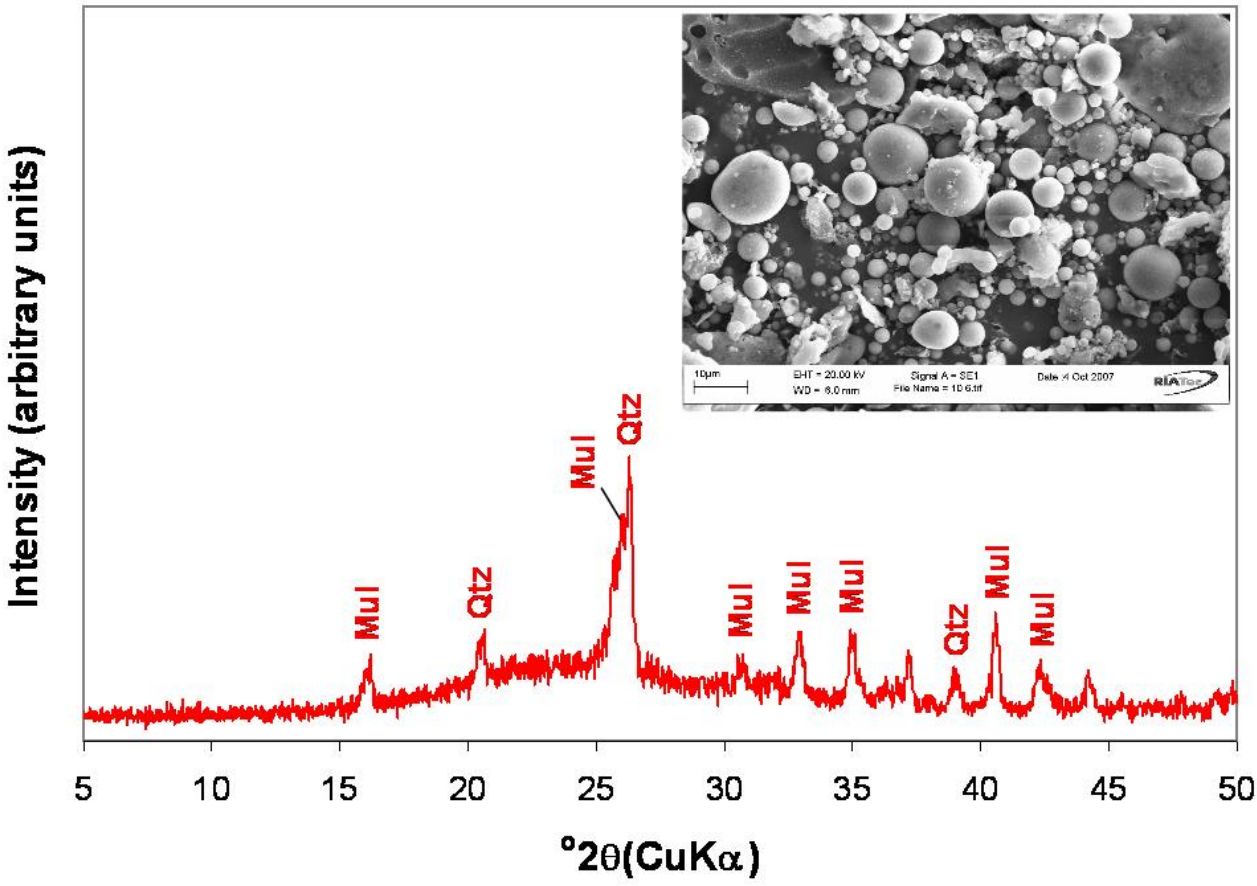

Figure 4.10. XRD pattern of FA and its SEM image. Qtz, quartz; Mul, mullite.

Recent studies have focused on determining the suitability of FA in the synthesis of zeolites for different applications (Moreno *et al*., 2004; Brindle and McCarthy, 2006). The SiO_2/Al_2O_3 ratio is an important parameter for zeolite synthesis, and the ratio of 1.2 is appropriate for the synthesis

of low-Si zeolitic materials with high CEC. The very low contents of Fe and Ca is also important, because Fe-bearing minerals, such as magnetite can show an inert behaviour and Ca-bearing phases promote the formation of C-S-H phases (Juan *et al*., 2007). Figure 4.11 illustrates several aspects about the morphology of FA particles.

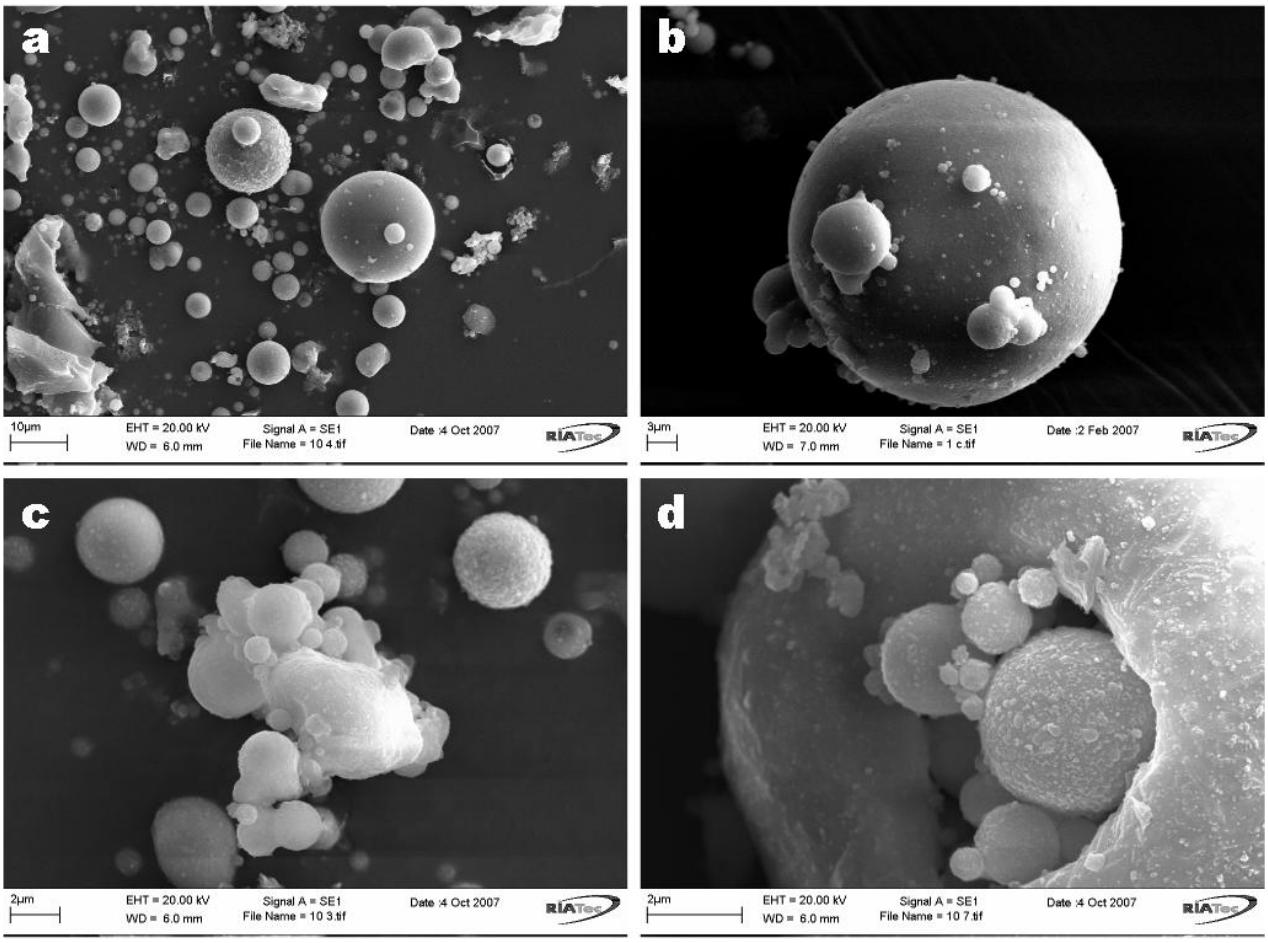

Figure 4.11. SEM images of the FA morphology. (a) Typical view of the FA particles with a predominantly spherical morphology. (b) Smaller particles attached to the surface of a larger particle serving as a substrate. (c) Hollow and empty spheres (cenospheres). (d) Hollow sphere containing smaller spheres (plerosphere).

In general, FA particles are predominantly spherical in shape with a relatively smooth surface texture (Figure 4.11a). In some cases smaller particles are attached to the surface of larger particles, serving as substrates (Figure 4.11b). The spherical particles are either solid or hollow. They are generally hollow and empty (cenospheres, Figure 4.11c), although some may contain

smaller spheres in their interiors (plerospheres, Figure 4.11d). Cenospheres show a large variation in their dimensions and are believed to be formed by the expansion of CO_2 and H_2O gas, evolved from minerals within the burning coal (Fisher *et al*., 1976). The variation in the dimensions of cenospheres depends on the conditions of the thermal plants during which the FA has been expelled (Raghavendra *et al.*, 2003). Plerospheres expose the smaller spheres as a consequence of a breaking or dissolution part of the shell of the larger sphere. However, it is probable that plerospheres were empty before being cracked, being progressively filled with smaller spheres during the FA collection process.

The FT-IR spectrum for FA (Figure 4.12a) shows the three wide bands characteristic of aluminosilicates. The peak observed at 1045 cm^{-1} is associated with T-O asymmetric stretching vibrations and may be attributed to the presence of quartz. The broadening of this peak may be due to the merging of FT-IR peaks corresponding to the other metal oxides present in FA. The bands appearing at 800 and 557 cm^{-1} can correspond to quartz and mullite, respectively, present in FA. The band at 420 cm^{-1} is associated with T-O bending vibrations. The ^{29}Si and ^{27}Al MAS NMR spectra of the original FA are shown in Figure 4.12b. The ^{29}Si MAS NMR spectrum of FA exhibits a broad resonance in the chemical shift range from −65 to −125 ppm (characteristic of amorphous or poorly crystallized materials). Such signals are generated by many slightly different environments around nominally equivalent Q^n(mAl)-type silicons, leading to a substantial number of overlapping lines with slightly different chemical shifts (Fernández-Jiménez *et al*., 2006). In this spectrum peaks detected at -79.2, -88.8, -96.2 and -108.6 ppm are attributed to the different Si environments of the FA similar to what is reported by Palomo *et al*. (2004) and Fernández-Jiménez *et al*. (2006). The peaks with chemical shifts at -88.8 and -108.6 ppm can be attributed, respectively, to a crystalline phase like mullite (Gomez and François, 2000) and to Q^4(0Al) environments in quartz (Klinowski, 1984; Engelhardt and Michel, 1987). The signal detected at -79.2 ppm is associated with the presence of less condensed, monomer and dimer species (Fernández-Jiménez *et al*., 2006). There is severe line broadening caused by a paramagnetic component in FA, which accounts for the intense spinning sidebands (between 0 and -50 and -150 and -200 ppm). The main component appears to have a Q^4 type of environment. However, it is quite difficult to detect the silicon because of this. The ^{27}Al MAS NMR spectrum of FA shows two peaks at 43.7 and -3.4 ppm. The signal at 43.7 ppm should be assigned to 4-coordinated Al in mullite, in which one oxygen atom is shared by three surrounding Al tetrahedra as proposed by Merwin *et al*. (1991), whereas the signal at -3.4 ppm corresponds to 6-coordinated Al in mullite (He *et al*., 2004). The intense sidebands result from a relatively high level of paramagnetic impurities in FA. Figure 4.12c shows the TG and its first

derivative (DTG) curves of FA, which is characterized by a weight loss between 450 and >700 °C, with the temperature for maximum weight loss occurring ~ 647 °C.

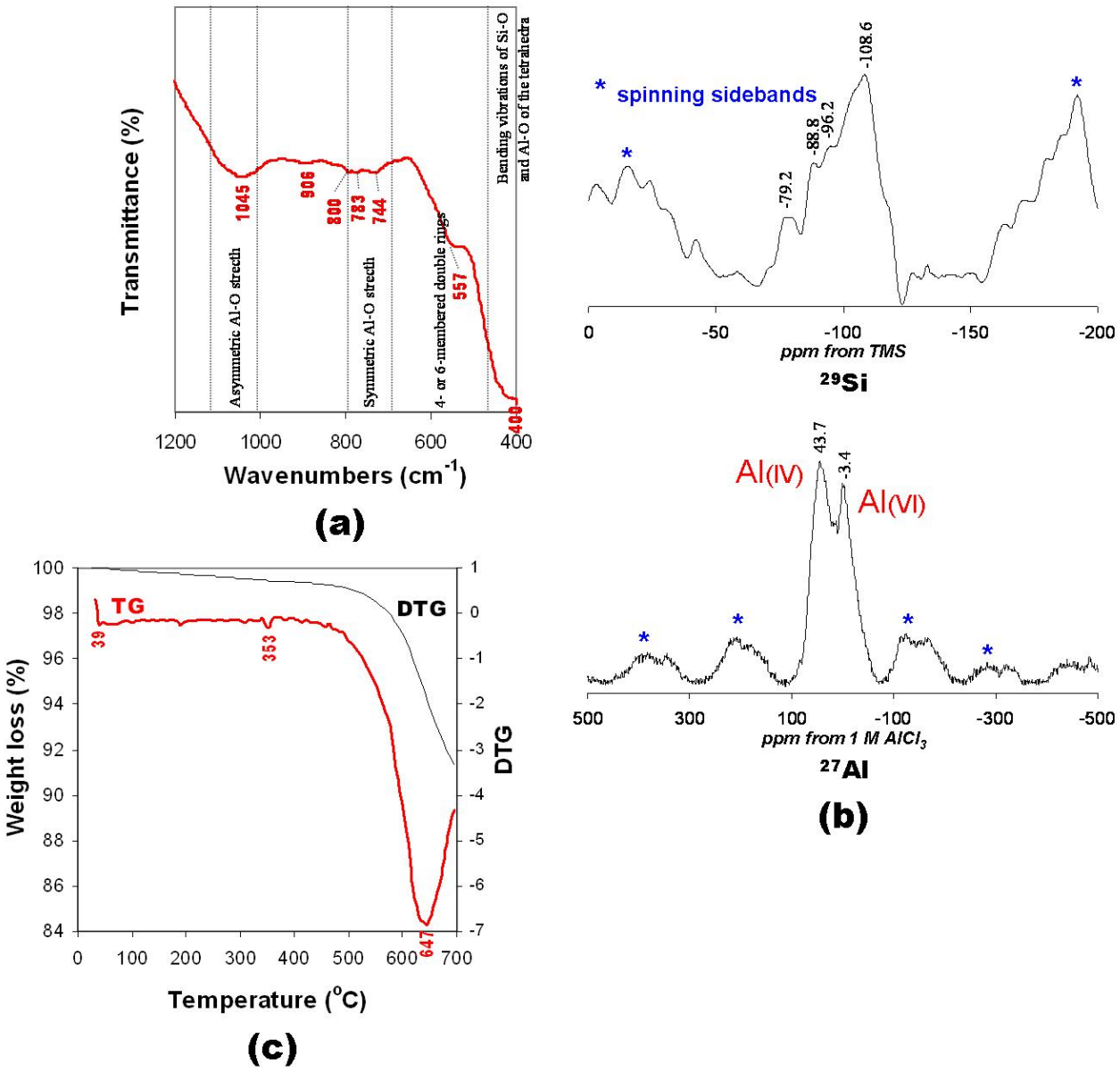

Figure 4.12. (a) FT-IR spectrum, (b) ^{29}Si and ^{27}Al MAS NMR spectra and (c) TG/DTG curves between 25-700 °C for FA.

4.4. Conclusions to Chapter 4

From the physicochemical characterization results, it can be concluded that the raw materials used in this study have properties suitable for zeolite synthesis and can be, in principle, useful sources of silica and alumina. The SiO_2/Al_2O_3 ratios of the starting materials are appropriate for the synthesis of low-Si zeolitic materials with high CEC. In addition, the very low contents of impurities, such as Fe and Ca is also important, taking into account that Fe-bearing and Ca-bearing phases can show an inert behaviour and promote the formation of C-S-H phases, respectively. Finally, considering new applications for these raw materials, their thorough characterization provided very important data useful in determining their behaviour in zeolite synthesis and remediation of polluted waters.

Chapter 5

Chapter 5. Synthesis of kaolinite-based zeolitic materials

This chapter discuss the results obtained after activation of KAO and MTK in different chemical systems. In recent years, the increasing interest in zeolite synthesis from low-cost materials, such as clays, promoted the development of various studies on their conversion into zeolitic materials, giving rise to an extensive literature.

5.1. Kaolinite as a starting material

Table 5.1 summarizes the starting reaction conditions for the conversion of KAO into zeolites according to the aqueous media (alkaline, fluoride and carbonate). Using NaOH was probably more effective during the hydrothermal conversion of KAO than KOH, and particularly when a fluoride medium was used. The main synthesis products obtained using NaOH as mineralizer include KAO-LTA, KAO-SOD, KAO-CAN, KAO-FAU, KAO-GIS, KAO-ANA and KAO-JBW. After conversion of KAO in KOH solutions, KAO-CHA, KAO-EDI and kalsilite and leucite were obtained. The hydrothermal reaction of KAO in the presence of aqueous fluoride media did not produce good results, although traces of KAO-FAU, KAO-GIS, KAO-CHA, KAO-SOD and KAO-CAN were obtained. The conversion of KAO in the system CaO-SiO_2-Al_2O_3-H_2O led to the study of KAO-HYD and KAO-TOB formation. The latter is among the first phases formed and invariably appears before KAO-TOB.

Table 5.1. Synthesis conditions for the conversion of KAO into zeolitic materials using the conventional hydrothermal synthesis.

Test	Chemical reagents									L/S	Hydrothermal reaction		Molar gel composition	Zeolitic phases and other synthesis products	Residual phases
	H_2O (g)	NaOH (g)	KOH (g)	NaF (g)	NH_4F (g)	CaO (g)	SDA (g)	SiO_2 (g)	KAO (g)	(ml/g)	T / °C	t / h			
1	18.00	0.96							3.10	6.12	100	6	$Na_2O:Al_2O_3:2SiO_2:86.3H_2O$	LTA, SOD, CAN	KAO
2	18.00	0.96							3.10	6.12	100	72	$Na_2O:Al_2O_3:2SiO_2:86.3H_2O$	LTA, SOD, CAN	KAO
3	18.00	0.96							3.10	6.12	100	120	$Na_2O:Al_2O_3:2SiO_2:86.3H_2O$	LTA, SOD, CAN	KAO
4	18.00	2.87							3.10	6.73	100	6	$3Na_2O:Al_2O_3:2SiO_2:88.3H_2O$	LTA, SOD, CAN	–
5	18.00	2.87							3.10	6.73	100	72	$3Na_2O:Al_2O_3:2SiO_2:88.3H_2O$	LTA, SOD, CAN	–
6	18.00	2.87							3.10	6.73	100	120	$3Na_2O:Al_2O_3:2SiO_2:88.3H_2O$	LTA, SOD, CAN	–
7	18.00	2.87							3.10	6.73	200	24	$3Na_2O:Al_2O_3:2SiO_2:88.3H_2O$	SOD, CAN, JBW	–
8	18.00	2.87							3.10	6.73	200	96	$3Na_2O:Al_2O_3:2SiO_2:88.3H_2O$	SOD, CAN, JBW	–
9	18.00	2.87							3.10	6.73	200	168	$3Na_2O:Al_2O_3:2SiO_2:88.3H_2O$	SOD, CAN, JBW	–
10	18.00	0.96						0.24	3.10	6.12	100	24	$Na_2O:Al_2O_3:2.3SiO_2:86.3H_2O$	LTA, FAU, GIS, SOD, CAN	KAO
11	18.00	0.96						0.24	3.10	6.12	100	48	$Na_2O:Al_2O_3:2.3SiO_2:86.3H_2O$	LTA, FAU, GIS, SOD, CAN	KAO
12	18.00	0.96						0.24	3.10	6.12	100	72	$Na_2O:Al_2O_3:2.3SiO_2:86.3H_2O$	LTA, FAU, GIS, SOD, CAN	–
13	18.00	0.96						0.24	3.10	6.12	100	96	$Na_2O:Al_2O_3:2.3SiO_2:86.3H_2O$	LTA, FAU, GIS, SOD, CAN	–
14	18.00	0.96					TPAB		3.10	6.12	100	6	$Na_2O:Al_2O_3:2SiO_2:0.5TPAB:86.3H_2O$	LTA, SOD, CAN	–
15	18.00	0.96					TPAB		3.10	6.12	100	72	$Na_2O:Al_2O_3:2SiO_2:0.5TPAB:86.3H_2O$	LTA, SOD, CAN	–
16	18.00	0.96					TPAB		3.10	6.12	100	120	$Na_2O:Al_2O_3:2SiO_2:0.5TPAB:86.3H_2O$	LTA, SOD, CAN	–
17	18.00	0.96					TEA		3.10	6.12	100	72	$Na_2O:Al_2O_3:2SiO_2:0.5TEA:86.3H_2O$	LTA, SOD, CAN	–
18	18.00	0.96					TEA		3.10	6.12	100	144	$Na_2O:Al_2O_3:2SiO_2:0.5TEA:86.3H_2O$	LTA, SOD, CAN	–
19	18.00	0.96					TEA		3.10	6.12	100	216	$Na_2O:Al_2O_3:2SiO_2:0.5TEA:86.3H_2O$	LTA, SOD, CAN	–
20	18.00	0.96					TEA		3.10	6.12	100	72	$Na_2O:Al_2O_3:2SiO_2:TEA:86.3H_2O$	LTA, SOD, CAN	–
21	18.00	0.96					TEA		3.10	6.12	100	168	$Na_2O:Al_2O_3:2SiO_2:TEA:86.3H_2O$	LTA, SOD, CAN	–
22	18.00	0.96					TEA		3.10	6.12	100	264	$Na_2O:Al_2O_3:2SiO_2:TEA:86.3H_2O$	LTA, SOD, CAN	–
23	18.00	0.96					TEDA		3.10	6.12	100	24	$Na_2O:Al_2O_3:2SiO_2:0.5TEDA:86.3H_2O$	LTA, SOD, CAN	–
24	18.00	0.96					TEDA		3.10	6.12	100	48	$Na_2O:Al_2O_3:2SiO_2:0.5TEDA:86.3H_2O$	LTA, SOD, CAN	–
25	18.00	0.96					TEDA		3.10	6.12	100	72	$Na_2O:Al_2O_3:2SiO_2:0.5TEDA:86.3H_2O$	LTA, SOD, CAN	–
26	18.00	0.96					TLAM		3.10	6.12	200	6	$Na_2O:Al_2O_3:2SiO_2:0.5TLAM:86.3H_2O$	SOD, CAN	–
27	18.00	0.96					TLAM		3.10	6.12	200	24	$Na_2O:Al_2O_3:2SiO_2:0.5TLAM:86.3H_2O$	SOD, CAN	–
28	18.00	0.96					TLAM		3.10	6.12	200	48	$Na_2O:Al_2O_3:2SiO_2:0.5TLAM:86.3H_2O$	SOD, CAN, JBW	–
29	18.00	2.87					TLAM		3.10	6.73	200	6	$3Na_2O:Al_2O_3:2SiO_2:0.5TEAM:88.3H_2O$	SOD, CAN	–
30	18.00	2.87					TLAM		3.10	6.73	200	24	$3Na_2O:Al_2O_3:2SiO_2:0.5TEAM:88.3H_2O$	SOD, CAN	–
31	18.00	2.87					TLAM		3.10	6.73	200	48	$3Na_2O:Al_2O_3:2SiO_2:0.5TEAM:88.3H_2O$	SOD, CAN, JBW	–
32	18.00			1.01					3.10	6.13	100	360	$2NaF:Al_2O_3:2SiO_2:86.6H_2O$	FAU, GIS, CHA	KAO
33	18.00			1.01					3.10	6.13	100	600	$2NaF:Al_2O_3:2SiO_2:86.6H_2O$	FAU, GIS, CHA	KAO
34	18.00			1.01					3.10	6.13	100	840	$2NaF:Al_2O_3:2SiO_2:86.6H_2O$	FAU, GIS, CHA	KAO
35	18.00				0.89		TPAB		3.10	6.09	175	120	$2NH_4F:Al_2O_3:2SiO_2:0.5TPAB:85.1H_2O$	GIS, SOD, CAN	KAO
36	18.00				0.89		TPAB		3.10	6.09	175	168	$2NH_4F:Al_2O_3:2SiO_2:0.5TPAB:85.1H_2O$	GIS, SOD, CAN	KAO
37	18.00				0.89		TPAB		3.10	6.09	175	216	$2NH_4F:Al_2O_3:2SiO_2:0.5TPAB:85.1H_2O$	GIS, SOD, CAN	KAO
38	18.00				2.66		TPAB		3.10	6.66	175	120	$6NH_4F:Al_2O_3:2SiO_2:0.5TPAB:85.4H_2O$	GIS, SOD, CAN	KAO
39	18.00				2.66		TPAB		3.10	6.66	175	216	$6NH_4F:Al_2O_3:2SiO_2:0.5TPAB:85.4H_2O$	GIS, SOD, CAN	KAO
40	18.00				2.66		TPAB		3.10	6.66	175	312	$6NH_4F:Al_2O_3:2SiO_2:0.5TPAB:85.4H_2O$	GIS, SOD, CAN	KAO
41	18.00		1.35						3.10	6.24	100	27	$K_2O:Al_2O_3:2SiO_2:86.3H_2O$	CHA	KAO
42	18.00		1.35						3.10	6.24	100	240	$K_2O:Al_2O_3:2SiO_2:86.3H_2O$	CHA	KAO
43	18.00		1.35						3.10	6.24	100	528	$K_2O:Al_2O_3:2SiO_2:86.3H_2O$	CHA	KAO
44	18.00		4.03						3.10	7.11	100	27	$3K_2O:Al_2O_3:2SiO_2:88.3H_2O$	CHA, EDI	–
45	18.00		4.03						3.10	7.11	100	240	$3K_2O:Al_2O_3:2SiO_2:88.3H_2O$	CHA, EDI	–
46	18.00		4.03						3.10	7.11	100	528	$3K_2O:Al_2O_3:2SiO_2:88.3H_2O$	CHA, EDI	–
47	18.00		1.35						3.10	6.24	175	24	$K_2O:Al_2O_3:2SiO_2:86.3H_2O$	EDI	KAO
48	18.00		1.35						3.10	6.24	175	216	$K_2O:Al_2O_3:2SiO_2:86.3H_2O$	EDI	KAO
49	18.00		1.35						3.10	6.24	175	312	$K_2O:Al_2O_3:2SiO_2:86.3H_2O$	EDI	KAO
50	18.00		4.03						3.10	7.11	175	24	$3K_2O:Al_2O_3:2SiO_2:88.3H_2O$	Kal, Leu	–
51	18.00		4.03						3.10	7.11	175	216	$3K_2O:Al_2O_3:2SiO_2:88.3H_2O$	Kal, Leu	–
52	18.00		4.03						3.10	7.11	175	312	$3K_2O:Al_2O_3:2SiO_2:88.3H_2O$	Kal, Leu	–
53	18.00					5.20			3.40	6.82	175	0	$7CaO:Al_2O_3:2SiO_2:77.9H_2O$	P, CSH, Qtz	KAO
54	18.00					5.20			3.40	6.82	175	0.5	$7CaO:Al_2O_3:2SiO_2:77.9H_2O$	P, CSH, Qtz	KAO
55	18.00					5.20			3.40	6.82	175	1	$7CaO:Al_2O_3:2SiO_2:77.9H_2O$	P, CSH, Qtz	KAO
56	18.00					5.20			3.40	6.82	175	1.5	$7CaO:Al_2O_3:2SiO_2:77.9H_2O$	P, CSH, HYD, α-C_2SH, Qtz, Cal	KAO
57	18.00					5.20			3.40	6.82	175	2	$7CaO:Al_2O_3:2SiO_2:77.9H_2O$	P, CSH, HYD, α-C_2SH, Qtz, Cal	KAO
58	18.00					5.20			3.40	6.82	175	18	$7CaO:Al_2O_3:2SiO_2:77.9H_2O$	P, CSH, HYD, α-C_2SH, Qtz, Cal	–
59	18.00					5.20			3.40	6.82	175	24	$7CaO:Al_2O_3:2SiO_2:77.9H_2O$	P, CSH, HYD, TOB, α-C_2SH, Qtz, Cal	–

LTA, zeolite LTA; SOD, sodalite; CAN, cancrinite; JBW, JBW-type zeolite; ANA, analcime; FAU, faujasite; GIS, zeolite Na-P1; CHA, chabazite; PHI, phillipsite; EDI, zeolite Barrer-KF; P, portlandite; CSH, calcium silicate hydrate phase; H, hydrogarnet; T, tobermorite; α-C_2SH (Hartmann et al., 2007); Kal, kalsilite; Leu, leucite; Cal, calcite; Qtz, quartz. Weighed amounts of SDAs: TPAB (0.92 g), TEA (0.61-1.22 g), TEDA (0.67 g); TLAM (0.90 g); L/S, activator solution/KAO ratio.

As shown in Table 5.2, following the fusion approach, KAO-LTA and KAO-CAN were obtained using NaOH as an activator. No attempts to activate KAO with KOH by this method were made, due to the unsuccessful results obtained using NC and FA as starting materials.

Table 5.2. Synthesis conditions for the conversion of KAO into zeolitic materials using the alkaline fusion method.

Test	Chemical reagents to be fused				Alkaline fusion		L/FP	Aging	Hydrothermal reaction		Molar gel composition	Zeolitic phases and other synthesis products	Residual phases
		RM (g)	NaOH (g)	KOH (g)	T / °C	t / h	(ml/g)	t / h	T / °C	t / h			
60	*	6.20	7.44		600	1	4.9	5.5^{s}	60	24	$3.9Na_2O:Al_2O_3:2SiO_2:153.9H_2O$	LTA	---
61	*	6.20	7.44		600	1	4.9	5.5^{s}	60	48	$3.9Na_2O:Al_2O_3:2SiO_2:153.9H_2O$	LTA	---
62	*	6.20	7.44		600	1	4.9	5.5^{s}	60	96	$3.9Na_2O:Al_2O_3:2SiO_2:153.9H_2O$	LTA	---
63	*	6.20	7.44		600	1	4.9	21.5^{s}	60	92	$3.9Na_2O:Al_2O_3:2SiO_2:153.9H_2O$	CAN	---

LTA, zeolite LTA; CAN, cancrinite; L/FP, water/fused product; s stirring conditions.

5.2. Conversion of kaolinite in the system Na_2O-SiO_2-Al_2O_3-H_2O

5.2.1. Chemical and mineralogical analyses

The XRD patterns of unreacted and reacted KAO treated with alkaline solutions are presented in Figure 5.1. The most distinct changes in the XRD patterns are the reduction in intensity of the KAO peaks and the appearance of new crystalline phases. The hydrothermal treatment of KAO in the presence of NaOH without the addition of precipitated SiO_2 or SDAs resulted in the co-crystallization of KAO-SOD and KAO-CAN, along with metastable KAO-LTA (Figures 5.1a and 5.1b). It is seen that a higher NaOH concentration in the synthesis solution leads to faster dissolution of the original KAO, accompanied by more crystalline zeolitic materials, as shown by an increase of the relative intensity of the XRD peaks of these feldspathoids. When precipitated SiO_2 was used, high Si/Al ratio zeolites (KAO-LTA, KAO-FAU, KAO-GIS and KAO-ANA) with traces of KAO-SOD and KAO-CAN formed (Figure 5.1c), which is reflected in strong peaks for these zeolite-type structures and relatively weak peaks for the feldspathoids, compared with evidence in Figures 5.1a and 5.1b. In general, at low temperature and shorter reaction times the raw KAO is dominant with respect to the as-synthesized products, which display low intensity peaks compared with those at longer reaction times. The activation of KAO at higher NaOH concentration and temperature promoted the co-crystallization of highly crystalline KAO-JBW with traces of KAO-SOD and KAO-CAN and (Figure 5.1d). Lin *et al*. (2004) concluded that the reaction at higher temperature is advantageous for the synthesis of JBW. The JBW-type structure is one of the lesser-studied zeolites, which was first reported by Barrer and White (1952). According to Healey *et al*. (2000a), a subsequent work referred to this zeolite inappropriately as ‘nepheline hydrate I’ and Its crystal structure was solved partially in 1982 by

Hansen and Fälth (1982). The JBW-type structure is unusual because one part of its structure is separated from the next by what is effectively a layer of the cristabolite structure containing non hydrated cations (Hansen and Fälth, 1982). No interesting changes were observed using SDAs at low temperature. However, the use of SDAs (TLAM), at high temperature (Figures 5.1e and 5.1f) reveals a clear evidence of a phase transformation KAO-SOD + KAO-CAN → KAO-JBW, as shown by the co-crystallization of KAO-SOD and KAO-CAN at shorter reaction times (6 h), followed by the formation of the JBW-type structure, as main crystalline phase, at longer reaction times (24-48 h). However, the final synthesis products are composed by a mixture of KAO-SOD, KAO-CAN and KAO-JBW, similar to what is observed in Figure 5.1d. In general, at high temperature, the raw KAO was quickly dissolved; the crystallinity of the KAO-based feldspathoids showed a constant behaviour, except using a high NaOH concentration and adding TLAM, which promoted a decrease in the crystallinity of KAO-SOD and KAO-CAN at longer reaction times. On the other hand, the grade of crystallinity of the JBW-type structure increased using a high NaOH concentration and longer reaction times.

XRD patterns (Figure 5.2) of the raw KAO and crystallization products in the reactant mixture obtained using an alkaline fusion step followed by hydrothermal treatment at 60 ^{o}C indicate that the reaction of KAO with NaOH is shown by the disappearance of its characteristic peaks. On the other hand, there is a marked influence in the zeolitic products obtained when a longer or a shorter stirring time was used for dissolving the alkali fused solid in water. KAO-LTA crystallized after using a shorter stirring time in spite of the hydrothermal reaction time, which indicates that this phase was stable over 24-96 h period (Figure 5.2a). Additional tests (Figure 5.2b) were done to estimate the effect of aging under stirring conditions. When a longer stirring time was used, KAO-CAN was the single phase obtained after 92 h of reaction of KAO.

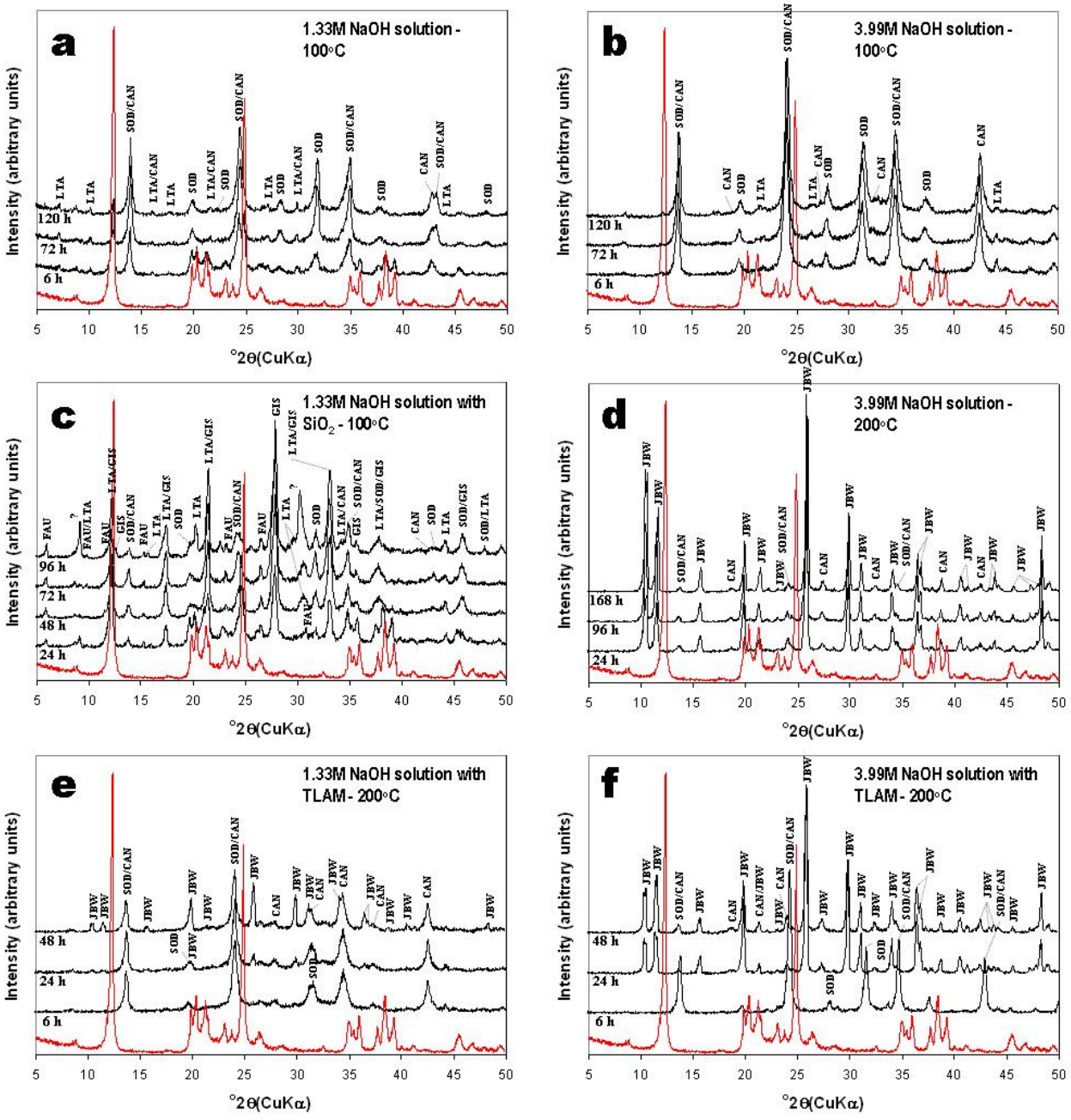

Figure 5.1. XRD patterns of the unreacted (in red) KAO and representative as-synthesized products obtained after hydrothermal reaction of KAO in NaOH solutions.

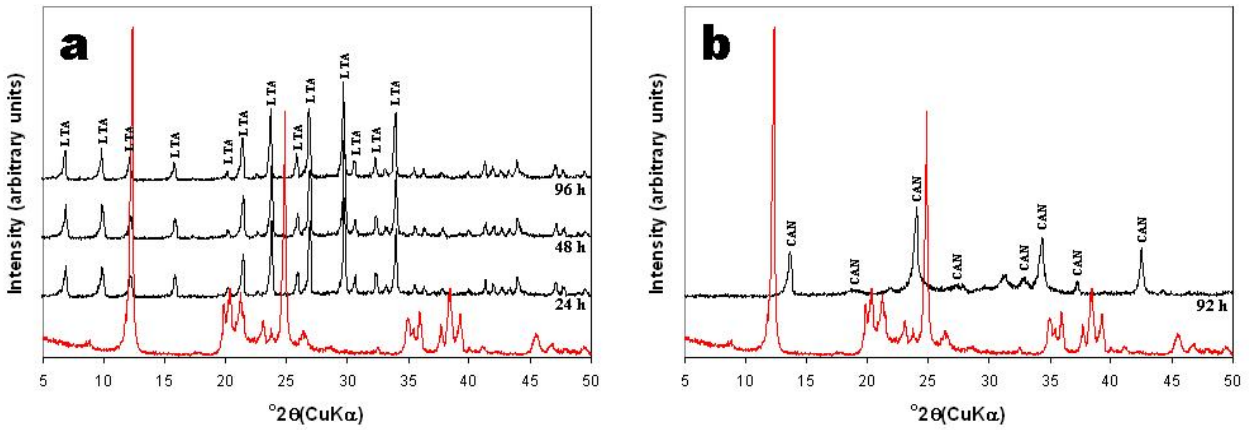

Figure 5.2. XRD patterns of the KAO (in red) and representative as-synthesized products obtained by the alkaline fusion approach, aging the hydrogel under stirring conditions for (a) shorter and (b) longer reaction times.

SEM images of the morphology of the as-synthesized zeolitic products obtained after activation of KAO in NaOH solutions are exhibited in Figure 5.3. The observed morphologies in this work are similar to those reported in previous studies (de Vos Burchart *et al*., 1989; Gerson and Zheng, 1997; Barnes *et al*., 1999a, b, c; Porcher *et al*., 2000; Deng *et al*., 2003; Mashal *et al*., 2004, 2005; Zhao *et al*., 2004; Mon *et al*., 2005; Traa and Thompson, 2002; Lapides and Heller-Kallai, 2007).

Figure 5.3a shows a SEM image of the treated KAO in which KAO-SOD and KAO-CAN that show lepispheric morphology grew out onto the surface of a well-developed cube of KAO-LTA displaying fluorite-type interpenetration-twinning, which indicates that KAO-LTA is a thermodynamically metastable phase that was successively replaced by more stable phases, such as KAO-SOD and KAO-CAN. The lepispheric morphology is characteristic in mixtures of cancrinite and sodalite (Chorover *et al*., 2003; Deng *et al*., 2003, 2006; Qafoku *et al*., 2003; Mashal *et al*., 2004, 2005). Remnants of hexagonal platy crystals of KAO as aggregates of parallel plates that did not react with NaOH coexist with the zeolitic products. The transformation of KAO-SOD into KAO-CAN is illustrated in Figure 5.3b. KAO-SOD shows a wedge-shaped blade structure whereas KAO-CAN occurs as lepispheres composed of intergrown thin disks. The phase transformation sodalite → cancrinite has been reported elsewhere (Barnes *et al*., 1999a, b, c; Choi *et al*., 2005). These morphological features are consistent with the mixture of KAO-LTA, KAO-SOD and KAO-CAN observed in the XRD patterns. Figure 5.3c illustrates an

epitaxial growth between KAO-LTA and KAO-FAU arranged in a spherical aggregate, with KAO-LTA, displaying a perfect cubic morphology and interpenetration-twinning, and KAO-FAU, showing an octahedral morphology with spinel-type contact twinning. These aggregates are similar to the overgrowths of faujasite onto zeolite LTA described by several authors (de Vos Burchart *et al*., 1989; Porcher *et al*., 2000; and Traa and Thompson, 2002; Lapides and Heller-Kallai, 2007). However, in this study a reverse relationship between these zeolitic phases was observed, with KAO-LTA growing after KAO-FAU. In general, it is common to observe twin growth and intergrowth of polycrystals, which can be explained by agglomeration of nuclei early (Gora *et al*., 1997). A molecular intergrowth model is suggested by de Vos Burchart *et al*. (1989) in which sodalite cages are strain-free bound to the framework (through a double four-ring) of zeolite LTA as well as to the framework (through two double six-rings) of faujasite. Characteristic long prismatic lath-like crystals of KAO-JBW, with pseudohexagonal cross sections, are illustrated in Figure 5.3d. Similar morphologies were observed by Wei *et al*. (2007) in JBW-type zeolite obtained by phenol solvothermal synthesis. A KAO-JBW crystal with a tubular morphology associated to lepispheric aggregates of KAO-CAN is observed in Figure 5.3e. Healey *et al*. (2000b) reported similar tubular morphologies in aluminogermanate possessing the zeolite JBW framework topology. Prismatic lath-like and tubular crystals of KAO-JBW, with pseudohexagonal cross sections, are illustrated in Figure 5.3f.

Using the alkaline fusion approach, a contrast in morphology between the fused and as-synthesized products was observed. The fused KAO exhibited amorphous spherical aggregates interspersed with crystalline material in general showing acicular morphology. On the other hand, after hydrothermal reaction, at short reaction time (24 h) the synthesis product consists of small crystals that have grown in amorphous aggregates, whereas increasing the reaction time to 96 h (Figure 5.4a) cubes with truncated edges of KAO-LTA that display occasionally intergrown twins appeared with a mean particle size of 1 μm. Alfaro *et al*. (2007) observed that at longer reaction time, KAO-LTA shows a smaller crystal size compared with that at shorter aging time. Figure 5.4b illustrates the occurrence of lepispheric morphology (intergrown thin disks) typical of KAO-CAN.

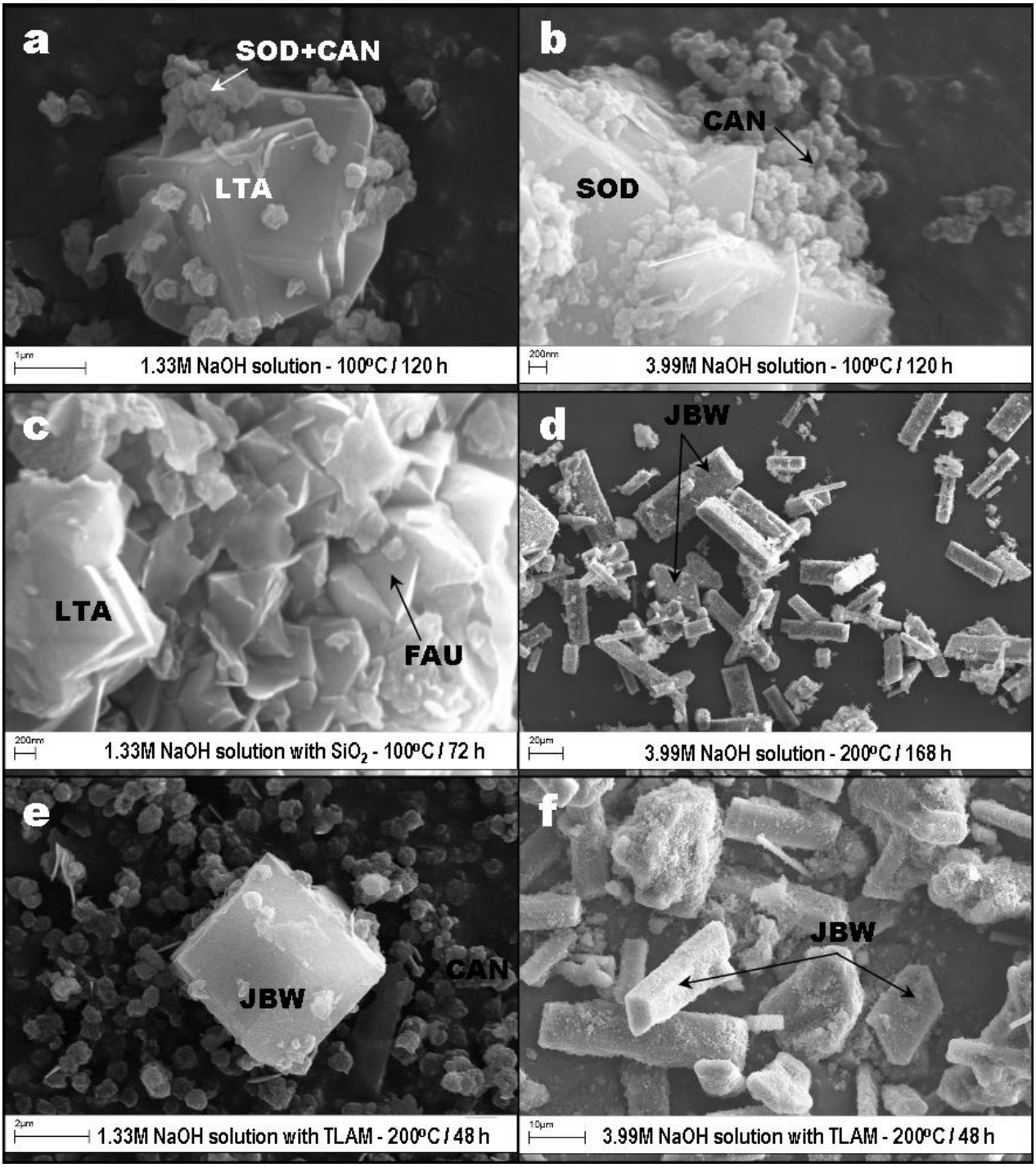

Figure 5.3. SEM images showing the occurrence of representative synthesis products obtained via hydrothermal treatment of KAO in NaOH solutions.

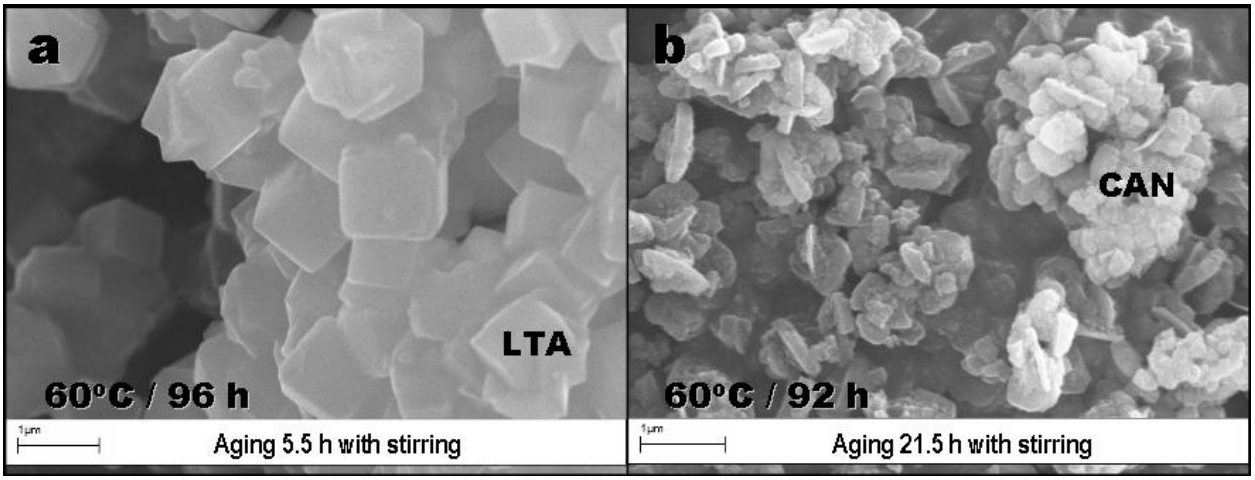

Figure 5.4. SEM images of representative synthesis products obtained by the alkaline fusion approach, with NaOH as an activator, aging the hydrogel under stirring conditions for (a) shorter and (b) longer reaction times.

5.2.2. Fourier Transform Infrared Spectroscopy

The FT-IR spectra of the original KAO and as-synthesized products obtained after its hydrothermal treatment with alkaline solutions are shown in Figure 5.5. The characteristic OH-stretching vibrations in KAO at 3687 cm^{-1} (surface OH stretching) and 3619 cm^{-1} (inner OH stretching), as well as the peaks at 1116, 1031, 1008, 938 (surface OH bending), 913 (inner OH bending), 797, 790 and 754 cm^{-1}, which disappeared with reaction time. In general, the characteristic peaks of KAO shift of absorbance to lower wavenumbers indicates that there are more Al substitution in tetrahedral sites of the silica framework with NaOH acting as a structure modifier as has been suggested in other studies (Aronne *et al*., 1997, 2002; Park *et al*., 2000a). However, at shorter reaction times, using a low NaOH concentration and temperature (tests 1 and 7), these peaks were preserved. The absorption bands of the synthesis products at low temperature show the asymmetric and symmetric vibration bands characteristic for a mixture of KAO-LTA, KAO-SOD and KAO-CAN in the region 1200-400 cm^{-1}. Barnes *et al*. (1999b) summarized the reported assignments of vibrations for sodalite and cancrinite in this range. Coincident with the disappearance of KAO, characteristic zeolite bands appeared on the spectra, including the asymmetric Al-O stretch located in the region of 1250-950 cm^{-1}, and their symmetric Al-O stretch located in the region of 770-660 cm^{-1}. The region 1200-850 cm^{-1} shows a single vibration band centred at 960-965 cm^{-1}, associated to the presence of KAO-CAN, except

adding precipitated SiO_2 (975 cm^{-1}, characteristic in KAO-SOD, test 9) or using lower reaction times (tests 1 and 7, unreacted KAO). The absorbance for the asymmetric stretch for the Si-O-Al framework of sodalite consists of a single peak at 980 cm^{-1}, which split into four peaks at 1110, 1050, 1020 and 960 cm^{-1} in the cancrinite (Barnes *et al*., 1999b). However, in this study is reported only the peaks at 975 and 960-965 cm^{-1}, corresponding to KAO-SOD and KAO-CAN, respectively. The region 850-750 cm^{-1} reveals a weak vibration band at 766-768 cm^{-1} (tests 10, 13, 29 and 31), characteristic of KAO-CAN. Several peaks in the region 750-650 cm^{-1} indicate the presence of a mixture of KAO-SOD and KAO-CAN in the as-synthesized products. The bands in the region of 650-500 cm^{-1} are related to the presence of the double rings (D4R and D6R) in the framework structures of the zeolitic materials (Breck, 1974). In this region is reported for the first time three characteristic vibration bands, which can be attributed to the presence of six-rings of the dehydrated region and eight-rings of the hydrated section of the structure KAO-JBW. The bands in the region of 500-420 cm^{-1} are related to internal tetrahedron vibrations of Si-O and Al-O of the synthetic zeolites. The region 800-400 cm^{-1} can be consider as the 'fingerprint' region not only for KAO-LTA, KAO-SOD and KAO-CAN as suggested in previous studies (Barnes *et al*., 1999b; Aronne *et al*., 2002) but also for KAO-JBW.

5.2.3. ^{29}Si and ^{27}Al Magic Angle Spinning Nuclear Magnetic Resonance

Figure 5.6 shows the ^{29}Si and ^{27}Al MAS NMR spectra of the raw KAO and representative synthesis products obtained using NaOH as an activator. The ^{29}Si MAS NMR spectrum of KAO (Figure 5.6a) shows two signals at -90.9 and -91.4 ppm attributed to the existence of two different but equally populated silicon sites. Three resonances at -83.6, -86.3 and -91.2 ppm are clearly distinguished in Figure 5.6b. The chemical shifts at -83.6 and -86.3 ppm can be attributed to Q^4(4Al) environments in KAO-SOD and KAO-CAN (Wilson, 1987). The presence of the two Si sites indicates imperfect Al/Si ordering in tetrahedral sites. It was demonstrated that there was a good correlation (r^2 = 0.968) between the sodalite unit cell size and the chemical shift (Engelhardt *et al*., 1989; Jacobsen *et al*., 1989; Kempa *et al*., 1991). Cancrinite was reported to have a chemical shift of - 87.3 ppm (Barnes *et al*., 1999b). In this study the signal at -86.3 ppm can be presumably attributed to KAO-CAN. In some studies, ^{29}Si MAS NMR has been used to differentiate between sodalite and cancrinite (Buhl and Löns, 1996; Buhl, 1991a; Mundus *et al*., 1996). However, according to Barnes *et al*. (1999b), no difference in chemical shift between sodalite and cancrinite can be recognized in terms of ^{29}Si MAS NMR. Therefore, as the

framework stoichiometry and the bonding between oxygen, aluminium and silicon is similar for these phases, any difference in chemical shift would be likely be caused by the position of the different ions in the cages or channels (Barnes *et al*., 1999b). The -91.2 ppm chemical shift can be assigned to the presence of residual KAO. Two resonances peaks at -85.8 and -87.9 ppm are observed in Figure 5.6c. Similar results have been reported by Healey *et al*. (2000a) and Lin *et al*. (2004) to confirm the characteristic framework of the structure of the KAO-JBW. The framework is ordered and the tetrahedral silicon atoms possess chemical shift values (ca. -80 to -90 ppm) consistent with silicon being surrounded by four O-Al groups (Q^4(4Al) sites in KAO-JBW) as has been suggested by Healey *et al*. (2000a). They assume that three silicon atoms occupy two distinct sites with occupancies of 2:1, as shown by the area beneath the two resonance peaks, and attributed the smaller of the two peaks (at -85.8 ppm) to Si(1), whereas the other two chemically similar silicon atoms, Si(2) and Si(3), lead to the larger of the two peaks (at -87.9 ppm). Therefore, the atomic ratio of Si/Al in the framework is 1.0 for this as-synthesized zeolite-type structure. These confirm the framework characteristics of the KAO-JBW proposed by Hansen and Fälth (1982). A single resonance at -86.3 ppm (Figure 5.6d) can be attributed to Q^4(4Al) of the KAO-CAN (Si/Al ratio = 1.0) obtained after activation of KAO by the fusion approach. The ^{27}Al MAS NMR spectrum of the unreacted KAO (Figure 5.6a) consists of a single resonance at -3.4 ppm and is largely octahedral aluminium. Single resonances at 59.5, 56.8 and 60.1 ppm, respectively, in Figures 5.6b, 5.6c and 5.6d, can be assigned to tetrahedral Al in the framework of the zeolitic products, but with some octahedral Al (Figure 5.6b) corresponding to the presence of residual KAO, presumably microcrystalline as it is not detected by XRD. The reaction of the KAO with NaOH as mineralizer resulted in a shift of Al from octahedral to tetrahedral coordination, which is likely due to the dissolution of KAO and the subsequent precipitation of tectosilicates. The amount of Al(6) is greatest in KAO (Figure 5.6a) where the initial Al concentration was larger compared with that in the synthesis products (Figures 5.6b-5.6d). The decrease in the Al(6)/Al(4) ratio can be explained by the dissolution of KAO, with Al coordination changing from octahedral to tetrahedral, which is consistent with the formation of zeolite-type materials. These results corroborate the XRD and FT-IR results (Figure 5.5).

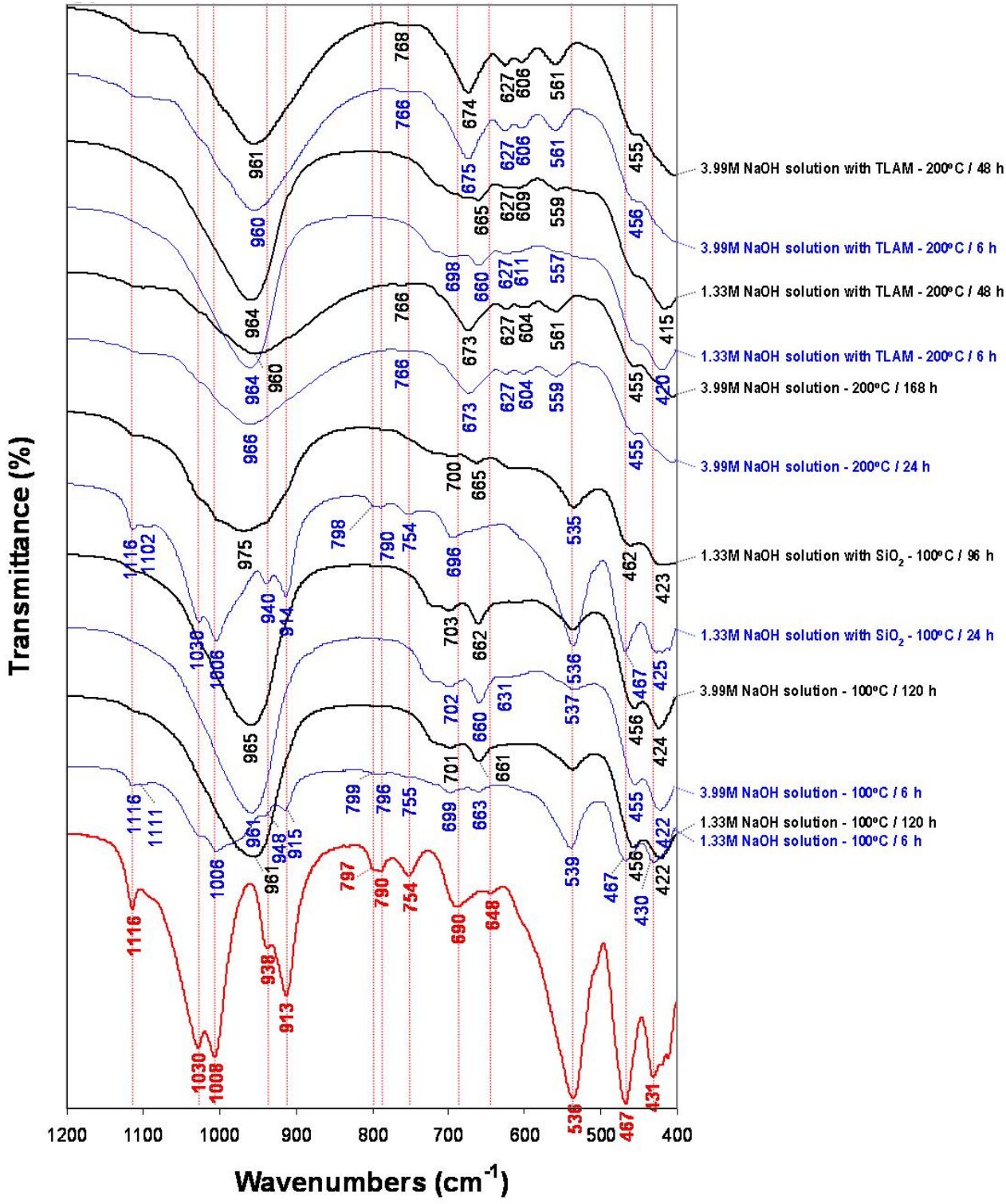

Figure 5.5. FT-IR spectra of the unreacted (in red) KAO and representative as-synthesized products obtained after hydrothermal reaction of KAO in NaOH solutions.

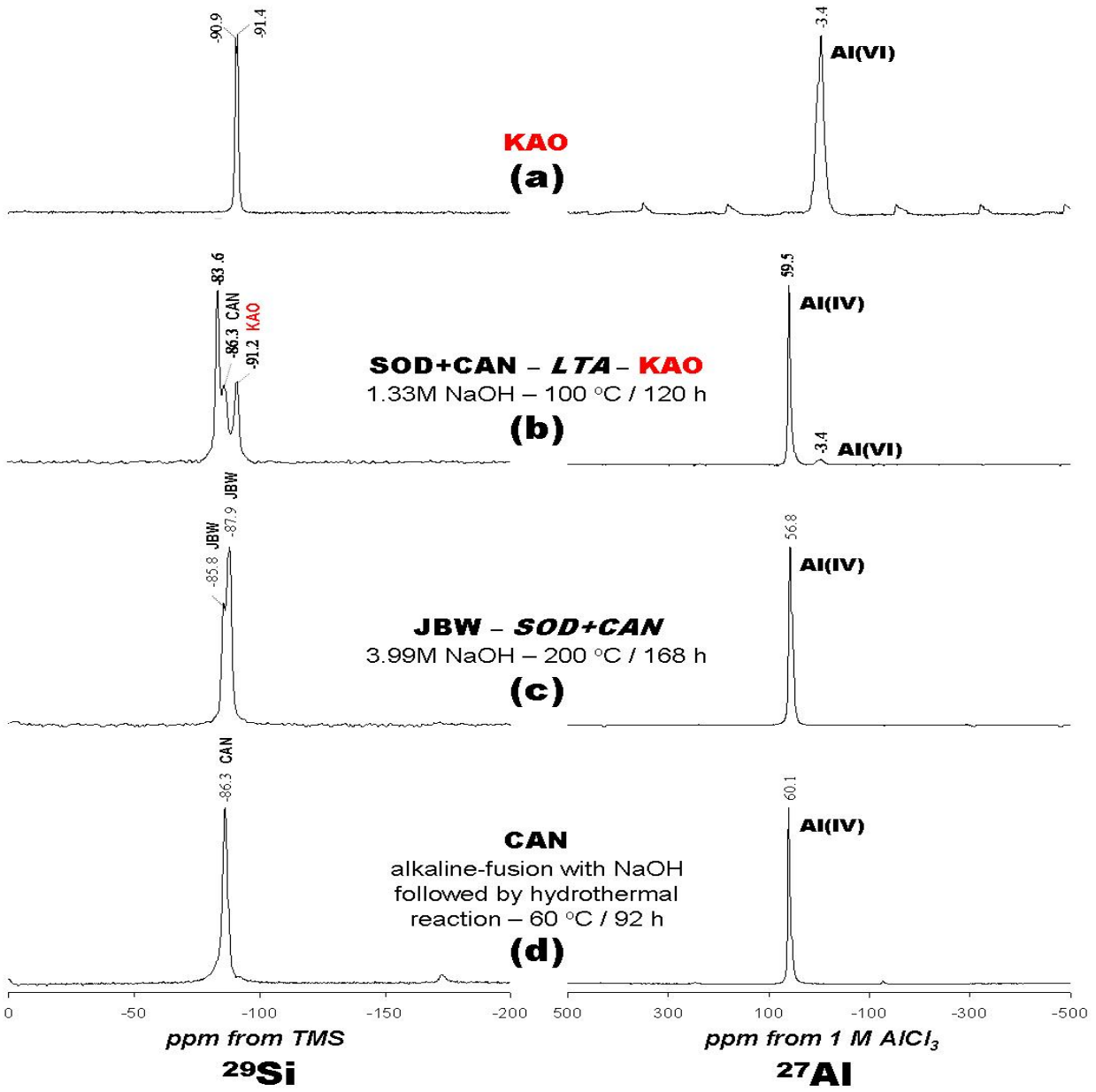

Figure 5.6. ^{29}Si and ^{27}Al MAS NMR spectra of the (a) raw KAO and (b-d) representative synthesis products obtained after alkaline activation of KAO with NaOH as mineralizer. Main and minor phases are indicated in uppercase regular and italic fonts, respectively; starting material phases in uppercase regular font (red colour).

5.2.4. Thermogravimetric analysis

DTG curves of the KAOZs are shown in Figure 5.7. The as-synthesized products show three or

four dehydration steps. The position of these DTG peaks and the number of dehydration steps has been attributed to the different compensating cation-water binding energies, as well as to the different energy associated with the diffusion of the desorbed water through the porous structure of the zeolitic materials. Their weight loss percentages reflect the water loss from the zeolite structure, and the amount of desorbed water is related with the number of compensation cations in the zeolite framework (Covarrubias *et al*., 2006). The peaks observed between 39-52 ^{o}C correspond to surface water in zeolitic materials; the peaks observed between 100-162 ^{o}C indicate zeolitic water, although in some cases in this temperature range up to two peaks occur, which can be explained by the heterogeneous nature of the as-synthesized products. There are also some peaks between 216-257 ^{o}C. The peaks at 223 and 244 ^{o}C are related to the SDA vaporizing. However, sometimes these peaks are broad, indicating that water and the SDA are coming out from the zeolite. A broad peak ~ 500 ^{o}C indicates the SDA burning. The as-synthesized products obtained after hydrothermal transformation of KAO in solutions of 1.33M NaOH + precipitated SiO_2 at 100 °C for 96 h display the highest weight loss (17.88%), which indicates that these zeolitic products have a higher amount of water. On the other hand, zeolitic products obtained after hydrothermal transformation of KAO in alkaline solutions show a decrease in weight loss with increasing of NaOH concentration. The lowest weight loss (8.10%) was obtained for zeolitic materials formed after reaction of KAO in solutions of 3.99M NaOH + triethanolamine at 200 °C for 48 h.

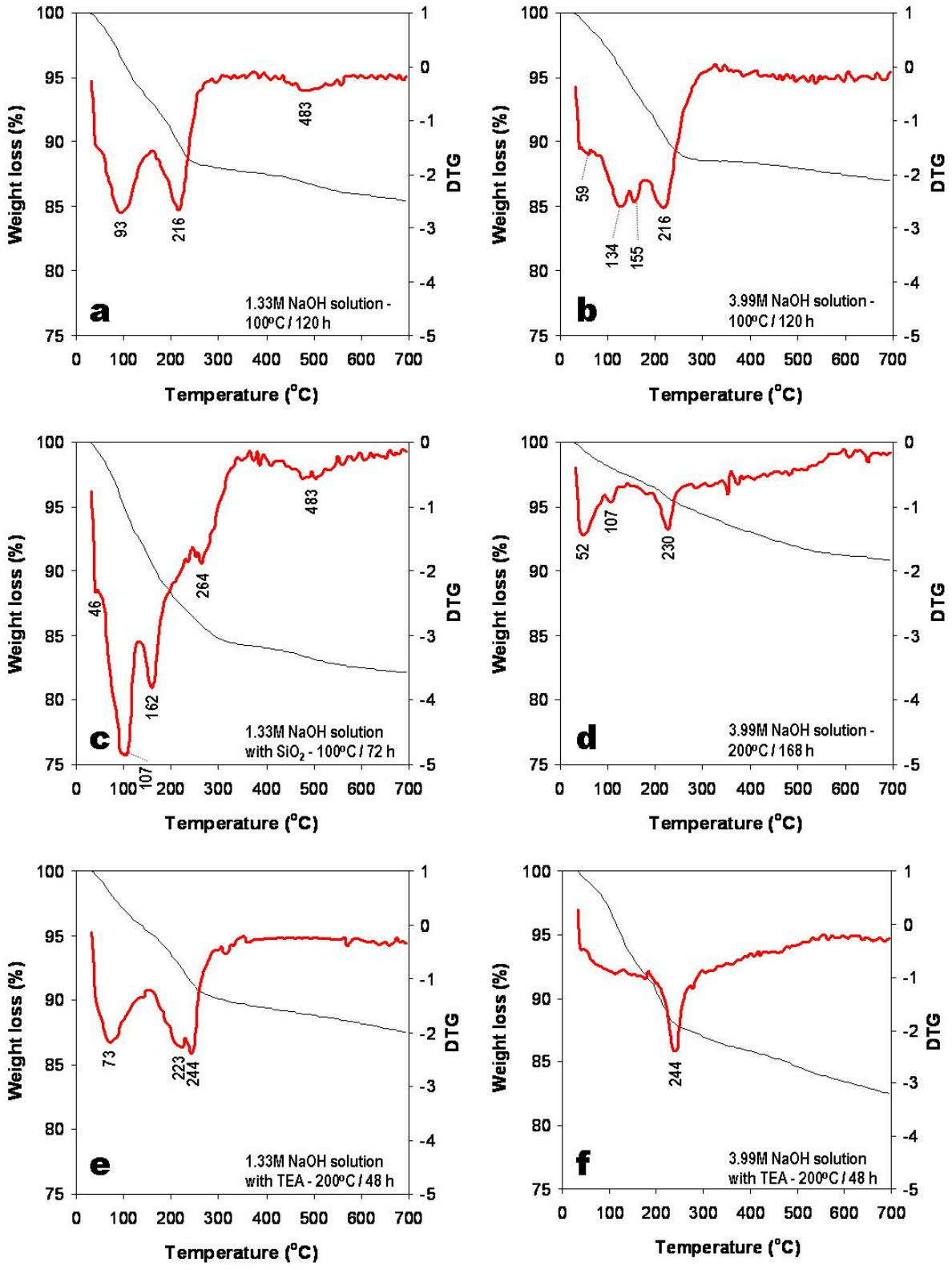

Figure 5.7. TG/DTG curves between 25-700 ºC of representative synthesis products obtained after alkaline activation of KAO using NaOH as mineralizer.

5.2.5. Phase transformation

The mineral transformation and the stability of the end products were controlled by experimental parameters like NaOH concentration, temperature and Si/Al ratio. However, they were likely affected by several factors, such as the formation of intermediate metastable phases and the occurrence of different chemical processes, including precipitation and dissolution of a gel phase, nucleation and growth of zeolitic phases, dissolution of the early metastable phases, nucleation and growth of more stable phases (sodalite and cancrinite), with a dissolution of the initial crystals and nucleation and growth of the crystalline phases that reached chemical equilibrium. Recently, Ríos *et al*. (2008b) described the mechanism of synthesis of zeolite LTA as the result of two main stages: (1) the dissolution of aluminosilicate phases of the raw material or its alkaline fused product releasing Si and Al and the zeolite crystallization. Deng *et al*. (2006) have demonstrated that the mineral formation/transformation rates increased with temperature and the mineral transformation at low temperature were:

At 22ºC – poorly crystalline aluminosilicate → zeolite LTA (~ 1 week)

At 50ºC – poorly crystalline aluminosilicate → zeolite LTA (< 1 day) → cancrinite + sodalite (~ 6 weeks)

At 80ºC – poorly crystalline aluminosilicate → zeolite LTA (< 2 h) → cancrinite + sodalite (< 1 day) → cancrinite (< 32 weeks)

The hydrothermal transformation of KAO at low temperature presumably reveals a similar sequence of reactions, starting with an amorphous material after dissolution of KAO, followed by KAO-LTA as the first and metastable phase formed, a mixture of KAO-SOD and KAO-CAN and finally KAO-CAN (apparently more stable than KAO-SOD) as the stable and final synthesis product. These mineral transformations did not occur in the solid state and therefore represent a solution-mediated mechanism (Barnes *et al*., 1999a; Deng *et al*., 2006). However, according to XRD diffraction analysis a co-crystallization of KAO-LTA, KAO-SOD and KAO-CAN, being very difficult to establish a phase transformation due to the very constant behaviour of the XRD peaks of these zeolite phases and to the overlapping of the diffraction peaks of sodalite and cancrinite, which makes difficult to quantifying sodalite and cancrinite phase mixtures. SEM data reveal phase relationships in which (1) lepispheric aggregates of KAO-SOD and KAO-CAN grow onto the surface of cubic crystals of KAO-LTA or (2) KAO-CAN growing at the expense of KAO-SOD. Under the experimental conditions considered by Deng *et al*. (2006) there is enough evidence

about the phase transformations that occur in this chemical system. However, in this study a slight higher temperature (100 ^{o}C) was used, which can explain why KAO-LTA (a metastable phase) occurs as a minor phase, compared with the presence of KAO-SOD and KAO-CAN.

KAO-JBW crystallized as the main crystalline phase at high temperature, along with KAO-ANA KAO-SOD and KAO-CAN. Results indicate that the use of SDAs, particularly TLAM, is not necessary for crystallization of the JBW-type structure from SDA-free hydrogels. Lin *et al*. (2004) reported the phase transformations from zeolite LTA to JBW and from sodalite to cancrinite using MTK as starting material, the first of them for the first time. However, these authors do not consider the phase relationships between the zeolite-type materials involved in such phase transformations. Therefore, taking into account the sequence of reactions observed at low temperature, the metastable character of zeolite LTA and sodalite compared with the stable cancrinite and the fact that the JBW-type structure crystallized at longer reaction times, the sequence of phase transformations KAO-SOD → KAO-CAN → KAO-JBW is proposed for the first time in this study. However, the only two evidences to support this are the absence of KAO-JBW at shorter reaction times as revaled by the

The alkaline fusion of KAO with NaOH, followed by dissolution in water and hydrothermal treatment, resulted in KAO-CAN formation. The fused products correspond to large amounts of sodium silicate and amorphous aluminosilicate, which indicates that the fusion process was very effective in extracting the silicon species in these mixtures. Adding FA to KAO in the mixture to be fused did not exert an important control either in the fusion process or the hydrothermal treatment of the fused product, taking into account that CAN was the single crystalline phase obtained. The use of an alkaline fusion approach included a previous aging step of the aluminosilicate hydrogels, which promotes the increase of ionic species in solution and produces a liquid phase with a composition more similar to that of the bulk composition (Szostak, 1989).

5.2.6. Summary

Using the classic hydrothermal method several zeolitic products were obtained depending on the experimental conditions. The main crystalline phases obtained at low NaOH solutions and temperatures were KAO-SOD, KAO-CAN and KAO-LTA. At high SiO_2/Al_2O_3 ratio solutions, KAO-FAU and KAO-GIS also crystallized. On the other hand, at high NaOH solutions and temperatures, KAO-JBW, KAO-SOD and KAO-CAN were obtained, with the feldspathoids

occurring as trace phases without the use of SDAs. There were two major chemical processes involved in the reaction between KAO and alkaline solutions: dissolution of KAO followed by the formation of zeolitic materials. The structural similarity between zeolites and feldspathoids explain why they can coexist in the as-synthesized products and the dominant crystalline phase depends on formation conditions.

Using an alkaline fusion step prior to hydrothermal treatment, KAO-LTA and KAO-CAN were obtained. This approach promoted the dissolution of larger amounts of aluminosilicates and played an important role in enhancing the hydrothermal conditions for zeolite synthesis.

5.3. Hydrothermal transformation of kaolinite in the system K_2O-SiO_2-Al_2O_3-H_2O

A crystallization sequence illite → zeolite K-F → K-phillipsite → K-feldspar, reported by Bauer *et al*. (1998) was monitored during the hydrothermal treatment of KAO in solutions of KOH (Table 5.1, tests 41-52). However, in this study a different reaction sequence was documented, due to the probable absence of illite and the presence of three metastable phases (KAO-CHA, KAO-EDI and an unidentified potassium aluminosilicate) and two stable final crystalline phases (kalsilite and leucite). On the other hand, the synthesis was carried out at shorter reaction times compared with those used by Bauer *et al*. (1998).

5.3.1. Chemical and mineralogical analyses

The XRD patterns in Figure 5.8 reveals that the hydrothermal treatment of KAO in KOH solutions is characterized by the dissolution of KAO and the formation of amorphous aluminosilicate and crystalline phases (three metastable phases, KAO-CHA, KAO-EDI and an unidentified potassium aluminosilicate, and two stable phases, kalsilite and leucite). The unidentified peaks in the XRD patterns should represent the still remaining KAO or some potassium aluminosilicate phases.

As can be seen from the XRD patterns in Figure 5.8a, very weak peaks indicate that KAO-CHA was the only crystalline phase formed when a low KOH concentration and temperature were

used. There was no change in crystallinity over 240-528 h period. At high KOH concentration (Figure 5.8b), an intense dissolution of the starting KAO was accompanied by the precipitation of three different zeolitic phases (KAO-CHA and KAO-EDI), which increased in crystallinity with reaction time. However, it could be said that KOH concentration increase promoted the KAO-EDI formation. Figure 5.8c shows that KAO-EDI crystallized at low KOH concentration and high temperature, although their crystallinity tended to be constant over 216-312 h period, with a large amount of amorphous aluminosilicate material at shorter reaction times (24 h), as evident by a hump between 25 and 35° 2θ. The increase in temperature had a negative effect in KAO-CHA formation. The XRD patterns in Figure 5.8d show that a mixture of kalsilite ($KAlSiO_4$) and leucite ($KAlSi_2O_6$) formed at high KOH concentration and temperature, without a change in crystallinity during the monitored time.

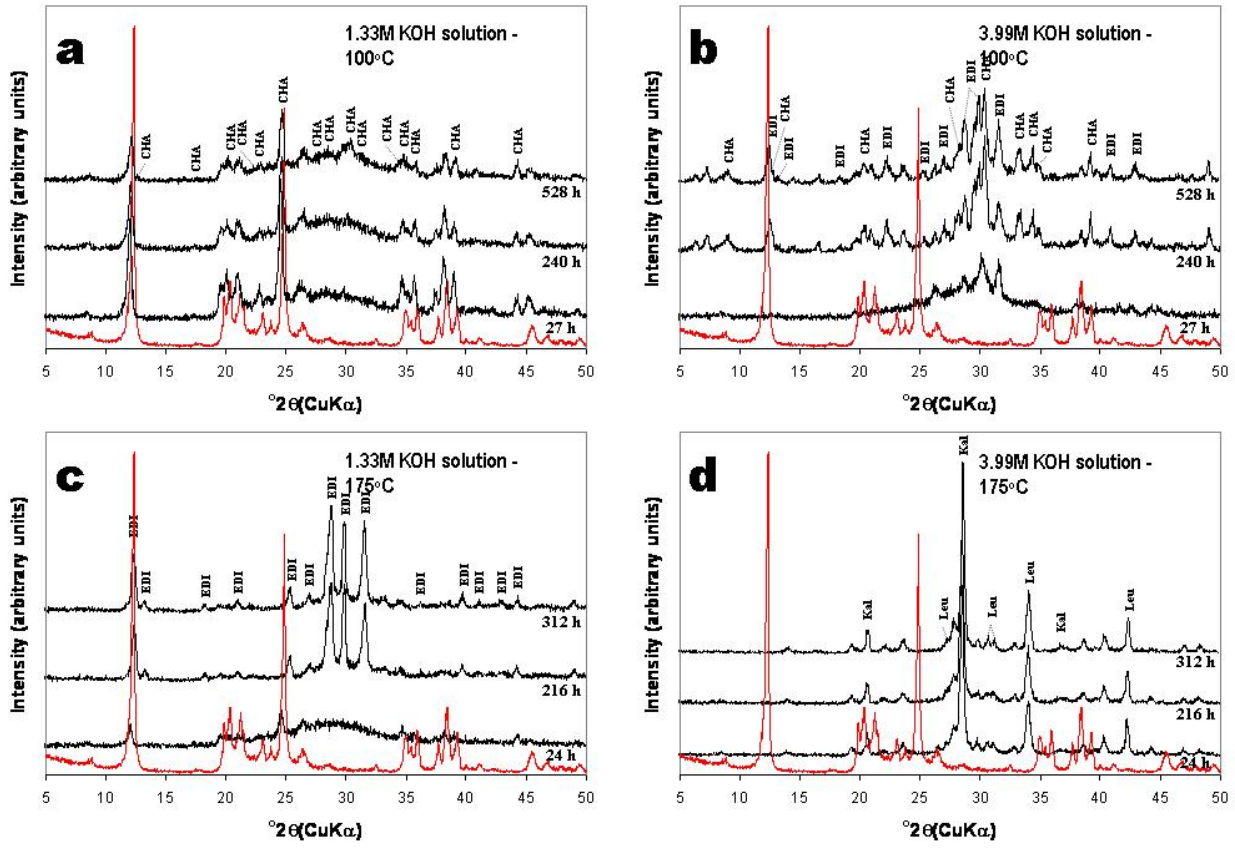

Figure 5.8. XRD patterns of the unreacted (in red) KAO and representative as-synthesized products obtained after hydrothermal reaction of KAO in KOH solutions.

SEM images (Figures 5.9 and 5.10) shows interesting morphologies that provide new clues on the phase reaction history after the hydrothermal transformation of kaolinite in the system K_2O-SiO_2-Al_2O_3-H_2O.

Figure 5.9a illustrates an example of the dissolution of KAO, revealed by its different morphology in the boundary region, which may indicate the formation of illite. The arrows indicate the position of developed illite. However, the Initial precipitation of the metastable KAO-CHA could affect the activity of K and inhibits precipitation of illite. On the other hand, some Fe should be released by dissolution of impurities in KAO to promote the formation of illite. Figure 5.9b illustrates aggregates of cauliflower-shape morphology of bladed crystals of KAO-CHA. In Figure 5.9c is revealed the presence of neoformed crystals of KAO-EDI and an unidentified potassium aluminosilicate, which have grown at the expense of spheroidal aggregates of KAO-CHA. An intergrowth between prismatic crystals of KAO-EDI developing cruciform penetrating twinning and a potassium aluminosilicate phase with hexagonal plate-like morphology is illustrated in Figure 5.9d. Observe also the occurrence of stacks of face-to-face relict KAO flakes with euhedral pseudohexagonal crystals with regular edges. The hexagonal morphology of the unidentified potassium aluminosilicate is similar to that observed in the hexagonal polymorph of faujasite (EMT) or in the zeolite MCM-61 (MSO), which have been synthesized only in the presence of 1,4,7,10,13,16-hexaoxacyclooctadecane (18-Crown-6) (Annen *et al*., 1991; Dougnier *et al*., 1992; Burkett and Davis, 1993) or using 18-Crown-6 in the presence of potassium cations (Shantz *et al*., 1999), respectively. In spite of XRD and SEM data providing some evidences on the presence of a potassium aluminosilicate phase associated to KAO-CHA and KAO-EDI, it is difficult to speculate that this phase could correspond to the EMT or MSO-type structure.

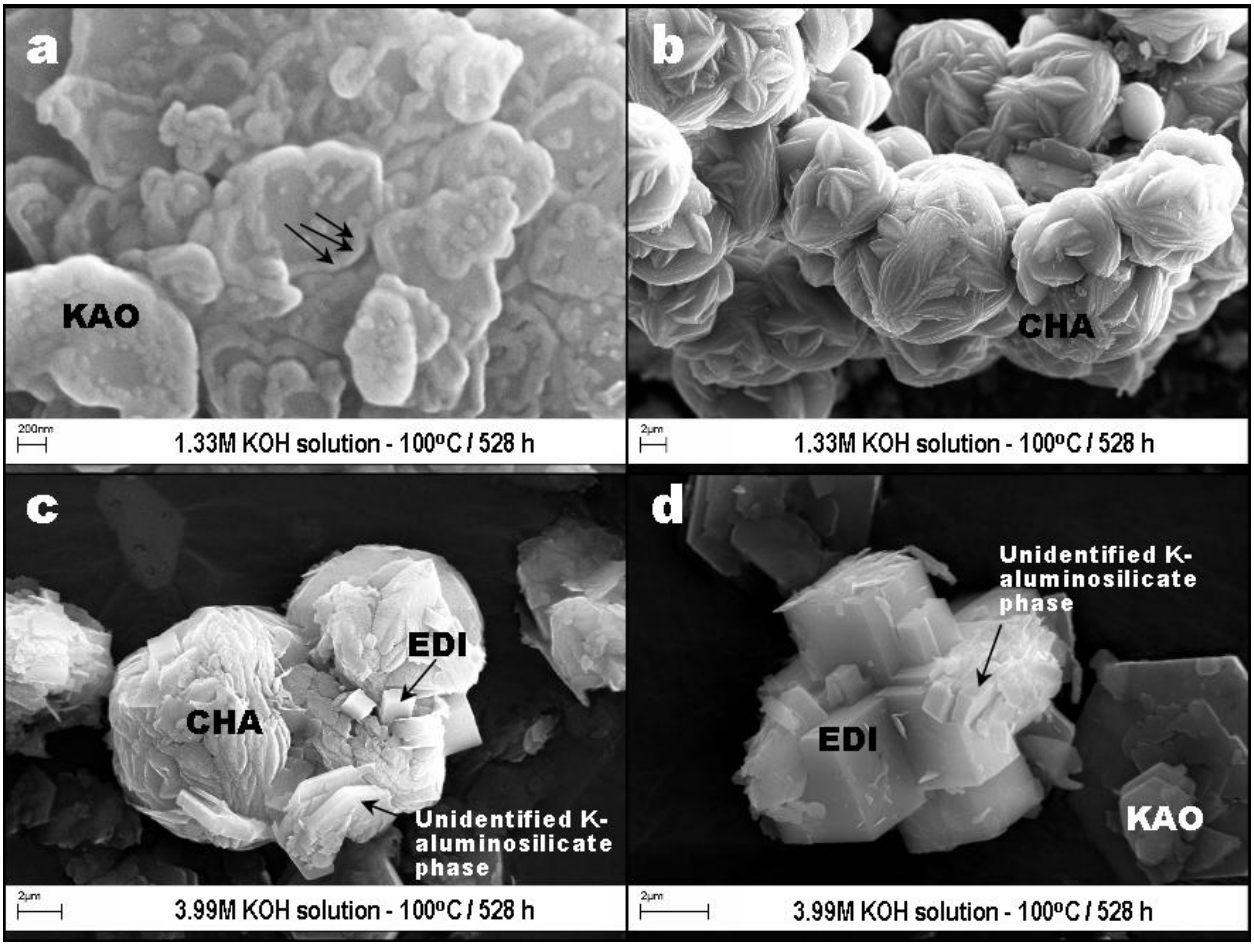

Figure 5.9. SEM images showing the occurrence of representative synthesis products obtained via hydrothermal treatment of KAO in KOH solutions at 100 ºC.

Figure 5.10a shows an additional evidence of the dissolution of KAO (as indicated by the arrows) at low KOH concentration and reaction time and high temperature, comparable with what is observed in Figure 5.9a. In Figure 5.10b is illustrated a radial array of tetragonal prismatic crystals of KAO-EDI, which grew from the centre of a spherule, showing a typical growth mechanism from a nucleating point in an essentially amorphous material. A similar morphology for KAO-EDI has been achieved by Juan *et al*. (2007) after activation of FA in KOH solutions at 150 ºC. As shown in Figure 5.10c, flaky and blocky morphologies reveal the presence of the starting KAO along with a very fine grain-sized aggregate of kalsilite and leucite. The occurrence of these potassium aluminosilicates is illustrated in Figure 5.10d. It is proposed that after KAO dissolution in KOH solutions, KAO-CHA represents the first zeolitic phase that crystallized, followed by a crystallization of KAO-EDI, which is progressively accompanied by the presence of an additional potassium aluminosilicate phase, developing intergrowths with KAO-EDI, and finally the formation of the stable mixture composed by kalsilite and leucite.

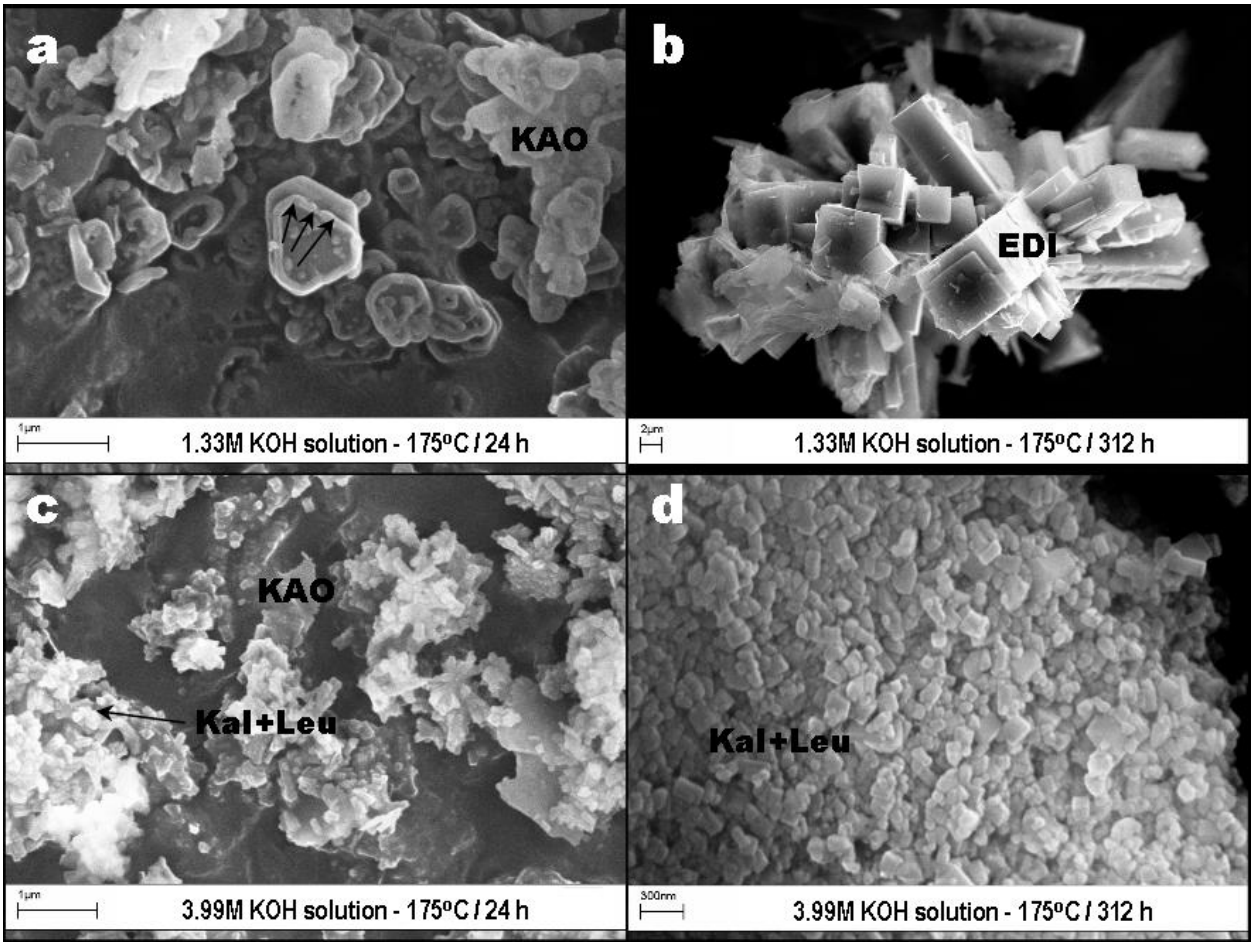

Figure 5.10. SEM images showing the occurrence of representative synthesis products obtained via hydrothermal treatment of KAO in KOH solutions at 175 ºC. Kal, kalsilite; Leu, leucite.

Under experimental conditions similar to those used in this study, Barrer and co-workers demonstrated the formation of zeolite K-F (EDI-type structure) predominantly at temperatures between 80-170 ºC over a range of KOH concentrations. KAO-CHA stability is controlled by KOH concentration and temperature, whereas KAO-EDI formation is promoted increasing KOH molarity and temperature. According to Mackinnon *et al*. (2006), at high temperatures (200-350 ºC), the dominant potassium aluminosilicate phase is either kalsilite or kaliophyllite depending on the starting composition. Syntheses at higher temperatures favour the feldspathoids such as leucite and analcime (e.g. Barrer and Marcilly, 1970). However, the synthesis of stable phases, such as kalsilite and leucite, at lower temperature (175 ºC) have been demonstrated in this study, different to what is reported by these authors.

5.3.2. Fourier Transform Infrared Spectroscopy

Figure 5.11 illustrates the FT-IR spectra of the raw KAO and as-synthesized products obtained after its hydrothermal treatment in KOH solutions. The characteristic peaks of KAO have not disappeared, but weakened after reacting with 1.33M KOH, while they disappeared after reacting with 3.99M KOH. At low KOH concentration and temperature (tests 41 and 43), the characteristic vibration bands of the original KAO just showed a small decrease with reaction time, but they tend to be preserved. However, increasing the KOH concentration, the IR vibration bands of KAO disappeared, accompanied by the appearance of new vibration bands as follows. In the region of 1200-850 cm^{-1}, a peak centred at 976 cm^{-1} (test 44) moved to a lower frequency (953 cm^{-1}, test 46) with reaction time. An additional peak (862 cm^{-1}, test 44) was seen at shorter reaction time. In the region of 850-550 cm^{-1}, a single peak at 696 cm^{-1} (tests 41 and 43) appeared using a low KOH concentration and temperature. However, two different peaks appeared using a high KOH concentration, 704 and 677 cm^{-1} (test 44), which shifted to higher (729 cm^{-1}) and lower (662 cm^{-1}) frequencies, respectively, with reaction time, accompanied by an additional peak at 594 cm^{-1} (test 46). In the region of 550-400 cm^{-1}, the vibration bands tended to disappear at high KOH concentration. At high temperature and low KOH concentration, peaks centred at 1007 and 874 cm^{-1} (test 47) disappeared and new weak peaks appeared with reaction time. At high temperature and KOH concentration, the synthesis products are characterized by much better IR absortion spectra (tests 50 and 52), with sharp peaks revealing a material with high grade of crystallinity, which has a very constant behaviour in spite of the reaction time. Several vibration bands particularly in the 850-550 cm^{-1} (T-O-T symmetrical stretching mode) and 550-400 cm^{-1} (T-O bending mode) regions can be attributed to the presence of kalsilite and leucite. The vibrations bands at 474, 564, 606, 682 and 964 cm^{-1} and at 461, 564 and 606 cm^{-1} can be assigned to the presence of kalsilite and leucite, respectively. These assignments correspond to the spectra reported by Dimitrijevic and Dondur (1995).

5.3.3. ^{29}Si and ^{27}Al Magic Angle Spinning Nuclear Magnetic Resonance

Figure 5.12 shows the ^{29}Si and ^{27}Al MAS NMR spectra of the raw KAO and representative synthesis products obtained using KOH as an activator agent. The ^{29}Si MAS NMR spectrum of KAO is given on Figure 5.12a shows two signals at -90.9 and -91.4 ppm corresponding to different but equally populated silicon sites in KAO. Figure 5.12b shows a spectrum with a sharp

peak centred at -91.2 ppm attributed to residual KAO that is superimposed on a broader resonance at -89.1 ppm, which can be presumably attributed to $Q^4(4Al)$ sites of KAO-CHA and is characteristic of amorphous or poorly crystallized materials. Two well resolved resonances at -85.2 and -89.0 ppm are distinguished in Figure 5.12c, indicating the presence of KAO-EDI and KAO-CHA, respectively. These peaks can be attributed to $Q^4(4Al)$ sites in the zeolite phases. Figure 5.12d shows a resonance at -85.3 ppm that can be attributed to $Q^4(4Al)$ sites in KAO-EDI (Si/Al ratio = 1.0). A weak signal - 91.3 ppm, revealing the presence of $Q^4(4Al)$ sites, corresponding with the presence of unreacted KAO. A single resonance at -85.8 ppm (Figure 5.12e) can be attributed to the presence of $Q^4(4Al)$ sites of kalsilite and leucite. Barbosa and MacKenzie (2003) have reported a similar signal for these potassium aluminosilicates in geopolymers. The ^{27}Al MAS NMR spectrum of the unreacted KAO (Figure 5.12a) consists of a single resonance at -3.4 ppm and is largely octahedral aluminium. Strong resonances at 57.6, 58.5, 60.7 and 59.8 ppm, respectively, can be assigned to tetrahedral Al in the framework of the zeolitic products (Figures 5.12b, 5.12c, 5.12d and 5.12e). However, in Figures 5.12b and 5.12d, weak signals at -4.0 and -4.2 ppm, respectively, correspond to the small amount of Al(6) due to residual KAO. The amount of Al(6) was greatest in KAO (Figure 5.12a) where the initial Al concentration was larger compared with that in the synthesis products (Figures 5.12b-5.12e). ^{29}Si and ^{27}Al MAS NMR results indicates that KAO was or total or partially dissolved (as revealed by the signals corresponding to residual KAO in some of the synthesis products), in agreement with XRD and FT-IR results.

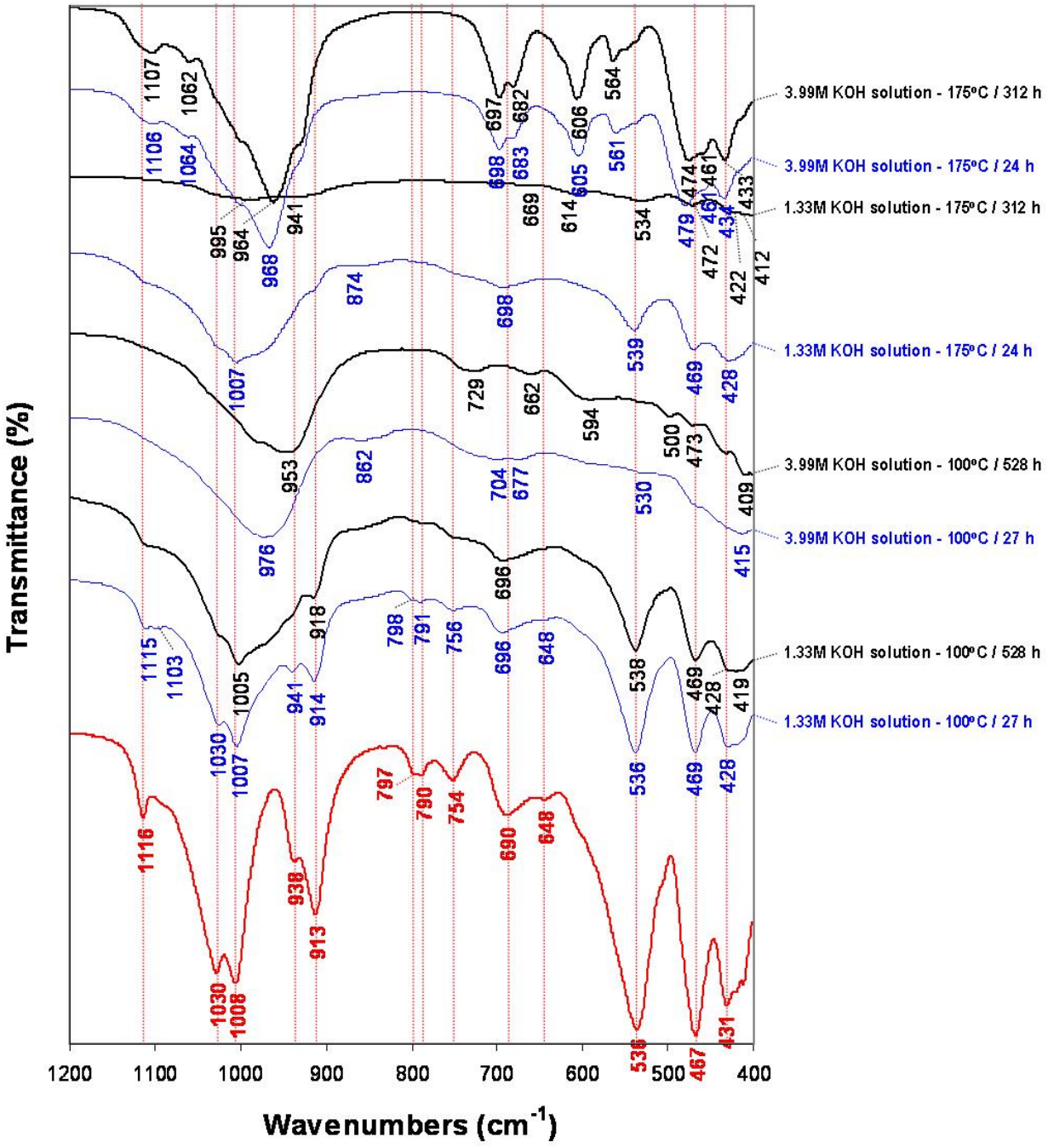

Figure 5.11. FT-IR spectra of the unreacted (in red) KAO and representative as-synthesized products obtained after hydrothermal reaction of KAO in KOH solutions.

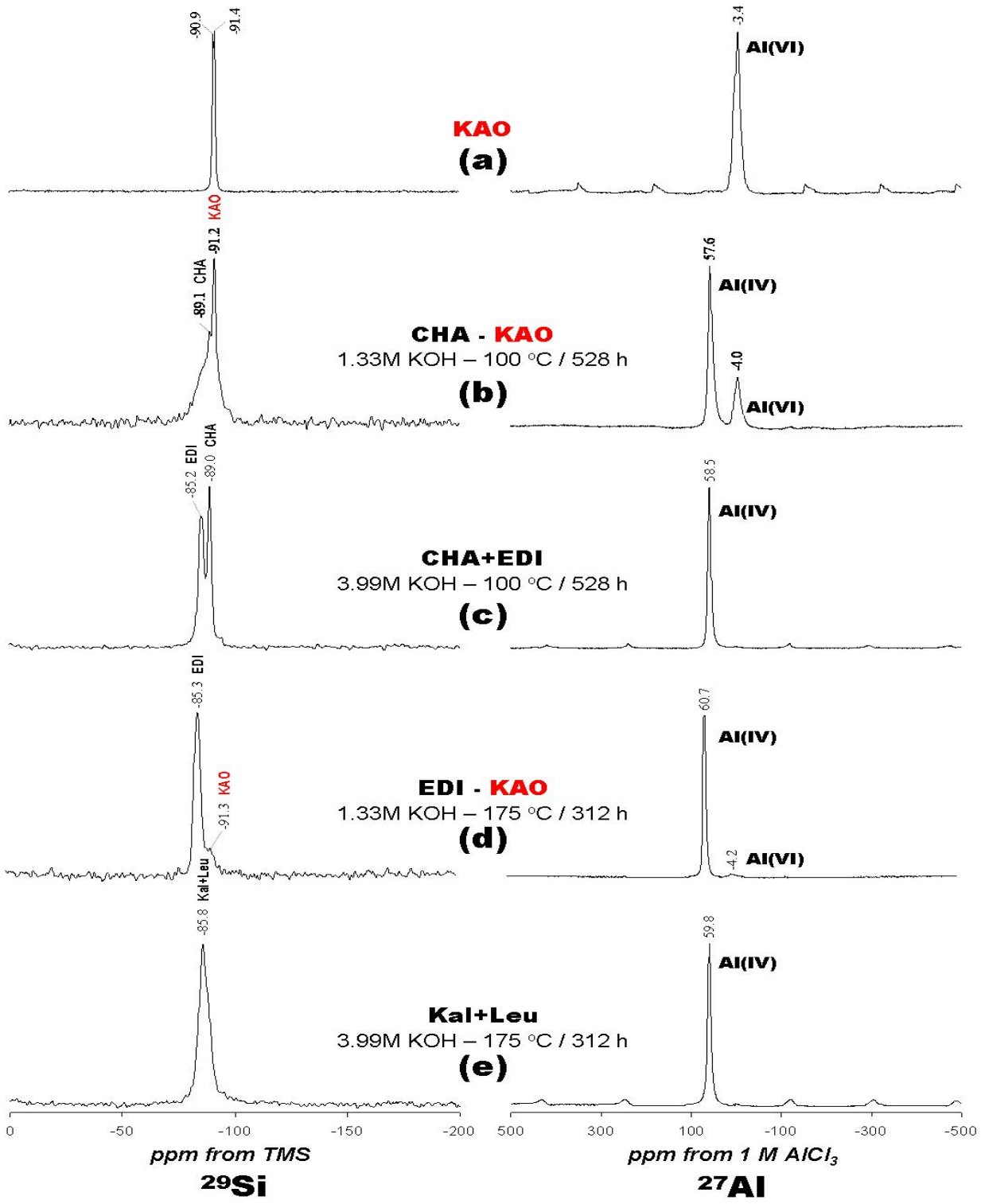

Figure 5.12. ^{29}Si and ^{27}Al MAS NMR spectra of the (a) raw KAO and (b-e) representative synthesis products obtained via hydrothermal treatment of KAO with KOH as mineralizer. Kal, kalsilite; Leu, leucite. Main phases are indicated in uppercase (except Kal and Leu) regular fonts, respectively; starting material phases in uppercase regular font (red colour).

5.3.4. Thermogravimetric analysis

Figure 5.13 shows TG/DTG curves obtained for representative as-synthesized products obtained after hydrothermal reaction of KAO in KOH solutions. The as-synthesized zeolitic materials show up to four dehydration steps, which could be explained as a consequence of water molecules dehydrated at lower temperatures that could re-enter the zeolite with or without affecting its framework linkages. The occurrence of a peak at 490 °C (Figure 5.13a) is attributed to the dehydroxylation of KAO still remaining in the synthesis product, which is not observed in Figure 5.13b.

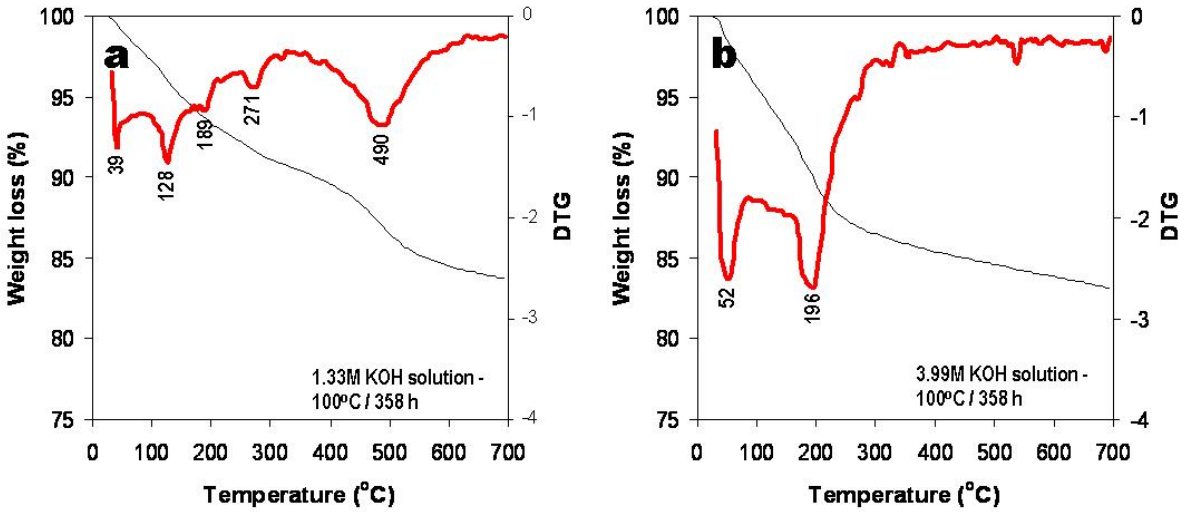

Figure 5.13. TG/DTG curves between 25-700 °C of representative synthesis products obtained after alkaline activation of KAO using KOH as mineralizer.

5.3.5. Summary

Experimental data from the syntheses in potassium aluminosilicate systems are contradictory and confusing. In addition, the nomenclature for potassium zeolites has evolved over a period of decades since the early discovery of hydrothermal synthesis routes by Barrer and co-workers.

The transformation of KAO in KOH solutions can be explained by two different processes: (1) dissolution and (2) precipitation. A dissolution process of a series of crystalline phases summarized by the reaction sequence KAO → KAO-CHA → KAO-EDI → unidentified potassium

aluminosilicate phase → kalsilite + leucite was identified in the system K_2O-SiO_2-Al_2O_3-H_2O. A similar sequence of phase transformation has not been reported in previous studies. In general, the synthesis products are characterized by the occurrence of a large amount of an amorphous aluminosilicate phase from which several crystalline phases formed, although with a low grade of crystallinity. Therefore, a higher concentration of KOH as an activating agent would be required, in relation to NaOH, in order to attack aluminosilicate phases from the starting KAO. In fact, a total dissolution of KAO was achieved with high KOH concentration and temperature, with an amorphous potassium aluminosilicate phase at shorter reaction times. Longer reaction times were required to obtain crystalline phases (zeolites), which display a low grade of crystallinity. Therefore, to achieve a similar level of attack on KAO with KOH compared to that using NaOH, it would be necessary to use higher KOH concentrations, alkaline solution/KAO ratios and longer reaction times, under controlled experimental conditions, to obtain the desired zeolitic phases.

5.4. Metakaolinite as a starting material

Table 5.3 summaries the starting reaction conditions for the conversion of MTK into zeolites by the classic hydrothermal treatment. MTK-LTA was the main crystalline phase obtained after conversion of MTK. However, similar to observations while using KAO as starting material, the synthesis products can be different according to the aqueous media (alkaline, fluoride and carbonate), being strongly dependent on experimental conditions. During the hydrothermal conversion of MTK, NaOH was more effective compared with the results obtained when a fluoride medium was used. The synthesis products formed by the conventional hydrothermal treatment method were MTK-LTA, MTK-SOD, MTK-CAN and traces of MTK-JBW and MTK-ANA. The hydrothermal reaction of MTK in the presence of aqueous fluoride media did not produce successful results, although traces of MTK-FAU, MTK-GIS and MTK-CHA crystallized. The conversion of MTK in the system CaO-SiO_2-Al_2O_3-H_2O promoted the formation of C-S-H phases, including MTK-TOB and MTK-HYD. As shown in Table 5.4, MTK-LTA was obtained using NaOH as an activator following the fusion approach.

Table 5.3. Synthesis conditions for the conversion of MTK into zeolitic materials using the conventional hydrothermal synthesis.

Test	Chemical reagents									L/S	Hydrothermal reaction		Molar gel composition	Zeolitic phases and other synthesis products	Residual phases
	H_2O (g)	NaOH (g)	KOH (g)	NaF (g)	NH_4F (g)	CaO (g)	SDA (g)	SiO_2 (g)	MTK (g)	(ml/g)	T / ºC	t / h			
1	18.00	0.96							2.67	7.10	100	22	$Na_2O:Al_2O_3:2SiO_2:84.2H_2O$	LTA, SOD, CAN	---
2	18.00	0.96							2.67	7.10	100	28	$Na_2O:Al_2O_3:2SiO_2:84.2H_2O$	LTA, SOD, CAN	---
3	18.00	0.96							2.67	7.10	100	52	$Na_2O:Al_2O_3:2SiO_2:84.2H_2O$	LTA, SOD, CAN	---
4	18.00	0.96						0.24	2.67	7.10	100	24	$Na_2O:Al_2O_3:2.3SiO_2:84.2H_2O$	LTA	---
5	18.00	0.96						0.24	2.67	7.10	100	48	$Na_2O:Al_2O_3:2.3SiO_2:84.2H_2O$	LTA	---
6	18.00	0.96						0.24	2.67	7.10	100	72	$Na_2O:Al_2O_3:2.3SiO_2:84.2H_2O$	LTA	---
7	18.00	0.96						0.24	2.67	7.10	100	96	$Na_2O:Al_2O_3:2.3SiO_2:84.2H_2O$	LTA	---
8	18.00	2.87						0.24	2.67	7.82	200	6	$3Na_2O:Al_2O_3:2.3SiO_2:86.2H_2O$	LTA, SOD, CAN, FAU, ANA	---
9	18.00	2.87						0.24	2.67	7.82	200	24	$3Na_2O:Al_2O_3:2.3SiO_2:86.2H_2O$	LTA, SOD, CAN, FAU, ANA	---
10	18.00	2.87						0.24	2.67	7.82	200	48	$3Na_2O:Al_2O_3:2.3SiO_2:86.2H_2O$	LTA, SOD, CAN, FAU, ANA	---
11	18.00	0.96					TPAB		2.67	7.10	100	22	$Na_2O:Al_2O_3:2SiO_2:0.5TPAB:84.2H_2O$	LTA, SOD, CAN	---
12	18.00	0.96					TPAB		2.67	7.10	100	28	$Na_2O:Al_2O_3:2SiO_2:0.5TPAB:84.2H_2O$	LTA, SOD, CAN	---
13	18.00	0.96					TPAB		2.67	7.10	100	52	$Na_2O:Al_2O_3:2SiO_2:0.5TPAB:84.2H_2O$	LTA, SOD, CAN	---
14	18.00	0.96					TEA		2.67	7.10	100	24	$Na_2O:Al_2O_3:2SiO_2:0.5TEA:84.2H_2O$	LTA, SOD, CAN	---
15	18.00	0.96					TEA		2.67	7.10	100	48	$Na_2O:Al_2O_3:2SiO_2:0.5TEA:84.2H_2O$	LTA, SOD, CAN	---
16	18.00	0.96					TEA		2.67	7.10	100	72	$Na_2O:Al_2O_3:2SiO_2:0.5TEA:84.2H_2O$	LTA, SOD, CAN	---
17	18.00	0.96					TEA		2.67	7.10	100	24	$Na_2O:Al_2O_3:2SiO_2:TEA:84.2H_2O$	LTA, SOD, CAN	---
18	18.00	0.96					TEA		2.67	7.10	100	48	$Na_2O:Al_2O_3:2SiO_2:TEA:84.2H_2O$	LTA, SOD, CAN	---
19	18.00	0.96					TEA		2.67	7.10	100	72	$Na_2O:Al_2O_3:2SiO_2:TEA:84.2H_2O$	LTA, SOD, CAN	---
20	18.00			1.01					2.67	7.12	100	360	$2NaF:Al_2O_3:2SiO_2:83.5H_2O$	FAU, GIS, CHA	MTK
21	18.00			1.01					2.67	7.12	100	600	$2NaF:Al_2O_3:2SiO_2:83.5H_2O$	FAU, GIS, CHA	MTK
22	18.00			1.01					2.67	7.12	100	840	$2NaF:Al_2O_3:2SiO_2:83.5H_2O$	FAU, GIS, CHA	MTK
23	18.00					4.90			3.00	7.63	175	0	$6.5CaO:Al_2O_3:2SiO_2:74H_2O$	P, CSH, Cal	---
24	18.00					4.90			3.00	7.63	175	0.5	$6.5CaO:Al_2O_3:2SiO_2:74H_2O$	P, CSH, C_2ASH_8, Cal	---
25	18.00					4.90			3.00	7.63	175	1	$6.5CaO:Al_2O_3:2SiO_2:74H_2O$	P, CSH, C_2ASH_8, C_4AH_{13}, Cal	---
26	18.00					4.90			3.00	7.63	175	1.5	$6.5CaO:Al_2O_3:2SiO_2:74H_2O$	P, CSH, C_2ASH_8, Cal	---
27	18.00					4.90			3.00	7.63	175	2	$6.5CaO:Al_2O_3:2SiO_2:74H_2O$	P, CSH, H, C_2ASH_8, Cal, Qtz	---
28	18.00					4.90			3.00	7.63	175	18	$6.5CaO:Al_2O_3:2SiO_2:74H_2O$	P, CSH, H, C_2ASH_8, α-C_2SH, Cal, Qtz	---
29	18.00					4.90			3.00	7.63	175	24	$6.5CaO:Al_2O_3:2SiO_2:74H_2O$	P, CSH, H, C_2ASH_8, α-C_2SH, Cal, Qtz	---

LTA, zeolite LTA; SOD, sodalite; CAN, cancrinite; JBW, JBW-type zeolite; ANA, analcime; FAU, faujasite; GIS, zeolite Na-P1; CHA, K-chabazite; zeolite Barrer-KF; P, portlandite; CSH, calcium silicate hydrate phase; H, hydrogarnet; T, tobermorite; α-C_2SH (Hartmann et al., 2007); C_2ASH_8 and C_4AH_{13} (Frías and Cabrera, 2002); Cal, calcite; Qtz, quartz. Weighed amounts of SDAs: TPAB (0.92 g), TEA (0.61-1.22 g); L/S, activator solution/MTK ratio.

Table 5.4. Synthesis conditions for the conversion of MTK into zeolitic materials using the alkaline fusion method.

Test	Chemical reagents to be fused				Alkaline fusion		FP:L	Aging	Hydrothermal reaction		Molar gel composition	Zeolitic phases and other synthesis products	Residual phases
	RM (g)		NaOH (g)	KOH (g)	T / ºC	t / h	(ml/g)	t / h	T / ºC	t / h			
30	*	6.20	7.44		600	1	4.9	5.5^s	60	24	$3.3Na_2O:Al_2O_3:2SiO_2:130.7H_2O$	LTA	---
31	*	6.20	7.44		600	1	4.9	5.5^s	60	48	$3.3Na_2O:Al_2O_3:2SiO_2:130.7H_2O$	LTA	---
32	*	6.20	7.44		600	1	4.9	5.5^s	60	96	$3.3Na_2O:Al_2O_3:2SiO_2:130.7H_2O$	LTA	---

LTA, zeolite LTA; L/FP, water/fused product; s stirring conditions.

5.5. Hydrothermal transformation of metakaolinite in the system Na_2O-SiO_2-Al_2O_3-H_2O

5.5.1. Chemical and mineralogical analyses

In Figure 5.14 the XRD patterns of MTK and the resulting as-synthesized products after its hydrothermal reaction with alkaline solutions are illustrated. The most important change observed in the XRD patterns is the appearance of the characteristic peaks of MTK-LTA, MTK-SOD and MTK-CAN with traces of MTK-JBW and MTK-ANA. The as-synthesized MTK-LTA has several common peaks located at 7.14°, 10.10°, 12.38°, 16.20°, 21.58°, 23.92°, 27.00°, 29.82° and 34.08° 2θ on its XRD pattern (Figure 5.14a). Figure 5.14b indicates that when precipitated SiO_2 was used at low temperature and NaOH concentration, the as-synthesized product is characterized by peaks corresponding to MTK-LTA at shorter reaction time (24 h), which tend to be constant, and disappear with reaction time to produce an amorphous aluminosilicate material (96 h). On the other hand, the addition of precipitated SiO_2 at high temperature and NaOH concentration (Figure 5.14c) produced a mixture of MTK-LTA, MTK-SOD, MTK-CAN, MTK-JBW and MTK-ANA, which show an almost constant crystallinity during the monitoring time. As occurred with KAO, the use of SDAs produced a reduction in the intensity of the peaks of MTK-LTA and associated phases (Figures 5.14d and 5.14e). Figure 5.14f shows the XRD patterns of the treated MTK following the fusion approach, which indicates that only MTK-LTA crystallized in spite of the hydrothermal reaction time, which indicates that this phase was stable over 24-96 h period.

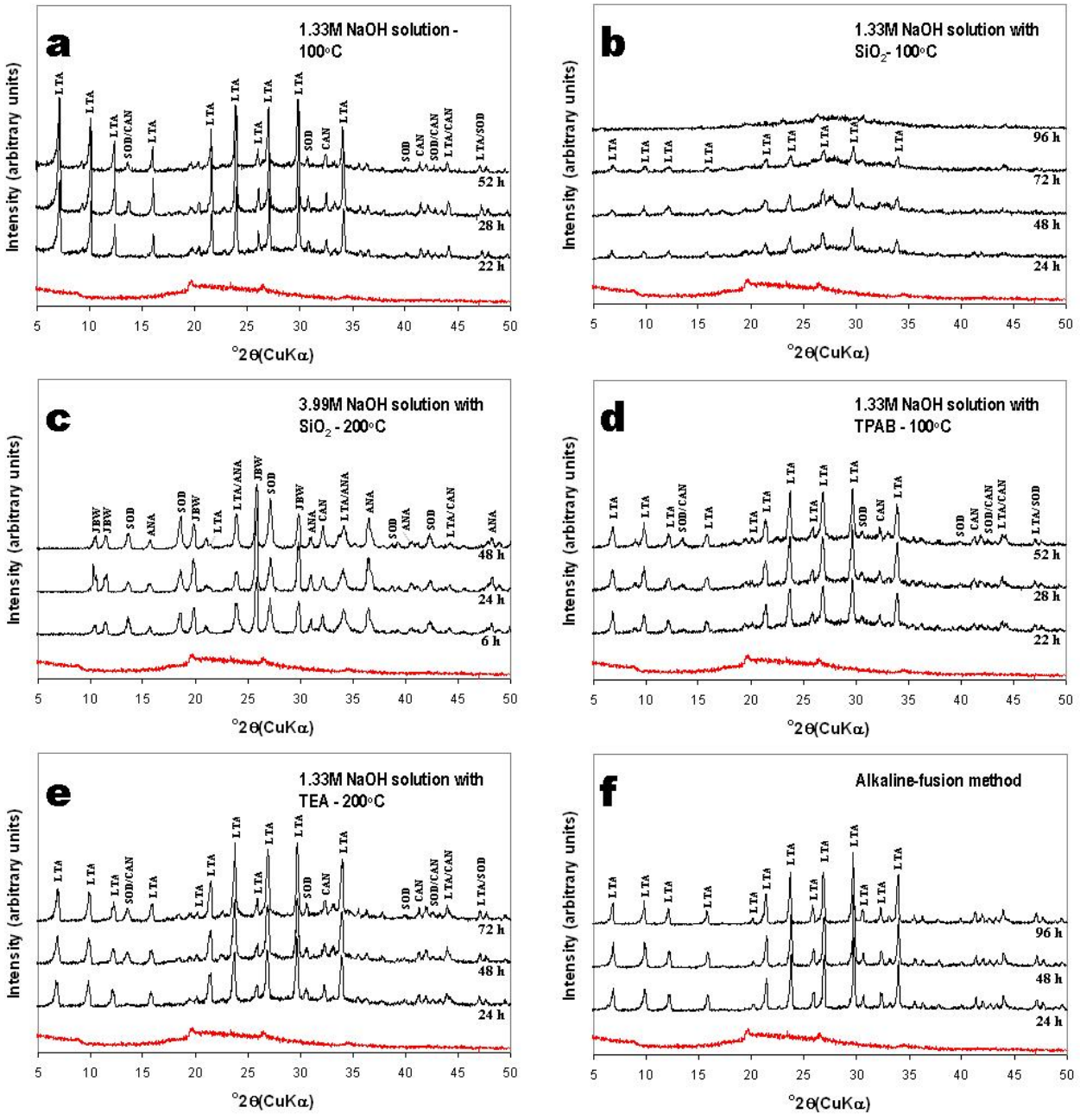

Figure 5.14. XRD patterns of the unreacted (in red) MTK and representative as-synthesized products obtained via (a-e) hydrothermal reaction of MTK in NaOH solutions with addition of SDAs or SiO_2 and (f) alkaline fusion method.

SEM images in Figure 5.15 illustrates several aspects on the occurrence of representative as-synthesized products obtained using MTK as a starting material, with cubic crystals of MTK-LTA as the main synthesis product.

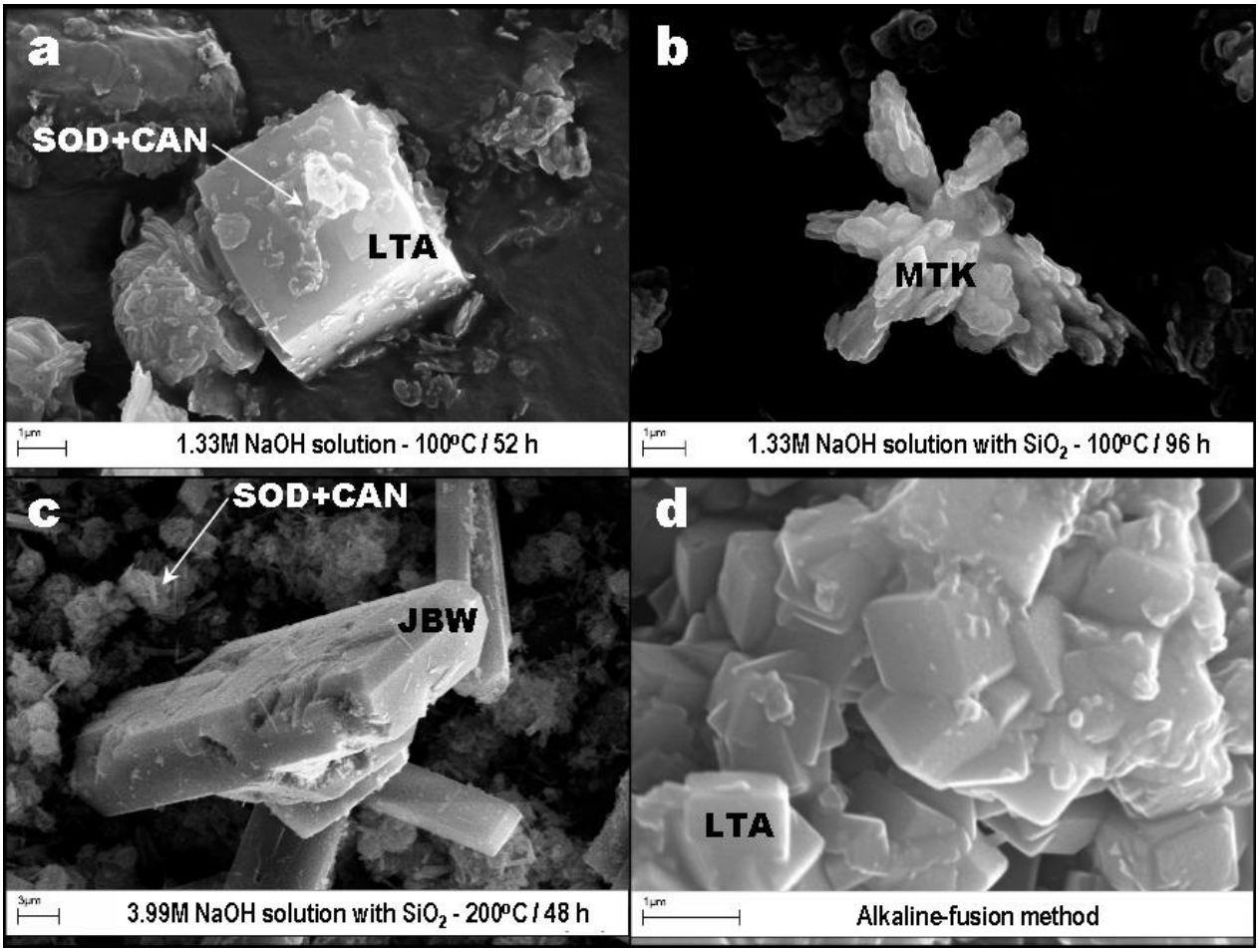

Figure 5.15. SEM images showing the occurrence of representative as-synthesized products obtained via (a-c) hydrothermal reaction of MTK in NaOH solutions and (d) alkaline fusion method with NaOH as an activator.

Lepispheric morphologies corresponding to MTK-SOD and MTK-CAN grow at the surface of cubic crystals of MTK-LTA (Figure 5.15a), which sometimes display interpenetrating twinning, at 1.33M NaOH solutions at 100 ºC for 52 h. Some deformed pseudohexagonal platelets of the original KAO still remain after its activation. When MTK was treated at low NaOH concentration and temperature with the addition of precipitated SiO_2, amorphous spheroidal morphologies, from which relicts of unreacted MTK (morphology showing distorted pseudohexagonal platelets) can be observed in a radial arrangement (Figure 5.15b). At higher NaOH concentration and temperature, a co-crystallization of MTK-SOD and MTK-CAN was followed by MTK-JBW formation (Figure 5.15c). Lin *et al*. (2004) described a similar relationship, describing a phase

transformation from zeolite LTA to JBW-type structure. However, in this study is suggested a phase transformation from metastable LTA to SOD- and CAN-type structures prior to JBW formation. Figure 5.16d illustrates the occurrence of MTK-LTA obtained by alkaline fusion of MTK followed by hydrothermal treatment, which is characterized by a cubic morphology with varying expression of facets and surface terraces, and occasionally intergrown twins with a particle size of 1 μm (average). This indicates that nuclei were formed in a slow and homogeneous way, with consequent uniform growth during the crystallization. Agger *et al*. (1998) first discussed the growth mechanisms of zeolite LTA crystals assessed by atomic force microscopy images, which revealed the occurrence of surface terraces of crystals; from the shape of these terraces, mechanisms based on terrace-ledge-kink growth were proposed.

5.5.2. Fourier Transform Infrared Spectroscopy

Figure 5.16 illustrates the FT-IR spectra of the unreacted and reacted MTK. The characteristic vibration bands of MTK disappeared, accompanied by the appearance of new peaks that reveal the occurrence of MTK-LTA. The band at 1047 cm^{-1} was shifted to lower frequency bands (at 973-980 cm^{-1}); the band at 800 cm^{-1} disappeared in the zeolitic products; the low intensity bands at 635 and 565 cm^{-1} were shifted to higher (at 673-690 cm^{-1}) and lower (at 530-538 cm^{-1}) frequency bands, respectively. The band at 424 cm^{-1} was shifted to lower frequency bands (at 411-417 cm^{-1}). The typical bands of MTK-LTA representing the asymmetric Al-O (973-980 cm^{-1}) and symmetric Al-O (673-690 cm^{-1}) stretches, double rings (530-538 cm^{-1}) in the framework structures of the zeolitic materials were observed and they show a constant intensity. In general, the activation of MTK resulted in a shift to lower wavenumbers, which indicates that there are more Al substitution in tetrahedral sites of the silica framework. The FT-IR peak width is an indication of the level of the crystallinity of the synthesis products. The alkaline fusion approach produced MTK-LTA (spectra 30 and 32 in Figure 5.16), which shows a much better defined IR spectra, with sharp peaks centred at 549-551 and 463-464 cm^{-1}, which reveals a pure synthesis product with higher crystallinity. This is in agreement with the XRD data. On the other hand, this can also be attributed to the occurrence of better defined structures (zeolite LTA) containing more Al in tetrahedral coordination as discussed below from NMR analysis.

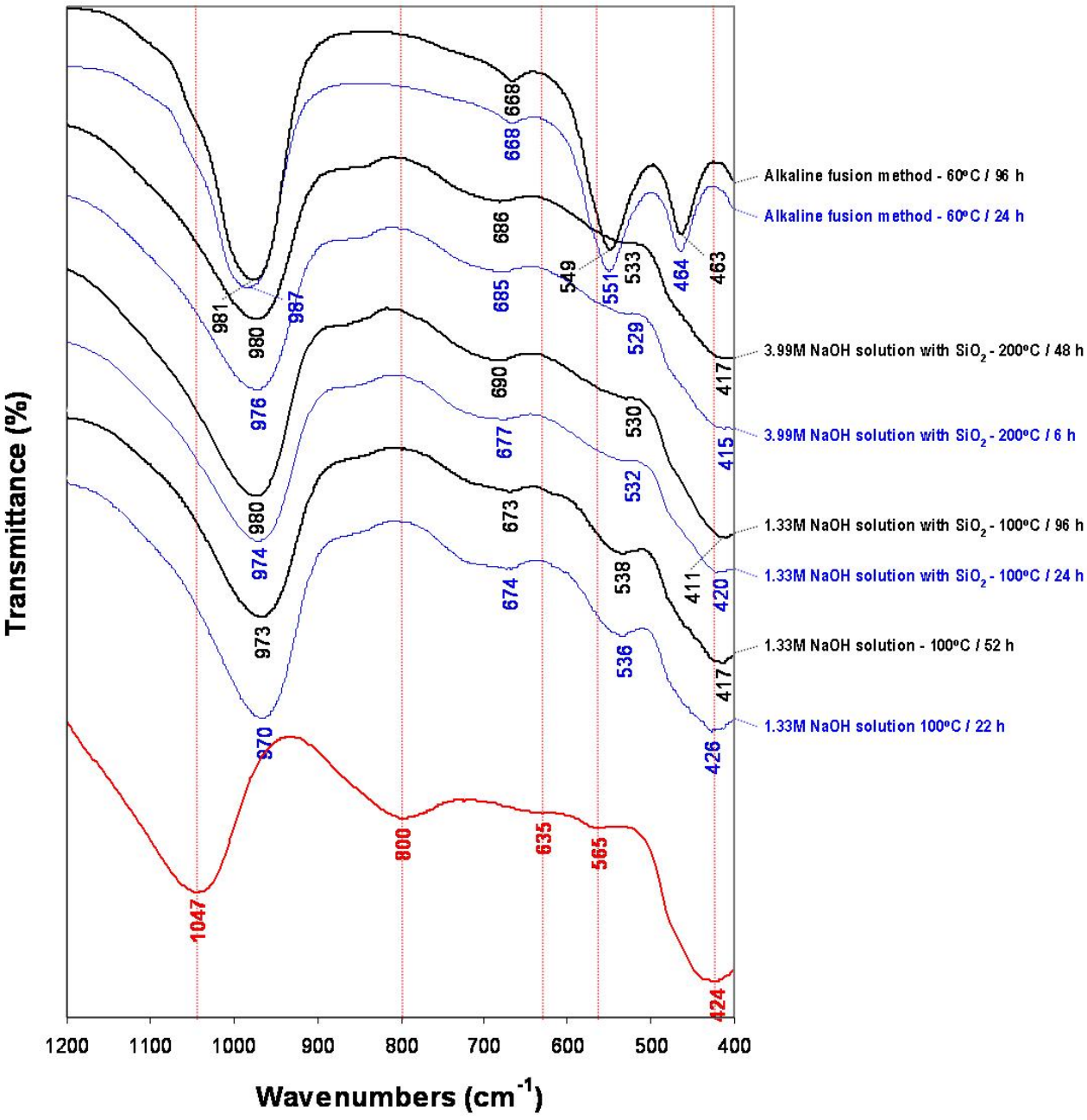

Figure 5.16. FT-IR spectra of the unreacted (in red) MTK and representative as-synthesized products obtained after alkaline activation of MTK using NaOH as mineralizer.

5.5.3. ^{29}Si and ^{27}Al Magic Angle Spinning Nuclear Magnetic Resonance

Figure 5.17 shows the ^{29}Si and ^{27}Al MAS NMR spectra of the MTK and representative synthesis

products obtained using NaOH as mineralizer. The ^{29}Si MAS NMR spectrum of MTK (Figure 5.17a) shows a broad single resonance centred at -96.3 ppm, attributed to a range of Q^4 environments. Figure 5.17b shows a sharp ^{29}Si signal at -89.5 ppm, which is characteristic of Q^4(4Al) sites in MTK-LTA, similar to that observed by Akolekar *et al*. (1997). A weak signal at -85.9.0 ppm can be attributed to the contribution of Q^4(4Al) sites of MTK-SOD and MTK-CAN. ^{29}Si NMR points out the change of the silica morphology from amorphous SiO_2 in MTK to crystalline SiO_2 in MTK-based aluminosilicates, with the total dissolution of the starting MTK to form zeolite-type structures and the incorporation of aluminium. The ^{27}Al MAS NMR spectrum of the unreacted MTK (Figure 5.17b) shows two resonances at -0.3 and 23.4 ppm can be attributed to 6- and 5-coordinated Al. Figure 5.17b shows a single resonance at 58.2 ppm, which can be assigned to tetrahedral Al in the zeolitic product.

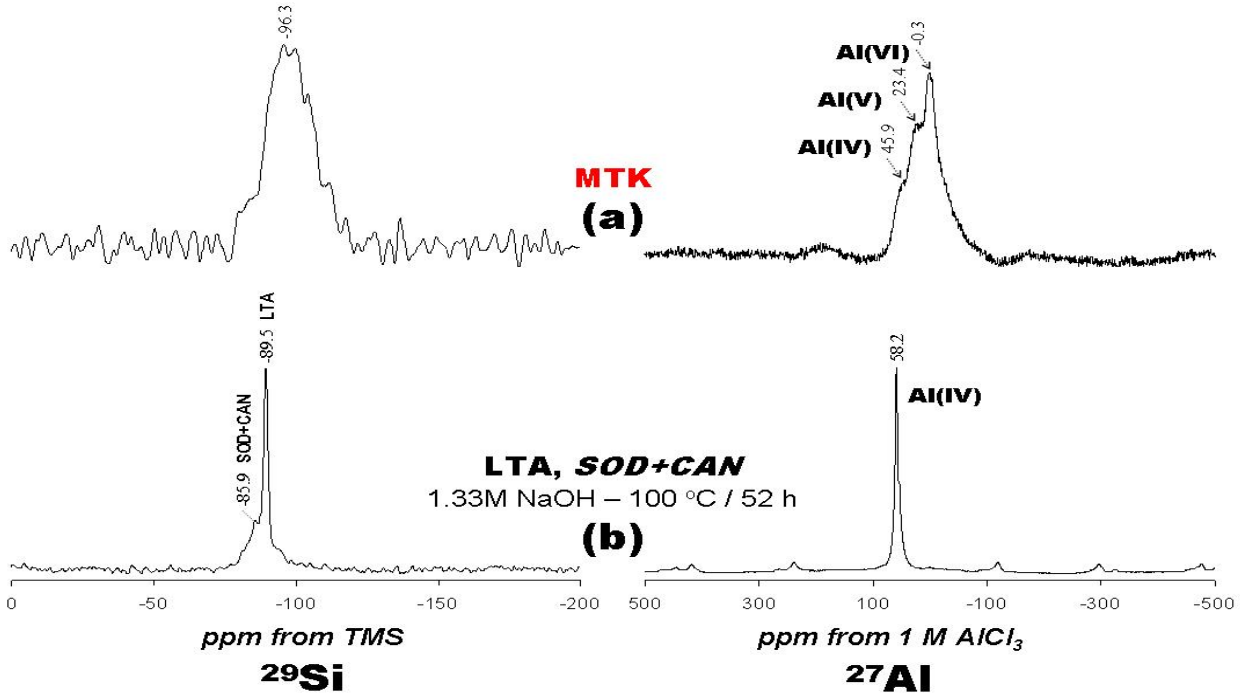

Figure 5.17. ^{29}Si and ^{27}Al MAS NMR spectra of the (a) raw MTK and (b) representative synthesis products obtained after hydrothermal reaction of MTK with NaOH as mineralizer. Main and minor phases are indicated in uppercase regular and italic fonts, respectively; starting material phases in uppercase regular font (red colour).

5.5.4. Thermogravimetric analysis

DTG curves of the MTK-based zeolitic materials (MTKZs) are shown in Figure 5.18. The as-synthesized products generally show two dehydration steps. The peaks observed between 39-52 ^{o}C correspond to surface water in zeolitic materials; the peaks observed between 100-162 ^{o}C indicate zeolitic water, although in some cases in this temperature range up to two peaks occur, which can be explained by the heterogeneous nature of the as-synthesized products. The synthetic zeolitic products obtained after hydrothermal transformation of MTK in solutions of 1.33M NaOH at 100 °C for 52 h shows the highest weight loss (19.48%).

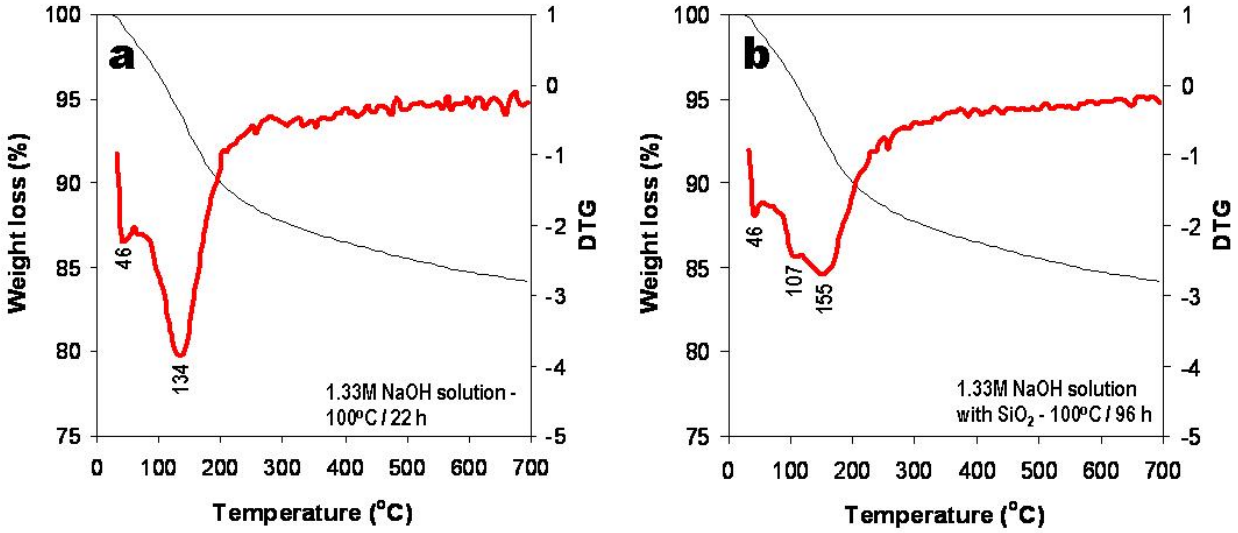

Figure 5.18. TG/DTG curves between 25-700 ^{o}C of representative synthesis products obtained after alkaline activation of MTK using NaOH as mineralizer.

5.5.5. Summary

Zeolite LTA was successfully synthesized after alkaline hydrothermal treatment of MTK. However, the synthesis product was controlled by the experimental method, taking into account that the classic hydrothermal transformation of MTK produced a mixture of different zeolite-type structures, whereas the alkaline fusion approach promoted the crystallization of pure MTK-LTA. The addition of precipitated SiO_2 at low NaOH concentrations and temperature produced only MTK-LTA, although with a constant low grade of crystallinity and the presence of an amorphous aluminosilicate phase at longer reaction times. However, using this silica source at high NaOH

concentrations and temperature, several crystallinity phases (MTK-LTA, MTK-SOD, MTK-CAN, MTK-JBW and MTL-ANA) were obtained. The use of SDAs produced a reduction in the intensity of the peaks of MTK-LTA and associated phases. The alkaline activation of MTK following the fusion approach favoured the crystallization of pure MTK-LTA stable for 96 h of monitoring time. This synthesis product is characterized by a high grade of crystallinity and uniform crystal size distribution (1.0 μm).

5.6. Hydrothermal transformation of kaolinite and metakaolinite in the system $CaO\text{-}SiO_2\text{-}Al_2O_3\text{-}H_2O$

The structure and properties of C-S-H phases, typically found in hydrated Portland cement products, has been the subject of considerable research for decades (Taylor, 1990). The C-S-H system is highly complex and is comprised of crystalline to amorphous phases with variable composition that build up a wide family of phases, which are interesting for the variety of their structural arrangements, the peculiarity of the transformation processes in which they are involved and the relationships with compounds which form during the hydration of the Portland cement (Bonaccorsi and Merlino, 2004). On the other hand, $Ca(OH)_2$ (portlandite) is formed in large quantities as one of the cement hydration products and easily reacts with reactive aggregates or glasses. A blended cement consisting of Portland cement and pozzolan is desirable, because the pozzolanic reaction is effective in decreasing the quantity of $Ca(OH)_2$, increasing the ultimate strength and conserving energy in production.

The synthesis of C-S-H phases, hydrogarnet (HYD) and tobermorite (TOB) has been investigated from a range of starting materials and industrial by-products (Coleman, 2005). However, several studies have been carried out on the hydrothermal transformation of KAO or MTK into cement hydrates. From the different hydrated calcium silicates which occur in nature as hydrothermal alteration products of calcium carbonate rocks and as vesicle fillings in basalts, particular attention has focused on TOB, which can also be easily synthesized in hydrothermal conditions (Siauciunas and Baltusnikas, 2003). The interest in the structure and crystal chemistry of the minerals of the TOB group stemmed from their close relationships with the C-S-H phases formed during the hydration processes of Portland cement (Taylor, 1992; 1997). The present study examines the hydrothermal synthesis of C-S-Hs from KAO and MTK at 175 ºC for

24 h in the system $CaO\text{-}SiO_2\text{-}Al_2O_3\text{-}H_2O$, which is especially important in cement chemistry, establishing the reaction sequence and nature of the phases formed.

5.6.1. Chemical and mineralogical analyses

The XRD patterns and assignments of the peaks of original KAO and MTK and their synthesis products are presented in Figure 5.19. It is evident that C-S-H forming reactions of C-S-Hs started very rapidly, after hydrothermal reaction of the starting materials.

Figure 5.19a shows that the characteristic reflection peaks of KAO (at 12.34° and 24.64° 2θ) decreased with reaction time. $Ca(OH)_2$ and C-S-H were the main phases identified at 0 h, along with relicts of KAO. The amount of $Ca(OH)_2$ increased with curing time and reached a maximum after 1 h. KAO-HYD and C-S-H were the reaction products formed after 1.5 h of treatment, with the maximum and minimum amounts of KAO-HYD and C-S-H, respectively, after 24 h. KAO-HYD did not disappear after 24 h of treatment, and the formation of KAO-TOB was observed after 2 h and its amount increased gradually with reaction time. During the last stages of reaction, $\alpha\text{-}C_2SH$, as reported by Hartmann *et al*. (2007), and calcite also appeared. In Figure 5.19b the XRD patterns of MTK and the resulting as-synthesized products after hydrothermal reaction with CaO solutions are illustrated. MTK showed a poor crystalline nature, with low-intensity peaks corresponding to quartz and muscovite, and was characterized by the appearance of an amorphous aluminosilicate (see the broad hump at 2θ = 13-33°). According to Ríos *et al*. (2007) this persists between 600-950 ^oC, with relicts of the original KAO and mullite as the main crystalline phase at 1000 ^oC. After MTK/lime reaction, the most important hydrated phases were $Ca(OH)_2$, MTK-HYD, C_2ASH_8 and C_4AH_{13} at the early stages. Metastable phases, such as C_2ASH_8 and C_4AH_{13} were also reported by Frías and Cabrera (2002). C-S-H, $\alpha\text{-}C_2SH$, MTK-HYD and MTK-TOB were observed at the late stages.

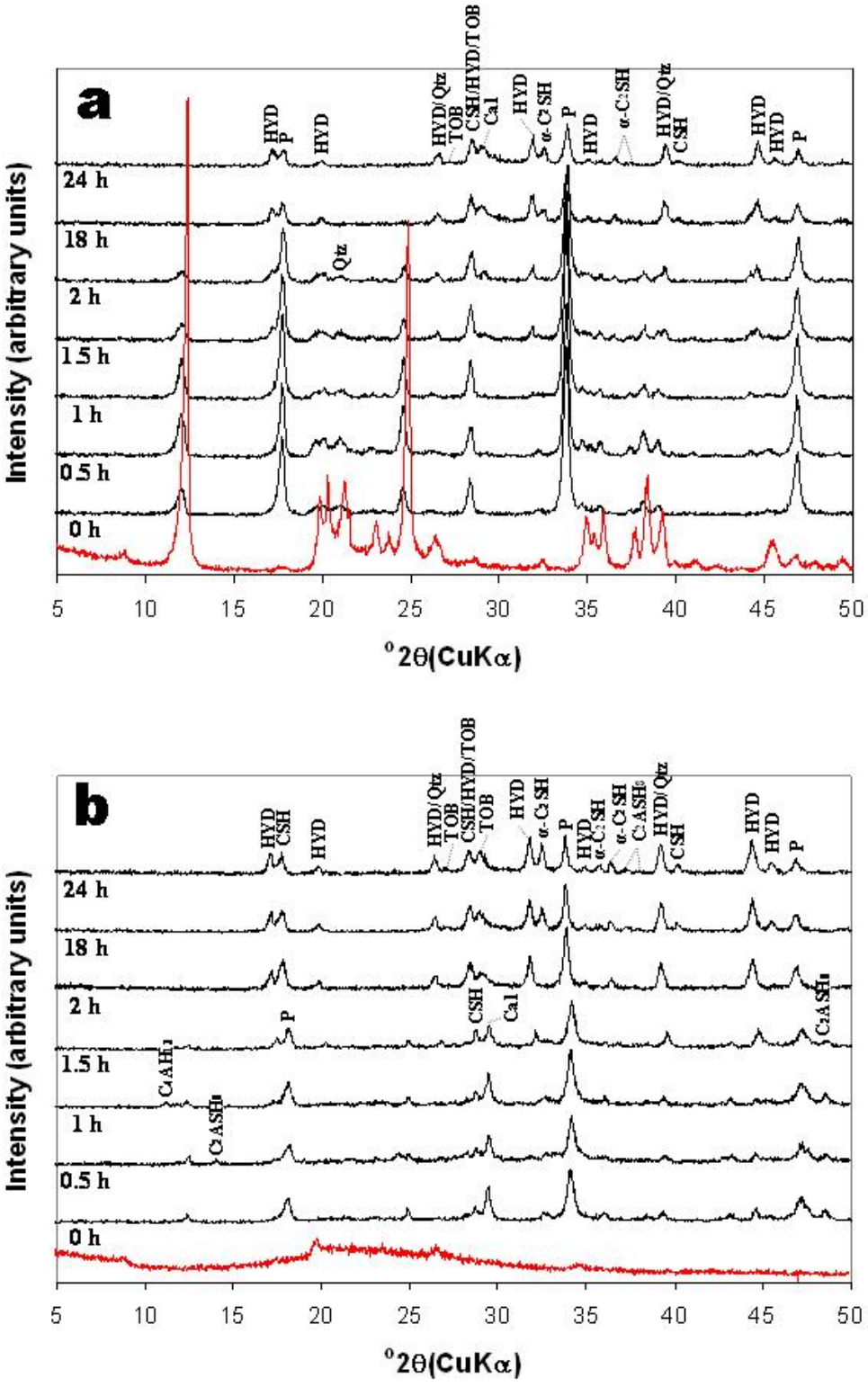

Figure 5.19. XRD patterns of representative as-synthesized products obtained after hydrothermal treatment of: (a) KAO and (b) MTK with CaO at 175 ºC for a monitoring time of 24 h. XRD patterns of the raw materials are indicated in red.

It is evident that in the investigated systems, HYD invariably appeared before 11 Å TOB, as reported in previous studies. However, the occurrence of metastable phases, such as C_2ASH_8 and C_4AH_{13}, remains unclear. It is suggested that they were quickly converted to MTK-HYD, followed by MTK-TOB, with curing time. Le Saoût *et al*. (2006) reported the occurrence of the polymorphs of $CaCO_3$ (calcite and aragonite), with calcite as the main crystalline material at the surface. Our XRD analysis did not detect it due to its very small crystal size, although the thermogravimetric analysis reveals the presence of $CaCO_3$, as will be discussed later. The occurrence of $CaCO_3$ can be explained by dissolution of carbon dioxide in the solution producing CO_3^{2-} ions, which react with Ca^{2+} (Le Saoût *et al*., 2006), and the Ca^{2+} ions required by these reactions are obtained by the dissolution of C-H and by lowering the Ca/Si ratio of the C-S-H (Taylor, 1997).

XRD reveals that several poorly crystalline materials, with un-reacted $Ca(OH)_2$ occurred at shorter reaction times. HYD was always among the first phases formed and invariably appeared before 11 Å TOB. However, later, with increasing reaction time, they started to fracture and their quantity reduced almost in half for 24 h. With increasing reaction time, HYD tended to undergo breakdown and its amount decreased and finally disappeared; CaO present in the further reaction with SiO_2 formed C-S-Hs, and released Al^{3+} ions were inserted into the Al-substituted TOB crystal lattice (Siauciunas and Baltusnikas, 2003). Different research groups have classified C-S-Hs based on morphological and chemical data to compensate for scarce structural data. Taylor (1990) classified C-S-H as C-S-H(I) and C-S-H(II) based on the Ca:Si ratio, with C-S-H(I) being obtained with Ca:Si<1.5 and C-S-H(II) produced using Ca:Si>1.5. Therefore, it is considered that C-S-H(II) is the metastable phase that coexists with HYD and TOB, taking into account that a ratio Ca:Si>1.5 used to prepare gel compositions, as precursors of the synthetic C-S-H phases obtained in the present study.

Figure 5.20 shows SEM images of representative as-synthesized products autoclaved at 175°C for 0 and 24 h. Synthesis products obtained from KAO/lime mixtures are characterized by the occurrence of flaky crystals of relict KAO associated with C-S-H (Figure 5.20a) and progressively with reaction time the breakdown of KAO-HYD, which in general shows an apparently intact surface, as shown in Figure 5.20b. The typical octahedral morphology of MTK-HYD occurring in twinned crystals, developing clusters, obtained after MTK/lime mixtures is illustrated in Figure 5.20c, whereas with reaction time MTK-TOB with a typical 'Hebel' microstructure (intergrown bladelike crystals) grew onto the MTK-HYD (rounded morphology) surface prior to its breakdown (Figure 5.20d).

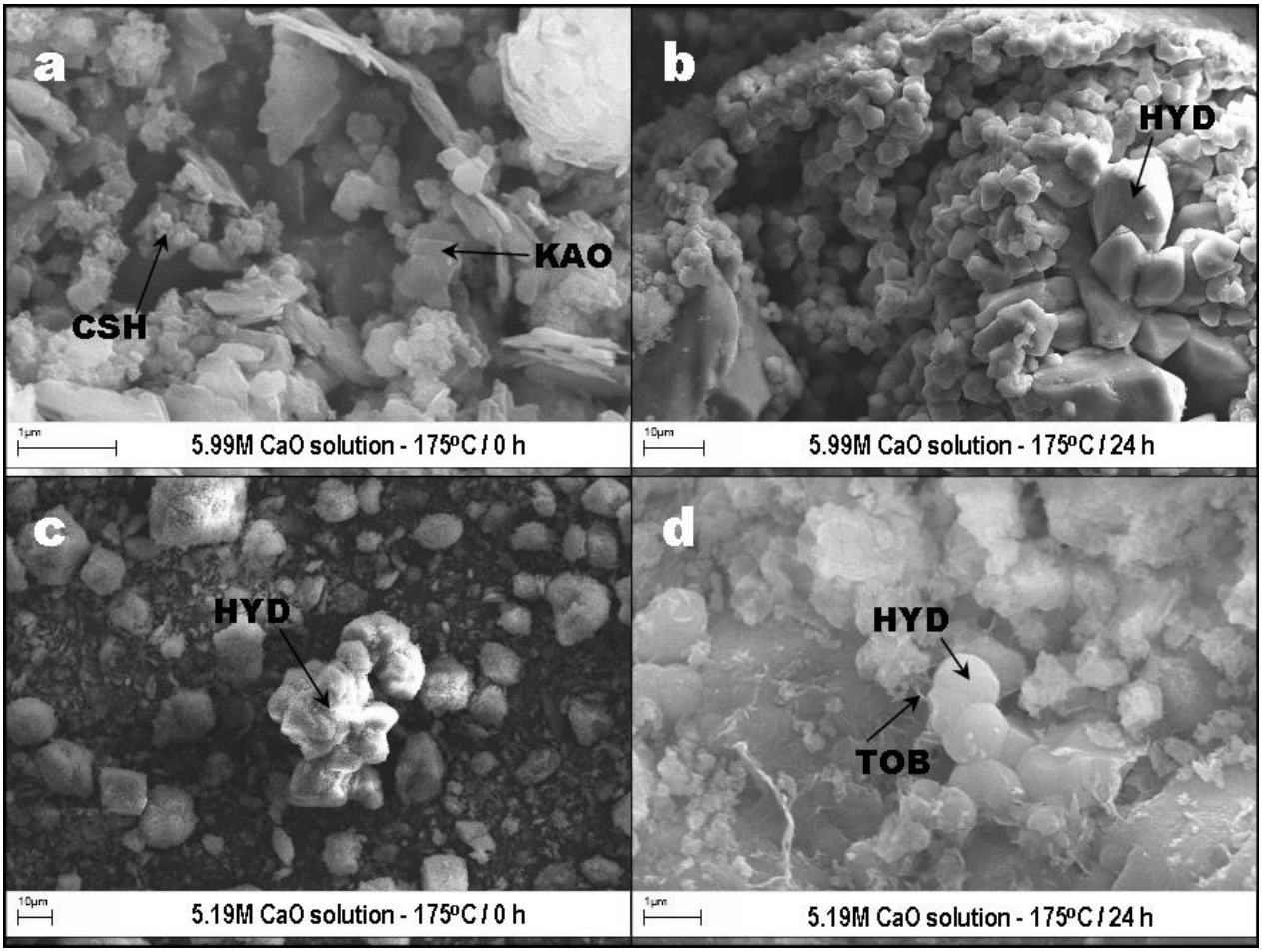

Figure 5.20. SEM images showing the morphology of representative as-synthesized hydrated phases obtained after hydrothermal treatment of (a-b) KAO and (c-d) MTK in CaO solutions.

5.6.2. Fourier Transform Infrared Spectroscopy

The structure of C–S–H gel is very complex. FT-IR has been found to be very useful in delineating the complex chemistry involved in the cement due to the poor crystallinity of silicate hydrates (Yu *et al*., 1999). The FT-IR spectra in the region of 1200-400 cm^{-1} of the as-synthesized products from the two investigated mixtures are illustrated in Figure 5.21.

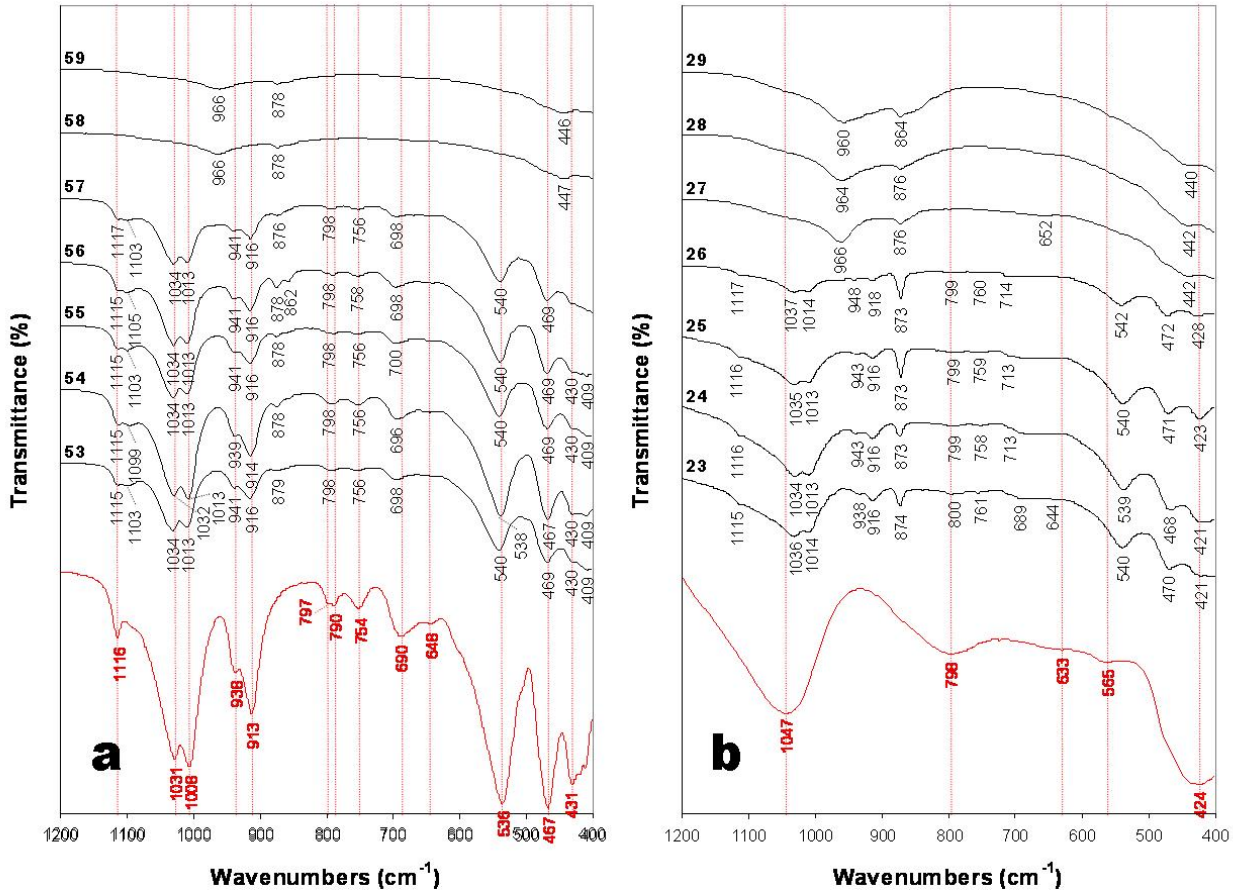

Figure 5.21. FT-IR spectra of the raw materials (in red) and representative as-synthesized products obtained after the hydrothermal treatment of: (a) KAO and (b) MTK with CaO as an activator at 175 ºC for 24 h. The numbers indicating XRD patters correspond to the first column (Test) in Tables 5.1 (KAO) and 5.3 (MTK).

The broad band centred at 1115–1117 cm^{-1} suggests the presence of C–S–H gels. This band decreases in intensity and exhibits a slight shift to lower frequencies with reaction time, and disappeared after 1.5 h. Al–O stretching vibrations of tetrahedral AlO_4 groups lie at 1020–990 cm^{-1}. The band at 970 cm^{-1} is attributed to Si–O stretching vibrations in C–S–H gels with jennite type structure (Hidalgo *et al*., 2007). The shoulder at 914-918 cm^{-1} may be assigned to OH bending vibrations in Al–OH–Al bonds (octahedral aluminium). The band appearing at 798-800 cm^{-1}, which is assigned to stretching vibrations modes of O–T–O groups (T=Al, Si), is attributed to polymerization and Si replacement by Al in tetrahedral sites of C–S–H. The bands at 873-879 and 696-700 cm^{-1} can be attributed to calcite.

5.6.3. ^{29}Si and ^{27}Al Magic Angle Spinning Nuclear Magnetic Resonance

Hydration phases, such as calcium hydroxide (C-H) and calcium-silicate-hydrate (C-S-H) are closely linked, although C-H and C-S-H are considered as crystalline and nearly amorphous materials, respectively. Therefore, its structure must be studied by other methods and/or by analogy with natural or synthetic minerals, such as zeolites. Some information on the structure of these compounds can be obtained by MAS NMR. ^{29}Si and ^{27}Al MAS NMR were performed on CaO-activated raw materials, revealing important information on the structure of the as-synthesized hydrated phases, as shown in Figures 5.22 and 5.23.

The ^{29}Si and ^{27}Al MAS NMR spectra of KAO and its synthesis products are presented in Figure 5.22. The ^{29}Si MAS NMR spectrum of KAO (Figure 5.22a) shows a single resonance centred at -91.4 ppm, which is characteristic of a layered silicate and assigned to Si linked via oxygens to three other Si atoms (Rocha and Klinowski, 1990; Jiugao *et al*., 1997). The chemical shift values in the ^{29}Si MAS NMR spectra of the treated KAO for 0 and 24 h are illustrated in Figures 5.22b and 5.22c, respectively, indicating the occurrence of silicon sites of several C-S-H phases and residual KAO. A single resonance line at -91.3 ppm is observed in Figure 5.22b, which can be attributed to the silicon site Q^4(3Al) of the unreacted KAO, whereas three resonance lines at -79.5, -85.3 and -91.0 ppm were recognized in Figure 5.22c, which according to previous studies (Wieker *et al*., 1982; Komarneni *et al*., 1985) can be assigned to the silicon sites Q^1, Q^2(1Al) and Q^3(1Al) of C–S–H phases, respectively. The signal at -91.0 ppm can be attributed to the presence of KAO-HYD and therefore are no related with relict KAO, taking into account that this clay mineral was completely dissolved after 24 h of curing. A similar resonance peak was reported by Rivas *et al*. (2007), who ascribed the presence of a ^{29}Si NMR peak at -89.5 ppm to the formation of $[SiO_4]_4$ groups in hydrogarnet. According to them, this signal corresponded to isolated $[SiO_4]$ groups in Q^0(4Al) environments. The presence of a tobermorite-type structure is confirmed by the resonance peak at -85.3 ppm, in agreement with ^{29}Si MAS NMR data reported by Komarneni *et al*. (1985) on tobermorite that showed resonances at -85.7 and -95.7 ppm representing chain middle groups (Q^2) and branching sites (Q^3), respectively. The ^{27}Al MAS NMR spectrum in Figure 5.22a consists of a single resonance at -3.4 ppm that is assigned to 6-coordinated Al in KAO. ^{27}Al MAS NMR spectra of the treated KAO (Figures 5.22b and 5.22c), with a single resonance at -3.7 ppm (Figure 5.22b) attributed to 6-coordinated Al and three resonance lines at 2.0, 11.6 and 55.4 ppm (Figure 5.22c); the double peak (composed by the first two resonances) is assigned to 6-coordinated Al, while the last one is attributed to 4-coordinated Al. The occurrence of KAO-TOB in the synthesis products obtained after 24 h of

curing is confirmed by the signal at 55.4 ppm, which has been reported by Komarneni *et al*. (1985).

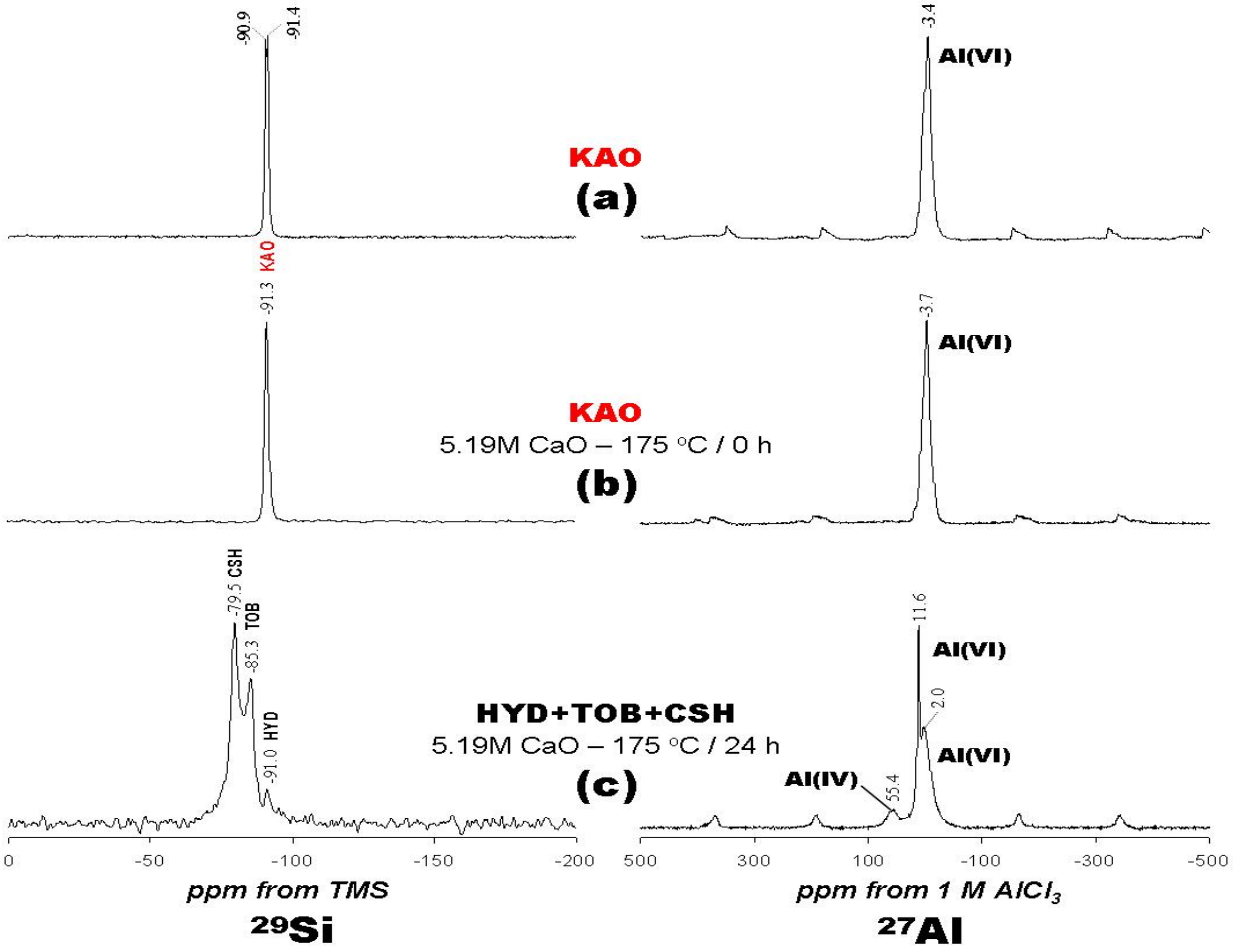

Figure 5.22. ^{29}Si and ^{27}Al MAS NMR spectra of the (a) raw KAO and (b-c) representative synthesis products obtained after alkaline activation of KAO with CaO as an activator. Main phases are indicated in uppercase regular fonts; starting material phases in uppercase regular font (red colour).

The ^{29}Si and ^{27}Al MAS NMR spectra of MTK and representative synthesis products are given in Figure 5.23. The ^{29}Si MAS NMR spectrum of MTK (Figure 5.23a) displays a broad resonance in the chemical shift range from -75 to -125 ppm, centred at -96.3 ppm, which can be assigned to the variety of silicon sites with Si linked to four other Si atoms in silica polymorphs (Smith and Blackwell, 1983) and indicates the presence of amorphous silica (Hartmann *et al*., 2007). According to Mackenzie *et al*. (1985), when KAO is dehydroxylated, the Si atoms undergo a range of environments of different distortion and the broadness of the MTK line is attributed to these variations in the Si-O-Si(Al) bond angles. The chemical shift values of the ^{29}Si MAS NMR spectra of the treated MTK for 0 and 24 h are illustrated in Figures 5.23b and 5.23c, respectively. A single resonance line at -91.2 ppm is observed in Figure 5.23b, being attributed to Q^0(4Al) environments of MTK-HYD, which was quickly formed, whereas two resonance lines at -79.4 and -85.6 ppm attributed to the silicon sites Q^1 and Q^2(1Al) of C-S-H phases were observed in Figure 5.23c, with the second one attributed to the presence of a tobermorite-type structure. The ^{27}Al MAS NMR spectrum of MTK (Figure 5.23a) displays two other resonances at -0.3 ppm (assigned to 6-coordinated Al) and 23.4 ppm (attributed to 5-coordinated Al), which are, however, different compared with those reported by Rocha and Klinowski (1990) and Jiugao *et al*. (1997). The broader and asymmetrical peak shapes of MTK show its disordered structure (Liu *et al*., 2001). ^{27}Al MAS NMR spectra of the treated MTK show a single resonance at -1.9 ppm (Figure 5.23b) attributed to 6-coordinated Al and three resonance lines at 3.9, 11.7 and 55.6 ppm (Figure 5.23c); the double peak (composed by the first two resonances) is assigned to 6-coordinated Al, while the last one is attributed to 4-coordinated Al. The last of these peaks confirms the presence of MTK-TOB.

^{29}Si MAS NMR data reveal that silicon of the raw materials is completely converted with reaction time into C-S-H phases, including HYD and TOB. 11 Å TOB exhibits two resonances at -85.7 and -95.7 ppm attributed to chain middle group (Q^2) and branching site (Q^3) (Wieker *et al*., 1989). It is considered that the resonances at -85.3 (Figure 5.22c) and -85.6 (Figure 5.23c) ppm can be assigned to 11 Å KAO-TOB. However, the lack of the resonance at -95.7 ppm reported by Wieker *et al*. (1989) in Figures 5.22c and 5.23c can be explained by an overlapping of resonances corresponding to different C-S-Hs. Komarneri *et al*. (1985) showed that the substitution of aluminium in TOB caused a low field shift of the Q^3 units from -95.7 to -91.5 ppm, which can also explain the occurrence of the resonance at -91.0 ppm in Figure 5.22c. ^{27}Al MAS NMR data indicate the appearance of KAO-TOB at longer reaction time (24 h), although it is

difficult to suggest the occurrence of Al-substituted KAO-TOB or other Al-substituted C-S-H phase, as reported by other studies (Komarneni *et al*., 1985; Smith and Blackwell, 1983; Mackenzie *et al*., 1985; Faucon *et al*., 1998; Liu *et al*., 2001). The ^{29}Si and ^{27}Al MAS NMR data were in agreement with the XRD and FT-IR analysis.

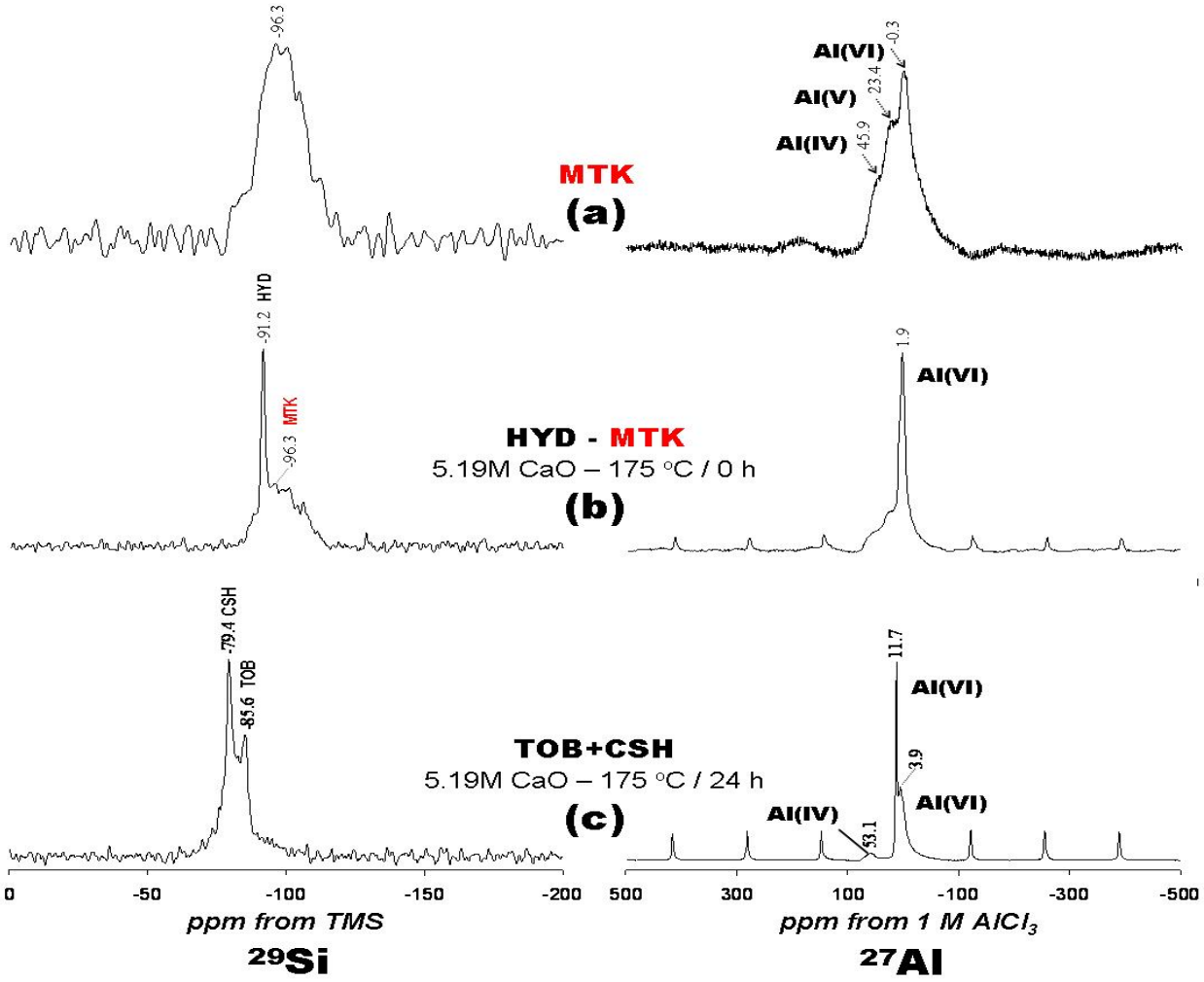

Figure 5.23. ^{29}Si and ^{27}Al MAS NMR spectra of the (a) raw MTK and (b-c) representative synthesis products obtained alkaline activation of MTK with CaO as an activator. Main phases are indicated in uppercase regular fonts; starting material phases in uppercase regular font (red colour).

5.6.4. Thermogravimetric analysis

Thermogravimetry (TG) and derivative thermogravimetry (DTG) are valuable tools for evaluating the nature of hydration products according to different stages of cement hydration, as well as quantifying the different phases (Fordham and Smalley, 1985; Chandra and Flodin, 1990; Ollitrault-Fichet *et al*., 1998; Tisivilis *et al*., 1998; Dweck *et al*., 2000). The identity of the amount of the hydrated phases was estimated from thermogravimetric analysis, as illustrated in Figure 5.24. Hydration products, mainly C-S-H gel and portlandite ($Ca(OH)_2$), are the result of hydration of the main components of cement. The hydration rate of cement can be evaluated by measuring the mass loss of hydrated compounds $\leq$700 °C. Different DTG peaks or temperature ranges were obtained when the C-S-H gel was heated between 25-700 ^oC: 100 °C, dehydration of pore water; 100-250 ^oC, different stages of C-S-H dehydration; ~250-350 ^oC, presence of a member of the HYD group; ~350-500 ^oC, decomposition of $Ca(OH)_2$; ~500 °C, dehydroxylation of $Ca(OH)_2$; ~573 ^oC: crystalline inversion of quartz; ~700 °C, decarbonation of $CaCO_3$. Much water is released between 100-250 ^oC, when the C-S-H gel began to decompose. According to Klimesch and Ray (1998), HYD amount increased slightly up to 2 h, followed by a decrease, clearly demonstrating that this phase was decomposed and consumed with reaction time. C-S-H formation was enhanced with the use of the MTK/lime mixture as indicated by the size and presence of several endotherms, compared with the other two mixtures, which indicates that the SiO_2 source originating from MTK is more reactive than that from precipitated SiO_2 and KAO. MTK-TOB appeared after 2 h of autoclaving and increased with reaction time. However, the addition of MTK to the mixture promoted a decrease in MTK-TOB formation. A weight loss of 23.36 and 27.06% was obtained when KAO and MTK, respectively, were activated with CaO. The MTK/lime mixture produced the highest weight loss, which indicates that this mixture had high water contents. However, it should be noted that the weight loss is overlapped by C-S-Hs, which are known to dehydrate gradually and differently over a wide temperature range $\leq$ 800 ^oC (Okada *et al*., 1994). Differences in their dehydration behaviour are due to compositional and structural variations (Pushnyakova *et al*., 1975).

In general, the results of the thermogravimetric analysis indicate that the addition of CaO to KAO and MTK produced several water containing phases between 25-350 ^oC. On the other hand, the DTA curves show the decomposition of portlandite (at ~440 ^oC) and calcite (at ~680 ^oC). Two interesting aspects observed are: a crystalline inversion of quartz (peak at 551 ^oC in Figure 5.24a) and the presence of C_2ASH_8 and C_4AH_{13} (Figure 5.24b), as reported by Frías and Cabrera (2002).

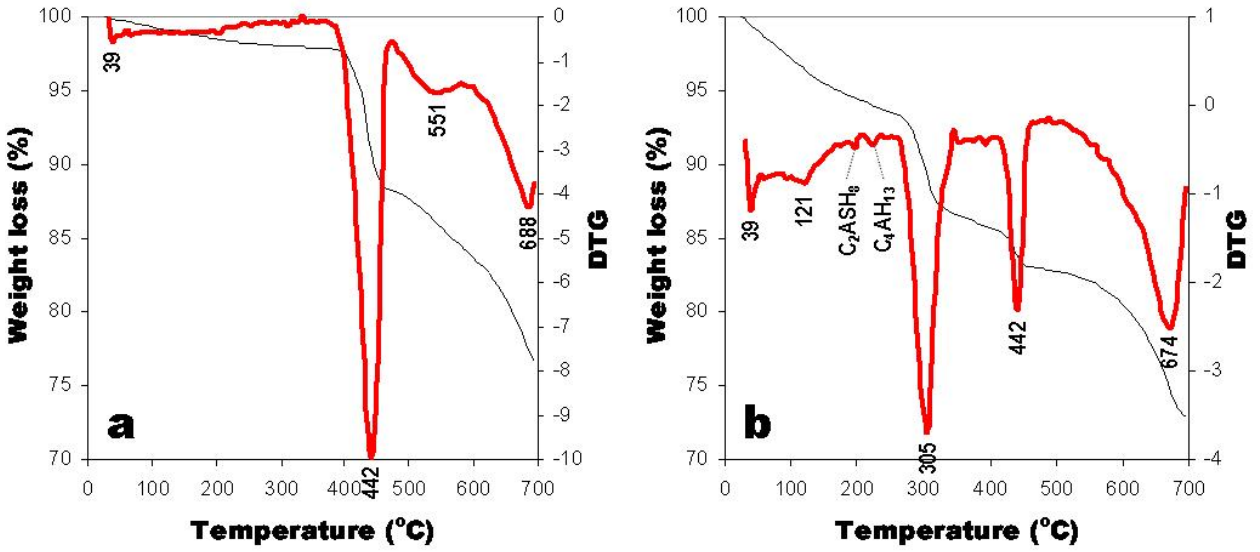

Figure 5.24. (a) TG/DTG curves between 25-700 °C of representative synthesis products obtained after hydrothermal treatment of: (a) KAO and (b) MTK, using CaO as mineralizer at 175 °C for 0 h.

5.6.5. Summary

Different C-S-H materials were synthesized in the system CaO-SiO_2-Al_2O_3-H_2O under hydrothermal conditions at 175 °C for a monitoring time of 24 h. The morphological, chemical and structural data determined by several analytical techniques are consistent and show good agreement with the literature. Some of the advantages to use an Al_2O_3 source, such as KAO or MTK, is that Al accelerates TOB formation from C-S-H. This inhibits the conversion to xonotlite, which reduces the strength properties of the synthetic product, and extends the temperature range over which TOB is stable (Larosa and Grutzeck, 1996). MTK is a more reactive phase than KAO for release of Al to form Al-TOB.

Several poorly crystalline materials occurred with un-reacted $Ca(OH)_2$ at shorter reaction times. HYD and TOB are interesting phases formed in the treated samples at longer curing times, which should promote the strength development of the synthesis products. HYD was always among the first phases formed and invariably appeared before 11 Å TOB. However, later, with increasing reaction time, they start to fracture and their quantity is reduced almost in half during 24 h.

Results indicate that HYD is always one of the first phases formed. However, its continued existence in the final product depends on factors, such as reaction time and bulk composition. In the subsequent autoclaving process the reaction continues and TOB is formed, which is known to provide hardness and strength to the final material.

5.7. Conclusions to Chapter 5

The conversion of KAO and MTK led to the formation of new crystalline structures, although their mineral chemistry would depend on the type of raw material, the mineralizer used to activate them, the presence of cations or compounds non-reactive in aqueous media, and the experimental conditions of synthesis. The alkaline media, particularly using NaOH, favoured a more intense transformation of the raw materials and higher crystallinity of the synthesis products than the hydrothermal treatment in KOH solutions. However, it is necessary to highlight that the introduction of an alkaline fusion step prior to the hydrothermal reaction demonstrated to be a more efficient method due to (1) the optimal extraction of aluminosilicates from the starting materials for zeolite synthesis, (2) the reduction of curing time and (3) the formation of purer and more crystalline products.

The production of zeolite-type materials by the reaction of KAO or MTK does not represent a new synthesis, but provides valuable scientific knowledge on their transformation on the nucleation and growth of aluminosilicates, with dissolution dominating initially and precipitation dominating in the later stages. The chemistry of evolution of the chemical systems investigated in this study can be affected by several factors, such as the formation of intermediate metastable phases and the occurrence of simultaneous reactions like precipitation and dissolution of a gel phase, nucleation and growth of zeolitic phases, dissolution of the early metastable phases, nucleation and growth of more stable phases. However, no previous effort has been made on the transformation of KAO and MTK using an alkaline fusion prior to the hydrothermal reaction, except by a study carried out by Meor Yusoff *et al*. (2007), which justify carrying out additional experimental studies. In the system CaO-SiO_2-Al_2O_3-H_2O, several poorly crystalline materials occurred with un-reacted $Ca(OH)_2$ at shorter reaction times, whereas at longer curing times HYD was always among the first phases formed and invariably appeared before 11 Å TOB.

KAO can be used for synthesis of low-silica zeolites (LSZs) because the contents of SiO_2 and Al_2O_3 are similar with each other. The alkaline activation of KAO and MTK to zeolites is well

known, with zeolite LTA as the most common synthesis product. In general, the SiO_2/Al_2O_3 ratios obtained from the as-synthesized zeolitic materials were quite similar to that from the starting materials. LSZs with Si/Al ratio of 1, such as zeolite A (LTA), sodalite (SOD), zeolite NA-P1 (GIS) and faujasite (FAU) are relatively rare, although they exhibit the highest ion exchange capacity and have important industrial applications.

Chapter 6

Chapter 6. Synthesis of natural clinker - based zeolitic materials

In this chapter the results corresponding to the synthesis products obtained using NC as starting material are discussed. The experimental conditions are summarized in Tables 6.1 and 6.2. Results indicate that NaOH was more efficient in the hydrothermal conversion of NC than KOH, and that through the two methods described above it was possible to carry out the transformation of NC into zeolite-type materials. The main as-synthesized NCZs obtained by the conventional hydrothermal treatment method include: NC-PHI, NC-SOD and NC-CAN. Using the fusion approach, NC-FAU, NC-LTA and feldspathoids (NC-SOD and NC-CAN) were obtained with NaOH as an activator, whereas no zeolitic material crystallized when KOH was used.

Table 6.1. Synthesis conditions for the conversion of NC into zeolitic materials using the conventional hydrothermal synthesis.

Test	Chemical reagents				L/S	Hydrothermal reaction		Molar gel composition	Zeolitic phases and other synthesis products	Residual phases
	H_2O (g)	NaOH (g)	KOH (g)	NC (g)	(ml/g)	T / °C	t / h			
1	18.00	0.96		3.10	6.12	100	6	$1.8Na_2O{:}0.1K_2O{:}0.4MgO{:}0.3Fe_2O_3{:}Al_2O_3{:}4.1SiO_2{:}140.2H_2O$	PHI, SOD, CAN	Qtz
2	18.00	0.96		3.10	6.12	100	24	$1.8Na_2O{:}0.1K_2O{:}0.4MgO{:}0.3Fe_2O_3{:}Al_2O_3{:}4.1SiO_2{:}140.2H_2O$	PHI, SOD, CAN	Qtz
3	18.00	0.96		3.10	6.12	100	72	$1.8Na_2O{:}0.1K_2O{:}0.4MgO{:}0.3Fe_2O_3{:}Al_2O_3{:}4.1SiO_2{:}140.2H_2O$	PHI, SOD, CAN, ANA	Qtz
4	18.00	2.87		3.10	6.73	100	6	$5.1Na_2O{:}0.1K_2O{:}0.4MgO{:}0.3Fe_2O_3{:}Al_2O_3{:}4.1SiO_2{:}141.9H_2O$	PHI, SOD, CAN	Qtz
5	18.00	2.87		3.10	6.73	100	24	$5.1Na_2O{:}0.1K_2O{:}0.4MgO{:}0.3Fe_2O_3{:}Al_2O_3{:}4.1SiO_2{:}141.9H_2O$	PHI, SOD, CAN	Qtz
6	18.00	2.87		3.10	6.73	100	72	$5.1Na_2O{:}0.1K_2O{:}0.4MgO{:}0.3Fe_2O_3{:}Al_2O_3{:}4.1SiO_2{:}141.9H_2O$	PHI, SOD, CAN	Qtz
7	18.00		1.35	3.10	6.24	100	6	$0.1Na_2O{:}0.9K_2O{:}0.4MgO{:}0.3Fe_2O_3{:}Al_2O_3{:}4.1SiO_2{:}140.2H_2O$	---	Qtz
8	18.00		1.35	3.10	6.24	100	24	$0.1Na_2O{:}0.9K_2O{:}0.4MgO{:}0.3Fe_2O_3{:}Al_2O_3{:}4.1SiO_2{:}140.2H_2O$	---	Qtz
9	18.00		1.35	3.10	6.24	100	72	$0.1Na_2O{:}0.9K_2O{:}0.4MgO{:}0.3Fe_2O_3{:}Al_2O_3{:}4.1SiO_2{:}140.2H_2O$	---	Qtz
10	18.00		4.03	3.10	7.11	100	6	$0.1Na_2O{:}02.6K_2O{:}0.4MgO{:}0.3Fe_2O_3{:}Al_2O_3{:}4.1SiO_2{:}141.9H_2O$	---	Qtz
11	18.00		4.03	3.10	7.11	100	24	$0.1Na_2O{:}02.6K_2O{:}0.4MgO{:}0.3Fe_2O_3{:}Al_2O_3{:}4.1SiO_2{:}141.9H_2O$	---	Qtz
12	18.00		4.03	3.10	7.11	100	72	$0.1Na_2O{:}02.6K_2O{:}0.4MgO{:}0.3Fe_2O_3{:}Al_2O_3{:}4.1SiO_2{:}141.9H_2O$	---	Qtz

PHI, phillipsite; SOD, sodalite; CAN, cancrinite; ANA, analcime; Qtz, quartz; NC, natural clinker; L/S, activator solution/NC ratio.

Table 6.2. Synthesis conditions for the conversion of NC into zeolitic materials using the alkaline fusion method.

Test	Chemical reagents to be fused			Alkaline fusion		L/FP	Aging	Hydrothermal reaction		Molar gel composition	Zeolitic phases and other synthesis products	Residual phases
	RM (g)	NaOH (g)	KOH (g)	T / °C	t / h	(ml/g)	t / h	T / °C	t / h			
13	* 6.20	7.44		600	1	4.9	5.5^{s}	100	3	$6.6Na_2O{:}0.1K_2O{:}0.4MgO{:}0.3Fe_2O_3{:}Al_2O_3{:}4.1SiO_2{:}261.3H_2O$	FAU, LTA, SOD, CAN	Qtz
14	* 6.20	7.44		600	1	4.9	5.5^{s}	100	24	$6.6Na_2O{:}0.1K_2O{:}0.4MgO{:}0.3Fe_2O_3{:}Al_2O_3{:}4.1SiO_2{:}261.3H_2O$	FAU, LTA, SOD, CAN	Qtz
15	* 6.20	7.44		600	1	4.9	5.5^{s}	60	24	$6.6Na_2O{:}0.1K_2O{:}0.4MgO{:}0.3Fe_2O_3{:}Al_2O_3{:}4.1SiO_2{:}261.3H_2O$	FAU, SOD, CAN	Qtz
16	* 6.20	7.44		600	1	4.9	5.5^{s}	60	48	$6.6Na_2O{:}0.1K_2O{:}0.4MgO{:}0.3Fe_2O_3{:}Al_2O_3{:}4.1SiO_2{:}261.3H_2O$	FAU, SOD, CAN	Qtz
17	* 6.20	7.44		600	1	4.9	5.5^{s}	60	96	$6.6Na_2O{:}0.1K_2O{:}0.4MgO{:}0.3Fe_2O_3{:}Al_2O_3{:}4.1SiO_2{:}261.3H_2O$	FAU, SOD, CAN	Qtz
18	* 6.20		7.44	600	1	4.9	5.5^{s}	100	3	$0.1Na_2O{:}2.4K_2O{:}0.4MgO{:}0.3Fe_2O_3{:}Al_2O_3{:}4.1SiO_2{:}260.3H_2O$	---	Qtz
19	* 6.20		7.44	600	1	4.9	5.5^{s}	100	24	$0.1Na_2O{:}2.4K_2O{:}0.4MgO{:}0.3Fe_2O_3{:}Al_2O_3{:}4.1SiO_2{:}260.3H_2O$	---	Qtz

*RM, raw material; * NC; FAU, faujasite; LTA, zeolite LTA; CAN, cancrinite; SOD, sodalite; Qtz, quartz; NC, natural clinker; L/FP, water/fused product; ^{s} stirring conditions.*

6.1. Chemical and mineralogical analyses

6.1.1. Synthesis experiments in NaOH media

In the set of experiments at 1.33 M NaOH solutions (Table 6.1, tests 1–3), as shown in Figure 6.1a, the XRD patterns reveal the occurrence of mixture of several zeolite phases, such as NC-PHI, NC-SOD and NC-CAN, with traces of NC-ANA and unreacted quartz. The content of the zeolitic materials increased with reaction time. Ríos and Williams (2008) conducted the synthesis of zeolites under similar experimental conditions for longer reaction times (166 h); the grade of crystallinity of the synthesis products increased with reaction time, although the highest synthesis yields were obtained after 72 h, with quartz partially dissolved under these experimental conditions with no additional dissolution for longer reaction times. These results demonstrate that most of the amorphous aluminosilicate glass can be effectively converted to zeolitic materials, but not the crystalline quartz. At 3.99 M NaOH solutions (Table 6.1, tests 4-6, Figure 6.1b), the XRD patterns show a decrease in the intensity of the reflection peaks corresponding to the zeolitic products compared with those in Figure 6.1a, with the disappearance of some of the characteristic XRD peaks of NC, the absence of NC-ANA and the reduction of the intensity of the characteristic reflection peak of quartz at $2\theta = 26.6^{o}$ with reaction time. The SEM images of the treated NC in NaOH solutions reveal interesting morphologies. In Figure 6.2a several morphologies were observed; a complex aggregate containing large clusters of radiating tetragonal prisms of NC-PHI, a spheroid 'ball of yarn' of NC-SOD, intergrown thin disks typical of NC-CAN, and scarce crystals with a rounded morphology of NC-ANA. A mixture of irregular bladed crystals of NC-SOD and lepispheric aggregates of NC-CAN are observed in Figure 6.2b.

6.1.2. Synthesis experiments in KOH media

In the set of experiments at 1.33 M KOH solutions (Table 6.1, tests 7-9), as shown in Figure 6.1c, the XRD patterns indicate that no zeolitic products were detected, with evidence of the persistence of quartz, although hematite and muscovite peaks of the original NC disappeared completely during the reaction. At 3.99 M KOH solutions (Table 6.1, tests 10-12, Figure 6.1d), the XRD patterns show that the synthesis products have quite similar reflection peak intensities compared to those in Figure 6.4c, with quartz showing a reduction of intensity for the reflection peak at $2\theta = 26.6^{o}$ with reaction time. Using KOH solutions, several NCZs, such as NC-SOD, NC-PHI, NC-CHA and NC-EDI, not detected by XRD analysis were observed by SEM, which depicts the following features: 'ball of yarn'-like morphology comparable to that of NC-SOD associated with clusters of prismatic crystals of NC-PHI, developing a bow tie-like aggregate (Figure 6.2c), and intergrowth of phacolitic NC-CHA and prismatic NC-EDI (Figure 6.2d). However, in general, SEM indicated that the reaction between NC with KOH did not significantly change the microscopic structure of NC.

6.1.3. Synthesis experiments using a fusion process followed by hydrothermal reaction

The conversion of the raw NC into zeolitic materials via alkaline fusion followed by hydrothermal treatment reveals that the alkaline fusion process promoted the dry reaction between the crystalline mineral phases present in NC and the alkaline activator. The alkaline-fused product corresponds to amorphous sodium or potassium silicate or aluminate salts. This indicates that fusion was very effective in extracting the silicon and aluminium species from NC. Figure 6.3 reveals that several zeolite phases crystallized by using NaOH as alkaline activator (Table 6.1, tests 13-17), with NC-FAU as the main phase. The XRD patterns in Figure 6.3a indicate a mixture of NC-FAU, NC-LTA and NC-SOD or NC-CAN. From 3 to 24 h of reaction, a progressive increase in the intensity of the reflection peaks of the as-synthesized zeolitic materials occurred. On the other hand, from 24 to 96 h of reaction there was no observed a change of the crystallinity of the synthesis products (Figure 6.3c). The SEM image in Figure 6.3b shows the typical octahedral morphology of crystals of NC-FAU, displaying only some faces, associated with aggregate of bladed crystals of NC-SOD, representing two different populations of crystal size. A long reaction time (96 h) and low temperature of reaction produced an uniform crystal

size distribution (Figure 6.3d). The activation of NC with KOH (Table 6.1, tests 18-19, Figure 6.4) resulted in the formation of an amorphous phase (see the broad hump at 2θ = 22.5-37.5°, having a maximum at 2θ = ~28º), with weak peaks that correspond to residual crystalline quartz.

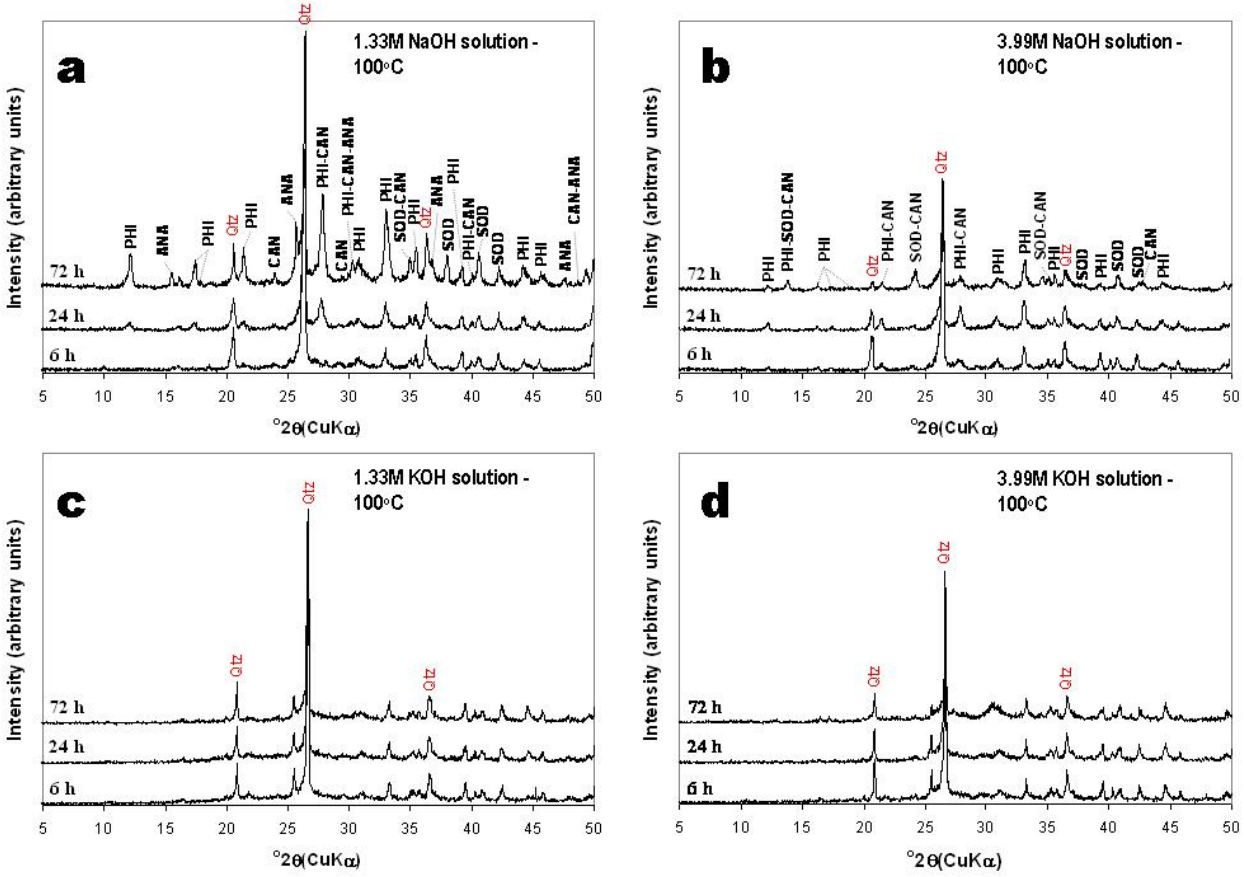

Figure 6.1. XRD patterns of the as-synthesized NCZs via hydrothermal treatment of NC in (a-b) NaOH and (c-d) KOH solutions.

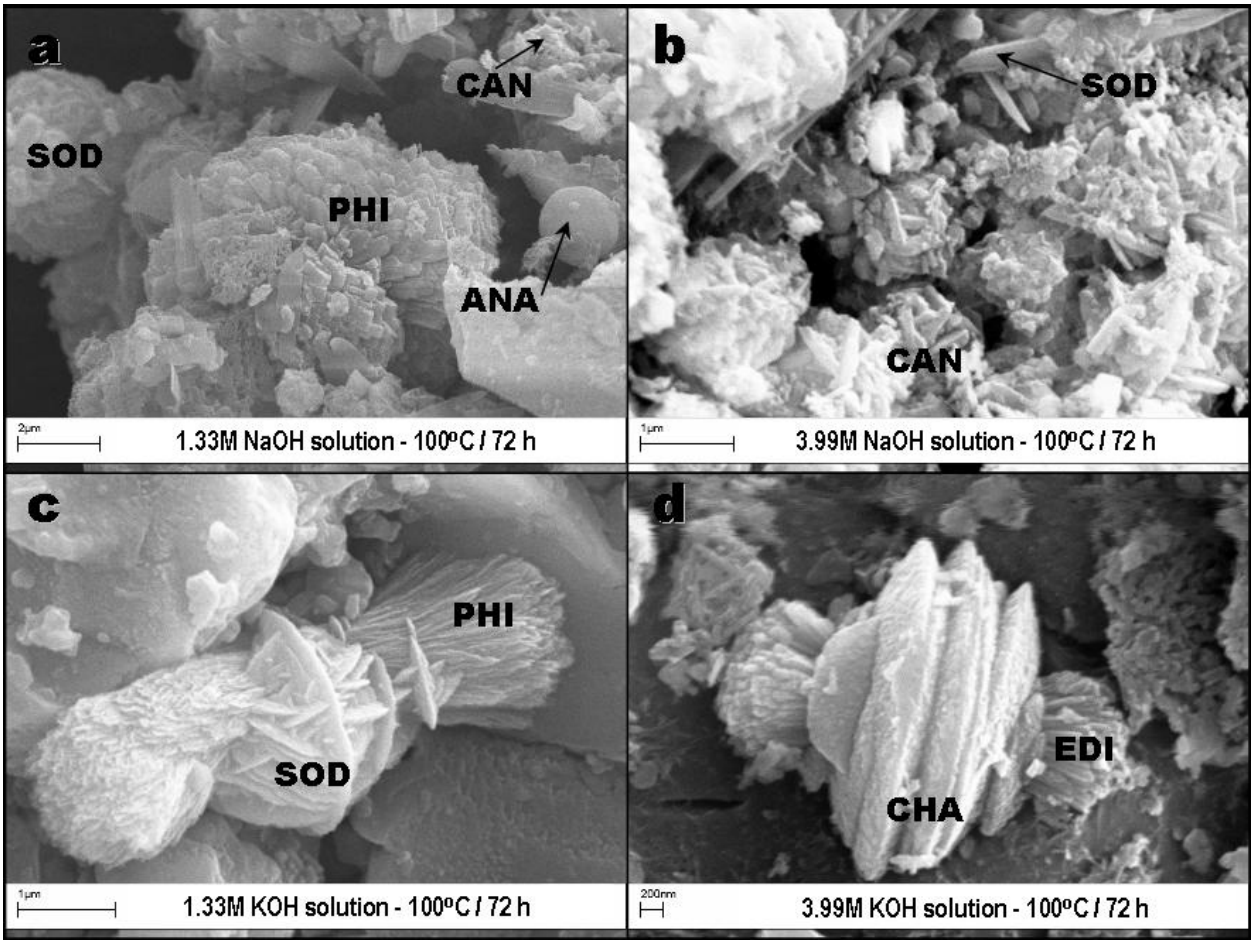

Figure 6.2. SEM images showing morphological aspects in the as-synthesized products obtained via hydrothermal treatment of NC in (a-b) NaOH and (c-d) KOH solutions.

As shown in Table 6.3, the weight percent of the major oxides in starting material has been reduced during zeolite synthesis, which was expected. After the hydrothermal synthesis, NC incorporated significant amount of Na or K due to their activation with NaOH and KOH, which is what have also been reported by Maruyama *et al*. (2002) using FA. These authors explains that an increase in Na and K contents in the synthesis product is caused by captured Na^+ and K^+ ions to neutralize the minus charge on aluminate in zeolite structure when a zeolite crystal is formed. The synthesis products obtained using the fusion approach showed higher Na or K contents. Fe content decreased after activation of NC, particularly using the alkaline fusion approach, whereas the other impurities in general were reduced.

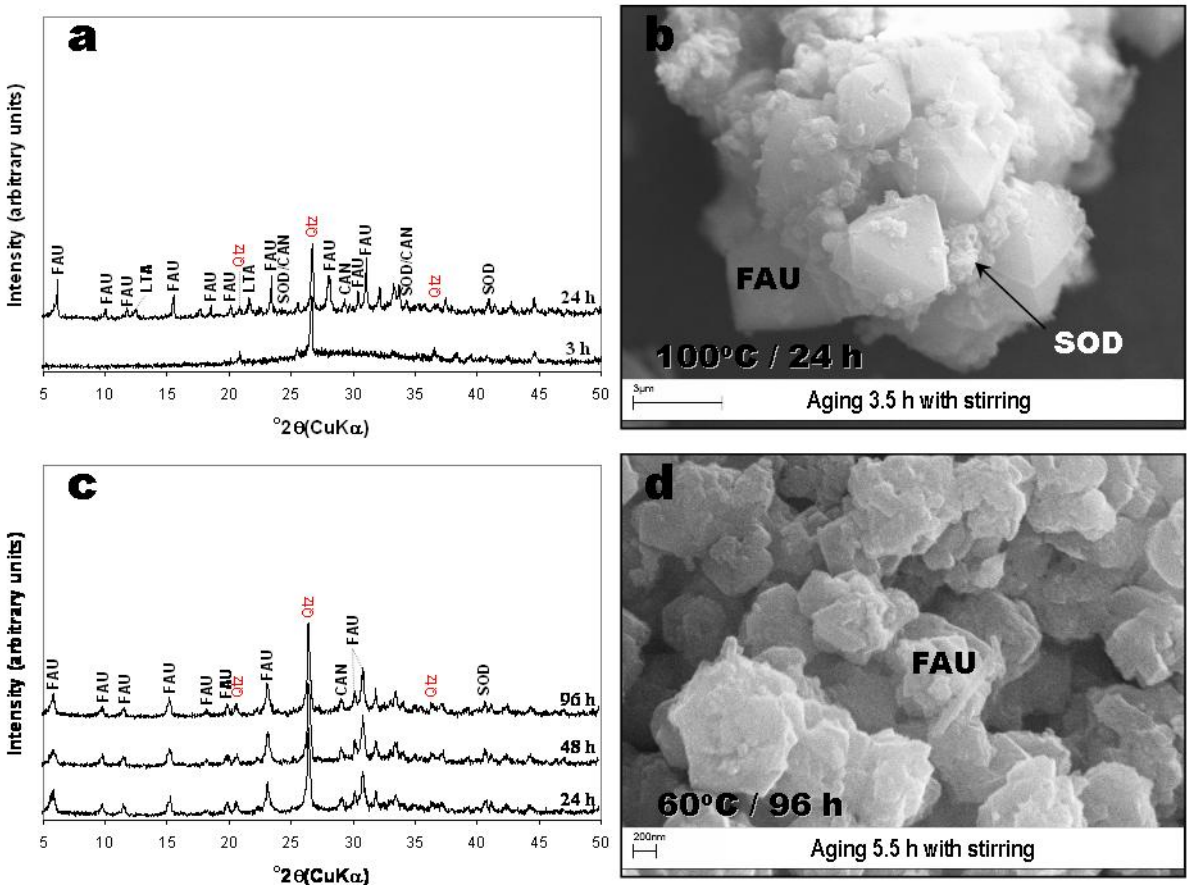

Figure 6.3. XRD patterns (a-c) and SEM images (b-d) of synthesis products obtained after activation of NC using the alkaline fusion method using NaOH as mineralizer.

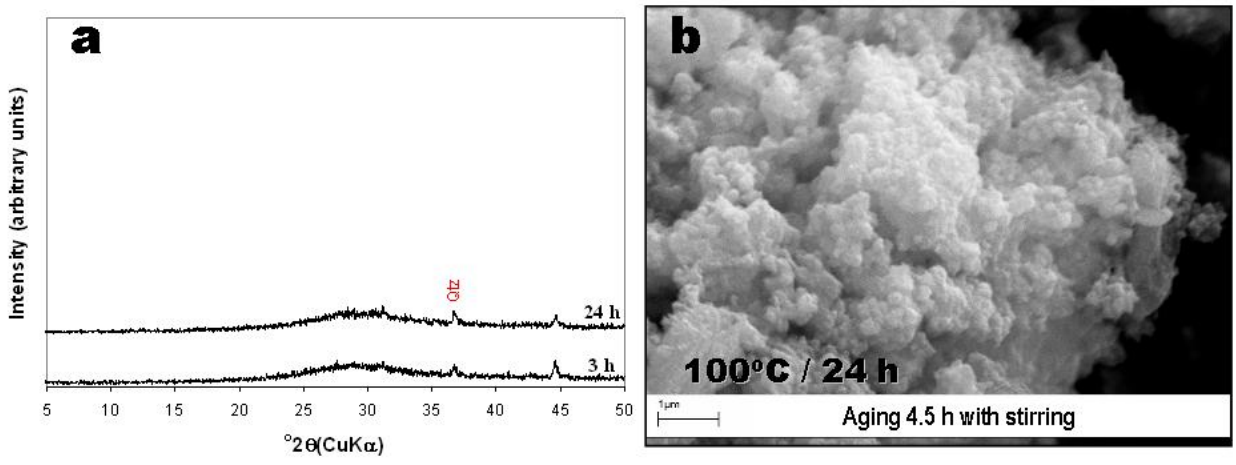

Figure 6.4. XRD patterns (a) and SEM image (b) of synthesis products obtained after activation of NC using the alkaline fusion method using KOH as mineralizer.

The SiO_2/Al_2O_3 ratio has a very significant impact on the zeolite performance in water treatment, since according to Misak (2000) generally a zeolite with a low SiO_2/Al_2O_3 ratio will tend to be hydrophilic, while a high silica zeolite (>2.00) will tend to be hydrophobic and organophillic. Zeolitic products showed different SiO_2/Al_2O_3 ratios, with lower ratios using NaOH solutions with higher concentrations and the fusion approach, higher ratios using KOH solutions with higher concentrations, similar ratios to that obtained for NC were obtained using alkaline solutions with lower concentration. Therefore, based on the low SiO_2/Al_2O_3 ratios determined in the as-synthesized zeolites, the expected results would be a higher concentration of terminal Al–OH species at the zeolite-water interface during the water treatment, as well as increased hydrophilic nature of the zeolite and subsequent enhanced ion exchange capacity.

Table 6.3. Chemical composition of the starting NC and representative synthesis products.

Material	Weight (%)										SiO_2/Al_2O_3 ratio
	SiO_2	Al_2O_3	Fe_2O_3	MgO	K_2O	Na_2O	CaO	MnO	TiO_2	SO_3	
NC	56.60	23.61	9.41	3.94	1.95	1.41	0.53	0.35	1.10	1.11	2.40
NCZ1	58.43	24.18	7.51	0.00	3.63	4.74	0.42	0.00	1.08	0.00	2.42
NCZ2	45.06	33.63	1.84	0.00	0.80	18.38	0.00	0.00	0.29	0.00	1.34
NCZ3	61.00	24.51	0.79	0.00	12.48	0.83	0.00	0.00	0.39	0.00	2.49
NCZ4	72.15	16.81	1.43	0.00	9.18	0.00	0.16	0.00	0.28	0.00	4.29
NCZ5	47.81	26.95	1.71	0.00	0.64	22.90	0.00	0.00	0.00	0.00	1.77
NCZ6	50.47	26.22	4.18	0.00	19.14	0.00	0.00	0.00	0.00	0.00	1.93

NC, natural clinker; NCZ1 (1.33M NaOH solution - 100 °C / 72h); NCZ2 (3.99M NaOH solution - 100 °C / 72h); NCZ3 (1.33M KOH solution - 100 °C / 72 h); NCZ4 (3.99M KOH solution - 100 °C / 72 h); NCZ5 and NCZ6 (following the fusion approach with NaOH and KOH as activators at 100 °C / 24 h
NCZ, NC-based zeolite

6.2. Fourier Transform Infrared Spectroscopy

The FT-IR spectra of the raw NC and as-synthesized products obtained after alkaline activation of NC are illustrated in Figures 6.5 and 6.6. The FT-IR spectra of the activated NC show interesting differences when compared with the spectrum of the raw NC. The FT-IR spectra of the activated NC show interesting differences when compared with the spectrum of the raw NC. Coincident with the progressive transformation of NC, characteristic zeolite bands appeared on the spectra. The bands in the region of 400-420 cm^{-1} are related to the pore opening or motion of the tetrahedral rings, which form the pore opening of zeolites (Breck, 1974). The bands in the region of 420-500 cm^{-1} are attributed to internal tetrahedron vibrations of Si-O and Al-O of the

zeolitic materials. The band at 461 cm^{-1} shifted to lower frequencies with reaction time, when a NaOH solution was used. A similar behaviour was observed using the alkaline fusion followed by hydrothermal treatment, although two different bands at 419 and 449 cm^{-1} were obtained when NaOH was used. A tendency for the progressive appearance of higher and lower frequencies was observed using KOH as mineralizer. The bands in the region of 500-650 cm^{-1} can be identified after NC activation in high concentration alkaline solutions or after its conversion by the second method using NaOH, with the tetrahedral secondary building units (SBUs), such as double rings (double, 4-membered ring, D4R, and double, 6-membered ring, D6R), in the framework structures of the zeolitic materials. The band at 704 cm^{-1} changed to lower frequencies, with the symmetric Al-O stretch located in the region of 660-770 cm^{-1} represented by the appearance of new vibration bands, using higher concentration of the alkaline activator, with new lower frequency bands using NaOH or higher frequency bands using KOH. Using NaOH as an activator in the alkaline fusion method, lower and higher frequencies were obtained. The bands at 785 and 804 cm^{-1} in general shifted to lower frequencies, except using KOH as an activator in the second method due to the disappearance of the band at 804 cm^{-1}. New bands at higher frequencies in the region of 834-917 cm^{-1} appeared by the classical hydrothermal synthesis, except when low concentration NaOH solutions were used. The band at 1053 cm^{-1} associated with asymmetric T–O stretching vibrations shifted to higher frequencies but, in general, it tended to disappear. New bands of lower frequencies appeared in the region of 975-1035 cm^{-1}, except when low concentration KOH solutions were used, and new bands of higher frequencies appeared in the region of 1090-1168 cm^{-1}, except when the second method was applied. The shift in absorption frequency has been related to compositional effects (Al/Si ratio) (Sitarz *et al*., 1999).

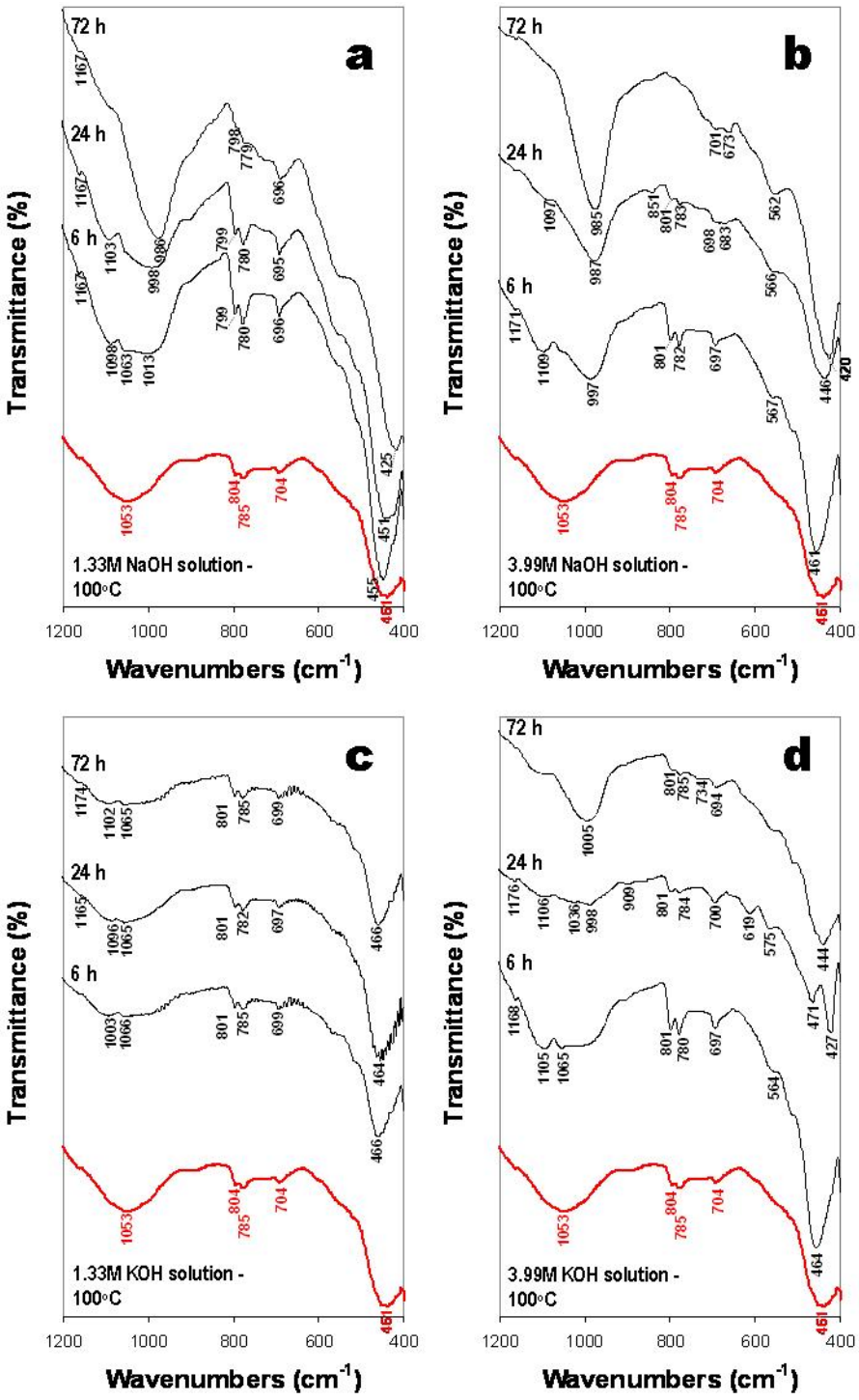

Figure 6.5. FT-IR spectra of NC (in red) and as-synthesized products obtained via hydrothermal treatment of NC in (a-b) NaOH and (c-d) KOH solutions.

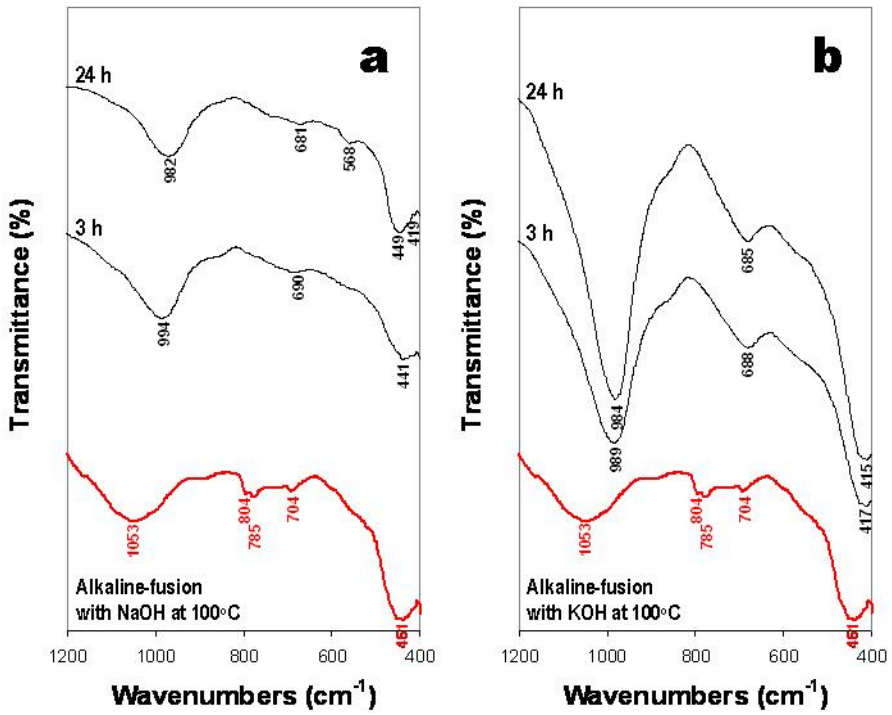

Figure 6.6. FT-IR spectra of NC (in red) and as-synthesized products obtained via alkaline fusion of NC prior to hydrothermal reaction using (a) NaOH and (b) KOH as activators.

6.3. ^{29}Si and ^{27}Al Magic Angle Spinning Nuclear Magnetic Resonance

The ^{29}Si and ^{27}Al MAS NMR spectra of NC and representative synthesis products are given in Figure 6.7 to better characterize the amorphous and poorly crystalline phases which occur in NC and to reveal important information on the zeolite structure. The most intense peak in ^{29}Si MAS NMR spectrum of NC (Figure 6.7a), centred at -107.6 ppm, can be assigned to highly polymerized Q^4Si sites [Si(4Si)] and attributed to quartz. The ^{29}Si MAS NMR spectrum of Figure 6.7b consists of six resonances at -85.4, -89.6, -93.2, -98.0, -103.0 and -107.3 ppm. A weak resonance peak at -85.4 ppm can be assigned to the Q^4(4Al) sites in FA-SOD and possibly FA-PHI. According to Engelhardt *et al*. (1989), the ^{29}Si chemical shift of the SOD-type structure is controlled by the Si-O-Al bond angle and lattice constants. Four well-resolved peaks at -89.6, -93.2, -98.0 and -103.0 ppm are clearly distinguished in Figure 6.7b, revealing the presence of Q^4(4Al), Q^4(3Al), Q^4(2Al) and Q^4(1Al) sites, respectively, in the framework of NC-PHI. Using the method of Engelhardt and Michel (1987), the relative size of these peaks was used to determine the Si/Al ratio in NC-PHI, which was found to be 2.3. Mashal *et al*. (2005) reported a ^{29}Si NMR

chemical shift at approximately -89.0 ppm, which is consistent with alternating Si and Al ordering in the Q^4(4Al) sites of cancrinite and sodalite. However, the absence of such resonance peak can explain why NC-CAN is no observed in the synthesis product. Therefore, the spectral signals corresponding to this zeolite-type structure can be overlapped and may not be easily detected. The resonance signal at -107.3 ppm is assigned to Q^4(0Al) sites of unreacted quartz. Figure 6.7c shows several resonance peaks at -85.9, -91.2, -96.7 and -107.0 ppm. The sharp peak at -85.9 ppm (Q^4(4Al) sites) is characteristic for the framework of NC-SOD; the Si/Al ratio calculated for this zeolite-type structure was found to be 1.0. The two weak peaks at -91.2 and -96.7 ppm, which include, respectively, contributions from Q^4(3Al) and Q^4(2Al) sites in the NC-PHI framework. The weak resonance peak at -107.0 ppm arises from Q^4(0Al) environments in unreacted quartz. From Figures 6.7b and 6.7c, a reduction in the intensity of the characteristic signal of quartz approximately at -107.0 ppm increasing the concentration of NaOH was observed. Figure 6.7d shows five well-resolved peaks at -84.3, -88.6, -93.0, -97.8 and -104.1 ppm, which can be attributed to the presence of Q^4(4Al), Q^4(3Al), Q^4(2Al), Q^4(1Al) and Q^4(0Al) sites, respectively, in zeolite phases. The relative peak areas of these peaks were used to calculate the Si/Al ratio for NC-FAU, which was found to be 1.4 in agreement with data reported by Fernández-Jiménez (2008). The first peak can be also attributed to the presence of NC-SOD (calculated Si/Al = 1.0). The spectral signal at -107.3 ppm is attributed to the presence of unreacted quartz. ^{27}Al MAS NMR spectrum of the unreacted NC (Figure 6.7a) consist of a single resonance at 50.3 ppm and is largely tetrahedral aluminium, but with some octahedral. The sharp resonances at 57.7 ppm (Figure 6.7b), 60.5 ppm (Figure 6.7c) and 61.5 ppm (Figure 6.7d) can be assigned to tetrahedral Al in the framework of the zeolitic products.

The structure of NCZs reveals that ^{29}Si occurs in various environments with different crystallographically Si sites and that ^{27}Al is predominantly tetrahedral. The intensity in the sidebands at the edges of the ^{29}Si and ^{27}Al MAS NMR spectra corresponding to NC confirms the occurrence of some paramagnetic impurities (hematite) in NC, which provide it with a high-intensity thermoremanent magnetization that appears to faithfully record the ambient geomagnetic field, allowing mapping of burn zones and tracing of magnetic reversals in ancient burns (Jones *et al*., 1984). These results are in agreement with XRD data.

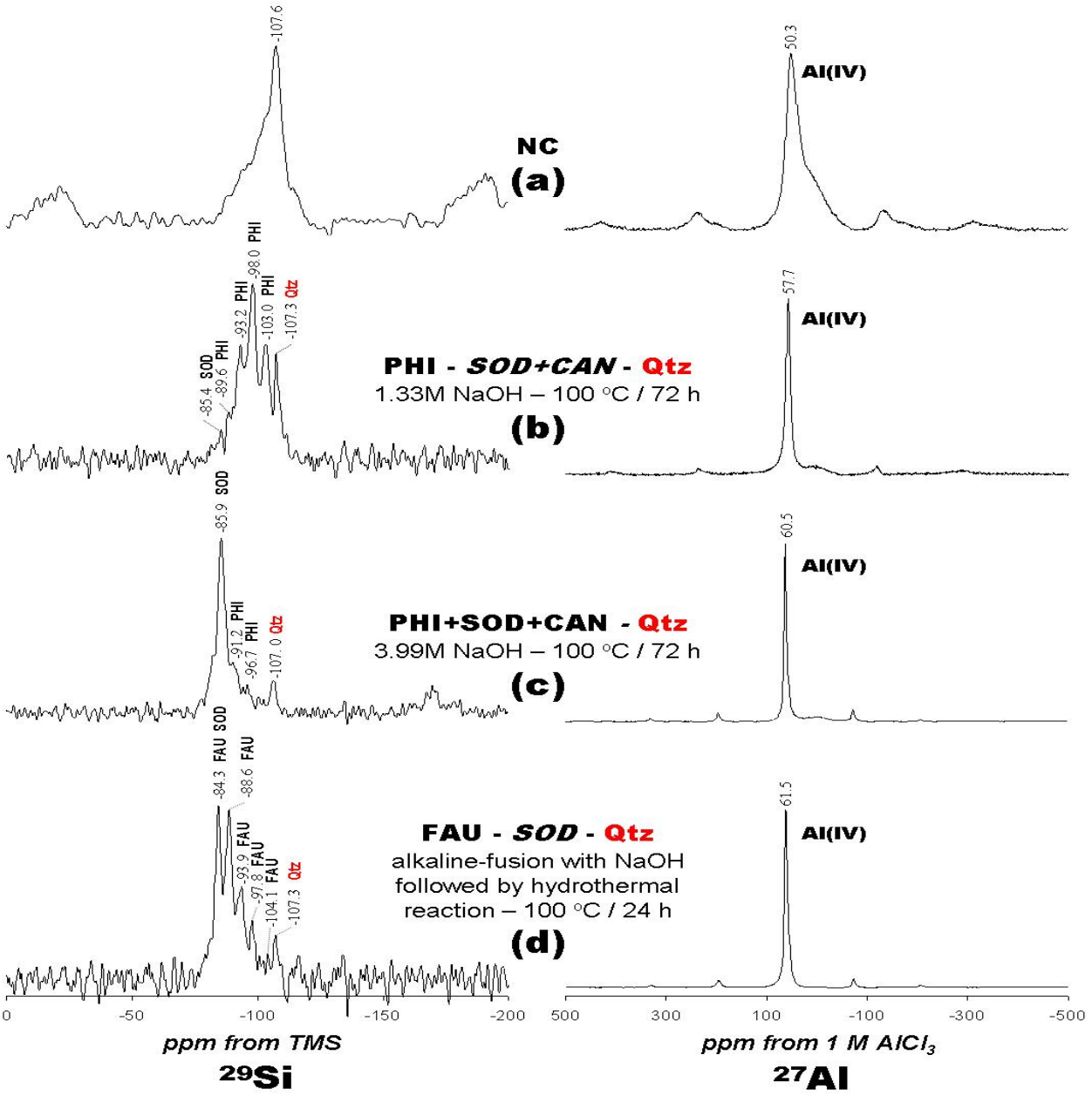

Figure 6.7. ^{29}Si and ^{27}Al MAS NMR spectra of the (a) raw NC and (b-d) representative synthesis products obtained after alkaline activation of NC with NaOH as mineralizer. Main and minor phases are indicated in uppercase regular and italic fonts, respectively; starting material phases in uppercase regular font (red colour).

6.4. Thermogravimetric analysis

DTG curves of the NCZs obtained after alkaline activation of NC by classical hydrothermal reaction (Figures 6.8a and 6.8b) and alkaline fusion followed by hydrothermal reaction (Figure 6.8c) show up to five DTG peak dehydration steps, depending on the thermogravimetric evolution of the NCZs.

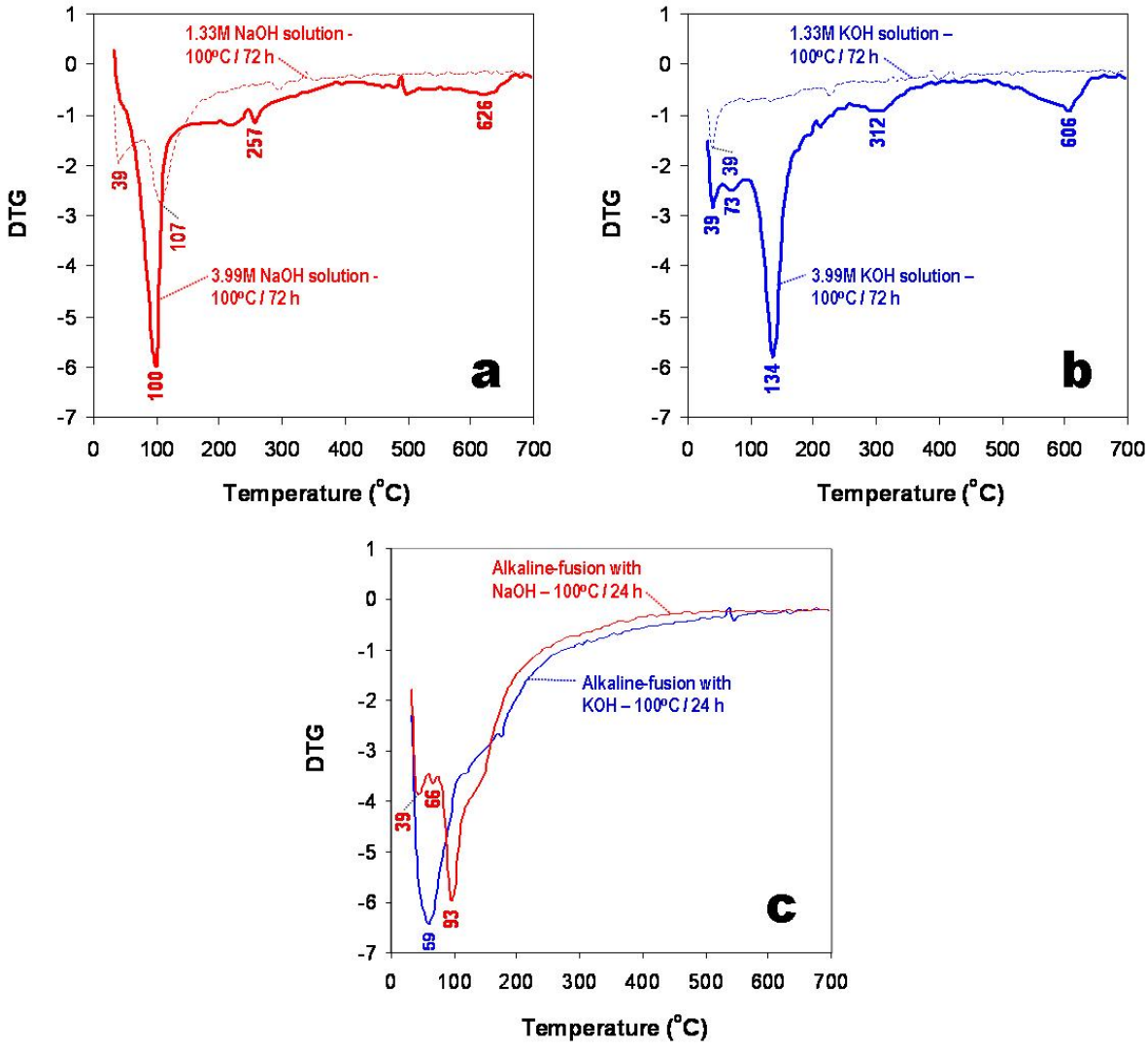

Figure 6.8. DTG curves between 25-700 ºC of representative as-synthesized NCZs obtained after alkaline activation of NC by the (a-b) classic hydrothermal treatment and (c) alkaline fusion method.

The DTG peaks observed between 25-150 ^{o}C correspond to the zeolite dehydration steps (up to 3 DTG peaks). The position of these DTG peaks and the number of dehydration steps has been attributed to the different compensating cation-water binding energies, as well as to the different energy associated with the diffusion of the desorbed water through the porous structure of the zeolites (Covarrubias, *et al*., 2006). The first group of peaks are observed between 25-90 ^{o}C and correspond to water desorption; between of 50-180 ^{o}C the second group of peaks are observed and are attributed to occluded water. In some cases, zeolites also show additional DTG peaks at 257 or 312 ^{o}C and 606 or 626 ^{o}C, which can be attributed to framework dehydroxilation of the NCZs. The synthetic products showed higher weight loss (LOI, loss of ignition = 4.98-24.41%) and Na_2O content than those of the starting material. The synthesis products obtained by the classic hydrothermal reaction produced least weight loss (4.98-9.05%), particularly using low concentration alkaline solutions, whereas those obtained by the alkaline fusion approach displayed most weight loss (15.63-24.41%).

6.5. Conclusions to Chapter 6

NC is a non-hazardous coal by-product, which can be used in several industrial applications and its recycling might save millions of dollars per year to the coal industry, avoiding landfill costs, generate cost-effective alternatives, minimize environmental damage and energy consumption and provide new synthetic materials with superior qualities and cheaper than natural ones. The characterization of NC revealed valuable mineralogical and structural data to improve our understanding on the potential environmental impact associated with its disposal. However, NC should be characterized in detail both before and after leaching or dissolution experiments, because its chemical composition plays a very important role in fluid-rock interaction processes. In turn, this helps us in finding better strategies to mitigate environmental problems associated with NC deposits and to enhance recycling methods. It has been demonstrated for the first time that the production of NCZs represents a new alternative synthesis process and provides valuable scientific knowledge on the transformation of NC, which can be summarized by two main stages. Firstly, the dissolution of NC or its aluminosilicate salts (produced after alkaline fusion) releases Si and Al, with a progressive formation and dissolution of an amorphous aluminosilicate gel. Secondly, the crystallization of the aluminosilicate products (NCZs), generally accompanied by relict phases of the raw NC.

The experimental method used in zeolite synthesis played an important role in determining the

type of zeolite formed. The chemistry of zeolite synthesis was subject to perturbations caused by the presence of impurities in the starting material, which may remain insoluble during crystallization and make undesired species to nucleate, developing mixtures of different zeolitic materials coexisting in the as-synthesized products, and the dominant crystalline phase depends on the conditions of formation. Higher conversion efficiency was obtained using NaOH as mineralizer compared with that using KOH, even at high concentration, taking into account that K^+ is the suppression factor for zeolite synthesis, causing a slow crystallization rate, similar to rates reported in different studies using FA as starting material. The alkaline fusion method has been successfully applied in the synthesis of zeolites from NC. However, the alkaline fusion step promoted the solid-state reaction between the NaOH powder and the crystalline phases of NC. As a result, a sodium aluminosilicate phase was formed at the fusion temperature. The fused product is generally dissolved in water more readily than quartz and hematite in NC. However, these phases still remain in the synthesis products, which may be explained by the presence of unburnt organic matter in the raw NC, which interferes in the fusion step thereby affecting the quality of fused product. Mixtures of different zeolitic materials coexist in the synthesis products, with NC-FAU as the main crystalline phase. The SiO_2/Al_2O_3 ratio in the initial mixture limited the formation of NC-LTA. In the fusion process, the product is more likely to be a highly crystalline zeolite (NC-FAU), obtained after short times of crystallization. The results on the alkaline activation of NC also prove that further studies should be carried out under optimized experimental conditions, to successfully prepare highly crystalline zeolites efficient in the purification of polluted effluents.

Chapter 7

Chapter 7. Synthesis of fly ash - based zeolitic materials

In this chapter the synthesis of zeolitic materials from FA via: (1) hydrothermal treatment in alkaline solutions and (2) dissolution of alkali-fused aluminosilicate salts in water followed by hydrothermal treatment is discussed. Results show that NaOH was more efficient in the hydrothermal conversion of FA than KOH. The main as-synthesized FAZs obtained by the classic hydrothermal treatment method include: FA-GIS, FA-SOD, FA-EDI, FA-CHA and FA-LTF, with traces of FA-TOB, FA-CAN and FA-HER. Using the alkaline fusion approach, FA-FAU and FA-CAN was obtained with NaOH as an activator, whereas no zeolitic material was crystallized using KOH.

7.1. Conversion of fly ash by alkaline hydrothermal treatment

Experimental parameters and results for the synthesis of FAZs by the classic hydrothermal method are presented Table 7-1.

7.1.1. Synthesis experiments in NaOH media

The main FAZs obtained after activation of FA in NaOH solutions were FA-GIS and FA-SOD (Table 7.1), with different yields, depending on the experimental conditions, although the last of them being the preferred product at higher temperature and NaOH concentration. The NaOH acts as a strong mineralizing agent, which forces the reactants into solution. The greater the OH^- concentration, the greater the concentration of reactants in solution and thus the greater the rate of crystal growth (Jansen, 1991). Along with these zeolitic products, FA-CAN, FA-TOB and FA-HER, crystallized as trace phases.

Table 7.1. Synthesis conditions for conversion of FA into zeolitic materials by the classic hydrothermal treatment.

Test	Chemical reagents				L/S	Hydrothermal reaction		Molar gel composition	Zeolitic phases and other synthesis products	Residual phases
	H_2O (g)	NaOH (g)	KOH (g)	FA (g)	(ml/g)	T / °C	t / h			
1	18.00	0.96		3.10	6.12	100	3	$0.9Na_2O{:}Al_2O_3{:}2.1SiO_2{:}76.4H_2O$	---	Qtz, Mul
2	18.00	0.96		3.10	6.12	100	24	$0.9Na_2O{:}Al_2O_3{:}2.1SiO_2{:}76.4H_2O$	GIS, SOD	Qtz, Mul
3	18.00	0.96		3.10	6.12	100	48	$0.9Na_2O{:}Al_2O_3{:}2.1SiO_2{:}76.4H_2O$	GIS, SOD	Qtz, Mul
4	18.00	0.96		3.10	6.12	100	120	$0.9Na_2O{:}Al_2O_3{:}2.1SiO_2{:}76.4H_2O$	GIS, SOD	Mul
5	18.00	0.96		3.10	6.12	100	288	$0.9Na_2O{:}Al_2O_3{:}2.1SiO_2{:}76.4H_2O$	GIS, SOD	Mul
6	18.00	2.87		3.10	6.73	100	3	$2.7Na_2O{:}Al_2O_3{:}2.1SiO_2{:}78.2H_2O$	---	Qtz, Mul
7	18.00	2.87		3.10	6.73	100	24	$2.7Na_2O{:}Al_2O_3{:}2.1SiO_2{:}78.2H_2O$	SOD, GIS	Qtz, Mul
8	18.00	2.87		3.10	6.73	100	48	$2.7Na_2O{:}Al_2O_3{:}2.1SiO_2{:}78.2H_2O$	SOD, GIS	Qtz, Mul
9	18.00	2.87		3.10	6.73	100	120	$2.7Na_2O{:}Al_2O_3{:}2.1SiO_2{:}78.2H_2O$	SOD, GIS	Qtz, Mul
10	18.00	2.87		3.10	6.73	100	288	$2.7Na_2O{:}Al_2O_3{:}2.1SiO_2{:}78.2H_2O$	SOD, GIS	Qtz, Mul
11	18.00	0.96		6.20	3.06	100	3	$0.5Na_2O{:}Al_2O_3{:}2.1SiO_2{:}38.2H_2O$	---	Qtz, Mul
12	18.00	0.96		6.20	3.06	100	24	$0.5Na_2O{:}Al_2O_3{:}2.1SiO_2{:}38.2H_2O$	GIS, SOD	Qtz, Mul
13	18.00	0.96		6.20	3.06	100	48	$0.5Na_2O{:}Al_2O_3{:}2.1SiO_2{:}38.2H_2O$	GIS, SOD	Qtz, Mul
14	18.00	2.87		6.20	3.37	100	3	$1.4Na_2O{:}Al_2O_3{:}2.1SiO_2{:}39.1H_2O$	---	Qtz, Mul
15	18.00	2.87		6.20	3.37	100	24	$1.4Na_2O{:}Al_2O_3{:}2.1SiO_2{:}39.1H_2O$	SOD, GIS	Qtz, Mul
16	18.00	2.87		6.20	3.37	100	48	$1.4Na_2O{:}Al_2O_3{:}2.1SiO_2{:}39.1H_2O$	SOD, GIS	Qtz, Mul
17	18.00	0.96		3.10	6.12	175	3	$0.9Na_2O{:}Al_2O_3{:}2.1SiO_2{:}76.4H_2O$	GIS, SOD, CAN, HER	Qtz, Mul
18	18.00	0.96		3.10	6.12	175	24	$0.9Na_2O{:}Al_2O_3{:}2.1SiO_2{:}76.4H_2O$	GIS, SOD, CAN, TOB, HER	Mul
19	18.00	0.96		3.10	6.12	175	48	$0.9Na_2O{:}Al_2O_3{:}2.1SiO_2{:}76.4H_2O$	GIS, SOD, CAN, TOB, HER	Mul
20	18.00	2.87		3.10	6.73	175	3	$2.7Na_2O{:}Al_2O_3{:}2.1SiO_2{:}78.2H_2O$	GIS, CAN, HER	Qtz, Mul
21	18.00	2.87		3.10	6.73	175	24	$2.7Na_2O{:}Al_2O_3{:}2.1SiO_2{:}78.2H_2O$	GIS, SOD, TOB, CAN, HER	Mul
22	18.00	2.87		3.10	6.73	175	48	$2.7Na_2O{:}Al_2O_3{:}2.1SiO_2{:}78.2H_2O$	GIS, SOD, TOB, CAN, HER	Mul
23	18.00	0.96		6.20	3.06	175	3	$0.5Na_2O{:}Al_2O_3{:}2.1SiO_2{:}38.2H_2O$	---	Qtz, Mul
24	18.00	0.96		6.20	3.06	175	24	$0.5Na_2O{:}Al_2O_3{:}2.1SiO_2{:}38.2H_2O$	GIS	Qtz, Mul
25	18.00	0.96		6.20	3.06	175	48	$0.5Na_2O{:}Al_2O_3{:}2.1SiO_2{:}38.2H_2O$	GIS	Qtz, Mul
26	18.00	2.87		6.20	3.37	175	3	$1.4Na_2O{:}Al_2O_3{:}2.1SiO_2{:}39.1H_2O$	GIS, CAN, HER	Qtz, Mul
27	18.00	2.87		6.20	3.37	175	24	$1.4Na_2O{:}Al_2O_3{:}2.1SiO_2{:}39.1H_2O$	GIS, CAN, TOB, HER	Mul
28	18.00	2.87		6.20	3.37	175	48	$1.4Na_2O{:}Al_2O_3{:}2.1SiO_2{:}39.1H_2O$	GIS, CAN, TOB, HER	Mul
29	18.00		1.35	3.10	6.24	100	3	$0.9K_2O{:}Al_2O_3{:}2.1SiO_2{:}76.4H_2O$	---	Qtz, Mul
30	18.00		1.35	3.10	6.24	100	24	$0.9K_2O{:}Al_2O_3{:}2.1SiO_2{:}76.4H_2O$	---	Qtz, Mul
31	18.00		1.35	3.10	6.24	100	48	$0.9K_2O{:}Al_2O_3{:}2.1SiO_2{:}76.4H_2O$	---	Qtz, Mul
32	18.00		4.03	3.10	7.11	100	3	$2.7K_2O{:}Al_2O_3{:}2.1SiO_2{:}78.2H_2O$	---	Qtz, Mul
33	18.00		4.03	3.10	7.11	100	24	$2.7K_2O{:}Al_2O_3{:}2.1SiO_2{:}78.2H_2O$	---	Qtz, Mul
34	18.00		4.03	3.10	7.11	100	48	$2.7K_2O{:}Al_2O_3{:}2.1SiO_2{:}78.2H_2O$	---	Qtz, Mul
35	18.00		1.35	6.20	3.12	100	3	$0.5K_2O{:}Al_2O_3{:}2.1SiO_2{:}38.2H_2O$	---	Qtz, Mul
36	18.00		1.35	6.20	3.12	100	24	$0.5K_2O{:}Al_2O_3{:}2.1SiO_2{:}38.2H_2O$	---	Qtz, Mul
37	18.00		1.35	6.20	3.12	100	48	$0.5K_2O{:}Al_2O_3{:}2.1SiO_2{:}38.2H_2O$	---	Qtz, Mul
38	18.00		4.03	6.20	3.55	100	3	$1.4K_2O{:}Al_2O_3{:}2.1SiO_2{:}39.1H_2O$	---	Qtz, Mul
39	18.00		4.03	6.20	3.55	100	24	$1.4K_2O{:}Al_2O_3{:}2.1SiO_2{:}39.1H_2O$	---	Qtz, Mul
40	18.00		4.03	6.20	3.55	100	48	$1.4K_2O{:}Al_2O_3{:}2.1SiO_2{:}39.1H_2O$	CHA, SOD, PHI	Qtz, Mul
41	18.00		1.35	3.10	6.24	175	3	$0.9K_2O{:}Al_2O_3{:}2.1SiO_2{:}76.4H_2O$	---	Qtz, Mul
42	18.00		1.35	3.10	6.24	175	24	$0.9K_2O{:}Al_2O_3{:}2.1SiO_2{:}76.4H_2O$	EDI	Mul
43	18.00		1.35	3.10	6.24	175	48	$0.9K_2O{:}Al_2O_3{:}2.1SiO_2{:}76.4H_2O$	EDI	Mul
44	18.00		4.03	3.10	7.11	175	3	$2.7K_2O{:}Al_2O_3{:}2.1SiO_2{:}78.2H_2O$	---	Qtz, Mul
45	18.00		4.03	3.10	7.11	175	24	$2.7K_2O{:}Al_2O_3{:}2.1SiO_2{:}78.2H_2O$	CHA, LTF	---
46	18.00		4.03	3.10	7.11	175	48	$2.7K_2O{:}Al_2O_3{:}2.1SiO_2{:}78.2H_2O$	CHA, LTF	---
47	18.00		1.35	6.20	3.12	175	3	$0.5K_2O{:}Al_2O_3{:}2.1SiO_2{:}38.2H_2O$	---	Qtz, Mul
48	18.00		1.35	6.20	3.12	175	24	$0.5K_2O{:}Al_2O_3{:}2.1SiO_2{:}38.2H_2O$	EDI	Mul
49	18.00		1.35	6.20	3.12	175	48	$0.5K_2O{:}Al_2O_3{:}2.1SiO_2{:}38.2H_2O$	EDI	Mul
50	18.00		4.03	6.20	3.55	175	3	$1.4K_2O{:}Al_2O_3{:}2.1SiO_2{:}39.1H_2O$	---	Qtz, Mul
51	18.00		4.03	6.20	3.55	175	24	$1.4K_2O{:}Al_2O_3{:}2.1SiO_2{:}39.1H_2O$	CHA, LTF	---
52	18.00		4.03	6.20	3.55	175	48	$1.4K_2O{:}Al_2O_3{:}2.1SiO_2{:}39.1H_2O$	CHA, LTF	---

GIS, gismondine; PHI, phillipsite; SOD, sodalite; CAN, cancrinite; TOB, tobermorite; HER, herschelite; EDI, zeolite Barrer-KF; CHA, chabazite; LTF, zeolite LTF; Qtz, quartz; Mul, mullite; L/S, activator solution/FA ratio.

In the set of experiments at 100 °C (Table 7.1, tests 1–16, Figure 7.1), XRD showed that FA-GIS and FA-SOD were the dominant synthesis products at 1.33 and 3.99 M NaOH, respectively. For shorter reaction times (3 h), the XRD intensities of quartz and mullite showed a small decrease and zeolitic materials were not detected. With reaction time, the intensities of quartz progressively decreased, whereas those of mullite did not change, indicating that it was a

relatively stable phase during the hydrothermal reaction, and weak reflection peaks of the zeolitic products appeared, which showed increasing intensity with reaction time. However, the characteristic XRD peaks of mullite and quartz still remain after 48 h of hydrothermal reaction, which demonstrated the low reactivity of these phases in alkaline solutions. In this case**,** the only source of Si and Al for zeolite crystallization should be the glass phase (Juan *et al*., 2007).

The synthesis of FA-GIS and FA-SOD was conducted using different NaOH concentrations at 100 ^{o}C for longer reaction times, with higher grade of crystallinity and the complete dissolution of quartz using 1.33M NaOH solutions (Figures 7.1c) and lower crystallinity and the persistence of quartz and mullite using 3.99M NaOH solutions (Figures 7.1d), compared with what is observed in Figures 7.1a and 7.1b, respectively. Using low activation solution/FA ratios, it was observed that using a low NaOH concentration (Figure 7.1e) a quite similar grade of crystallinity to that observed in Figure 7.1a was obtained, whereas that using a high NaOH concentration (Figure 7.1f) a reduction in crystallinity of the synthesis products with respect to that in Figure 7.1.b occurred. The highest NaOH activation efficiencies were obtained using 1.33M NaOH solutions, reaction time (120-288 h) and high activation solution/FA ratio (6.12 ml/g). Mullite was only partially attacked and no additional dissolution of this phase was observed for periods > 48 h, after which quartz was completely dissolved. Therefore, the increase in yield of FA-GIS after 48 h of activation would be due to the bringing into solution of some components of aluminosilicate glass by alkaline reaction and reaction times > 72 h do not improve the FA-GIS yield similar to what is reported by (Juan *et al*., 2007).

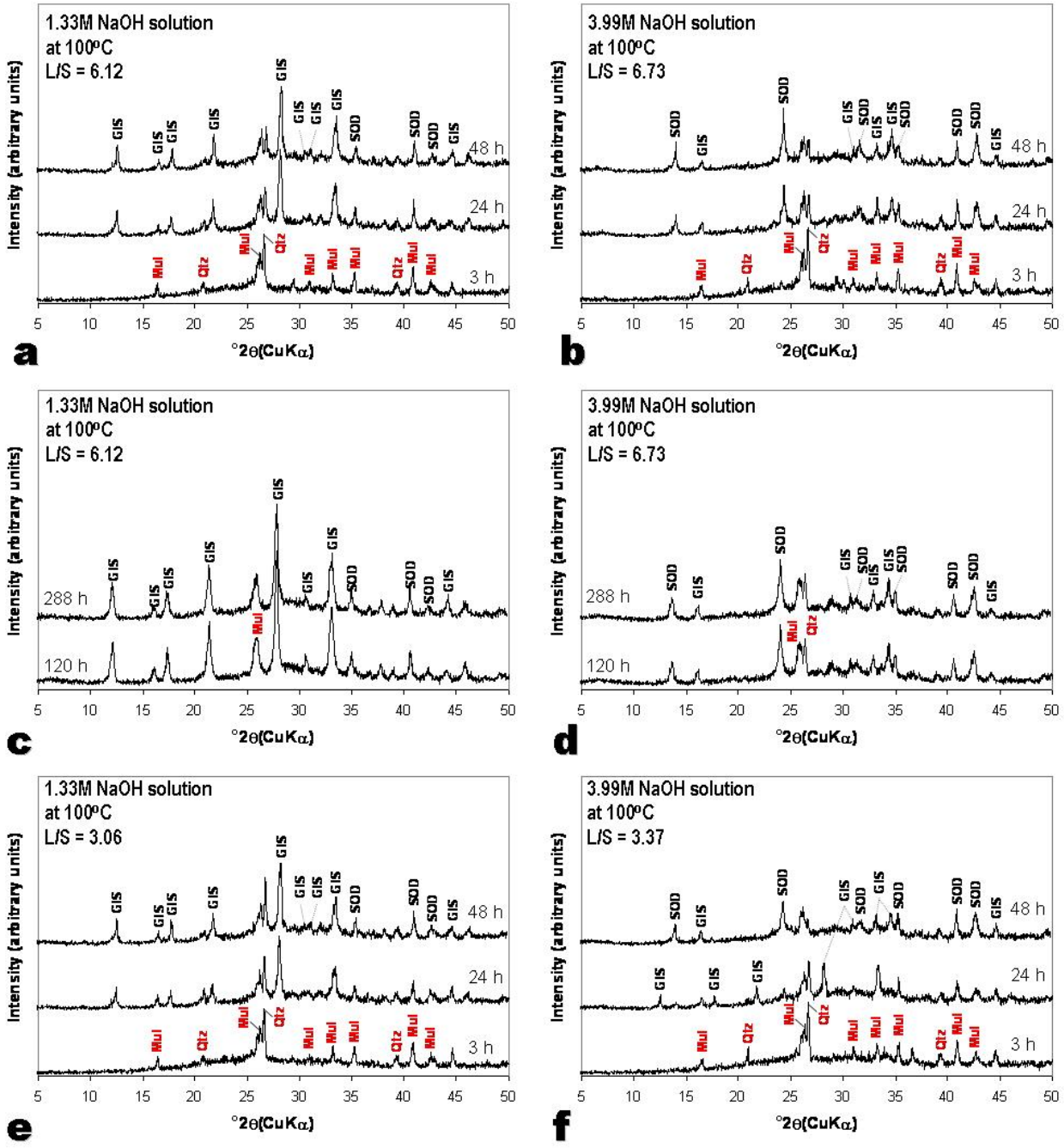

Figure 7.1. XRD patterns of the synthesis products obtained after hydrothermal reaction of FA in NaOH solutions at 100 ºC. L/S, alkaline solution/FA ratio.

In the set of experiments at 175 ºC (Table 7.1, tests 17-28, Figures 7.2a to 7.2d), XRD showed that FA-GIS and FA-SOD were still the dominant synthesized types, accompanied by traces of FA-TOB, FA-CAN and FA-HER at higher activation solution/FA and a mixture of FA-GIS, FA-TOB, FA-CAN and FA-HER was obtained at lower activation solution/FA.

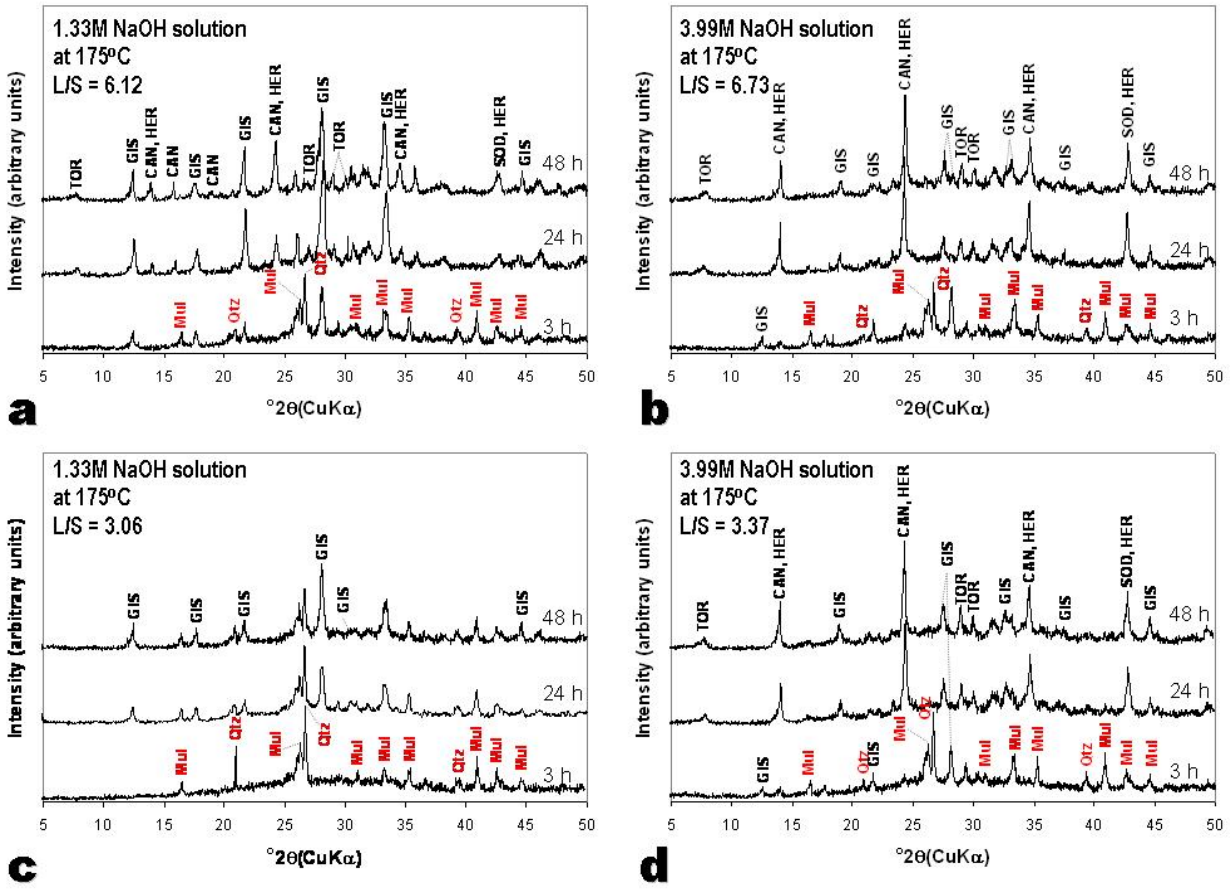

Figure 7.2. XRD patterns of the synthesis products obtained after hydrothermal reaction of FA in NaOH solutions at 175 ºC. L/S, alkaline solution/FA ratio.

A difference in the XRD patterns was recognized after 3 h, compared with those obtained at lower temperature, which is shown by the occurrence of weak reflection peaks of the zeolitic products. A total dissolution of quartz and mullite occurred after 24 h when a higher activation solution was used. However, at lower activation solution and higher activation solution/FA ratios, quartz dissolved after 24 h while mullite only after 48 h. These crystalline phases exhibited a similar behaviour using lower NaOH concentrations and activation solution/FA ratios, with a progressive decrease of their intensities during 24 h of reaction, which however increased over 24-48 h period. Under these reaction conditions, it was observed that the reaction time probably was an important factor controlling the synthesis process over 3-24 h period, although after this reaction time a fairly constant behaviour of the reflection peak intensity was observed.

SEM images in Figure 7.3 illustrate the occurrence of the as-synthesized zeolitic products

obtained after activation of FA in NaOH solutions, revealing a change in morphology of the original surface of the FA particles, which can be explained by the dissolution of the amorphous aluminosilicate phase in the raw FA and the crystallization of zeolitic materials onto the external surface of FA spheres as pseudomorphs, taking into account that the zeolitic aggregates retain the original shape of the FA spheres after alkaline activation. Figures 7.3a to 7.3d illustrate examples of the presence of FA-SOD, which developed aggregates of randomly oriented and intersecting blade-shaped crystals (in some cases growing onto the surface of a sphere of the original FA). This phase can be associated with large clusters of radiating crystals of FA-GIS showing an orthorhombic stick-like shape (Figures 7.3a and 7.3c). A similar morphology has been reported by Kang *et al*. (1998). These zeolitic materials seem to nucleate and grow outward from the surface of the FA spheres. The covering of the spherical particles with small crystallites becomes apparent as well as the presence of large crystals of FA-GIS after alkaline activation. The occurrence of different FAZs, such as FA-TOB, FA-GIS, FA-CAN, FA-SOD and FA-HER, in which aggregates showing fibrous or flaky appearance, likely corresponding to FA-TOB, are recognized in Figures 7.3e to 7.3h. However, Figure 7.3g shows that no zeolitic product crystallized except an unidentified phase with hair-like morphology.

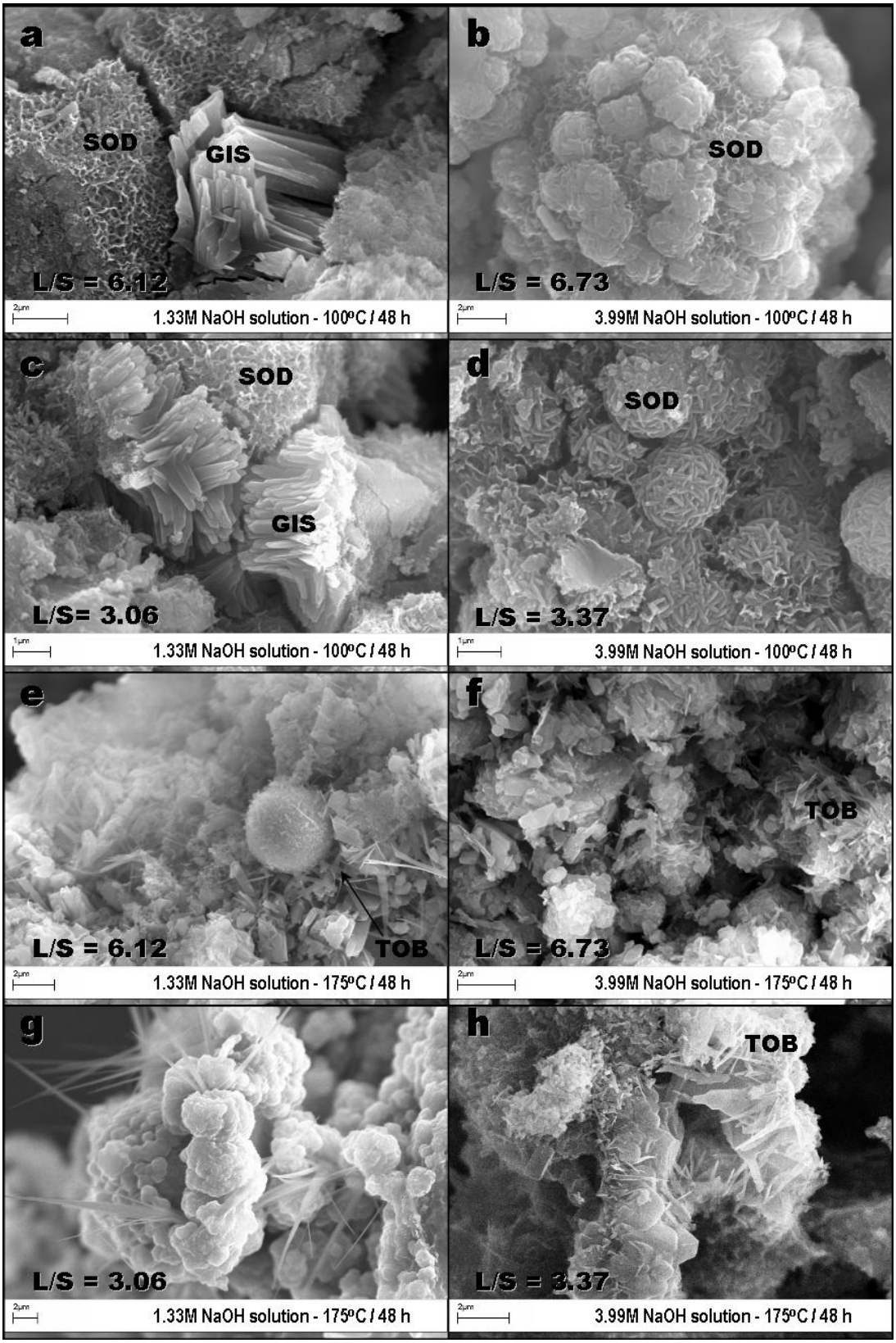

Figure 7.3. SEM images of the synthesis products obtained after hydrothermal reaction of FA in NaOH solutions at (a-d) 100 and (e-h) 175 ^{o}C. L/S, alkaline solution/FA ratio.

7.1.2. Synthesis experiments in KOH media

Results from KOH treatments are shown in Table 7.1, indicating that KOH concentration, activation solution/FA ratio and temperature play important roles in determining the type of zeolitic material to be synthesized in KOH media. However, the KOH solutions showed lower conversion efficiency than the NaOH solutions, although several FAZs were obtained, which included FA-EDI as the main zeolitic product, with traces of FA-CHA, FA-LTF and FA-PHI. According to Juan *et al*. (2007), FAZs prepared by KOH activation show a different behaviour of the zeolite layer synthesized on the surface of the external surface of the FA spheres with regards to the FAZs obtained by NaOH activation. The fact that most K-zeolites firmly adhere to the FA particles makes these FAZs attractive for use in water treatment by cation exchange. No difference can be identified in the XRD patterns between the FA and the synthesis products obtained after its activation in KOH solutions for 3 h, as shown by the occurrence of the aluminosilicate phases (mullite and quartz). The formation of K-zeolites was promoted at longer reaction time (24 h). The XRD patterns of the FAZs tend to increase with reaction time for 24 h, while correspondingly those of mullite and quartz greatly lowered, indicating the dissolution of aluminosilicates in the KOH medium, except when higher activation solution/FA and lower temperature were used. Generally, over 24-48 h period, the peak intensities of the as-synthesized zeolites exhibited a constant behaviour.

In the set of experiments at 100 ^{o}C (Table 7.1, tests 29-40, Figures 7.4a to 7.4d), XRD shows that quartz and mullite were not attacked by the KOH solution, as shown by the fairly constant behaviours of their reflection peaks, except when higher KOH concentration and lower activation solution/FA ratios were used. This resulted in the progressive dissolution of quartz and mullite and the corresponding crystallization of FA-CHA and FA-SOD over 24-48 h period (Table 7.1, tests 39-40, Figure 7.4d).

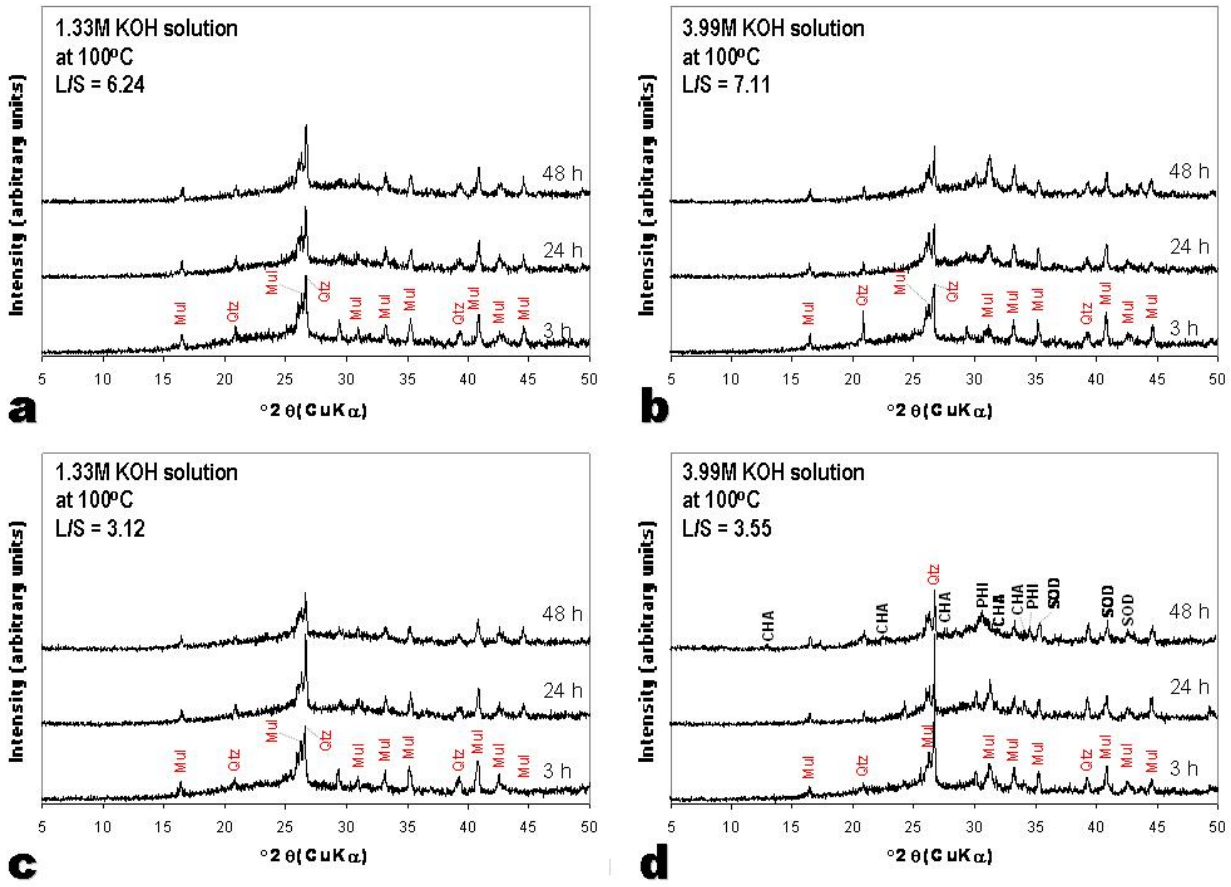

Figure 7.4. XRD patterns of the synthesis products obtained after hydrothermal reaction of FA in KOH solutions at 100 ºC. L/S, alkaline solution/FA ratio.

In the set of experiments at 175 ºC (Table 7.1, tests 41-52, Figures 7.5a to 7.5d), XRD shows that in spite of the activation solution/FA ratios, a lower KOH concentration (Table 7.1, tests 42-43, 48-49) promoted the formation of FA-EDI as the main zeolitic phase. However, with a higher KOH concentration (Table 7.1, tests 45-46, 51-52), FA-CHA and FA-LTF became the dominant phases. In both cases, the intensities of quartz progressively decreased and disappeared after 24 h, whereas those of mullite decreased during 24 h, being constant over 24-48 h period. These zeolitic products were accompanied by traces of FA-CHA, FA-PHI and FA-SOD. Results also showed that high conversion efficiencies could be achieved in short periods of time by increasing KOH concentration. At higher concentration, in spite of the activation solution/FA ratio, quartz and mullite were completely dissolved over 24-48 h period.

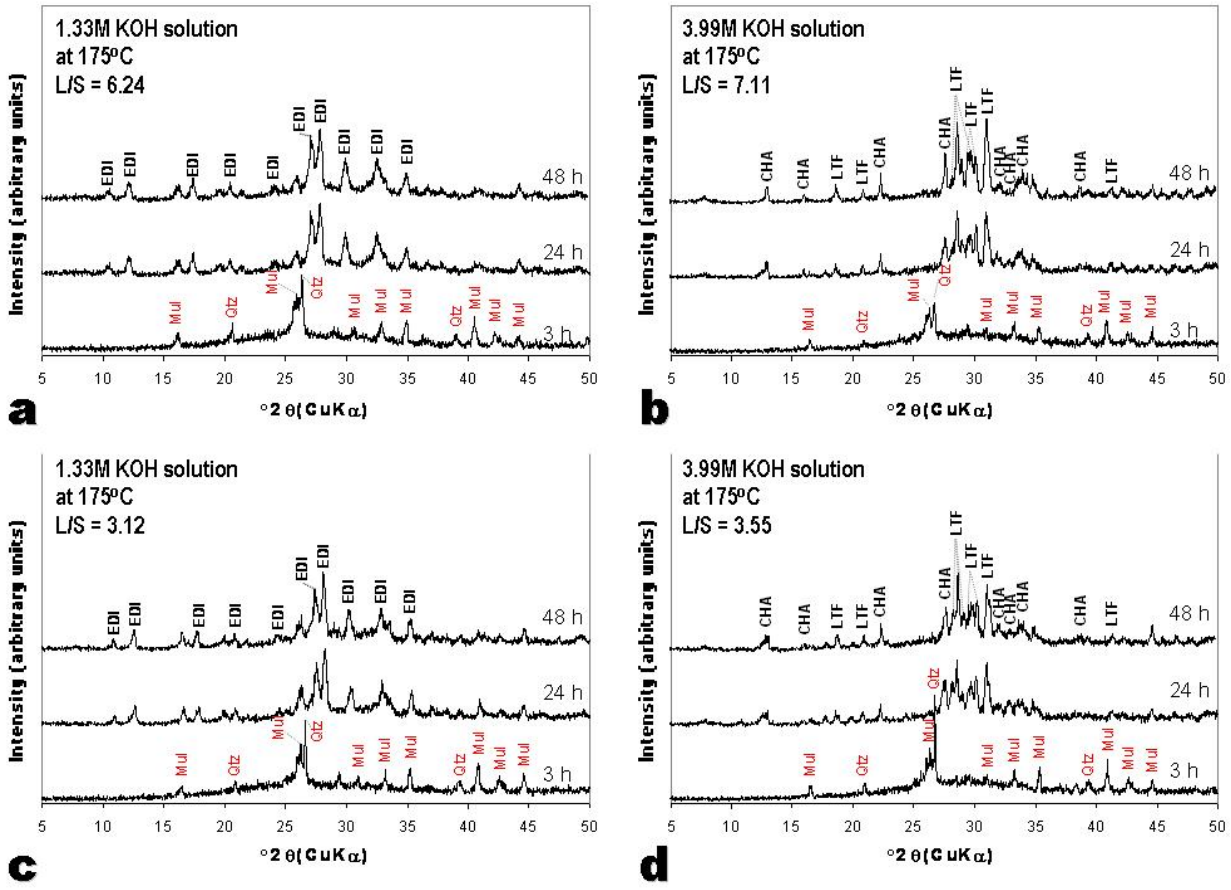

Figure 7.5. XRD patterns of the synthesis products obtained after hydrothermal reaction of FA in KOH solutions at 175 ºC. L/S, alkaline solution/FA ratio.

In general, when higher KOH solutions are used, the main factor controlling the synthesis of FAZs seems to be the L/S ratio, even in short reaction periods (Juan *et al*., 2007). Figure 7.6 illustrates examples of the structural aspects of the treated FA using KOH as an activator. The un-reacted surface of the FA spheres is observed in Figures 7.6a to 7.6c. Hexagonal plates of FA-CHA with a phacolitic aspect associated to FA-SOD are illustrated in Figure 7.6d. Figures 7.6e and 7.6g show examples of typical stubby tetragonal prisms of FA-EDI, arranged into radiating clusters. Observe how the zeolitic crystals have grown onto amorphous material. An intergrowth between FA-LTF and FA-CHA is shown in Figures 7.6f and 7.6h.

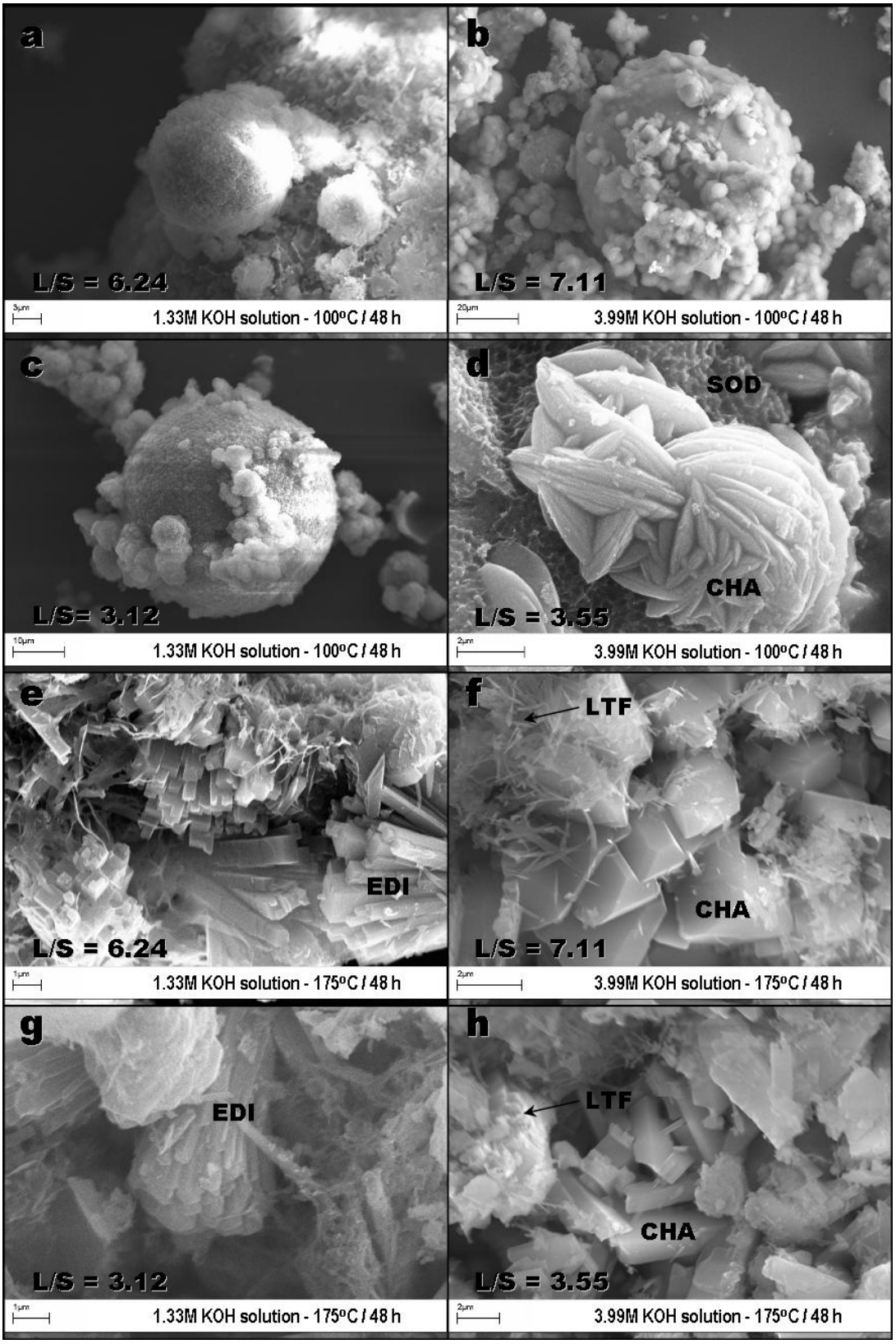

Figure 7.6. SEM images of the synthesis products obtained after hydrothermal reaction of FA in KOH solutions at (a-d) 100 and (e-h) 175 ºC. L/S, alkaline solution/FA ratio.

7.2. Conversion of fly ash by using an alkaline fusion step prior to hydrothermal reaction

The conversion of FA into zeolitic materials using an alkaline fusion, followed by hydrothermal treatment (Table 7.2), revealed that KOH showed a poor efficiency to activate FA, compared with that when NaOH was used as an activator. The alkaline-fused products correspond to sodium silicate and amorphous aluminosilicate, which indicate that fusion was very effective in extracting silicon species in FA. The reaction of quartz and mullite of the starting FA with NaOH is indicated by the disappearance of their characteristic peaks. On the other hand, when the fused product was dissolved in water and heated, zeolitic phases crystallized, using NaOH as an activator. However, the occurrence of an amorphous phase with a geopolymeric paste appearance, particularly using KOH as an activator, reveals a non-successful zeolite synthesis process. This suggests that most of crystalline aluminosilicate has been geopolymerised to amorphous geopolymer during the synthesis as reported by several researchers (Swanepoel and Strydom, 2002; van Jaarsveld *et al*., 2003; Steveson and Sagoe-Crentsil, 2005; Li *et al*., 2006). Therefore, the alkaline fusion method can be applied to evaluate the transformation of the crystalline phases in FA to amorphous geopolymers prior to the synthesis of zeolites.

Table 7.2. Synthesis conditions for conversion of FA by using an alkaline fusion step prior to hydrothermal reaction.

Test	Chemical reagents to be fused			Alkaline fusion		L/FP	Aging	Hydrothermal reaction		Molar gel composition	Zeolitic phases and other synthesis products	Residual phases
	RM (g)	NaOH (g)	KOH (g)	T / °C	t / h	(ml/g)	t / h	T / °C	t / h			
53 *	6.20	7.44		600	1	4.9	21.5^{s}	60	92	$3.5Na_2O{:}Al_2O_3{:}2.1SiO_2{:}141.1H_2O$	FAU	---
54 **	6.20	7.44		600	1	4.9	21.5^{s}	60	92	$3.7Na_2O{:}Al_2O_3{:}2SiO_2{:}149H_2O$	CAN	---
55 ***	6.20	7.44		600	1	4.9	21.5^{s}	60	92	$3.5Na_2O{:}Al_2O_3{:}2.1SiO_2{:}141.1H_2O$	CAN	---
56 *	6.20	7.44		600	1	4.9	5.5^{s}	60	24	$3.5Na_2O{:}Al_2O_3{:}2.1SiO_2{:}141.1H_2O$	---	---
57 *	6.20	7.44		600	1	4.9	5.5^{s}	60	48	$3.5Na_2O{:}Al_2O_3{:}2.1SiO_2{:}141.1H_2O$	CAN	---
58 *	6.20	7.44		600	1	4.9	5.5^{s}	60	96	$3.5Na_2O{:}Al_2O_3{:}2.1SiO_2{:}141.1H_2O$	CAN	---
59 *	6.20	7.44		600	1	4.9	5.5^{s}	60	4	$3.5Na_2O{:}Al_2O_3{:}2.1SiO_2{:}141.1H_2O$	CAN	---
60 *	6.20	7.44		600	1	4.9	5.5^{s}	60	24	$3.5Na_2O{:}Al_2O_3{:}2.1SiO_2{:}141.1H_2O$	CAN	---
61 *	6.20	7.44		600	1	4.9	24^{s}	60	4	$3.5Na_2O{:}Al_2O_3{:}2.1SiO_2{:}141.1H_2O$	---	---
62 *	6.20	7.44		600	1	4.9	24^{s}	60	24	$3.5Na_2O{:}Al_2O_3{:}2.1SiO_2{:}141.1H_2O$	FAU	---
63 *	6.20	7.44		600	1	4.9	2.5^{ws}	60	4	$3.5Na_2O{:}Al_2O_3{:}2.1SiO_2{:}141.1H_2O$	FAU	---
64 *	6.20	7.44		600	1	4.9	2.5^{ws}	60	24	$3.5Na_2O{:}Al_2O_3{:}2.1SiO_2{:}141.1H_2O$	FAU	---
65 *	6.20	7.44		600	1	4.9	2.5^{s}	100	4	$3.5Na_2O{:}Al_2O_3{:}2.1SiO_2{:}141.1H_2O$	CAN	---
66 *	6.20	7.44		600	1	4.9	2.5^{s}	100	24	$3.5Na_2O{:}Al_2O_3{:}2.1SiO_2{:}141.1H_2O$	CAN	---
67 *	6.20		7.44	600	1	4.9	2.5^{s}	60	4	$2.5K_2O{:}Al_2O_3{:}2.1SiO_2{:}140.1H_2O$	---	---
68 *	6.20		7.44	600	1	4.9	2.5^{s}	60	24	$2.5K_2O{:}Al_2O_3{:}2.1SiO_2{:}140.1H_2O$	---	---
69 *	6.20		7.44	600	1	4.9	2.5^{s}	100	4	$2.5K_2O{:}Al_2O_3{:}2.1SiO_2{:}140.1H_2O$	---	---
70 *	6.20		7.44	600	1	4.9	2.5^{s}	100	24	$2.5K_2O{:}Al_2O_3{:}2.1SiO_2{:}140.1H_2O$	---	---

*RM, raw material; * FA; ** FA+KAO; *** KAO; FAU, faujasite; CAN, cancrinite; L/FP, water/fused product; ^{s} stirring conditions; ^{ws} without stirring conditions.*

The XRD patterns in Figure 7.7a show the effect of addition of KAO to the mixture to be fused,

under the following experimental conditions: aging of hydrogel with stirring for 21.5 h, followed by heating at 60 ^{o}C for 92 h (Table 7.2, tests 53-55). FAU was the single crystalline phase obtained when FA was activated. However, when a mixture of FA+KAO was used, CAN was crystallized. This phase was also obtained using only KAO as raw material, which indicates that the addition of KAO to the mixture controlled both the reactant mixture and the synthesis products. However, this can not be assumed for adding FA to KAO, taking into account that the only CAN would be obtained. Aging of hydrogel with stirring for 5.5 h, followed by heating at 60 ^{o}C for 24, 48 and 96 h (Figure 7.7b, Table 7.2, tests 56-58), and produced an amorphous phase at shorter reaction time (24 h) from which FA-CAN start to crystallize with reaction time (48 h). This case illustrates the effect of reaction time using shorter aging time under stirring conditions. This zeolite-type structure shows a higher grade of crystallinity at longer reaction time (96 h). The effect of aging time under stirring conditions is illustrated in Figure 7.7c (Table 7.2, tests 59-62); using a shorter aging time (2.5 h), FA-CAN formed, showing a constant grade of crystallinity during the 24 h of reaction, whereas using a longer aging time (24 h), an amorphous phase and FA-FAU with a very low grade of crystallinity formed after 4 and 24 h, respectively. Additional tests (Figure 7.7d) show the effect of changing aging conditions. Aging without stirring for 24 h at 60 ^{o}C (tests 63-64 in Table 7.2) a poor crystalline FA-FAU was obtained after for 24 h, although the synthesis products tend to be highly amorphous at shorter reaction time. Aging with stirring for 2.5 h at 100 ^{o}C (tests 65-66 in Table 7.2), FA-CAN was the single crystalline phase identified, which show a constant grade of crystallinity during 24 h of reaction.

The reaction between FA with KOH following the alkaline fusion approach (Table 7.2, tests 67-70) did not produced zeolites. The synthesis products correspond to amorphous aluminosilicates with geopolymeric appearance.

These results reveal the progress of zeolite synthesis by the fusion method. The X-ray diffraction patterns after short reaction times generally shows no XRD peaks, typical of amorphous aluminosilicate solids in the gel, evidencing the fact that the reaction time for both nucleation and growth of zeolitic phases was not long enough. However, after longer reaction times, FAU or CAN appear. The addition of KAO to FA in the starting mixture to be fused with NaOH, produced the maximum grade of crystallinity aging the hydrogel 21.5 h under stirring conditions, followed by heating at 60 ^{o}C for 92 h. Under similar experimental conditions FAU showed the higher grade of crystallinity, compared with the results obtained changing the aging conditions. The crystallization of CAN is favoured generally using shorter aging times (2.5 h) under stirring conditions and the reaction time and temperature have not a strong influence in the grade of

crystallinity of this phase. The above observations also suggest that longer aging times under static conditions could accelerate the crystallization of FAU. It is clearly seen that the synthesis products and the grade of crystallinity were influenced significantly by the way of aging.

Therefore, FAZ crystallization was assessed to be in some cases fairly unsuccessful, as revealed by the presence of a substantial percentage of FA-CAN, with some quartz and mullite, and a poor crystalline FA-FAU. However, in other cases a high degree of well developed crystalline FA-FAU was obtained. Therefore, there is evidence that FA-FAU can be transformed to FA-CAN, which can be attributed to excessive enrichment of the FAZs with the alkaline activator (Rayalu *et al*., 2000).

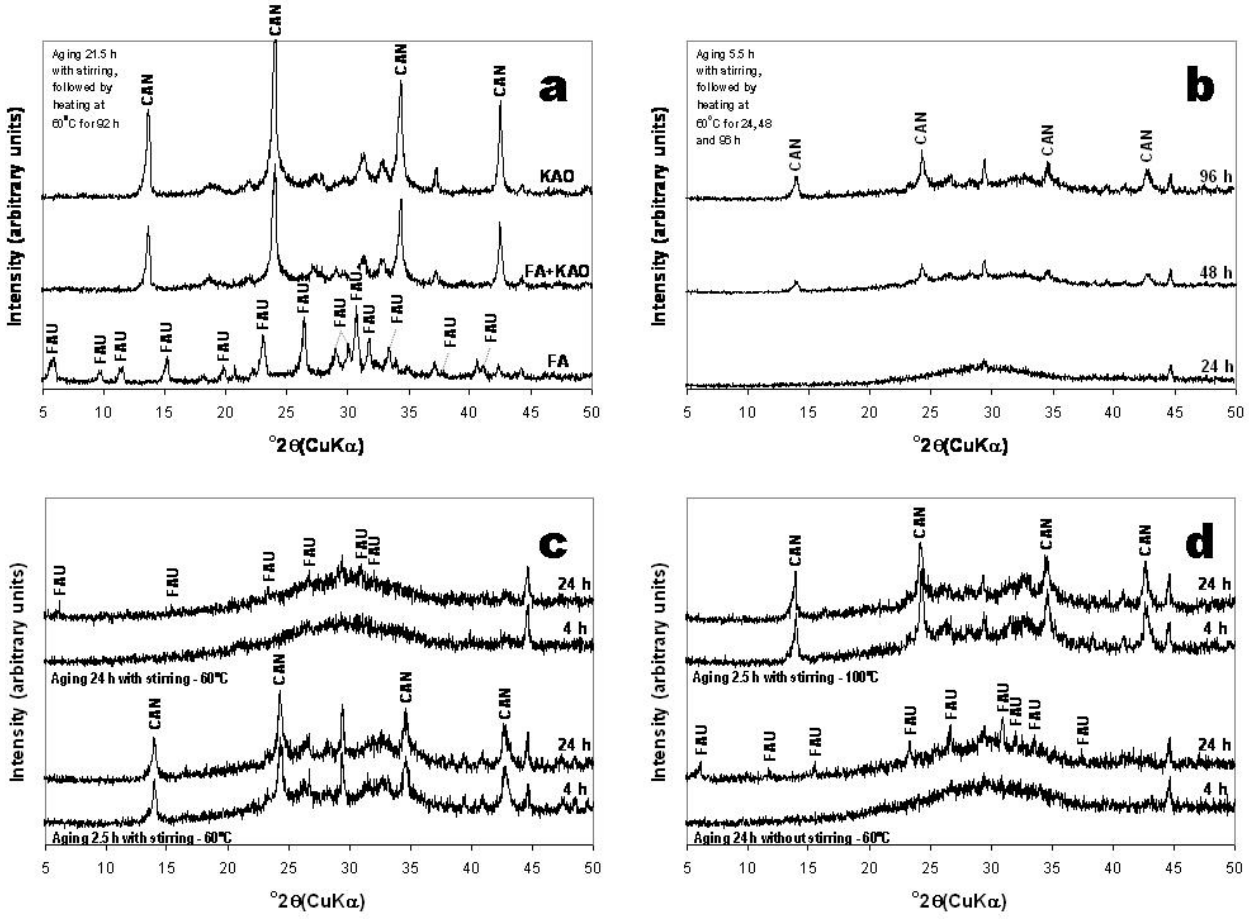

Figure 7.7. XRD patterns of the activation of (a) three different starting mixtures in the fusion step and (b-d) FA showing the effect of aging conditions of the hydrogel; alkaline fusion method with NaOH as an activator.

SEM images in Figure 7.8 show general aspects on the conversion of FA using the alkaline fusion method. Aging conditions strongly affected the morphology of the synthesis products. A uniform crystal size distribution of FA-FAU was obtained aging the slurry for 24 h without stirring, followed by heating at 60 °C for 24 h (Figure 7-8a). This process was repeated but aging the slurry with stirring, although a very poor crystalline zeolitic material was obtained. Two populations of grain size, corresponding to FA-FAU, were observed after aging the slurry for 21.5 h with stirring, followed by heating at 60 °C for 92 h; FA-FAU occurred as single large bipyramidal crystals. These grew at the expense of an aggregate of small FA-FAU cubic crystals (Figure 7.8b). In general, the synthesis products obtained after activation of FA with KOH are similar to polymeric pastes. The presence of the spherical particles in the treated FA indicates that a total conversion of FA to crystalline zeolite was not carried out during hydrothermal treatment.

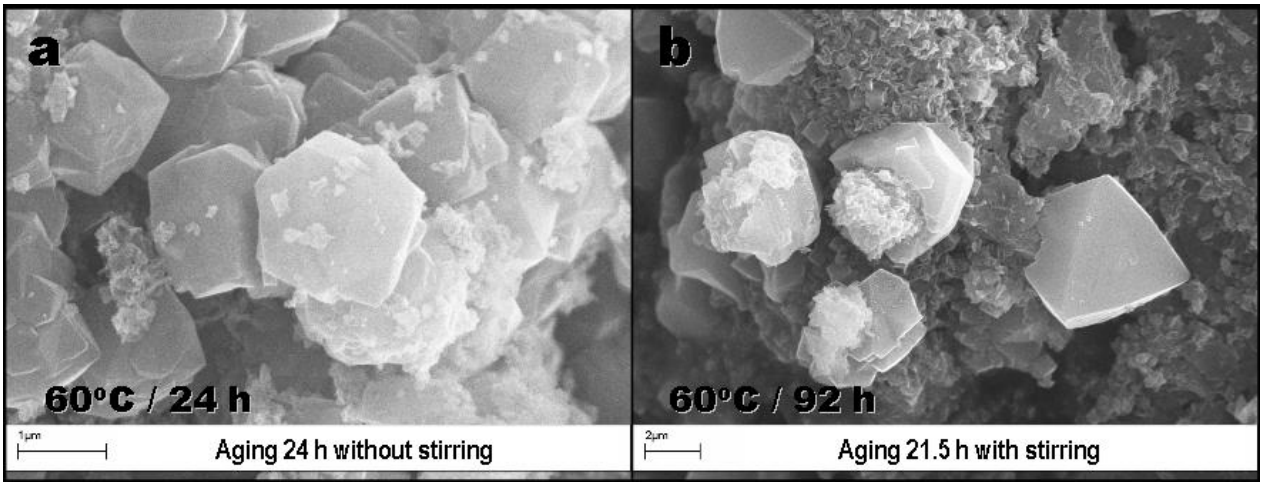

Figure 7.8. SEM images of representative synthesis products obtained via alkaline fusion method with NaOH as an activator.

As expected, the SEM images exhibited a great difference in the particles size distribution for the two different processes of aging of the reaction gel under static and stirring conditions. Aging the aluminosilicate gel without stirring promoted the formation of crystals of FA-FAU with a narrow size distribution (1.5-2.0 µm) as shown in Figure 7.8a, which indicates that nuclei were formed in a slow and homogeneous way, with consequent uniform growth during the crystallization. This reveals a high nucleation rate occurring during aging and the growth occurring during crystallization. Figure 7.8b shows the presence of small particles of 0.5-1.0 µm together with particles of up to 6.0 µm formed after aging the hydrogel under stirring conditions.

The formation of different nucleation sites (nuclei) occur and, following the Ostwald ripening rule, larger crystallites, which usually possess a lower surface free energy contribution and are more stable, destabilize smaller cubic coexisting crystals of the same phase, decreasing crystal size distribution and promoting the growth of progressively fewer octahedral crystals. In other words, numerous small crystals early formed eventually disappear, except those that still continue growing at the expense of the smallest crystals, acting as nutrients for the growth of the largest crystals. Therefore, this process is characterized by a simultaneous growth and dissolution of particles separated in the same media.

The considerable amount of unreacted or not totally consumed FA spheres indicate a moderate degree of reaction in the system. This might suggest that the precipitation of the reaction products quickly forms a layer on still unreacted spheres, which would inhibit its activation and could justify the moderate degree of reaction already observed in these systems (Palomo *et al*., 2004). In some cases, no zeolite crystals were detected through the SEM observations of some samples in spite of zeolitic materials being detected by XRD, which could be due to a very small size of the zeolite crystals (Fernández-Jiménez and Palomo, 2005).

Table 7.3 shows that the weight percent of the major oxides in raw FA has changed during zeolite synthesis. After the hydrothermal synthesis, FA incorporated significant amount of Na or K due to their activation with NaOH and KOH, in agreement with Maruyama *et al*. (2002). At high NaOH and KOH Molarity, higher SiO_2/Al_2O_3 ratios were obtained, with the corresponding increase of Na_2O and K_2O in the synthesis products. Using the fusion approach also promoted the increase in Na or K contents. Fe content showed a slight increase after alkaline activation of FA, except using low concentration alkaline solutions; Ca content increased during the synthesis process; other impurities in general tend to decrease, although the fusion method favoured the increase of some of them. The SiO_2/Al_2O_3 ratio can be used to predict whether the FA could successfully used in the treatment of contaminated effluents, with FAZs high SiO_2/Al_2O_3 ratios (>2.00) being more adequate for this proposal. Zeolitic products showed different SiO_2/Al_2O_3 ratios, with higher ratios using low molarity NaOH and KOH solutions or the fusion approach with KOH as activator. The lowest SiO_2/Al_2O_3 ratio (0.88) was obtained using NaOH as activator. Therefore, based on the low SiO_2/Al_2O_3 ratios determined in the as-synthesized zeolites.

Table 7.3. Chemical composition of the starting FA and representative synthesis products.

Material	Weight (%)										SiO_2/Al_2O_3 ratio
	SiO_2	Al_2O_3	Fe_2O_3	MgO	K_2O	Na_2O	CaO	MnO	TiO_2	SO_3	
FA	52.96	43.60	0.41	0.33	1.30	0.33	0.48	0.00	0.14	0.45	1.21
FAZ1	56.03	25.80	0.00	0.00	0.85	15.87	1.45	0.00	0.00	0.00	2.17
FAZ2	34.74	21.47	0.59	0.00	0.16	38.40	3.52	0.00	1.12	0.00	1.62
FAZ3	53.39	23.21	0.00	0.00	19.41	0.91	3.08	0.00	0.00	0.00	2.30
FAZ4	41.11	27.22	0.46	0.00	30.66	0.00	0.55	0.00	0.00	0.00	1.51
FAZ5	33.15	37.53	0.77	0.00	0.00	17.42	9.84	0.00	1.31	0.00	0.88
FAZ6	44.07	21.62	1.55	1.43	20.25	1.10	7.82	0.00	2.17	0.00	2.04

FA, fly ash; FAZ1 (1.33M NaOH solution - 100 °C / 288); FAZ2 (3.99M NaOH solution - 100 °C / 288 h); FAZ3 (1.33M KOH solution - 175 °C / 48 h); FAZ4 (3.99M solution - 175 °C / 48 h); FAZ5 (following the fusion approach with NaOH as activator - 60 °C / 92 h); FAZ6 (following the fusion approach with KOH as activator - 60 °C / 24 h)
FAZ, FA-based zeolite

7.3. ^{29}Si and ^{27}Al Magic Angle Spinning Nuclear Magnetic Resonance

The raw FA and synthesis products were studied by ^{29}Si and ^{27}Al MAS NMR (Figure 7.9), which is a powerful technique that reveals important information on the local structure of the [SiO_4] and [AlO_4] tetrahedra in aluminosilicates. These results corroborate the FT-IR results.

7.3.1. ^{29}Si MAS NMR spectra

The ^{29}Si MAS NMR spectrum of FA (Figure 7.9a) exhibits a broad resonance in the chemical shift range from −65 to −125 ppm due to many slightly different environments around nominally equivalent Q^n(mAl)-type silicons, leading to a substantial number of overlapping lines with slightly different chemical shifts (Fernández-Jiménez *et al*., 2006). There is severe line broadening caused by a paramagnetic component in the FA, which accounts for the intense spinning sidebands (between 0 and -50 and -150 and -200 ppm). In this spectrum peaks detected at -79.2, -88.8, -96.2 and -108.6 ppm are attributed to the different Si environments of the FA (Palomo *et al*., 2004; Fernández-Jiménez *et al*., 2006). The peaks with chemical shifts at -88.8 and -108.6 ppm can be attributed to mullite (Gomez and François, 2000) and quartz (Klinowski, 1984; Engelhardt and Michel, 1987), respectively. The ^{29}Si MAS NMR spectrum of Figure 7.9b consists of five resonances at -88.5, -92.9, -98.3, -103.7 and -107.8 ppm, revealing the presence of Q^4(4Al), Q^4(3Al), Q^4(2Al), Q^4(1Al) and Q^4(0Al) sites, respectively. A distinct peak at −88.5 ppm can be assigned to the Q^4(4Al) species in FA-SOD (Brough *et al*., 2001), with a

calculated Si/Al ratio = 1.0. However, zeolite-type structure exhibit a single resonance over a wide range of chemical shifts dependent upon composition; the ^{29}Si chemical shift depend upon the Si-O-Al bond angle and lattice constants (Weller and Wong, 1988; Engelhardt *et al*., 1989). Mullite can also contribute to this signal (Palomo *et al*., 2004). Three well resolved signals at -92.9, -98.3 and -103.7 ppm include, respectively, contributions from Q^4(3Al), Q^4(2Al) and Q^4(1Al) sites in FA-GIS (Engelhardt and Michel, 1987; Zubowa *et al*., 2008). According to Zubowa *et al*. (2008), the ranges of chemical shift over which these resonances occur are reasonably characteristic of the composition of the first coordination sphere and the NMR spectra reflect the local Si/Al distributions in simple zeolite lattices. FA-GIS has only one type of T atom in the unit cell and only one resonance line is observed for each locally different silicon surroundings (Zubowa *et al*. 2008). The relative size of these peaks was used to determine the Si/Al ratio in FA-GIS. The ratio was found to be 1.8 and explain why no local silicon environments with four Al neighbours (Si(4Al)) are present with a chemical shift range of -80 to -90 ppm. The signal at -107.8 ppm can be attributed to Q^4(0Al) sites due to the presence of unreacted quartz. Figure 7.9c shows two resonance peaks at -87.2 and -93.5 ppm. The sharp peak at -87.2 ppm can be assigned to Q^4(4Al) sites of FA-SOD. According to Weller and Wong (1988), this chemical shift is in agreement with the expected chemical shift for a lattice parameter of 8.905(2) Å in sodalite, whose structure is formed by four-member rings, with each silicon tetrahedron surrounded by four aluminium tetrahedral in strict alternation of Si and Al atoms and hence Si/Al ratio = 1 (as has been obtained in this study). The weak peak at -93.5 ppm can be attributed to a contribution from Q^4(3Al) sites of FA-GIS. Figure 7.9d shows several resonance peaks at -85.6, -89.6, -94.2, -98.3 and -103.1 ppm, which are assigned to Q^4(4Al), Q^4(3Al), Q^4(2Al), Q^4(1Al) and Q^4(0Al) sites, respectively, and can be presumably attributed to FA-EDI. Figure 7.9e displays a sharp peak at -84.0 ppm and a weak signal at -89.0 ppm, which are assigned to Q^4(4Al) and Q^4(3Al) sites, respectively, of FA-FAU. The faujasite structure is formed by linking the sodalite cage through double six membered rings. It can display up to five peaks in the range of -80 to -110 ppm assignable to Si atoms surrounded by 4, 3, 2, 1 and 0 atoms of Al, whose intensities vary as a function of the Si/Al ratio (Klinowski, 1984; Engelhardt and Michel, 1987). The as-synthesized FA-FAU has a calculated Si/Al ratio = 1.1, with the -84.0 ppm signal predominating with respect to the low intensity signal at -89.0 ppm. The other spectral signals corresponding to this zeolite can be overlapped and may not be easily detected due to the lower Si/Al ratio as suggested by Fernández-Jiménez *et al*. (2008).

7.3.2. ^{27}Al MAS NMR spectra

The ^{27}Al MAS NMR spectrum of the original FA (Figure 7.9a) shows two peaks at 43.7 and -3.4 ppm due to tetrahedral non-framework Al(4) and octahedral non-framework Al(6) co-ordination, respectively. The intense sidebands result from a relatively high level of paramagnetic impurities in FA. The ^{27}Al MAS NMR spectra of the as-synthesized materials are mostly tetrahedral aluminium, consisting of a single resonance, corresponding to zeolite $Al(OSi)_4$ sites. Figure 7.9b shows a signal at 58.8 ppm (FA-GIS), which is ascribed to 4-coordinated Al, similar to what is reported by Zubowa *et al*. (2008), although there is a small amount of extra-framework 6-coordinated Al at -5.3 ppm. This small amount of Al(6) may be due to the presence of residual mullite. The spectrum in Figure 7.9c shows a signal at 59.9 ppm in FA-SOD in agreement with previous studies (Engelhardt and Michel, 1987; Jacobsen *et al*., 1989). However, there a weak signal at -6.3 ppm corresponding to residual mullite. Figures 7.9d (FA-EDI) and 7.9e (FA-FAU) are characterized by a maximum intensity at 58.5 and 53.8 ppm, respectively. The spectra in Figures 7.9c to 7.9e show peaks have a much narrower linewidth than that in FA, which are predominantly tetrahedral aluminium. The outlying peaks are spinning sidebands. The ^{27}Al MAS NMR spectra clearly distinguish tetrahedrally and octahedrally co-ordinated aluminium. Al in higher co-ordination can typically result from the water co-ordinating to the Al in the zeolite, the presence of extra-framework Al species, often observed in calcined samples or the presence of impurities, usually alumina.

7.4. Reaction mechanism during zeolite synthesis

The reaction mechanisms of zeolite synthesis from alkali activation of FA have been investigated by several authors (Maruyama *et al*., 2002; Fernández-Jiménez and Palomo, 2005; Fernández-Jiménez *et al*., 2005; Inada *et al*., 2005; Juan *et al*., 2007), and can be divided into a number of stages. The chemistry of evolution of the system is very complex due to several factors. However, the reaction history of the zeolite synthesis developed in this study can be summarized as follows.

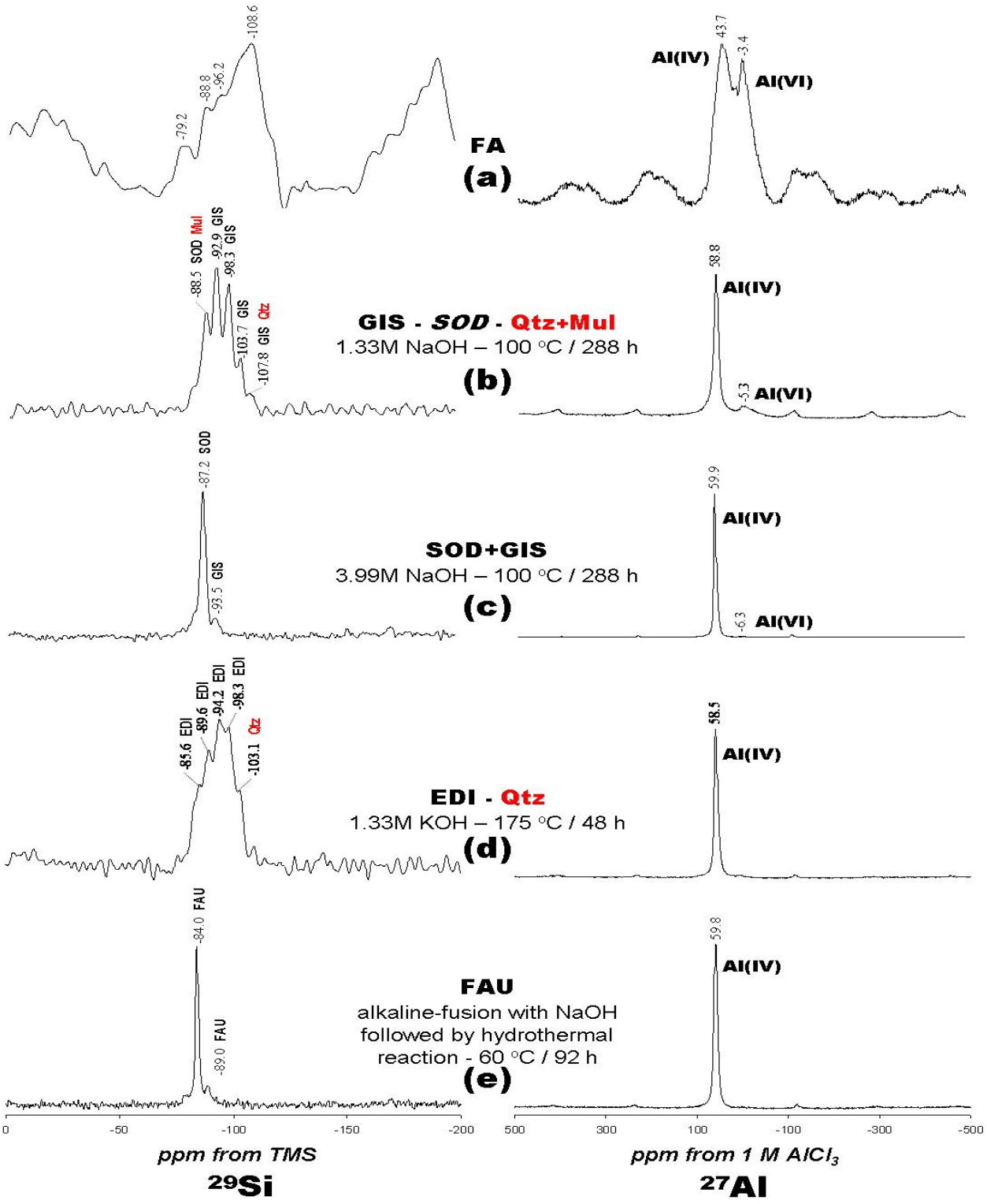

Figure 7.9. ^{29}Si and ^{27}Al MAS NMR spectra of the (a) raw FA and (b-e) representative synthesis products obtained after alkaline activation of FA with NaOH and KOH as mineralizers. Main and minor phases are indicated in uppercase regular and italic fonts, respectively; starting material phases in uppercase regular font (red colour).

The dissolution reaction of FA occurs in a temperature range of 20-120 ^{o}C as a first step and the amount of OH^- in the alkaline solution makes a great contribution to this reaction (Maruyama *et al*., 2002). In general, dissolution strongly depends on the pH of the alkali medium, with NaOH or KOH acting as mineralizers. Following the alkaline approach, the crystalline phases in FA were dissolved completely by fusion with the alkaline activators, with the formation of sodium or potassium aluminosilicate salts, which can be easily dissolved in H_2O. The dissolution of FA or alkali aluminosilicate phases released ionic species which were transported to the nucleation sites. As the condensation of aluminate and silicate ions took place, the particle surface of FA was covered with the precipitation of an aluminosilicate gel.

During nucleation, the gel composition was significantly affected by thermodynamic and kinetic parameters (Fernández-Jiménez and Palomo, 2005; Fernández-Jiménez *et al*., 2005). The formation of different nucleation sites occurred and, following the Ostwald rule, larger crystallites (usually with lower surface free energy contribution and more stable) destabilized smaller coexisting crystals of the same phase, decreasing crystal size distribution and promoting the growth of progressively fewer zeolite crystals (metastable phases). With reaction time, more stable phases formed at the expense of the initial metastable phases. Finally, the stable phases reached the required equilibrium conditions to promote the crystal growth of the final zeolitic materials. Therefore, following dissolution of the FA in alkaline solutions or its alkali fused products in water, new phases crystallized. A polymerization should be the process that forms the zeolitic precursors, which contains tetrahedra of Si and Al randomly distributed along the polymeric chains that are cross-linked so as to provide cavities sufficiently large to accommodate the charge balancing alkali ions. Finally, the crystallization generally involved the assimilation of material from solution by a growth process, which began when the nuclei reached a critical size and the crystals started to grow. Consequently, reaction products were generated at the expense of the spheres of FA, until the ash particles were completely or almost completely dissolved.

In general, the conversion of FA can be described by two main stages: (1) the dissolution of aluminosilicate phases of the FA releasing Si and Al and (2) the crystallization of zeolitic materials. FA-GIS is favoured at higher Si/Al ratios, whereas higher Al and NaOH concentrations promoted the FA-SOD formation. It is suggested that this FA-SOD appeared more stable than FA-GIS and would be the final product, whereas FA-GIS and amorphous material would be the transition phases, and that during the hydrothermal transformation of FA an initial formation of FA-GIS occurred with subsequent transformation to FA-SOD. The crystallization of FA-EDI was

favoured by higher pH and temperature conditions. The factor determining the crystallization rate was the presence of Na^+ in solution, as demonstrated by Maruyama *et al*. (2002). Na^+ cations also play very important roles during zeolitization, because they stabilize the sub-building units of zeolite frameworks and are fundamental for zeolite synthesis under hydrothermal conditions (Ojha *et al*., 2004). On the other hand, K^+ in solution promotes the slow crystallization rate in KOH solution and therefore it is the suppression factor for zeolite synthesis (Maruyama *et al*., 2002).

During the alkaline fusion step, a solid-state reaction between the alkaline activator and the crystalline phases of FA such as quartz and mullite occurred. As a result, most of the FA particles were converted into sodium or potassium silicate and aluminate salts at the fusion temperature (600 °C). These newly formed compounds dissolved in water more readily than quartz and mullite in the starting FA.

7.5. Conclusions to Chapter 7

FAZs were successfully synthesized via hydrothermal treatment and alkaline fusion followed by hydrothermal reaction using FA as starting material and NaOH and KOH as alkaline activators. In some cases, zeolite formation was assessed to be fairly unsuccessful, taking into account that the synthesis products contain a substantial percentage of FA-SOD, with some quartz and mullite also present, while only a very small fraction of a desired zeolitic phase can be observed. The chemical characterization of FAZs reveals the occurrence of the characteristic XRD reflection peaks of the zeolitic materials formed after FA conversion or relict quartz and mullite from the original FA. On the other hand, SEM images of the FAZs show that after alkaline activation, the original surface of the FA spheres became rough, which indicates that zeolite crystallized on the surface of the FA particles. The type of zeolite formed depends strongly on the experimental conditions, such as temperature, reaction time, alkali hydroxide concentration and solid/solution ratio. Experimental data suggest that the FA could be converted into beneficial products, which can be used as ion exchangers in removing heavy metals from wastewaters. Therefore, it is necessary to develop further experiments under well-optimized conditions, to successfully prepare highly crystalline zeolites. The efficiency in the conversion of FA can be affected by the contents of non-reactive phases (mainly mullite and quartz) or glass as well as its grain size distribution. A low activation solution/FA ratio could be more appropriate from a commercial perspective, taking into account a drastic reduction in the activation time, although

an important decrease in the yields was observed with regards to that obtained with a high activation solution/FA ratio.

The alkaline fusion followed by hydrothermal reaction has the advantage of producing pure zeolite materials, instead of blend zeolite/residual FA particles obtained from the classic hydrothermal treatment. Although this method can selectively produce a specific type of zeolite, it was clear that the crystallinity of the synthesis products was not high enough. Therefore, attempts to convert FA into zeolitic materials without other zeolite phases and residual phases and having higher crystallinity are still clearly challenging.

Chapter 8

Application of different adsorbent materials for the removal of metal ions and ammonium from polluted effluents

Chapter 8. Application of different adsorbent materials for the removal of metal ions and ammonium from polluted effluents

8.1. Introduction

Water is the source of life and is necessary for human survival. However, severe water pollution and insufficient water source are major problems. The structural and physicochemical properties of zeolites make them very effective for the removal of toxic metal ions, radionuclides and ammonium from wastewaters. There are increasing demands for a healthy environment, particularly with regards to high-quality drinking water and removal of pollutants from industrial, agricultural and municipal wastewaters. Most technologies using zeolites for water purification are based on their unique cation-exchange behaviour through which dissolved cations are removed from water by exchanging with cations on a zeolite exchange sites. The most common cation in waters affecting the health of living beings is NH_4^+.

Wastewaters contaminated with heavy metals are produced from many industrial activities, such as tanneries, metal plating facilities, petroleum refining and mining operations, having the potential to harm life forms and the environment. Heavy metals are toxic priority pollutants because they are not biodegradable and tend to accumulate in organisms, causing numerous diseases and disorders (Inglezakis *et al*., 2003). Therefore, wastewaters containing heavy metals are required to be treated prior to discharge into receiving environments. Removal of heavy metals from polluted effluents is a challenging task all over the world regarding the correct management of wastewaters for a sustainable future. If not carefully managed, however, wastewater may produce both short- and long-term effects on human health and the ecological system. Wastewater treatment is the last line of defence against water pollution.

Several procedures for wastewater treatment, including chemical precipitation, electrodeposition, ion exchange, membrane separation and adsorption, have been developed (Diz and Novak, 1998; Webster *et al*., 1998; Feng *et al*., 2000; Mohan and Chander, 2001, 2006; Chartrand and Bunce, 2003; Santos *et al*., 2004; Gibert *et al*., 2005a, b; Johnson and Hallberg, 2005a, b; Wattena *et al*., 2005; Wei *et al*., 2005; Kalin *et al*., 2006), although adsorption has been the preferred method for heavy metal removal, because it is considered to be a particularly effective technique. Adsorption is usually quite a complex process, generally involving much

more than simple ion exchange into the pore openings of the ion exchanger. Factors such as pH, nature and concentration of the counter ion (metal ion), ion hydration, varying metal solubilities, presence of competing and complexing ions, all affect the amount of metal ion to be adsorbed (Ikhsan *et al*., 1999) and therefore the sorbent selectivity. There are two general categories of wastewater treatment which have been thoroughly investigated: (1) active treatment, which requires the use of chemical treatment systems to buffer acidity, and (2) passive treatment, which allows naturally occurring chemical and biological processes to do the work in a controlled system outside of the receiving stream. Activated carbon is considered to be a particularly competitive and effective sorbent for the removal of heavy metals. However; may not be suitable due to high costs associated with production and regeneration of spent carbon (Panday *et al*., 1985). Therefore, alternative low-cost liming substitutes are constantly sought. Such adsorbents should be readily available, economically feasible and easily regenerated.

In this study, different sorbents were investigated to examine their metal ion and ammonium removal capacity and to investigate the relevant mechanisms for metal ion removal by equilibrium studies and kinetic studies. The working hypothesis was that the use of a product containing a higher dose of sorbent would raise pH and induce a favourable environment for ion exchange. Amongst the as-synthesized zeolitic materials, GIS, SOD, CHA and FAU were chosen to be utilized in batch reaction experiments, taking into account their CEC and low Si/Al ratio = 1.65. Such a low Si/Al ratio means that higher concentration of terminal Al-OH groups can be expected at the mineral/solution interface, as well as a zeolite with a more hydrophilic nature. This consequently leads to a greater capacity for ligand exchange and thus better performance during decontamination experiments (Alvarez-Ayuso *et al*., 2003; Misak, 2000; Semosa *et al*., 2002). The overall effect would thus be better performance in terms of metal removal from contaminated waters. Preliminary results obtained by ICP-AES of the treated solutions showed that the equilibrium concentration in the solution phase decreased with increasing adsorbent dose at a given initial metal concentration, since the fraction of metal removed from the aqueous phase increased with a higher sorbent dose. This trend can be anticipated, since raising the sorbent dose provides greater surface area and sorption sites of the zeolite (Gode and Pehlivan, 2003).

Laboratory-test experiments were conducted to evaluate metal ion and ammonium removal during the treatment of polluted solutions (synthetic or natural), to compare the capacity and selectivity of different sorbents during the treatment process and to confirm that zeolites have an advantage over other ion exchangers, taking into account their lower cost and high ion

selectivity. Important parameters such as sorbent dose (g) per effluent volume unit (ml), reaction time and metal concentration were examined in order to understand the removal mechanisms involved and to optimize the overall removal efficiency of the system.

8.2. Removal of heavy metals and ammonium from synthetic solutions

8.2.1. Preliminary experiment of treatment using fly ash and fly ash-based GIS-type zeolite

In a preliminary sorption test, FA and FA-based GIS-type zeolite (FA-GIS) were investigated in terms of their potential for the decontamination of model solutions, artificially polluted with selected metals, in order to compare the capacity and selectivity of these sorbents during treatment. Table 8.1 summarises the values of pH, EC and concentration of metal ions of an untreated synthetic solution (SS1) and those of the leachates obtained using a sorbent:SS1 mixture of 1 g / 50 ml for 7 days.

8.2.1.1. pH and EC

The pH and EC trends for the neutralization reactions between the SS1 and FA and FA-GIS are illustrated in Figure 8.1. Results show that the neutralization of the solution was initially very rapid, with pH increasing immediately from 3.57 to 11.95 (FA) and 10.33 (FA-GIS) within the first 30 min of reaction. Therefore, the breakthrough to alkaline pH was obtained during this period of time. The pH was stabilized within 1 h and then it showed plateau behaviour. Final pH values ranged from 11.92 (FA) and 10.56 (FA-GIS). EC ranged from 341 to 1526-2392 (FA) and 1639-1963 (FA-GIS) $\mu S\ m^{-1}$, with the largest values after 48 h. FA produced higher pH and EC values than FA-GIS.

Table 8.1. Water quality parameters recorded during 7 days of continuous shaking of FA and

FA-GIS with the SS1 in a batch experiment (sorbent:SS1 mixture of 1 g / 50 ml).

Contact time (min)	pH	EC (μS m^{-1})		Heavy metal concentration (ppm)				
				Cu	Pb	Zn	Cr	Ni
SS1*	3.57	341	20.1°C	7.40	6.00	6.04	3.20	5.89
Batch reaction of FA								
30	11.95	1526	18.8°C	0.00	0.00	0.00	0.11	0.00
60	12.10	1789	18.7°C	0.00	0.00	0.00	0.10	0.00
180	12.07	1770	19.9°C	0.00	0.00	0.00	0.08	0.00
360	12.10	1964	22.3°C	0.00	0.00	0.00	0.10	0.00
1440	12.13	2288	21.2°C	0.00	0.00	0.00	0.11	0.00
2880	12.09	2392	22.4°C	0.00	0.00	0.00	0.15	0.00
10080	11.92	1830	23.3°C	0.00	0.00	0.00	0.19	0.00
Batch reaction of FA-GIS								
30	10.33	1790	23.6°C	0.01	0.02	0.00	0.00	0.02
60	10.31	1639	23.3°C	0.03	0.01	0.00	0.01	0.00
180	10.37	1710	24.6°C	0.00	0.00	0.00	0.00	0.00
360	10.38	1760	26.5°C	0.00	0.00	0.00	0.00	0.00
1440	10.45	1879	24.7°C	0.00	0.00	0.00	0.00	0.00
2880	10.48	1963	24.8°C	0.00	0.00	0.00	0.00	0.00
10080	10.56	1836	21.4°C	0.00	0.00	0.00	0.00	0.00

** Parameters of synthetic solution 1*

In general, there is a strong positive correlation between the increase in pH and EC, particularly within the first 6 h of reaction, taking into account that for the rest of the time intervals the EC shows a progressive increase due to the dissolution of salts.

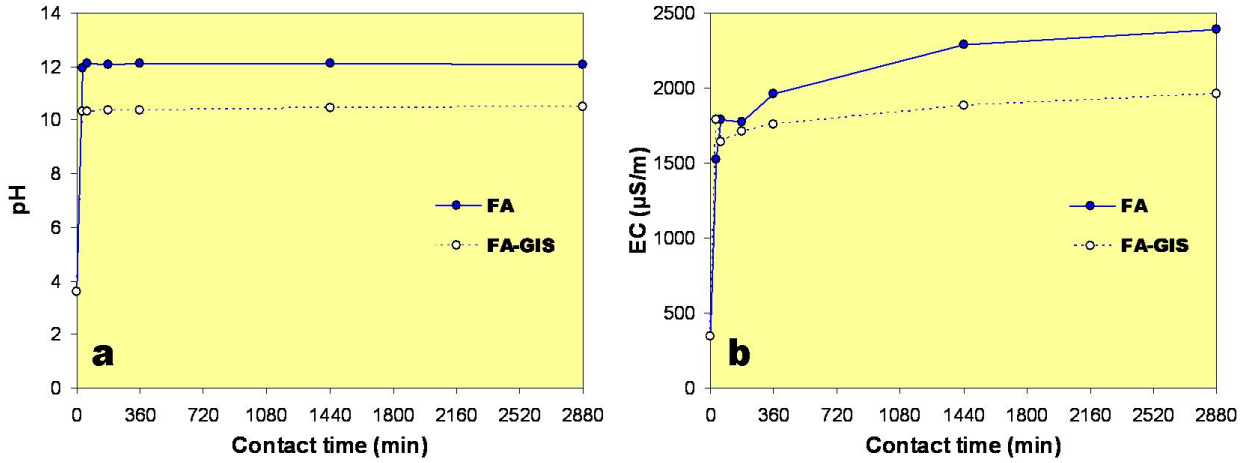

Figure 8.1. pH (a) and EC (b) variation as a function of time during a preliminary adsorption batch experiment with starting pH of 3.57 and EC of 341 μS m^{-1}, sorbent dose of 1 g and SS1 volume of 50 ml.

8.2.1.2. Heavy metal removal

The results obtained for heavy metal removal from the SS1 are shown in Figure 8.2. FA was effective in reducing the Cu, Pb, Zn and Ni concentration, indicating the complete removal of these metal ions, but not Cr, which can be reduced from the synthetic solution but not completely removed, as indicated by the residual concentrations ranging from 0.08-0.15 ppm (Figure 8.2a). It can be explained as a consequence of the dominant occurrence of $Cr(OH)_4^-$ at pH > 10, which increases Cr^{3+} solubility in FA. Pansini and Colella (1991) and Loizidou *et al*. (1992) considered that contrary to the reversible exchange character observed for a wide spectrum of heavy metals, the exchange of Cr is strongly irreversible. However, this does not agree with the Cr trend obtained after addition of FA to the synthetic solution. On the other hand, FA-GIS produced complete removal of Zn. Strong fluctuations in the concentration of Cu and Cr, and a progressive decrease in Pb and Ni, were observed at shorter reaction times, although after 3 h a complete removal of these metal ions was obtained. Heavy metals were chemically incorporated into FA and FA-GIS, but using the zeolitic product it was observed after a longer contact time. In general, most metal ions (except Cr for FA) were removed during an early step of reaction (within the first 3 h), which can be attributed to sorption and metal precipitation as hydroxides and carbonates, as suggested by Zagury *et al*. (2006). The pH of the solution played a very important role on the uptake of metal ions, since it determines the surface charge of the adsorbent (compare Figures 8.1 and 8.2). The uptake of heavy metal ions removed from solution increases rapidly from pH 3.57 to pH 11.95 (FA) or 10.33 (FA-GIS) within the first 30 min of reaction, with a complete removal of heavy metals, except in the case of Cr using FA as sorbent, and for the rest of the time intervals (with pH remaining almost constant), there was not a gradual increase on metals uptake due to the complete removal. In general, the amount of heavy metal ions removed from solution increased as the pH increased. Therefore, it is necessary to highlight that the change of pH in solution with the addition of FA (except for Cr) and FA-GIS has a strong influence in the removal of metal ions as a consequence of the pretty immediate increase in alkalinity, causing (almost certainly) the precipitation of hydroxyl-metal complexes. According to Alinnor (2007), at lower pH, the surfaces of the sorbents are positive, promoting the formation of metal complexes (e.g. $[Cu(OH)_4]^{2-}$), which can be adsorbed on the sorbent surfaces. Hydroxyl-metal complexes have higher affinity for adsorption than hydrated metal ion, because the formation of an OH group of the metal ion reduces the free energy required for adsorption (Cho *et al*., 2005). At higher pH, the surfaces of the sorbents were negative, increasing the uptake of heavy metals by the sorbent, which may be explained in terms of electrostatic interaction (Alinnor, 2007), as shown by the sharp increase on the amount

of metal ions uptake as pH increase from 3.57 to 11.95 (FA) or 10.33 (FA-GIS).

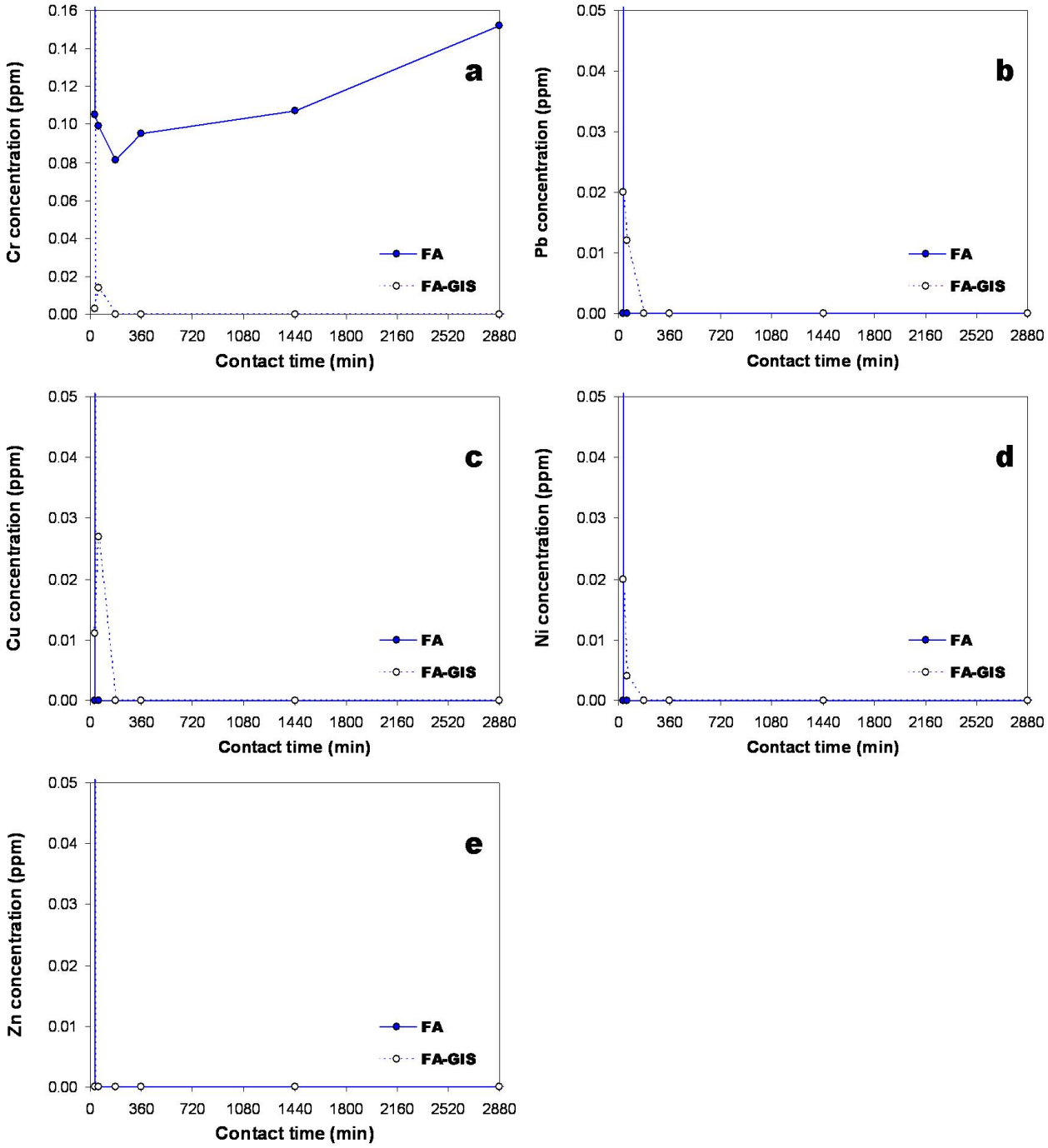

Figure 8.2. Heavy metal concentration variation as a function of time during a preliminary adsorption batch experiment with starting pH of 3.57 and EC of 341 $\mu S\ m^{-1}$, sorbent dose of 1 g and SS1 volume of 50 ml.

The increase in metal ions uptake by FA at higher pH values may be attributed mainly to SiO_2+Al_2O_3 content of the sorbents that provides alkalinity in the system raising the pH to strongly alkaline values, thereby facilitating the uptake of heavy metals, comparable to the alkalinity values obtained by Alinnor (2007). However, this author considers that calcium content and (SiO_2+Al_2O_3+Fe_2O_3) content are responsible of these strongly alkaline values, which is no assumed here due to the very low CaO and Fe_2O_3 of the sorbents (FA and FA-GIS) used in this study.

8.2.2. Treatment using kaolinite, natural clinker and fly ash

The raw materials were used as adsorbents in a second batch-mode experiment in order to establish their efficiency to clean-up an artificially polluted solution (SS2). Table 8.2 summarises the values of pH, EC and concentration of metal ions and ammonium of the untreated SS2 and those of the leachates obtained by using a sorbent:SS2 mixture of 0.50 g / 20 ml during 300 min.

8.2.2.1. pH and EC

Figure 8.3 illustrates the variation of solution pH and EC through time during the batch reactions of the raw materials with SS2. The monitoring of these parameters revealed that FA produced a quite different behaviour in the pattern of pH and EC compared with those obtained using the other two sorbents (NC and KAO).

Table 8.2. Water quality parameters recorded during 300 min of continuous shaking of the raw materials with the SS2 in a batch experiment (sorbent:SS2 mixture of 0.50 g / 20 ml).

Contact time (min)	pH	EC ($\mu S\ m^{-1}$)		Heavy metal concentration (ppm)					Ammonium ($mg\ l^{-1}$)
				Cu	Pb	Zn	Cr	Ni	
SS2*	3.82	376	15.5°C	8.12	6.35	3.56	8.32	6.27	8.1
Batch reaction of FA									
5	10.76	794	16.6°C	0.05	0.30	0.02	0.04	0.31	6.5
10	11.20	944	16.8°C	0.00	0.00	0.00	0.10	0.00	4.1
30	11.30	1027	16.6°C	0.00	0.00	0.00	0.08	0.00	4.9
45	11.67	1345	16.9°C	0.00	0.00	0.00	0.06	0.00	5.6
60	11.80	1331	17.2°C	0.00	0.00	0.00	0.08	0.00	6.0
120	11.67	1508	17.4°C	0.00	0.00	0.00	0.10	0.00	7.5
180	11.77	1453	18.0°C	0.00	0.00	0.00	0.09	0.00	6.8
240	11.71	1418	18.5°C	0.00	0.00	0.00	0.08	0.00	6.1
300	11.90	1526	19.1°C	0.00	0.00	0.00	0.10	0.00	6.4
Batch reaction of NC									
5	4.53	432	16.4°C	1.76	1.85	2.32	0.01	1.81	4.6
10	4.99	463	16.3°C	1.29	1.63	2.17	0.01	1.57	3.2
30	4.93	414	16.9°C	1.69	1.70	2.07	0.02	1.68	4.6
45	4.85	426	16.9°C	1.42	1.87	2.27	0.02	1.82	5.1
60	4.75	430	17.2°C	1.33	1.70	2.14	0.01	1.60	4.9
120	4.68	416	18.1°C	1.35	1.49	1.86	0.03	1.45	5.4
180	4.82	425	18.4°C	1.40	1.61	1.87	0.03	1.54	5.3
240	4.92	415	18.8°C	1.20	1.53	1.85	0.04	1.46	5.3
300	4.84	408	16.6°C	1.24	1.51	1.83	0.04	1.43	5.4
Batch reaction of KAO									
5	4.16	405	16.7°C	6.35	5.30	6.35	0.47	5.22	8.9
10	3.84	408	16.5°C	6.30	5.27	6.23	0.40	5.16	4.8
30	3.92	406	16.3°C	6.51	5.27	6.18	0.41	5.22	7.3
45	3.93	399	16.6°C	6.83	5.42	6.34	0.54	5.30	7.4
60	4.47	416	18.5°C	1.34	4.83	7.43	0.02	4.73	7.4
120	3.79	406	17.1°C	6.94	5.56	6.51	0.57	5.46	9.2
180	3.85	395	18.36°C	6.60	5.43	6.36	0.43	5.29	8.0
240	3.82	413	18.2°C	7.10	5.65	6.64	0.61	5.60	7.6
300	3.98	402	18.7°C	6.63	5.46	6.41	0.50	5.31	7.9

** Parameters of synthetic solution 2*

As shown in Figure 8.3(a), similar pH trends were observed using NC (4.53-4.99) and KAO (3.79-4.47), with no breakthrough to alkaline pH. However, the addition of FA to the model solution caused a considerable pH increase from 3.82 (untreated polluted solution) to 10.76-11.90 (leachates). Breakthrough to alkaline pH was obtained at 5 min. The kinetics of the neutralization reaction was initially very rapid for FA, with the pH increasing rapidly from 3.82-10.76 within the first 5 min, which cannot be explained as the result of the free CaO present in this solid waste material. This takes into account that FA added to the aqueous medium is a class F [$(SiO_2+Al_2O_3+Fe_2O_3)\geq 70\%$], with a very low CaO content. Therefore, during the

equilibration of FA with the aqueous phase, the neutralization of the solution pH can be attributed to the fact FA surface is spanned by charged OH-silanol groups and hydrolysis of these surface-SiOH sites (Hendricks, 2005). The reaction rate decreased as equilibrium was approached, with an apparent equilibrium pH of 11.80 being reached within 1 h. The pH increase can be also associated with dissolution of the sorbent during the shaking process. The lack of buffering capacity for the synthetic solution can be attributed to the very low concentration of Fe^{3+}/Fe^{2+}, Al^{3+} and Mn (Uhlmann *et al*., 2004). A buffering region is associated with oxidation and hydrolysis of Fe^{2+} which releases H^{+} ions and delays the rise in pH (Stumm and Lee, 1961). Solution pH had a very important role in the adsorption/removal of contaminants, probably due to the charge developed on the surfaces of the adsorbent as the pH increases. The EC (Figure 8.3b) also showed an abrupt increase from 376-794 $\mu S\ m^{-1}$within the first 5 min, which became stable after 1 h of contact time, when FA was used as sorbent. However, NC and KAO produced very constant behaviour.

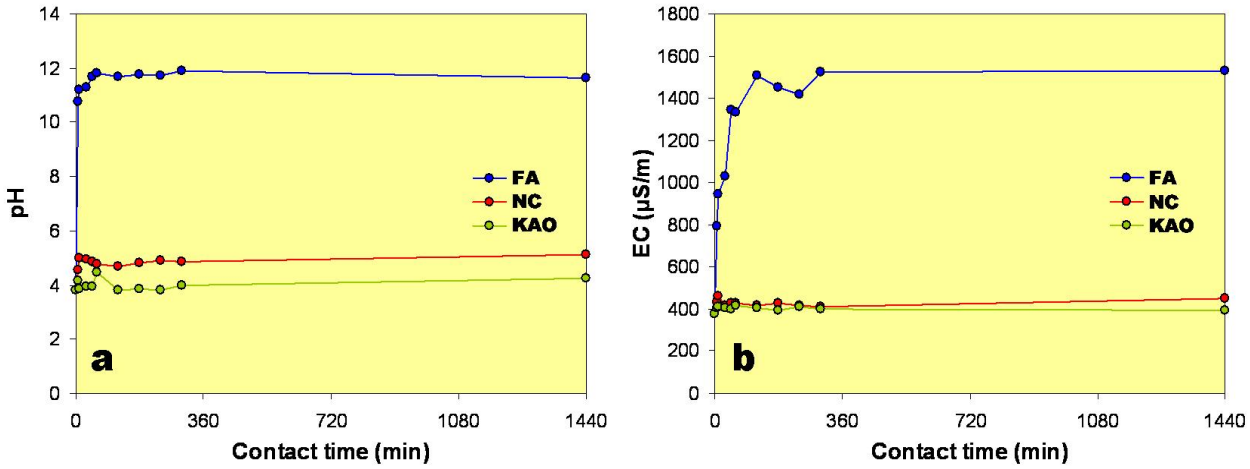

Figure 8.3. pH (a) and EC (b) variation as a function of time during an adsorption batch experiment with starting pH of 3.82 and EC of 376 $\mu S\ m^{-1}$, sorbent:SS2 mixture of 0.50 g / 20 ml.

8.2.2.2. Heavy metal removal

The removal of metal ions as a function of contact time after batch reaction is illustrated in Figures 8.4a to 8.4e. As mentioned before, the pH of the solution played a very important role on the uptake of metal ions (compare Figures 8.3 and 8.4), although with completely different pH

values after the addition of the sorbents. Results indicate that when FA was added to the synthetic solution, a steep decrease in Cu, Pb, Zn and Ni concentration was observed within the first 5 min, reaching very low residual concentrations. However, after 10 min plateau values were reached for the rest of the time intervals, indicating complete removal. However, Cr abruptly increased in concentration from 5 to 10 min (as a consequence of the dominant occurrence of $Cr(OH)_4^-$ at pH > 10, which increases the solubility of Cr^{3+} in FA). It then decreased from 10-45 min and increased again from 45-120 min, and stabilized at values between 0.08-0.11 ppm. With the exception of Cr, the heavy metals exchange character is irreversible. In general, Cu, Pb, Zn, Ni and Cr showed considerable inconsistency in concentration when NC and KAO were used as sorbents, which is shown by the fluctuations observed during the batch experiments. This indicates poor ion-uptake capacity with respect to FA. NC showed a higher selectivity for Cu, Ni and Pb than for Zn, whereas KAO showed a higher selectivity for Ni and Pb than for Zn and Cu, although the heavy metals exchange character of these materials is reversible. A possible reason for the low metal uptake shown by NC and KAO may be due to the competition between hydronium ions and metal ions for exchange sites (Hendricks, 2005), since the pH remained ~ 4 for the duration of the experiments. NC and KAO in general showed similar trends, with an abrupt increase at ~ 45 min, becoming constant after 1 h. The strong fluctuations in heavy metal concentration observed during the first 6 h of reaction when KAO was used as sorbent can be explained also by a recycling process of adsorption (precipitation) and dissolution. Furthermore, the gradual metal ion increase with a low pH for KAO can be attributed to colloidal and precipitation ions that may come into solution in reducing conditions (Johnson and Hallberg, 2005a, b).

It is necessary to highlight that the change of pH in solution with the addition of FA (except for Cr) has a strong influence in the removal of metal ions as a consequence of the pretty immediate increase in alkalinity, causing (almost certainly) the precipitation of hydroxyl-metal complexes. This effect was also observed with the addition of NC and KAO, although with a very small change in solution alkalinity and no significant heavy metal removal (except in the case of Cr). At lower pH, the surfaces of the sorbents are positive, promoting the formation of hydroxyl-metal complexes, which can be adsorbed on the sorbent surfaces, whereas at higher pH, the surfaces of the sorbents were negative, increasing the uptake of heavy metals by the sorbent, as shown by the sharp increase on the amount of metal ions uptake as pH increase from 3.82 to 10.76 (FA).

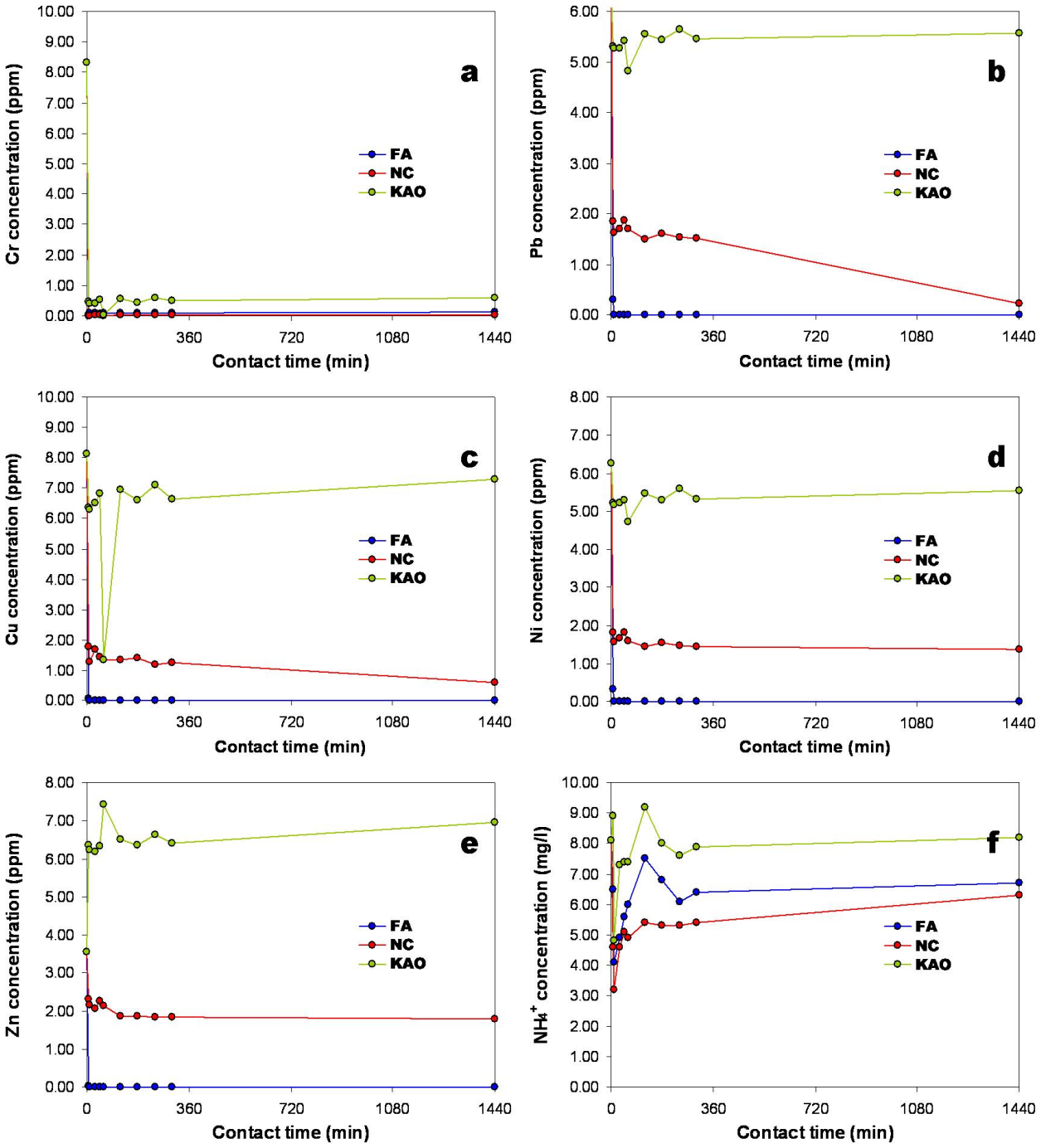

Figure 8.4. Heavy metal and ammonium concentration variation as a function of time during an adsorption batch experiment with starting pH of 3.82 and EC of 376 μS m^{-1}, sorbent:SS2 mixture of 0.50 g / 20 ml.

The immobilization of heavy metal ions from aqueous solutions is a complex process, which

consists of ion exchange and adsorption and is likely to be accompanied by precipitation of metal hydroxide complexes on active sites of the particle surface (Peric *et al*., 2004). However, it is important to determine whether the dominating mechanism in the retention of heavy metals was cation exchange or precipitation of solid species (Hendricks, 2005). According to Hendricks (2005)**,** the pH required to precipitate most metals from water ranges from pH 6-9 (except for Fe^{3+}, which precipitates at pH ~ 2.0-3.5). Therefore, the addition of an alkaline material, such as FA, to the solution increases pH > 9, and most of the metals will be hydrolyzed and precipitated, as proposed by Evangelou and Zhang (1995). The efficiency of FA with respect to metal retention and/or concentration control during its application for the treatment of metal-bearing aqueous media is governed by parameters, such as contact time, pH, temperature and FA origin (Hequet *et al*., 2000). On the other hand, the mechanisms of interactions, such as precipitation and adsorption, between a specific metal and FA are strongly influenced by pH.

8.2.2.3. Ammonium removal

As illustrated in Figure 8.4f, by using all three sorbents, ammonium removal was not very efficient, with a steep decrease in concentration from 8.1 to 4.1 (FA), 3.2 (NC) and 4.8 (KAO) mg/l within the first 10 min, although using KAO produced a sudden increase in concentration during the first 5 min. From this point, significant fluctuations were observed for the rest of the time intervals with residual concentrations of 6.4, 5.4 and 7.9 mg/l, respectively. After 4 h, smooth continuous plateau values can be observed. NC removed most ammonium.

Results reveal that FA had higher efficiency, particularly in removal of heavy metals with regard to NC and KAO, although NC removed most ammonium. On the other hand, FA produced the highest pH (11.90) after the batch reaction. Where the ion exchange process occurred in highly alkaline conditions, as those generated after reaction of FA with the polluted waters, the precipitation of solid phases probably occurred on the surface of the FA particles. These can act as crystallization seeds for the subsequent precipitation of the metal ion, promoting the enhancement of the metal ion-uptake (sorption) by the sorbent (ion exchanger), as established by Hendricks (2005). The batch experiments also showed poor performance for heavy metal reduction when NC and KAO were used as adsorbents. Heavy metals sorption was strongly affected by surface characteristics of these materials, which have no affinity for Cu, Pb, Zn and Ni. However, NC showed better efficiency in Cr and ammonium removal compared with FA. Therefore, neither NC nor KAO alone were found to be good adsorbents, which does not justify

their use in future sorption studies. However, taking into account that NC represents a novel starting material in zeolite synthesis, this coal by-product and its as-synthesized products can be used as sorbents, particularly to obtain valuable information on their performance in removing heavy metals and ammonium. Therefore, a modification of this geomaterial is suggested in order to reverse their surface charge and show strong affinities for heavy metals and ammonium.

8.2.3. Treatment using different zeolite-like materials

A third batch-mode experiment was conducted to establish the performance of several materials in removing heavy metals and ammonium from an artificially polluted solution (SS3), which included FAZs (FA-GIS, FA-SOD and FA-CHA), MTK-LTA and natural heulandite-type zeolite (HEU). Table 8.3 summarizes the values of pH, EC and concentration of metal ions and ammonium of the untreated SS3 and those of the leachates obtained using a sorbent:SS3 mixture of 0.50 g / 20 ml during 300 min.

8.2.3.1. pH and EC

The kinetics of the neutralization reaction was investigated by monitoring the pH and EC of sorbent:SS3 mixtures (0.25 g) for 300 min (Figure 8.5). The results show that the kinetics of the neutralization reaction was initially very rapid, with pH increasing from 4.94 to 10.32 (FA-SOD), 10.41 (FA-GIS), 10.46 (FA-CHA), 8.81 (MTK-LTA) and 5.82 (HEU) within 5 min. The reaction rates decrease as equilibrium is approached. The pH was stabilized within 1 h, and then it shows a progressive decrease. The final pH ranged from 5.98-10.09 and breakthrough to alkaline pH was obtained after 5 min (except when HEU was used as sorbent); FAZs produced quite similar pH trends, whereas HEU showed poor neutralization capacity. EC showed the following range of values: 773-1219 (FA-GIS), 695-1294 (FA-SOD), 1076-1506 (FA-CHA), 289-414 (MTK-LTA) and 277-297 (HEU) $\mu S\ m^{-1}$. The addition of the sorbents produced different EC trends; FA-CHA reached the higher EC values, FA-GIS and FA-SOD and MTK-LTA and HEU showed similar patterns, although the last two reached lower EC values.

Table 8.3. Water quality parameters recorded during 300 min of continuous shaking of the zeolite-like material with the SS3 in a batch experiment (sorbent:SS3 mixture of 0.25 g / 20 ml).

Contact time (min)	pH	EC (μS m^{-1})		Heavy metal concentration (ppm)					Ammonium (mg l^{-1})
				Cu	Pb	Zn	Cr	Ni	
SS3*	4.94	266	22.6°C	12.59	30.26	12.23	7.43	11.09	7.8
Batch reaction of FA-GIS									
5	10.41	773	21.6°C	0.01	0.06	0.03	0.03	0.06	4.5
10	10.35	857	21.7°C	0.02	0.05	0.03	0.03	0.05	4.4
30	10.42	986	21.9°C	0.01	0.02	0.02	0.02	0.04	4.6
45	10.38	1018	21.6°C	0.01	0.03	0.02	0.01	0.04	3.8
60	10.29	1055	21.7°C	0.01	0.00	0.01	0.01	0.03	3.4
120	10.45	1086	21.9°C	0.01	0.00	0.01	0.00	0.03	2.2
180	10.28	1200	22.4°C	0.01	0.06	0.01	0.02	0.01	1.7
240	10.20	1184	22.7°C	0.02	0.04	0.01	0.02	0.01	1.2
300	10.09	1219	23.3°C	0.02	0.09	0.02	0.03	0.00	1.1
Batch reaction of FA-SOD									
5	10.32	695	21.5°C	0.01	0.05	0.02	0.03	0.02	6.4
10	10.42	777	21.8°C	0.02	0.02	0.02	0.03	0.04	6.5
30	10.51	916	21.7°C	0.02	0.03	0.02	0.03	0.05	6.9
45	10.48	995	21.8°C	0.01	0.05	0.20	0.03	0.26	5.5
60	10.46	1062	21.8°C	0.02	0.01	0.02	0.03	0.04	4.7
120	10.50	1079	21.8°C	0.01	0.01	0.02	0.02	0.04	2.5
180	10.37	1271	22.3°C	0.01	0.00	0.01	0.02	0.03	1.5
240	10.21	1238	22.5°C	0.01	0.01	0.01	0.02	0.03	1.2
300	10.00	1294	23.1°C	0.00	0.02	0.01	0.01	0.03	0.9
Batch reaction of FA-CHA									
5	10.46	1076	21.7°C	0.01	0.04	0.03	0.03	0.04	6.1
10	10.42	1124	21.6°C	0.02	0.04	0.03	0.03	0.05	6.0
30	10.46	1239	21.9°C	0.02	0.06	0.03	0.03	0.04	6.8
45	10.45	1279	21.8°C	0.02	0.05	0.03	0.03	0.04	5.0
60	10.34	1351	21.7°C	0.01	0.01	0.03	0.02	0.05	4.1
120	10.67	1411	21.5°C	0.02	0.03	0.03	0.02	0.04	2.4
180	10.35	1466	22.5°C	0.01	0.00	0.02	0.01	0.04	1.5
240	10.32	1484	22.7°C	0.01	0.01	0.02	0.01	0.04	1.3
300	10.09	1506	23.3°C	0.00	0.02	0.01	0.01	0.03	1.2
Batch reaction of MTK-LTA									
5	8.81	289	21.5°C	0.02	0.05	0.03	0.04	0.05	0.9
10	9.25	301	21.7°C	0.02	0.05	0.02	0.04	0.05	0.8
30	9.35	305	21.8°C	0.02	0.06	0.03	0.04	0.06	1.2
45	9.44	323	21.8°C	0.02	0.07	0.02	0.04	0.05	1.1
60	9.33	321	21.7°C	0.02	0.06	0.03	0.04	0.05	1.0
120	9.49	360	21.8°C	0.02	0.05	0.03	0.04	0.05	0.9
180	9.42	402	22.2°C	0.02	0.04	0.02	0.03	0.04	1.0
240	9.28	402	22.3°C	0.00	0.01	0.01	0.03	0.03	0.8
300	9.06	414	22.9°C	0.00	0.00	0.01	0.02	0.03	0.9
Batch reaction of HEU									
5	5.82	282	21.6°C	6.10	2.27	9.00	1.02	8.61	3.9
10	5.89	277	21.6°C	6.72	1.59	8.87	1.19	8.37	2.8
30	5.91	280	21.7°C	6.69	0.81	8.61	1.17	8.23	3.2
45	5.90	284	21.5°C	6.43	0.33	8.35	0.99	8.33	2.3
60	5.97	281	21.8°C	5.81	0.21	7.67	0.82	7.88	4.4
120	6.26	289	22.0°C	4.31	0.04	7.11	0.50	7.84	2.0
180	6.05	293	22.2°C	4.38	0.01	6.77	0.54	8.01	1.7
240	6.12	297	22.4°C	4.69	0.03	6.97	0.60	8.21	1.8
300	5.98	288	22.9°C	3.92	0.01	6.38	0.34	8.02	1.7

** Parameters of synthetic solution 3*

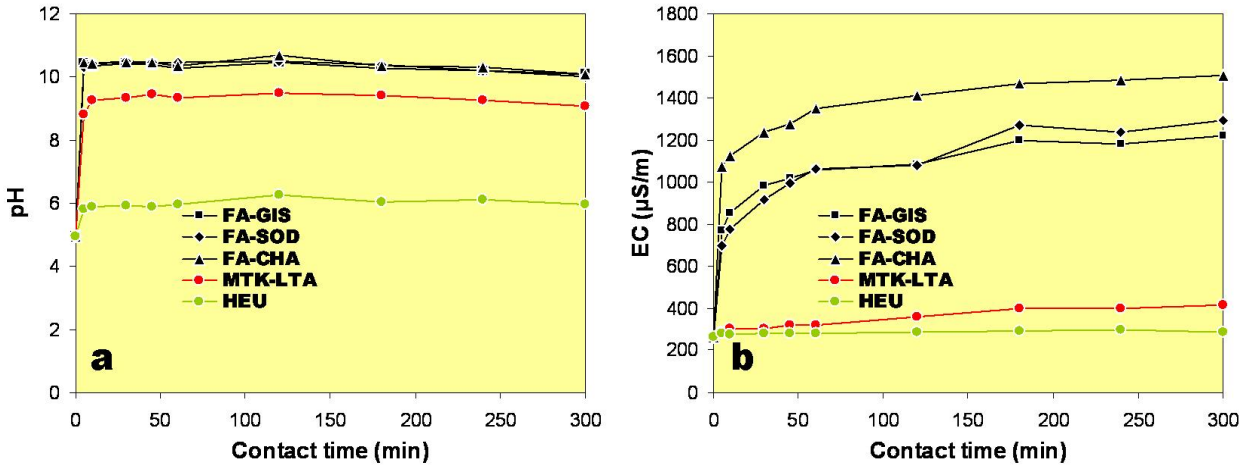

Figure 8.5. pH (a) and EC (b) variation as a function of time during an adsorption batch experiment with starting pH of 4.94 and EC of 266 μS m^{-1}, sorbent:SS3 mixture of 0.25 g / 20 ml.

8.2.3.2. Heavy metal removal

All sorbents, except HEU, produced similar trends of Zn and Ni (Figures 8.6a and 8.6b) with an abrupt decrease within the first 5 min, followed by a slight increase until 2 h (except for FA-GIS), reaching very stable behaviour after this time, although FA-SOD produced a sudden increase at 45 min, which can indicate sorbent contamination. On the other hand, using HEU, a sudden decrease in Zn and Ni within the first 5 min was followed by a progressive decrease, although showing the highest residual concentrations of these metal ions, which reveals the poor efficiency of HEU to remove Zn and Ni. Ni showed a progressive reduction with reaction time using FA-GIS, and it probably can be totally removed at longer reaction times. Cu concentration is illustrated in Figure 8.6c and is characterized by a steep decrease within the first 5 min, using all sorbents, reaching very stable behaviour after 1 h, although with HEU showing a poor efficiency to remove Cu and slight fluctuations in concentration. Cu probably was almost totally removed after longer reaction times using all sorbents, except when HEU was used. In the case of Cr (Figure 8.6d), an abrupt decrease was obtained within the first 5 min, followed by a progressive slight decrease until 1 h, when this metal ion tended to stabilize. However, during this period HEU produced slight fluctuations in concentration. The lowest Cr concentration was obtained after 2 h of reaction using FA-GIS and then a progressive increase with reaction time occurred, indicating a reversible character. The removal efficiency for Cr is in the following sequence: FA-GIS > FA-CHA > FA-SOD > MTK-LTA > HEU. Pb (Figure 8.6e) showed a steep decrease during the first 5 min using all sorbents, followed by slight fluctuations in concentration

for the remaining time intervals, with HEU and MTK-LTA showing the lower and higher efficiency, respectively, to remove Pb. All sorbents (except HEU) generally produced high metal removal efficiencies. Metal ion removal behaved distinctly when HEU was used, although Pb showed a different removal pattern, taking into account that this sorbent showed the best efficiency of Pb removal, with the lowest residual concentrations. HEU exhibited a slightly higher affinity for Pb respect to Cr, Cu, Zn and Ni. The low efficiency of the natural zeolite (HEU) used in this study on the removal of heavy metals can be explained by the presence of impurities, the coarser particle size, the difference between the relative cationic radius of metal and the porous diameter of the zeolite.

In general, as solution pH abruptly increases after 5 min of reaction, the heavy metal removal also increases due to the low competition between H^+ ions with heavy metal cations for the same exchange sites (Wingenfelder *et al*., 2005). The abrupt decrease in heavy metal concentration during the first 5 min of contact time can be explained as a consequence of a very fast diffusion of the metal species from the aqueous solution to an ion exchange site of the sorbents. However, some metals may be removed to a greater extent than others with more favourable equilibrium partitioning if the latter diffuse slower (Vaca *et al*., 2001).

The removal of all metal ions occurred very quickly (within 5 min) at the initial stage of sorption and no appreciable increase was observed beyond this time which proves the saturation of the active sites in the sorbents. It was also observed that under the experimental conditions, the removal of heavy metals by HEU is much slower and the sorption of these metal ions after 60 min of stirring is of little significance. For the HEU, the results demonstrate that around 90% of the metal ions are removed in the first 5 min. On the other hand, the retention efficiency of the metallic ions is in the order Pb > Cr > Cu >Zn > Ni.

In spite of the several factors that can affect the heavy metal removal of natural zeolites, the particle size is very important because it strongly control the rate and sorption capacity (Cui *et al*., 2006), taking into account that smaller particles can adsorb significantly more metal ions and have larger surface area and shorter pores than larger particles. The uptake of heavy metals increases when pH increases from 4.94. Given the behaviour of the zeolitic materials tested for heavy metal retention, they could be considered as low-cost sorbents for wastewater treatment, although the use of natural zeolites (e.g. HEU), which have relatively low ion exchange capacity would require their modification by physical or chemical methods to improve their ion exchange capacity.

However, the interpretation given above on the uptake of heavy metals by the sorbents by ion exchange may not represent the most important process to be considered. Therefore, it is necessary to highlight at this point that the pH of the solution has a strong influence on the heavy metal removal, as a consequence of surface charge of the adsorbent (compare Figures 8.5 and 8.6). The uptake of heavy metal ions removed from solution increases abruptly from pH 4.94 to pH 10.32-10.46 (FAZs), 8.81 (MTK-LTA) or 5.82 (HEU) within the first 5 min of reaction, with a complete removal of heavy metals, except in the case of HEU (lowest efficiency of uptake of heavy metals), and for the rest of the time intervals (with pH remaining almost constant), there was not a gradual increase on metals uptake due to the complete removal.

In general, the amount of heavy metal ions removed from solution increased as the pH increased. Therefore, the change of pH in solution with the addition of the sorbents has a strong influence in the uptake of metal ions as a consequence of the immediate increase in alkalinity, causing (almost certainly) the precipitation of hydroxyl-metal complexes onto the surface of the sorbents.

8.2.3.3. Ammonium removal

The removal of the ammonium from aqueous solution using zeolitic materials is due to the ion exchange reaction between NH_4^+ (solution) and Na^+ (zeolitic material), although the presence of other cations (K^+, Ca^{2+} or Mg^{2+}) in the solution decreased the uptake of ammonium due to cation competition (Lei *et al*., 2008). Figure 8.6f shows the ammonium trends are characterized by strong fluctuations within the first 60 min. An abrupt decrease in NH_4^+ concentration from 7.8 to 4.5 (FA-GIS), 6.4 (FA-SOD), 6.1 (FA-CHA), 0.9 (MTK-LTA) and 3.9 (HEU) mg l^{-1} was observed within the first 10 min, which can be explained by an increase in concentration of other exchangeable metal cations (Na^+, K^+, Ca^{2+} or Mg^{2+}) with a simultaneous strong absorption of NH_4^+ by the sorbent. From 10-30 min a sudden increase in NH_4^+ concentration occurred as a consequence of ion exchange, mainly with Na^+ and K^+. Finally, a progressive decrease in concentration with reaction time is related to NH_4^+ adsorption to the sorbent surface.

A different NH_4^+ uptake was found between the tested zeolites at shorter reaction times (< 2 h), with the following sequence of removal efficiency for NH_4^+: MTK-LTA > HEU > FA-GIS > FA-CHA > FA-SOD. Between the used FAZs, FA-GIS seems to be the material more favourable for NH_4^+ uptake. At longer reaction times (> 2 h), no difference in the pattern of NH_4^+ uptake was

observed with the following sequence of removal efficiency for NH_4^+: MTK-LTA > FA-SOD > FA-GIS > FA-CHA > HEU, although a complete removal of ammonium after 5 h was not obtained using these sorbents, with MTK-LTA producing the smallest residual concentrations. The selectivity order of ammonium ion over other cations would depend on the ion exchange capacity of the zeolitic material.

There are several factors that influence the sorption capacity of the ion exchangers used in this study, such as total capacity, concentration and type of ions to be sorbed, site accessibility, pH variation, temperature and agitation rate (Helfferrich, 1962). On the other hand, Hendricks (2005) described additional aspects playing very important roles in the reaction between specific sorbents and the aqueous medium, which include competing ions and interactions between sorbent and metal ions. In addition to the exchangeable metal contaminants to be removed, there are other species which interfere with the ion exchange process by competing for available exchange sites on the ion exchanger. This may adversely effect the process and therefore it is beneficial to investigate the effect of competing ions on the metal loading onto a given ion exchanger. It is also important to understand the dynamics involved in the reaction in the sorbent-solution interface, which should consider reactions such as ion exchange, surface hydrolysis, hydration, competing exchange reactions between metal ions in solution and free hydronium ions (H^+).

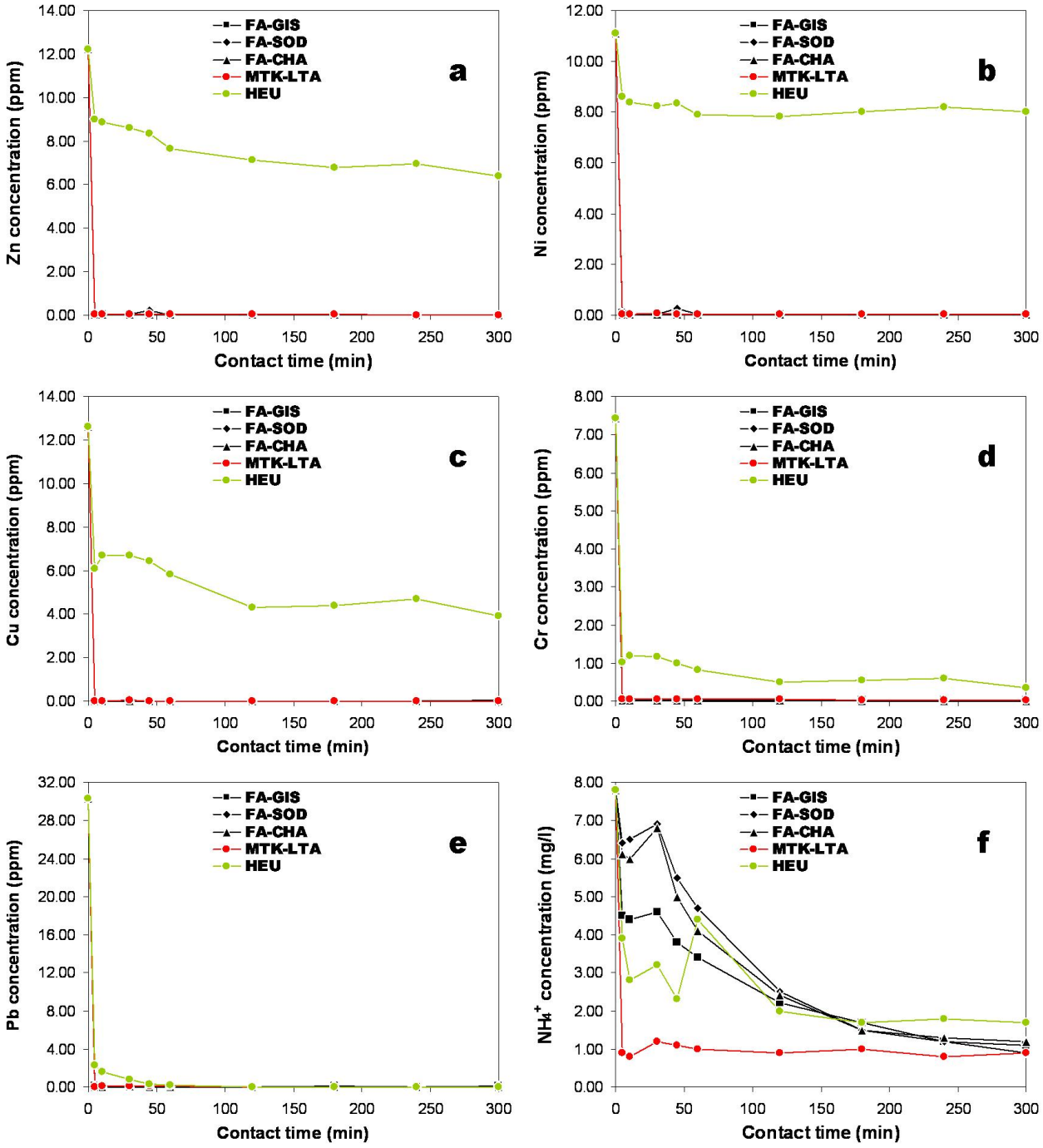

Figure 8.6. Heavy metal and ammonium concentration variation as a function of time during an adsorption batch experiment with starting pH of 4.94 and EC of 266 μS m^{-1}, sorbent:SS3 mixture of 0.25 g / 20 ml.

8.3. Removal of heavy metals and ammonium from acid mine drainage

8.3.1. Introduction

AMD is a widespread environmental problem associated with both working and abandoned mining operations, resulting from the microbial oxidation of pyrite in the presence of water and air, affording an acidic solution that may contain toxic metal ions. The generation of AMD and release of dissolved heavy metals is an important concern facing the mining industry. The aim of the present study is to examine, at the laboratory-scale, the effectiveness of low cost sorbents, such as FA and NC and synthetic zeolites in removing metal ions and ammonium from AMD generated at the Parys Mountain copper-lead-zinc deposit, Anglesey (North Wales). The potential use of FA, as well as the synthetic zeolites based on this solid waste material, in water purification has been evaluated by several research groups and the removal of heavy metals from contaminated water has been studied extensively (Moreno *et al*., 2001a, b; Petrik *et al*., 2003; Wingenfelder *et al*., 2005; Gitari *et al*., 2006). However, recent works showed that the addition of FA to a mining residue from the Iberian Pyrite Belt resulted in acid neutralization, metal retention in neoformed precipitates, and therefore, the improvement of leachate quality (Pérez-López *et al*., 2007a). In these conditions, a microencapsulation technology based in Fe-precipitation as a coating on pyrite surfaces was applied by Pérez-López *et al*. (2007b) in order to prevent interaction between oxidizing agents and pyrite grains, thus halting pyrite oxidation and AMD production. To our knowledge, no previous effort has been made to use NC or synthetic zeolites based on this material as sorbents in water treatment, except in a recent study by Ríos *et al*. (2008a).

8.3.2. Chemistry of acid mine drainage

AMD is generated by a complex series of geochemical reactions that occur when sulphide minerals are exposed to oxygen, in contact with water. Chemical oxidation of sulphide minerals occurs primarily via reactions catalyzed by microbiological action**.** Iron and sulphur are oxidized to ferric iron and sulphate, respectively, and during the oxidation process hydrogen ions are produced resulting in the production of sulphuric acid (Johnson, 1995). Iron sulphide minerals, especially pyrite (FeS_2), contribute most to AMD formation. The pyrite oxidation process has

been studied extensively. The following equations show the generally accepted sequence of pyrite reactions. During the first step, pyrite reacts with oxygen and water, producing ferrous iron and sulphuric acid (equation 8.1). The second step involves the oxidation of ferrous iron to ferric iron (equation 8.2), which is pH dependent. The third step corresponds to the hydrolysis of ferric iron with water to form a ferric hydroxide precipitate (ferrihydrite) and the release of additional acidity (equation 8.3), which is pH dependent. The fourth step involves the oxidation of additional pyrite by ferric iron (equation 8.4). The overall pyrite reaction series is among the most acid-producing of all weathering processes in nature.

$$FeS_2 + 3.5O_2 + H_2O \rightarrow Fe^{2+} + 2SO_4^{2-} + 2H^+ \quad (8.1)$$

$$4Fe^{2+} + O_2 + 4H^+ \rightarrow 4Fe^{3+} + 2\,H_2O \quad (8.2)$$

$$4Fe^{3+} + 12H_2O \rightarrow 4Fe(OH)_3(s)\downarrow + 12H^+ \quad (8.3)$$

$$FeS_2 + 14Fe^{3+} + 8H_2O \rightarrow 15Fe^{2+} + 2SO_4^{2-} + 16H^+ \quad (8.4)$$

The pyrite oxidation is controlled by bacterial species that have a definite pH growth range and pH growth optimum (Kuhn, 2005). The conversion of ferrous to ferric iron in the overall pyrite reaction sequence has been described as the ‘rate-determining step’ (Singer and Stumm, 1970), a chemistry term for the slowest step in a chemical reaction, which can be greatly accelerated by bacterial action. There are many mineral-degrading acidophiles in AMD, participating in the metabolism of pyrite and the metabolic pathways involved in this process are pyrite dissolution, iron oxidation, iron reduction and sulphur oxidation (Kuhn, 2005). The most common pyrite-oxidizing bacterium is *Acidithiobacillus ferrooxidans*, which is of great practical importance due to the extensive acid and metal pollution generated when this species releases metals from AMDs (Prescott *et al*., 1999). Once pyrite oxidation and acid production has begun, conditions are favourable for bacteria to further accelerate the reaction rate. At pH values of $\geq$ 6, bacterial activity is believed to be insignificant or comparable to abiotic reaction rates. High concentrations of iron are very common in AMD, because both ferric (Fe^{3+}) and ferrous iron (Fe^{3+}) are very soluble at pH < 2.5 (Baker and Banfield, 2003). The role of micro-organisms in the generation of AMD is very important because they influence metal mobility in different ways; some cause metal mobilization, while others contribute to metal retardation, although their influence on metal mobility depends on which of these processes dominates in a specific environment.

8.3.3. Characterization of acid mine drainage samples

The surface drainage waters at Parys Mountain are strongly acidic (pH < 2) and metal-rich, due to the oxidation of sulphide minerals, and its orange-brown colour is due to the very high concentrations of ferric iron in solution. Table 8.4 summarizes the values of pH, EC and concentration of metal ions and ammonium of the untreated AMD and those of the leachates obtained using a sorbent:AMD mixture of 0.25 g / 20 ml during different contact times ~~(Figure 8.8)~~. At Parys Mountain, there is very little detectable change in water chemistry along the drainage stream where AMD can be collected, which is characterized by high concentrations of Fe, Cu, Zn and sulphate (190-195 mg l^{-1}). Field data of AMD for 19 July 2007 were pH between 1.69-1.99; EC between 9.27 mS cm^{-1} (22.3 ^{o}C) and 3.89 mS cm^{-1} (21.0 ^{o}C) and ammonium concentration 7.0 mg l^{-1}. Laboratory data of AMD for 20 July 2007 were pH between 1.96-2.07; EC between 9.97 mS cm^{-1} (16.0 ^{o}C) and 5.05 mS cm^{-1} (17.0 ^{o}C) and ammonium concentration 3.0 mg l^{-1}. Thus, the AMD was very acidic and contained notable concentrations of metal ions, especially Fe. The acidic characteristic of the AMD results from the percolation of water through sulphide minerals, generally pyrite, which oxidizes and dissociates when in contact with air and water. Therefore, Fe^{2+} is released and rapidly oxidized to Fe^{3+}, which precipitates as hydroxides. After the onset of the reaction, a cyclic series of events takes place starting with the oxidation of Fe^{2+} to Fe^{3+}, which is subsequently reduced by pyrite, releasing Fe^{2+} which increases the solution acidity (Snoeyink and Jenkis, 1980). Alternatively other metals, such as Zn and Cu as well as minor Pb and As occurring in minerals associated with the volcanic-hosted massive Zn-Pb-Cu sulphide mineralization, can be solubilised and lixiviated as a consequence of the characteristic water acidity. Therefore, the concentration of these elements is often high, specially Zn and Cu. On the other hand, Smith *et al*. (1991) investigated the relationship between iron bacteria type, abundance, stream environment and water/sediment chemistry in AMDs and concluded that bacteria exert strong controls over the precipitation of Fe-Mn oxyhydroxides. This can attenuate the metal concentration by adsorption and precipitation of some metal species, such as sulphates. AMD characterization indicates that the effluents of the Parys Mountain copper-lead-zinc deposit were highly toxic to organisms and could destroy the natural ecosystem when disposed without previous treatment.

Table 8.4. Water quality parameters recorded during 24 h of continuous shaking of the raw FA and NC and their synthetic zeolitic products with AMD in a batch-mode experiment (sorbent:AMD mixture of 0.25 g / 20 ml).

Contact time (min)	pH	EC (mS cm^{-1})	T (°C)	Heavy metal concentration (ppm)							Ammonium (mg l^{-1})
				Cu	Pb	Zn	Cr	Ni	As	Fe	
AMD*	1.96	3.77	16.00	31.90	2.10	73.83	0.05	0.02	4.81	1355.33	3.0
Batch reaction of FA											
5	2.54	6.47	20.60	56.64	1.35	52.12	0.36	0.12	3.03	913.57	3.1
10	2.56	6.93	20.60	53.73	1.23	50.52	0.31	0.08	2.92	901.30	3.4
30	2.51	5.85	20.90	53.65	1.30	51.35	0.39	0.12	3.01	904.80	3.4
45	2.13	5.73	20.80	66.58	1.96	62.85	0.70	0.51	3.59	1068.04	1.4
60	2.46	5.48	21.50	55.73	1.60	52.41	0.58	0.42	3.01	906.62	3.5
120	2.38	5.01	21.20	55.28	1.41	51.86	0.46	0.24	3.00	914.04	7.3
180	2.38	5.00	21.70	56.62	1.58	53.49	0.55	0.38	3.03	941.46	3.3
240	2.34	5.13	22.70	55.17	1.46	53.23	0.54	0.32	3.13	916.34	5.3
1440	2.66	5.04	20.90	79.07	1.96	72.35	0.79	0.52	4.13	1156.62	---
Batch reaction of NC											
5	2.42	8.80	20.60	48.55	1.14	48.26	0.05	0.03	2.25	853.62	2.8
10	3.04	8.91	20.50	49.74	1.17	49.41	0.05	0.03	2.31	891.74	2.9
30	2.64	8.87	20.70	48.64	1.15	49.11	0.05	0.04	2.30	864.14	2.9
45	2.00	8.93	21.00	49.49	1.23	49.29	0.04	0.07	2.33	882.10	2.9
60	1.92	8.82	21.20	49.37	1.68	49.26	0.23	0.51	2.29	877.85	2.7
120	1.92	8.76	21.40	48.76	1.22	49.53	0.04	0.05	2.31	883.55	2.9
180	1.92	8.93	21.50	50.30	1.26	50.72	0.06	0.09	2.38	909.89	3.4
240	1.86	8.95	22.40	53.79	1.29	52.88	0.03	0.15	2.62	890.04	3.3
1440	1.86	10.38	20.50	76.41	2.40	71.04	0.39	0.85	3.61	1168.67	---
Batch reaction of FA-FAU											
5	3.04	4.96	20.60	42.32	0.16	47.07	0.01	0.19	0.08	80.66	4.8
10	3.64	4.97	20.60	43.47	0.12	47.50	0.01	0.20	0.05	43.99	6.4
30	3.69	5.13	20.70	41.01	0.14	47.27	0.00	0.24	0.04	15.09	1.3
45	3.80	5.32	20.80	38.62	0.23	46.42	0.01	0.31	0.04	9.05	1.1
60	3.85	5.57	21.00	31.10	0.16	43.79	0.01	0.28	0.05	3.11	1.0
120	3.89	5.71	21.20	30.65	0.26	43.36	0.01	0.36	0.06	2.10	1.5
180	4.02	6.14	21.50	25.28	0.32	42.91	0.01	0.44	0.06	0.73	1.6
240	3.99	6.23	22.20	30.62	0.30	46.17	0.00	0.42	0.07	1.67	1.1
1440	4.42	7.74	20.50	36.06	0.56	73.98	0.00	0.71	0.03	11.70	1.9
Batch reaction of NC-FAU											
5	3.40	5.80	20.70	39.25	0.10	44.68	0.02	0.11	0.02	33.09	4.8
10	3.52	5.94	20.60	38.38	0.09	45.13	0.02	0.12	0.02	25.68	4.0
30	3.98	6.30	20.60	35.45	0.10	44.13	0.03	0.12	0.05	6.26	0.9
45	4.03	6.34	20.80	34.58	0.13	45.14	0.06	0.16	0.07	5.87	1.0
60	3.63	6.37	21.00	37.87	0.10	46.31	0.04	0.13	0.06	7.52	1.1
120	4.10	6.58	21.20	37.14	0.16	47.63	0.09	0.18	0.06	2.16	1.4
180	4.15	6.75	21.50	37.19	0.19	49.13	0.10	0.21	0.07	1.59	1.3
240	4.09	7.25	22.10	37.96	0.14	50.72	0.06	0.18	0.09	1.39	1.3
1440	4.29	8.63	20.30	24.44	0.22	87.03	0.20	0.66	0.07	1.71	2.1
Batch reaction of NC-PHI											
5	2.99	4.53	20.80	51.37	1.06	49.03	0.05	0.03	1.73	783.65	3.3
10	2.67	4.72	20.60	52.50	0.81	51.32	0.04	0.04	0.95	638.34	2.4
30	3.06	4.80	20.70	50.64	0.67	49.95	0.01	0.08	0.42	491.02	3.7
45	2.76	4.84	20.90	52.31	0.76	50.69	0.06	0.22	0.33	460.02	2.0
60	2.62	4.56	21.60	53.46	0.99	51.91	0.09	0.16	0.97	669.31	3.1
120	2.90	5.00	21.60	49.49	0.51	51.48	0.13	0.39	0.10	179.00	2.4
180	2.95	5.07	21.30	56.16	0.29	54.47	0.12	0.17	0.11	179.45	2.8
240	2.84	5.17	22.10	54.84	0.48	53.52	0.00	0.06	0.47	446.60	1.6
1440	2.86	5.87	20.50	37.13	0.07	87.25	0.07	0.31	0.01	173.85	1.8

** Parameters of the acid mine drainage*

8.3.4. Acid mine drainage treatment using fly ash, natural clinker and synthetic zeolites

8.3.4.1. Kinetics of the neutralization reaction

Figure 8.7 shows the pH and EC trends, respectively, for the neutralization reactions between the investigated sorbents and the AMD (0.25 g / 20 ml). Figure 8.7a shows that a small increase of the initial pH (1.96) of the AMD occurred on contact with FA (2.54) and NC (2.42) and synthesis products (2.99–3.40) within the first 5 min of shaking. The reaction rates decrease as equilibrium is approached. Solution pH can increase as a consequence of the progressive dissolution of the sorbent during the shaking process, and it can decrease due to the release of relict organic matter. The pH was stabilized within 1 h when the FA and NC were reacted with AMD, whereas 2 h were required using the synthetic zeolites as sorbents. The final pH ranges from 1.86 to 2.66 (raw materials) to 2.86–4.42 (synthesis products), being higher when FAU was used. No breakthrough to alkaline pH was observed, which indicates that contact time did not affect alkalinity using a dose of 0.25 g, but using a higher sorbent ratio a strong change in pH was observed, as will be discussed later.

Figure 8.7b shows that EC ranges from 5.00-6.93 to 8.76-10.38 mS cm^{-1} for FA and NC, respectively, whereas the as-synthesized products showed EC ranges of 4.96-7.74, 5.80-8.63 and 4.53-5.87 mS cm^{-1}, respectively. A sudden increase in EC was observed during the first 5 min for all batch experiments, indicating that very soluble material dissolved very quickly resulted in a rapid and irregular increase in EC during the initial contact sorbent:AMD. After 1 h of reaction, the EC values remained fairly stable for the rest of the time intervals when NC was used. On the other hand, FA showed a regular and systematic decrease in EC, which can be associated with a reduction in sulphate accompanied by gypsum formation, whereas the use of zeolitic products promoted a progressive increase in EC, although showing slight fluctuations. After an initial very rapid increase in EC, the release of solutes to the solution slowed down during further reaction. Therefore, it is possible that ions from acid-generating and acid-neutralizing reactions can effectively increase both the salt concentration (salinity) of the AMD and its EC, which means that the sorbents released species in solution.

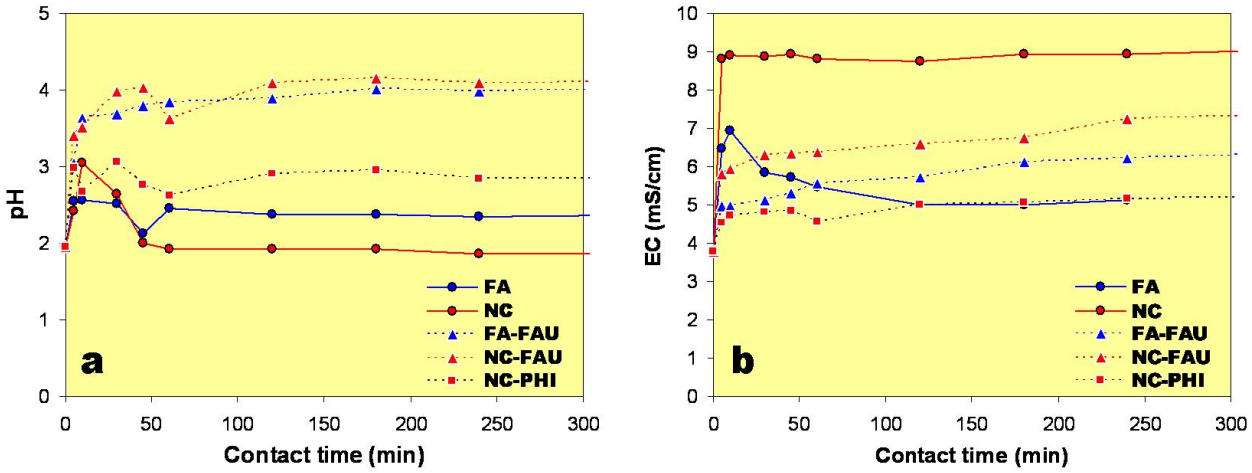

Figure 8.7. pH (a) and EC (b) variation as a function of time during the adsorption batch experiments with starting pH of 1.96 and EC of 3.77 mS cm^{-1}, sorbent dose of 0.25 g, and AMD volume of 20 ml.

8.3.4.2. Heavy metal removal

As shown in Figure 8.8, adsorption and desorption phenomena occurred very quickly in the early stages of the experimental tests, with metal concentrations almost constant for the rest of the time intervals, indicating approach to equilibrium, and the changes of metal ion concentrations differ considerably for the different metals in agreement with the results obtained by Cui *et al*. (2006).

Ni increased within the first 5 min and decreased between 5-10 min when the raw materials were used, whereas steep and slight increases were observed using FA- and NC-FAU and NC-PHI (Figure 8.8a). All sorbents produced a progressive increase between 10-45 min, although FA and NC showed a steep increase at 45 min and 1 h, respectively. During the first h of reaction, all sorbents produced inconsistent trends, characterized by strong fluctuations in concentration. After 2 h, NC and NC-PHI produced a progressive increase and decrease in Ni concentration, respectively. However, the concentration of this metal ion tended to increase at longer reaction times.

In general, Cr (Figure 8.8b) displayed very low concentrations, which tend to stabilize after sorbent:AMD reaction, except when FA was used, although complete Cr removal was not achieved. The addition of FA to AMD produced a steep increase in Cr, within the first 5 min, followed by a decrease between 5-10 min. Then a progressive increase was observed between 10-45 min, followed by a new decrease up to 2 h, showing a slight progressive increase with reaction time. Cr concentrations after FA-AMD interaction are higher than those contained originally in the raw AMD. This is due to the fact that FA releases Cr during dissolution. NC also produced very low Cr concentrations, with significant fluctuations, particularly at 1 h. When synthesis products were used, lower residual Cr concentrations were obtained, although with inconsistent behaviour. FAU produced similar trends, with Cr decreased within the first 10 min, slightly increasing up to 3 h, decreasing again between 3 and 4 h, after which it stabilized. The lowest residual concentrations were observed after 4 h using NCZs.

Pb showed a steep decrease during the first 5 min using faujasite, followed by a slight progressive increase for the rest of the time intervals (Figure 8.8c). The lower residual Pb concentrations were obtained using NC-FAU. FA produced a steep decrease in Pb concentration within the first 10 min, followed by a progressive increase between 10-45 min, and a new decrease between 45 min and 2 h, with slight concentration fluctuations for the remaining time intervals. The addition of NC and NC-PHI produced a steep decrease in Pb concentration within the first 5 min, followed by very stable behaviour and progressive decrease between 5-30 min using NC and NC-PHI, respectively; a sudden increase occurred between 30 min and 1 h, followed by a new decrease between 1 and 2 h, with slight concentration fluctuations for the remaining time intervals.

In the case of As, faujasite produced a steep decrease during the first 5 min, after which plateau values were reached with very low residual concentrations ($\sim$ 1 ppm) for the remaining time intervals, with an almost complete removal (Figure 8.8d). NC-PHI produced a steep decrease in As concentration during the first 45 min, with considerable inconsistency in concentration, as indicated by fluctuations in the plot. However, this zeolite shows a lower efficiency than that shown by faujasite. The addition of both coal by-products produced a steep decrease in As concentration within the first 5 min, followed by very stable behaviour for the remaining time intervals, although the FA produced a sudden increase at 45 min. All sorbents showed a very slight progressive increase after 2 h of reaction. It is well know that the complex chemistry of As will result in changes depending on its exposure. As is mostly found as arsenite (AsO_3^{3-}) or arsenate (AsO_4^{3-}), with arsenite being more soluble and therefore more toxic and more likely to

be absorbed than arsenate. Therefore, several arsenic treatment technologies are mainly based on transforming arsenite into arsenate, taking into account that the last one is less soluble, being easier removed from water, which can be explained by the fact that in the pH range of 4–10, the predominant arsenite species are neutral in charge, while arsenate species are negatively charged; the neutral charge on arsenite makes its removal efficiency poor in comparison with that of arsenate (U.S. EPA, 2001).

Cu concentration was characterized by a steep increase within the first 5 min, using all sorbents, which continued after 10 min, except when FA (small decrease) and NC-FAU were added (Figure 8.8e). FA-FAU produced a progressive decrease up to 3 h, followed by a new increase between 3-4 h. However, the trend after 1 h showed a quite stable behaviour. NC-FAU also produced a progressive decrease up to 45 min, followed by an increase between 45-60 min, and then stabilized for the remaining time intervals. NC-PHI produced slight concentration fluctuations. The addition of FA and NC promoted very stable behaviour of Cu concentrations, except by a significant fluctuation in concentration observed at 45 min using FA and a slight progressive increase after 2 h using NC. For all investigated materials, Cu concentrations after sorbent:AMD interaction is higher than those contained originally in the raw AMD, which can also be explained by dissolution of the sorbents releasing Cu.

All sorbents produced similar Zn trends (Figure 8.8f) with an abrupt decrease within the first 5 min, reaching a very stable behaviour, except by FA, which produced a sudden increase at 45 min. In general, Zn concentration tends to slightly increase at longer reaction time, particularly after 2 h.

In the case of Fe (Figure 8.8g), FAU produced a steep decrease during the first 5 min, followed by a progressive decrease up to 1 h, after which plateau values were reached with very low residual concentrations (~ 1 ppm) for the remaining time intervals, with an almost complete removal. NC-PHI showed a lower efficiency than that shown by FAU, producing a steep decrease within the first 5 min, followed by a progressive increase up to 45 min; then, an abrupt increase was observed at 1 h, followed by a new decrease at 2 h, decreasing again for the remaining time intervals. Therefore, this Fe trend showed inconsistent behaviour in concentrations characterized by significant concentration fluctuations. The addition of FA and NC produced a steep decrease within the first 5 min, tending to stabilize for the remaining time intervals, except by an abrupt increase in concentration observed at 45 min using FA. Based on the inherent alkalinity, induced by the alkaline activation of the raw materials, a higher pH was obtained upon zeolite addition. However, in conditions where the ion exchange process occurs

in considerably alkaline pH ranges, the precipitation of certain solid phases on the surface of the ion exchanger may be induced and, as such, they can act as crystallization seeds for the subsequent precipitation of the counter ion (Hendricks, 2005). The result would be the enhancement of metal uptake by the ion exchanger and this is what probably occurs during experiments with inorganic exchangers, such as the ones synthesized in this study.

It is interesting to highlight that the removal of As is associated with that of Fe, as shown by the correlation between the two elements in Figure 8.8, in agreement with results reported by Casiot *et al*. (2003). These authors calculated a As/Fe ratio in the range 0.13-1.3 from the amount of As and Fe removed from the aqueous phase, which reflects the formation of mixed As(V)–Fe(III) precipitates which occurs in some As-rich AMD (Carlson *et al*., 2002). The high selectivity of Fe-oxyhydroxides for As is often employed as a significant advantage in arsenic elimination strategies (Meng *et al*., 2002). As is associated with Fe oxides and the formation of $Fe_3(AsO_4)2{\cdot}8H_2O(s)$ or $FeAsO_4{\cdot}2H_2O(s)$ (Lenoble *et al*., 2005). Adsorptive materials like those used in this study, containing Fe oxides, could be capable of removing As^{3+} or As^{5+}. However, the removal of dissolved As from water is linked to the chemistry of the arsenite and arsenate species and thus to their relative distribution, simultaneously influenced by pH and redox conditions (e.g. Lombi *et al*., 1999).

In addition to ion exchange, sorption and surface precipitation, dissolution also takes place in the heavy metal AMD-sorbent interaction. It is concluded that the main mechanism for metal uptake is precipitation and not sorption and the increase in pH with the addition of the sorbents decreases metal concentrations probably due to precipitation on the sorbent surface. The process of precipitation works on the basis that the pH is reached at which the metals attain their minimum solubility and, as such, precipitate out (Hendricks, 2005). The pH of the AMD had a pronounced effect on the removal efficiency of heavy metals mainly due to the effect that this parameter has on metal speciation. Each metal portrays its own minimum solubility at its own characteristic pH. The pH required to precipitate most metals from water ranges from pH 6-9 (except for Fe, which precipitates at pH > 3.5), thus if sufficient alkaline material is added, such that pH is raised up to 9, most metals will be hydrolyzed and precipitated (Evangelou and Zhang, 1995). The experimental results show that the adsorption efficiency can depend on particle size, pH, adsorbent type and metal ion.

The treatment of AMD with alkaline materials like those used in this study leaves Na, K and Ca in the treated waters. Due to the high concentrations of Na, it is likely that protons are released to the aqueous phase through ion exchange with the excess of Na. At low pH in AMD, the ion

exchange would impact the mobility also by the pH effect. Heavy metals sorption could be also strongly affected by surface characteristics of these materials. In addition, it is probably that the behaviour of heavy metals be associated to relict organic matter in the sorbents and bacterial degradation.

8.3.4.3. Ammonium removal

The removal of ammonium from AMD using FA, NC and synthetic zeolites is illustrated in Figure 8.8h for a sorbent:AMD mixture of 0.25 g / 20 ml. FA produced an increase in ammonium after 10 min, which became stable between 10-30 min and then abruptly decreased to the lower concentration, although it shows strong fluctuations. This solid waste material seems to release ammonium after some time in contact with AMD, which has been observed in similar studies (Gitari *et al*., 2006). NC shows fairly stable behaviour in ammonium concentration after 1 h, and then it slightly increased between 1-3 h, followed by a gradual small decrease between 3-24 h. FAU showed an increase in ammonium after 5 or 10 min and then it abruptly decreased to lower concentrations, becoming stable after 30 min. Zeolitic materials showed a small increase in ammonium after 5 min and then it decreased after 10 min. However, the ammonium concentration shows strong fluctuations. On the other hand, the synthesis products show a capacity to adsorb ammonium, which could be mainly through ion-exchange.

Different factors can affect the sorbent surface charge and therefore its efficiency in NH_4^+ removal. The alkalinity of the tested sorbents leaves Na, K and Ca in the treated waters. These cations may compete with NH_4^+ for the adsorption sites on sorbents and hence decrease the exchangeable sites available for ammonium removal as has been suggested in several studies (e.g. Booker *et al*., 1995; Green *et al*., 1996; Singh and Prasad, 1997). On the other hand, the fluctuations in NH_4^+ concentration can be also explained as follows: an increase in the ammonium concentration reflects the intensive bacterial degradation of relict organic matter that can be found in coal by-products and their as-synthesized zeolites, whereas a decrease may be the result of ion-exchange reactions with sorbents.

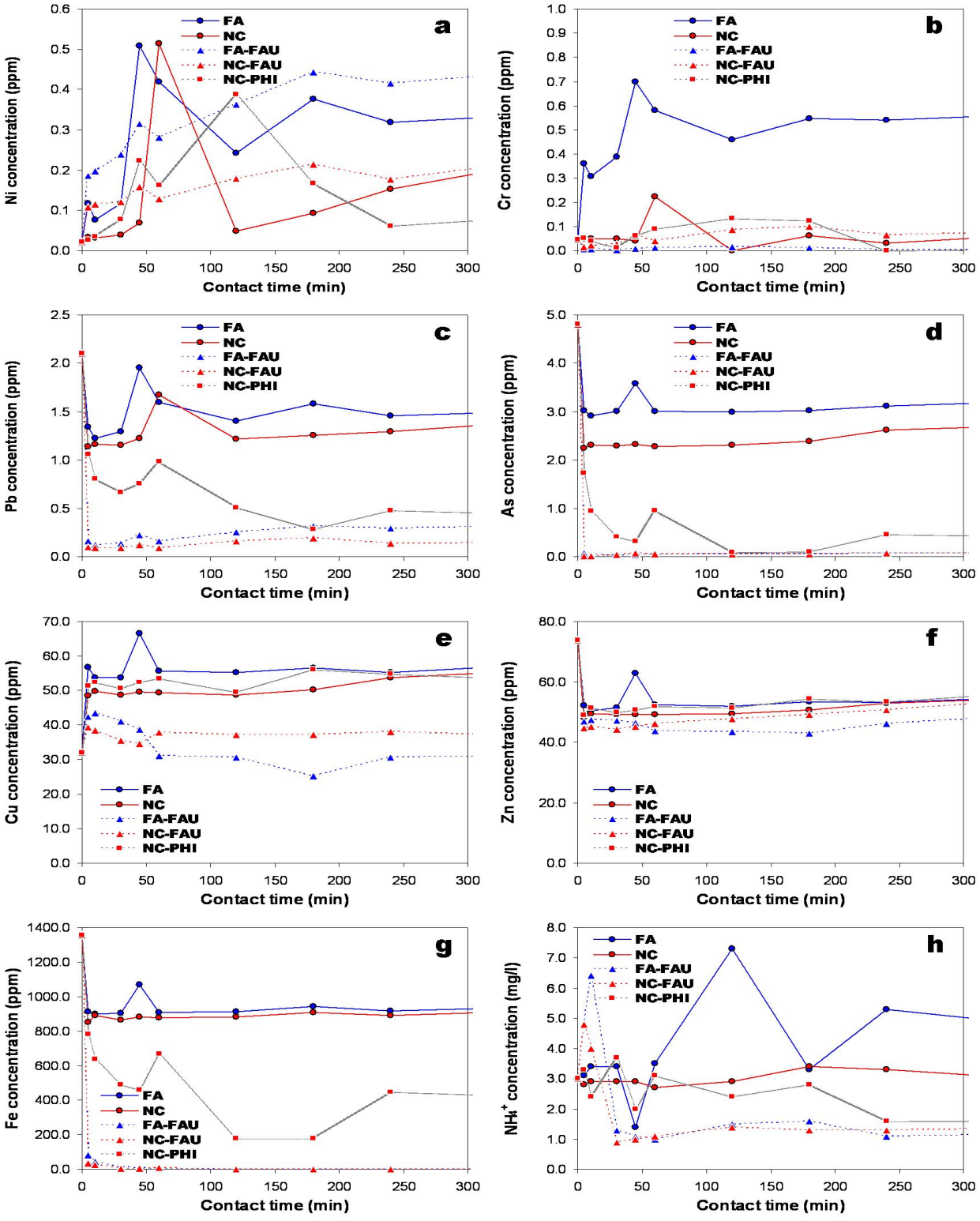

Figure 8.8. Heavy metal and ammonium concentration variation as a function of time during the adsorption batch experiments with starting pH of 1.96 and EC of 3.77 mS cm^{-1} and sorbent:AMD mixture of 0.25 g / 20 ml.

In general, the use of a small sorbent dose did not show good effect on solutions and the experiments showed inconsistent results as shown by the strong fluctuations in both heavy metal and ammonium concentration. The pH strongly affects the removal efficiency of heavy metals and ammonium, with precipitation of anionic hydr(oxide) complexes with little affinity for the sorbent surfaces that can reduce the removal efficiency or dissolution of the sorbent releasing metal ions. On the other hand, there was no clear relationship between the EC and uptake process, although the importance of this parameter should not be underestimated, taking into account that the fluctuations in EC can be explained by a combination of several factors, some of which may be difficult to predict, such as precipitation and evaporation by slight temperature oscillations.

8.3.4.4. Effect of sorbent dose

A sorbent:AMD mixture of 1 g / 20 ml was used to establish the effect of sorbent dose, and an increase of pH in the batch experiments occurred after 24 h of contact time, with final pH values from 4.20-9.43, except when NC was used (pH = 1.85). NC-FAU was selected to develop an additional batch reaction test (Table 8.5) to evaluate the removal of heavy metals and ammonium because it produced the highest pH (9.43).

Table 8.5. Water quality parameters recorded during 24 h of continuous shaking of NC-FAU with AMD in batch experiments (sorbent:AMD mixture of 1 g / 20 ml).

Contact time (min)	pH	EC (mS cm^{-1})	T (°C)	Heavy metal concentration (ppm)							Ammonium (mg l^{-1})
				Cu	Pb	Zn	Cr	Ni	As	Fe	
AMD*	1.96	3.77	16.00	31.90	2.10	73.83	0.05	0.02	4.81	1355.33	3.0
Batch reaction of NC-FAU											
5	7.70	9.42	20.50	0.05	0.06	0.02	0.08	0.04	0.00	0.28	0.3
10	8.05	9.78	20.50	1.65	0.02	3.35	0.02	0.04	0.00	0.24	0.7
30	8.32	9.71	20.50	0.02	0.07	0.11	0.27	0.06	0.02	0.27	0.8
45	8.45	10.44	20.70	0.06	0.13	0.12	0.12	0.03	0.03	0.28	0.9
60	8.34	10.03	20.60	0.06	0.09	0.10	0.10	0.07	0.01	0.20	0.7
1440	9.43	11.21	21.10	0.06	0.08	0.11	0.12	0.05	0.01	0.27	<<

** Parameters of the acid mine drainage*

Figure 8.9 illustrates the trends of pH, EC and ammonium and heavy metal concentrations in AMD treated with NC-FAU. The kinetics of the neutralization reaction is initially very rapid, with

pH (Figure 8.9a) increasing rapidly from 1.96-7.70 within the first 5 min on contact with the NC-FAU, which is probably the result of the free CaO present in the faujasite framework. The reaction rate decreases as equilibrium is approached, with an apparent equilibrium pH of 8.34 being reached within 1 h. The pH increase can also be associated with dissolution of the sorbent during the shaking process. However, a final pH similar to that obtained in our batch experiments has been attributed to hydrolysis of zeolites as well as cation exchange (Genç-Fuhrman *et al*., 2007). According to Kesraoui-Ouki and Kavannagh (1997) and Pitcher *et al*. (2004), the pH increase is almost unavoidable in zeolite heavy metal systems. The EC (Figure 8.9a) also shows an abrupt increase from 3.77-9.42 mS cm^{-1} within the first 5 min, which becomes stable after 1 h.

In Figure 8.9b is illustrated the ammonium removal. A sudden decrease from 3.0-0.3 mg l^{-1} of ammonium after 5 min was followed by an increase from 0.3-0.9 mg l^{-1} of ammonium between 5-45 min. After this monitoring time, uptake changed little (a progressive small decrease) for the rest of time intervals, reaching a complete removal of ammonium only after 24 h.

The removal trends of heavy metals in the treated AMD samples with NC-FAU (Figures 8.9c and 8.9d) indicates that after 5 min an abrupt decrease in all the analysed elements, except Ni and Cr, which showed a very small increase. Then, an abrupt increase in Zn and Cu, with a progressive decrease and increase in Pb and Ni, respectively was observed between 5-10 min, with Fe and As remaining constant. Cr displayed a very small decrease during this contact time. Between 10-30 min there was a sudden drop in Zn and Cu and an increase in Pb, Ni, Cr and As, with Fe remaining constant. A progressive increase in Pb and As, with a decrease in Ni, Zn and Cr occurred between 30-45 min. Finally, between 45-60 min a decrease in Pb and As, a very small decrease in Zn and Cr, and an increase in Ni, occurred. With contact time the concentration levels decreased to the lower values. However, during the monitoring range of time between 1 and 24 h an almost complete removal of Fe, Zn, Cu, As and Cr and partial removal of Pb and Ni was obtained.

In general, all metals showed a very steep concentration decrease during the first 5 min, reaching plateau values with very low residual concentrations for the remaining time intervals, although without complete removal. Pb and Ni exhibited a slight fluctuation in concentration during the first hour. The faster uptake indicates that the external mass transfer resistance played a strong role in the batch tests and that the agitation conditions of the sorbent can significantly reduce the time needed for the sorption study and hence the residence time needed for adsorption of metals from AMD (Cui *et al*., 2006). Solution pH had a very important role in the

adsorption/removal of the contaminants, probably due to the charge developed on the surfaces of the adsorbent as pH increased. On the other hand, a higher adsorbent ratio showed better efficiency in contaminant removal.

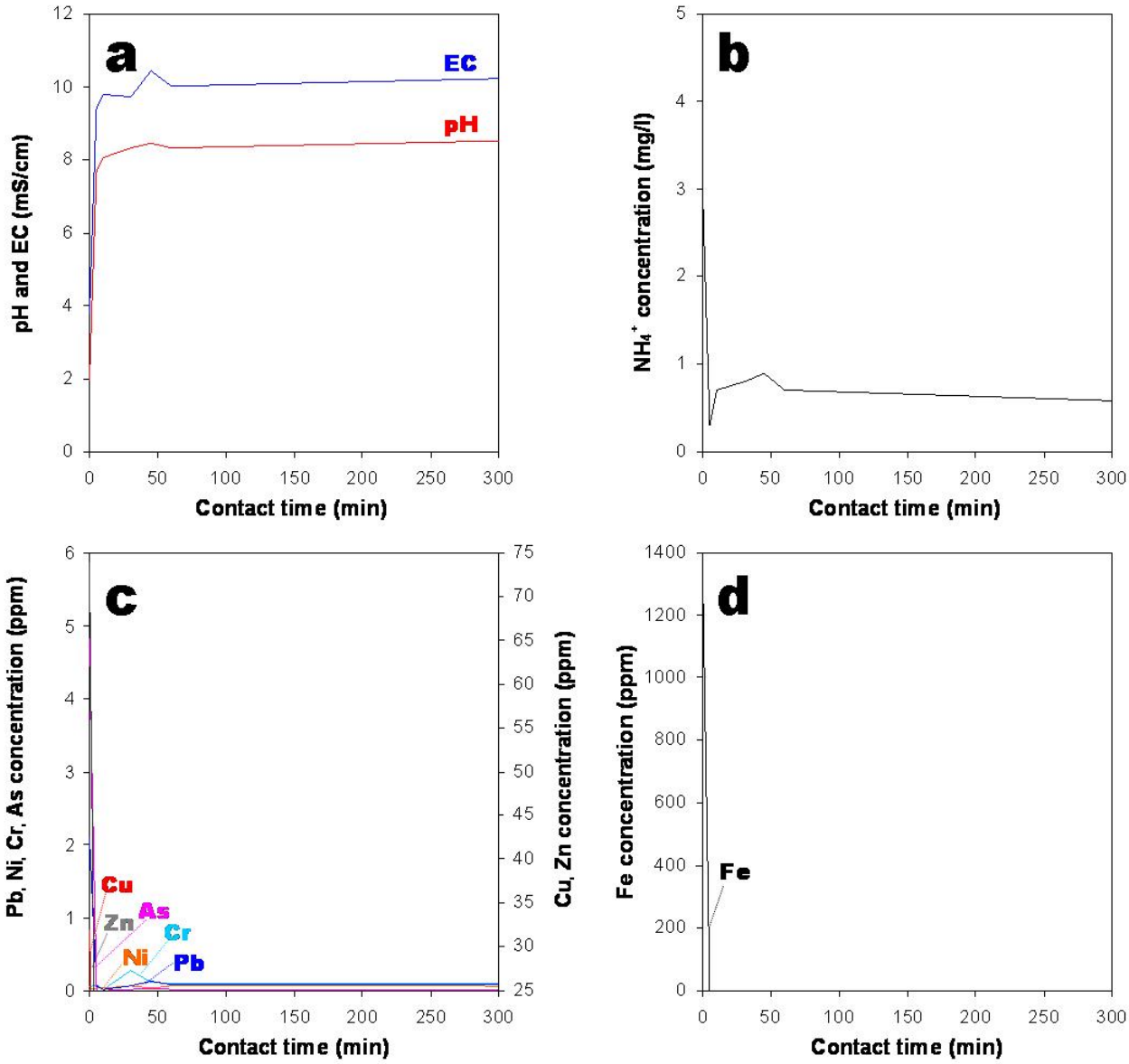

Figure 8.9. Variation of (a) pH and EC and concentration of (b) ammonium and (c-d) heavy metals as a function of time during the adsorption batch experiments (sorbent:AMD mixture of 1 g / 20 ml) with starting pH of 1.96 and EC of 3.77 mS cm^{-1}, using NC-FAU as the sorbent.

8.3.4.5. pH vs. dissolved metal content

The relationship between pH and the dissolved metal content in AMD can be summarized using 'Ficklin' diagrams (Ficklin *et al*., 1992; Plumlee *et al*., 1995; Seal *et al*., 2002; Desbarats and Dirom, 2007), as shown in Figure 8.10.

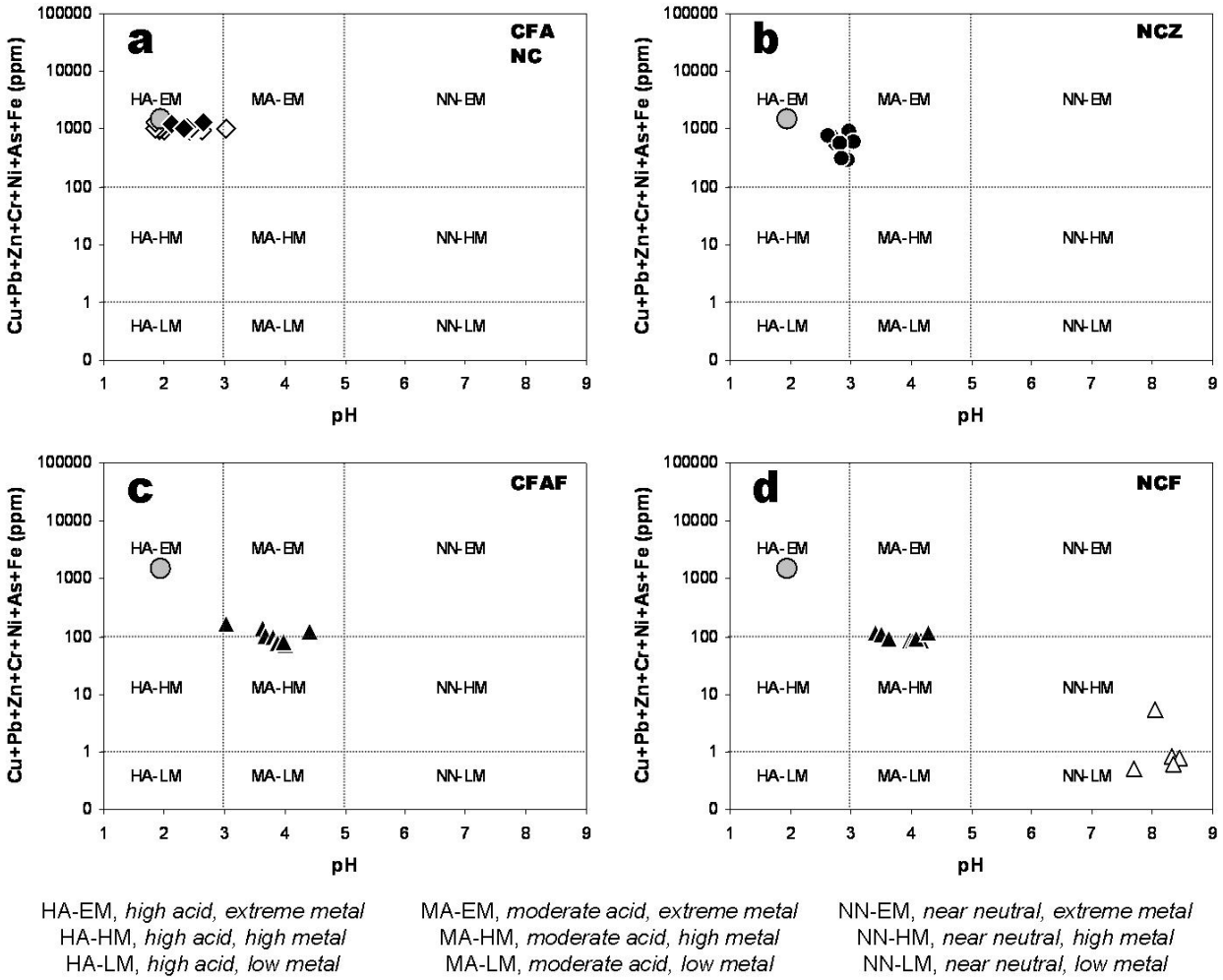

Figure 8.10. Ficklin diagrams showing the sum of aqueous base metal concentrations in AMD treated with: (a) FA and NC, (b) NC-PHI, (c) FA-FAU and (d) NC-FAU. AMD plot (grey circle) indicates the starting heavy metal concentration and pH, whereas the treated AMD data using a sorbent:AMD mixture of 0.25 g / 20ml are indicated by black rombs (FA); open rombs (NC); black circles (NC-PHI); black triangles (FAU). Open triangles indicate a NC-FAU:AMD mixture of 1 g / 20 ml.

These plots are very useful to do initial predictions of the potential impacts from mining sulphide-bearing mineral deposits, enabling an assessment of correlations between particular mineral-deposit types and the observed metal, metalloid, pH and sulphate chemistry in drainage (Bowell and Parshley, 2005). However, in this study the Ficklin diagrams are used to construct relationships between the metal concentration in treated AMDs and that corresponding to natural AMD associated with different mineral assemblages and geological conditions.

The plots of Figure 8.10 show that the raw AMD is characterized by high acid pH values and extreme metal concentrations and its plot falls within the field typically associated with pyrite-enargite-chalcocite-covelline in acid-altered rocks (Seal *et al*., 2002). The treated AMDs with FA and NC showed similar pH values and metal concentrations to those obtained for the starting AMD (Figure 8.10a). A similar result was observed when AMD was treated with NC-PHI (Figure 8.10b). When FA-FAU (Figure 8.10c) and NC-FAU (Figure 8.10d) were used during the AMD treatment, moderately acid pH values and extreme to high metal concentrations were obtained. This is equivalent to AMDs associated with pyrite-sphalerite-galena-chalcopyrite in carbonate-poor rocks. The effect of sorbent dose is also illustrated in Figure 8.10d. A sorbent:AMD mixture of 1 g / 20 ml, using NC-FAU as sorbent produced mainly near neutral pH and low metal concentrations, although after 5 min of reaction a near neutral pH and a high metal concentration was obtained, which is equivalent to AMDs associated with pyrite-poor sphalerite-galena veins and replacements in carbonate rocks or with pyrite-poor gold-telluride veins and breccias with carbonates. Therefore, the use of a higher sorbent dose in the treatment of AMD promoted increased pH and decreased metal concentrations.

8.3.4.6. Regeneration and long-term stability of the sorbents

In general, the sorbents used in the treatment of AMD are characterized by a good stability under strong acid conditions (pH < 2) for 24 h, although their grade of crystallinity showed a slight decrease. The starting FA and NC are more stable under the same conditions and show negligible change in crystallinity, faujasite represents a more stable phase compared with phillipsite, in agreement with results obtained by Ibrahim and Akashah (2004). Additional changes in the crystallinity of the sorbents are related to the appearance of new X-ray diffraction peaks corresponding to the precipitation onto the sorbent surface of new mineral phases, probably anionic hydr(oxide) complexes. On the other hand, the stability of the sorbents was confirmed by their intact morphology, although in some cases the surface morphology of the FA

spheres showed evidence of dissolution by AMD. However, there was also evidence of the precipitation of new phases; for example, cenospheres of FA revealed the precipitation of sulphate phases (gypsum crystals) growing on its inner surface after the batch reaction of FA with AMD for 24 h. The probable presence of sulphate or phosphate in the sorbent after its reaction with the acid solution (AMD) could modify its characteristics depending on the acidity of the aqueous media and consequently its stability. Therefore, the crystallinity and morphology of the sorbents used in this study remained intact following the treatment with AMD. Therefore, FA and NC as well as the synthesis products based in these low-cost and efficient materials appears to be promising for AMD treatment, with significant potential advantages relative to current treatment systems. However, in spite of the performance of the different sorbents used in the treatment of AMD, it is important to take into account some implications on these short half-live materials as suggested by Cama *et al*. (2005): (1) treated waters must be kept at near neutral pH and sorbents should be added periodically to the treated waters in order to compensate the loss of sorbent, and (2) water treatment applications that require a relatively short reaction time, the sorbent removed from the effluents should be kept dry in order to avoid its decomposition and the consequent release of the adsorbed metal to the environment. In addition to aspects related with the regeneration of the sorbent during the treatment of contaminated effluents, future experimental studies should consider the recycling of filtrates obtained after using a codisposal reaction in which different sorbents, mainly FA and NC, were reacted with AMD as has been done by Somerset *et al*. (2005a, 2005c). Alkaline hydrothermal zeolite synthesis would then be applied to these codisposal filtrates to convert coal by-products like FA and NC into zeolites. The application of FAZs in wastewater decontamination experiments with AMD showed that these FAZs can be used as low-cost and efficient sorbent in heavy metal uptake, particularly increasing the sorbent dose.

8.4. Conclusions to Chapter 8

The low-cost adsorbents used in this study were effective in removing mixed heavy metals and ammonium from artificially polluted solutions and AMD. The removal of heavy metals and ammonium from synthetic solutions using KAO, NC and FA was explored. It was found that FA exhibits a better sorption capacity for those pollutants, except by the uptake of Cr and NH_4^+, taking into account that NC showed a best affinity by them. KAO showed a poor efficiency during the sorption study due to surface effect. Moreover, the pH values did not change

significantly with the addition of this sorbent, similar to what occurs with NC, which means that KAO and NC did not act as a pH regulators. FA represents a low-cost adsorbent showing capability to adsorb particularly heavy metals. Metal ions sorption probably takes place in the form of metal hydroxide complexes and the high sorption capacity is related to the formation of soluble compounds on the internal surface of FA. However, to improve removal efficiencies and adsorption capacities of the raw materials used in this study, chemical modifications of these adsorbents should be done. The widespread uses of low-cost adsorbents for wastewater treatment applications are strongly recommended due to their availability, technical feasibility, engineering applicability and cost effectiveness.

The results obtained, particularly for short contact times suggests that the use of FAZs for the removal of metal ions from effluents contaminated with mixed heavy metals might became interesting in other different industrial applications. The as-synthesized FAZs had greater adsorption capabilities for heavy metals and ammonium than the original FA. FA-GIS exhibited the highest adsorption capacity with a metal ion selectivity of Cu > Zn > Cr > Ni > Pb. The experimental data suggest that FA could be converted into a beneficial product, which will be used in the future as an ion exchanger in removing heavy metals from wastewaters. MTK-LTA showed the best efficiency in the removal of heavy metals and ammonium compared with the FAZs and HEU.

In a case of study, FA, NC and synthetic zeolites were investigated in batch experiments as potential sorbents for treatment of AMD at a starting pH of 1.96, which changed after 24 h, particularly with sorbent dose, except when NC was used. This suggests that with sufficient reaction time (24 h), pH is strongly affected by the sorbent material rather than the AMD composition and with a higher sorbent dose. There are two competing processes here, release of alkalinity from FA and release of acidity from AMD components. At higher sorbent dose the acidity from AMD components is overwhelmed and pH is bound to increase, while with lower sorbent dose the alkalinity from the sorbent is overwhelmed by the acidity from the AMD components and pH remains low. Our experimental data reveal that the heavy metal removal depends on the sorbent material and the applied dose; NC and probably FA were not the best sorbents to neutralize the AMD, but their synthesis products are beneficial products as ion exchangers in removing acidity, Fe, Zn and Cu from AMD. In addition to cation exchange reactions, precipitation of hydroxide species (mainly of Fe) also played an important role in co-precipitation and adsorption, and thus immobilization of metals in the batch experiments.

The results of the absorption experiments suggest that FAU can be applied in wastewater

treatment as pollutant immobilizer. Selectivity of FAU for metal removal was, in decreasing order, Fe > As > Pb > Zn > Cu > Ni > Cr. From the above results, it is demonstrated that FAU was effective in decreasing Fe, As and Pb concentrations, indicating the complete removal of Fe and As with strong fluctuations and an incomplete removal of Pb, in spite of the dose of sorbent applied during AMD treatment. Cu and Zn were partially removed when 1 g of sorbent was reacted with the AMD. Ni showed a small progressive increase and displayed a similar trend to Pb, except when NC-PHI was used. The efficiency in ammonium removal was poor. However, the reaction between synthetic zeolites and AMD after 24 h of contact time produced the lower ammonium concentrations. NC-FAU shows a complete removal of ammonium after 24 h of contact time when a dose of 1 g was used.

In general, the different sorbents contain considerable amounts of minor phases that partly dissolve during the batch reaction, which may explain the sudden increase or decrease in metal concentration and, therefore, the release rate of these elements is controlled by sorbent dissolution. These results could assist in waste management scenarios and AMD management. However, it will be necessary to design and execute more detailed experiments to explore further applications of adsorbents for AMD cleaning. AMD can be treated at the mine to some degree, usually by neutralization at source by limestone, settling and tailings ponds or wetlands, although this process will never be fully efficient and accidents with the treatment system are probable.

In spite of the results obtained in this sorption study, the geochemical modelling can be a very useful tool to assist in the interpretation of the aqueous geochemical data, particularly with respect to speciation of metal ions in an aqueous solution, which significantly affects their interaction with the adsorbent. Several metal ions can be mainly present in solution as mononuclear hydrolysis products, although their species distributions are related to many factors, such as pH, ionic strength, anions and metal ion concentration.

Chapter 9

Chapter 9. Conclusions

In this chapter the specific aims of this study are reviewed to present an overview of the findings of this study and to make a critical evaluation.

9.1. Critical overview

The experimental work revealed new insights on the structures and behaviour of the raw materials and as-synthesized products, which are particularly important in understanding and predicting their applications under real-world conditions. Each characterization technique typically probed only a particular aspect of a specific material and therefore a combination of methods was necessary to obtain a balanced description of the starting materials as well as the frequently complex zeolitic products. This is very important to use and improve a zeolitic material for a specific application. Both natural and synthetic zeolites can be available in commercial quantities. However, the variable phase purity of the natural zeolites and the chemical impurities, which are costly to remove, can make the synthetic zeolites more attractive for specific applications, whereas where uniformity and purity are not important; the cheapness of a natural zeolite may favour its use (Sherman, 1999). This is why this research concentrates on using cheap and available materials such as KAO, NC and FA in zeolites synthesis, promoting the use of clean technologies to reduce capital and operating costs, energy requirements and adverse environmental impacts.

This research is innovative by two reasons. Firstly, unprocessed FA was used in zeolite synthesis in spite of advanced technologies generally require that FA be processed prior to the synthesis process. On the other hand, FA has shown to be a very versatile material that can be used as a silica and alumina source for the production of various FAZs with adequate physicochemical properties superior to any natural or commercial zeolites. Secondly, to our knowledge, no previous effort had been made to use NC as a raw material in zeolite synthesis, except in recent studies by Ríos *et al*. (2006, 2008a) and Ríos and Williams (2008). The bulk chemical composition similarity of this coal by-product with the volcanic materials from which the natural zeolites originate has motivated attempts to synthesize NCZs, justifying the development of future investigations in the field of the synthesis of new materials with potential industrial applications. In addition, NC was used in this study because: (1) it is a coal by-product thus it

adds value, reduces cost and enhances environmental conditions, (2) its potential application in zeolite synthesis and water technology is not utilized and (3) it is very resistant to weathering and erosion and highly workable.

Different zeolitic materials were successfully synthesized from KAO, NC and FA. In general, the synthesis products correspond to a mixture of zeolitic products, in some cases, containing relict phases of the starting materials. The chemical composition and particularly the SiO_2/Al_2O_3 ratio of the raw materials were appropriated for zeolite synthesis, which was conducted using two different methods: classic hydrothermal synthesis and alkaline fusion prior to hydrothermal synthesis. During the classic hydrothermal synthesis, several variables were considered: alkali activator (NaOH and KOH), concentration of the activator, reaction time, temperature and solution/raw material ratio. In the alkaline fusion approach, alkaline activator/raw material ratio for fusion, H_2O/alkali fused raw material ratio, reaction time and temperature were the considered parameters. Generally, the type and chemical composition of the as-synthesized zeolites were strongly dependent on the chemical composition of the starting material. However, other physicochemical factors probably played an important role in the thermodynamics and kinetics of zeolite formation. At this point, it is necessary to highlight that the introduction of an alkaline fusion step prior to the hydrothermal reaction demonstrated to be a more efficient method of zeolite synthesis compared with the classical hydrothermal synthesis, due to the reduction of curing time and the formation of more crystalline materials.

A very important issue of this study is the fact that the experimental data revealed the occurrence of several mineral assemblages. In the hydrothermal conversion of KAO in the system K_2O-SiO_2-Al_2O_3-H_2O, the phase transformation of KAO → KAO-CHA → KAO-EDI → unidentified potassium aluminosilicate phase → kalsilite + leucite could be similar in some steps to that reported for example by Bernhard and Barth-Wirsching (2002) after field and experimental studies performed to understand the formation conditions of the Nettetal zeolite deposit, Laach volcanic area, Germany. Potassium was essential to CHA, EDI and PHI crystallization, which represent metastable phases with respect to K-feldspar. The absence of ANA can be explained by the lack of sodium in the considered system, taking into account that Na is necessary for ANA formation. Hydrogel composition determined the mineral assemblages obtained and hence in those commonly found in nature. However, in this study it is demonstrated that a different sequence of reactions could occur in similar geological contexts.

Batch reaction experiments with simulated wastewaters revealed that the equilibrium metal ion concentration in solution decreased with increasing sorbent dose, with an optimum decrease

corresponding to 1 g sorbent / 20 ml of the polluted water. The contact time showed that a drastic decrease in metal concentration occurred within the first 30 min of contact and at this stage, equilibrium sorbent:solution was reached for almost all studied metals. The AMD treatment showed that in general the metal ion and ammonium removal trends are similar to those obtained after treatment of simulated wastewaters. The pH of the aqueous system played a very important role in the speciation of the metal ions, as well as the effective charge of the zeolite surface functional groups and as such changes the physicochemical reactions, which occur between the zeolite and effluent. Metal uptake could also occur through a more specific scenario involving the hydrolysed species. In this case, the hydrolysed metal ion associated with the zeolite as an inner-sphere complex via covalent bonding between the metal and the oxygen bridges of the functional groups (≡Si-O-Al≡) on the zeolite surface as reported by Hendricks (2005). According to this author, these reactions occurred at variable-charge sites on the zeolite surface, forming stable complexes between metal cations and silanol and/or aluminol functional groups. However, surface precipitation also becomes an appreciable process of metal retention. However, other mechanisms probably occurred during water treatment, which include specific and/or non-specific adsorption, outer-sphere complex formation and binuclear complex formation, thus considerably aiding the purification process (Hendricks, 2005).

Results confirmed the findings observed by the characterization analysis in terms of the successful zeolitization of the starting materials and effectively prove one of the major aims of this research that zeolites have advantages over other ion exchangers, based on their low-costs, as well as their ion selectivity, generated by their rigid porous structures.

9.2. Overall significance

Industrial waste solid materials, such as FA and NC can be successfully converted into zeolites and therefore their use serves a dual purpose. Firstly, due to the shortage of landfill sites and stricter environmental regulation the effective recycling of FA and NC into products of greater value is promoted to mitigate the depletion of resources and environmental impact, which can be achieved through their zeolitization. The recycling of these materials provides a low-cost source of Si and Al for the synthesis of zeolitic materials, which can show numerous potential applications that have not been analysed yet. As occurs with FA, the recycling of NC can become an increasing concern in the future due to increasing landfill costs and current interest in sustainable development. Secondly, this study contributes both to the management of these

industrial waste solid materials and their application as inorganic ion exchangers for treatment of contaminated effluents. FAZs and NCZs have great potential for immobilization of environmental pollutants, such as removal of heavy metals and ammonium ions from industrial wastewater.

9.3. Future work

Although the initial objectives were achieved, there are some aspects, which were not within the scope of this study and due to time/work limitations, concern on the physicochemical properties of the as-synthesized products and their performance in water treatment, taking into account that modern industrial technologies require the use of zeolitic materials and sorbents with very precisely specified parameters.

Future investigations will be required to explain some aspects of zeolite synthesis that are still unclear in the current work, which could give better perspectives in terms of possible applications. Some recommendations for further studies are:

1. A fundamental understanding on the conversion of the raw materials needs to be re-examined in order to establishing the role of cations in the kinetics and reaction mechanisms and to optimize experimental conditions. A mathematical model of the mechanism of zeolite formation should be developed in order to provide a quantitative understanding on how zeolites nucleate and grow, which is fundamental from both a scientific and technological point of view.

2. In spite of the results obtained in the sorption study, geochemical modelling can be a very useful tool to assist in the interpretation of the aqueous geochemical data, particularly with respect to speciation of metal ions in an aqueous solution, the effect of both cationic and anionic competition on metal removal capacity and on prevailing mechanisms, which significantly affects their interaction with the sorbent. Several metal ions can be mainly present in solution as mononuclear hydrolysis products, although their species distributions are related to many factors, such as pH, ionic strength, anions and metal ion concentration.

3. Zeolites generally show a limited capacity to sorb pollutants from contaminated water due to their hydrophilic properties. Therefore, the use of SDAs in the synthesis of zeolites (organozeolites) provide to them hydrophobic properties, which can improve the efficiency in the

removal of organic pollutants from wastewater compared with what is expected to be found in the unmodified zeolites.

4. A low-cost wastewater treatment process applied in this work, considering the fact that very cheap raw materials were used. However, the required dose of sorbent, particularly synthetic products, at an industrial scale would increase operating costs. Therefore, the use of zeolites in environmental remediation is restricted due to prohibitive costs and would not be economically viable at this stage. These issues can be resolved using low cost FAZs and NCZs.

5. Due to current problems associated with the potential leaching of heavy metals from some of the synthesis products used as sorbents in water purification, which would magnify when applied on a longer scale, their commercialization is not recommended at this stage. The problem of leaching needs to be eliminated, which may be achieved by treating the starting material to extract potential leachable elements. The process of synthesis should be optimized by applying a wide range of experimental conditions, taking into account parameters, such as reaction temperature, time, mineralizer concentration and solid/solution ratio, in order to avoid unnecessary operating costs.

6. Based on the fact that NC does not represent a hazardous material, new ways for its recycling should be quickly developed due to the shortage of landfill sites and stricter environmental regulations as also occurs with FA, which can be done through its zeolitization. Although its potential application could consume a small part of NC generated by coal combustion, the as-synthesized zeolites could reach an added value much higher than in the applications that at the moment this coal by-product has in the coal industry. It will certainly have a growing curiosity in terms of synthesis of NCZs with high CEC.

7. The principal disposal methods and possible recovery and recycling alternatives for the heavy metal saturated zeolitic materials should be considered. On the other hand, a study on the conditioning and regeneration methods under different experimental conditions and from an economical and feasibility point of view should be carried out.

8. It would be very important to apply the knowledge and techniques obtained in the synthetic systems studied here to design experimental petrology programmes to lead to an understanding of the conditions under which zeolites formed in a geological context. However, one of the criticisms given to the value of experimental petrology leading to an understanding of these low temperature systems is that the time involved is too long to be feasible (Sand, 1980). It is well-

known that geological processes take millions of years. Even if a minimal time-frame (i.e. about one million years is required for zeolites to crystallize completely from volcanic ash on the ocean floor) is assumed, this is still too long to entertain any sort of industrial application. Success in overcoming this problem would be especially based on: (1) Determining mineral assemblages in natural systems. (2) Carrying out phase equilibrium studies of zeolites formed in high temperature environments. (3) Determining the kinetics of phase transformations of zeolites formed in low temperature environments to other assemblages during burial metamorphism. (4) Correlating the crystallization from volcanic glass as a function of its lateral and vertical distribution within a zeolite deposit.

Bibliography

Bibliography

Abusafa, A. and Yucel, H. (2002). Removal of ^{137}Cs from aqueous solutions using different cationic forms of a natural zeolite: clinoptilolite. Separation and Purification Technology 28, 103-116.

Agger, J.R., Pervaiz, N., Cheetham, A.K. and Anderson, M.W. (1998). Crystallization in zeolite A studied by Atomic Force Microscopy, Journal of the American Chemical Society 120, 10754-10759.

Akolekar, D., Chaffee, A. and Howe, R.F. (1997). The transformation of kaolin to low-silica X zeolite, Zeolites 19, 359-365.

Alberti, A., Colella, C., Oggiano, G., Pansini, M. and Vezzalini, G. (1994). Zeolite production from waste kaolin containing materials, Materials Engineering (Modena, Italy) 5, 145-158.

Alfaro, S., Rodríguez, C., Valenzuela, M.A. and Bosch, P. (2007). Aging time effect on the synthesis of small crystal zeolite LTAs in the absence of organic template, Materials Letters 61, 4655-4658.

Alinnor, I.J. (2007). Adsorption of heavy metal ions from aqueous solution by fly ash, Fuel 86, 853-857.

Alkan, M., Hopa, C., Yilmaz, Z. and Guler, H. (2005). The effect of alkali concentration and solid/ liquid ratio on the hydrothermal synthesis of zeolite NaA from natural kaolinite, Microporous and Mesoporous Materials 86, 176-184.

Annen, M.J., Young, D., Arhancet, J.P., Davis, M.E. and Schramm, S. (1991). Investigations into the nature of the hexagonal polytype of faujasite, Zeolites 11, 98-102.

Altare, C.R., Bowman, R.S., Katz, L.E., Kinney, K.A. and Sullivan, E.J. (2007). Regeneration and long-term stability of surfactant-modified zeolite for removal of volatile organic compounds from produced water, Microporous and Mesoporous Materials 105, 305-316.

Alvarez-Ayuso, E., Garcia-Sanchez, A. and Querol, X. (2003). Purification of metal electroplating waste waters using zeolites, Journal of Water Research 37, 4855-4862.

American Public Health Association, American Water Works Association and Water Environment Federation (2005), Standard Methods for the Examination of Water and Wastewater, A.D. Eaton, L.S. Clesceri, E.W. Rice, A.E. Greenberg and M.A.H. Franson (Eds.), 21st Ed., 1368pp.

Amrhein, C., Haghnia, G.H., Kim, T.S., Mosher, P.A., Gagajena, R.C., Amanios, T., de La Torre, L. (1996). Synthesis and properties of zeolites from fly ash, Environmental Science and Technology 30, 735-742.

Argauer, R.J. and Landolt, G.R. (1972). U.S. Patent No. 3 702 886.

Armbruster, T. and Gunter, M.E. (2001). Crystal structure of natural zeolites. Natural Zeolites: Occurrence, Properties, Applications. In: Reviews in Mineralogy and Geochemistry 45, D.L. Bish and D.W. Ming (Eds.), Mineralogical Society of America, Washington, D.C., 1-67.

Aronne, A., Esposito S. and Pernice, P. (1997). FT-IR and DTA study of lanthanum aluminosilicates glasses, Materials Chemistry and Physics 51, 163–168.

Aronne, A., Esposito, S. Ferone, C., Pansini, M. and Pernice, P. (2002). FT-IR study of the thermal transformation of barium-exchanged zeolite A to celsian, Journal of Materials Chemistry 12, 3039–3045

Baccouche, A., Srasra, E. and Maaoui, M.E. (1998). Preparation of Na-P1 and sodalite octahydrate zeolites from interstratified illite-smectite, Applied Clay Sciences 13, 255-273.

Baerlocher, C., Meier, W.M. and Olson, D.H. (2001). Atlas of zeolite framework types, 5th Ed., Elsevier, Amsterdam, 302pp.

Bahruji, H. (2005). Synthesis of zeolite ferrierite from rice husk ash, characterization and activity towards friedel-crafts acylation for the formation of *p*-methoxypropiophenone. Unpublished Master's thesis. Universiti Teknologi Malaysia, 124p.

Balek, V. and Murat, M. (1996). The emanation thermal analysis of kaolinite clay minerals. Thermochimica Acta 282-283, 385–397.

Barbosa, V.F.F. and MacKenzie, K.J.D. (2003). Synthesis and thermal behaviour of potassium

sialate geopolymers, Materials Letters 57, 1477-1482.

Barnes, M.C., Addai-Mensah, J. and Gerson, A.R. (1999a). The mechanism of the sodalite-to-cancrinite phase transformation in synthetic spent Bayer liquor, Microporous and Mesoporous Materials 31, 287-302.

Barnes, M.C., Addai-Mensah, J. and Gerson, A.R. (1999b). A methodology for quantifying sodalite and cancrinite phase mixtures and the kinetics of the sodalite to cancrinite phase transformation, Microporous and Mesoporous Materials 31, 303-319.

Barnes, M.C., Addai-Mensah, J. and Gerson, A.R. (1999c). The solubility of sodalite and cancrinite in synthetic spent Bayer liquor, Colloids and Surfaces A 157, 106-116.

Barron, P.F., Frost, R.L., Skjemstad, J.O. and Koppi, A.J. (1983). Detection of two silicon environments in kaolins by solid-state silicon-29 NMR, Nature 302, 49–50.

Barrer, R.M. (1978). Zeolites and Clay Minerals as Sorbents and Molecular Sieves, Academic Press, London, 497pp.

Barrer, R.M. (1982). Hydrothermal Chemistry of Zeolites, Academic Press, New York, 360pp.

Barrer, R.M. and Denny, P.J. (1961). Hydrothermal chemistry of the silicates. Part X. A partial study of the field CaO-Al_2O_3-SiO_2-H_2O, Journal of the Chemical Society of London, 983-1000.

Barrer, R.M. and Marcilly, C. (1970). Hydrothermal chemistry of silicates. Part XV. Synthesis and nature of some salt-bearing aluminosilicates, Journal of Chemical Society (A), 2735-2745.

Barrer, R.M. and White, E.A.D. (1952). The hydrothermal chemistry of silicates. Part II. Synthetic crystalline sodium aluminosilicates, Journal of Chemical Society, 1561-1571.

Barrer, R.M., Cole, J.F. and Sticher, H. (1968). Chemistry of soil minerals. Part V. Low temperature hydrotermal transformations of kaolinite, Journal of Chemical Society (A), 2475-2485.

Basaldella, E.I. and Tara, J.C. (1995). Synthesis of LSX zeolite in the Na/K system. Influence of the Na/K ratio, Zeolites 11, 243-248.

Basaldella, E.I., Boneno, R.D. and Tara, J.C. (1993). Synthesis of NaY zeolite on preformed kaolinite spheres. Evolution of zeolite content and textural properties with the reaction time, Industrial and Engineering Chemistry Research 32, 751-757.

Basaldella, E.I., Kikot, A. and Tara, J.C. (1995). Effect of pellet pore size and synthesis conditions in the *in situ* synthesis of LSX zeolite, Industrial and Engineering Chemistry Research 34, 2990-2996.

Bauer, A., and Berger, G. (1998). Kaolinite and smectite dissolution rate in high molar KOH solutions at 35 ° and 80 °C, Applied Geochemistry 13, 905-916.

Bauer, A., Velde, B. and Berger, G. (1998). Kaolinite transformation in high molar KOH solutions, Applied Geochemistry 13, 619-629.

Baykal, B.B. (1998). Clinoptilolite and multipurpose filters for upgrading effluent ammonia quality under peak loads, Water Science and Technology 37, 235-242.

Benoît, L. and Lioubov, K-M. (2004). Synthesis of ZSM-5 zeolite in fluoride media: An innovative approach to tailor both crystal size and acidity, Microporous and Mesoporous Materials 74, 171-178.

Bergk, K.H., Porsch, M. and Drews, J. (1987). Conversion of solid primary and recycled raw materials to zeolite-containing products. Part VI: Continuous manufacture of zeolite A containing products, Chemische Technik 39, 308-310.

Berkgaut, V. and Singer, A. (1996). High capacity cation exchanger by hydrothermal zeolitization of fly ash, Applied Clay Sciences 10, 369-378.

Bernhard, F. and Barth-Wirsching, U. (2002). Zeolitization of a phonolitic ash flow by groundwater in the Laach volcanic area, Eifel, Germany, Clays and Clay Minerals 50, 710-725.

Bonaccorsi, E. and Merlino, S. (2004). Calcium silicate hydrate (C-S-H) minerals: Structures and transformations. Conference of the 32nd International Geological Congress, Florence, p. 215.

Booker, N.A., Cooney, E.L. and Priestley, A.J. (1995). A combined high-rate adsorption process for enhanced sewage treatment. In: Proceedings of the 16th Federal Convention,

Australian Water and Wastewater Association, Sydney, Australia, pp. 645-652.

Boukadir, D., Bettahar N. and Derriche, Z. (2002). Synthesis of zeolites 4A and HS from natural materials, Annales de Chimie - Science des Materiaux 27, 1-13.

Bowell, R.J. and Parshley, J.V. (2005). Control of pit-lake water chemistry by secondary minerals, Summer Camp pit, Getchell mine, Nevada, Chemical Geology 21, 373-385.

Breck, D.W. (1964). U.S. Patent No. 3 130 007.

Breck, D.W. (1974). Zeolite Molecular Sieves: Structure, Chemistry and Use, 1st Ed., John Wiley, New York, 313pp.

Brindle, J.H. and McCarthy, M.J. (2006). Chemical constraints on fly ash glass compositions, Energy and Fuels 20, 2580-2585.

Brindley, G.W. and Nakahira, M. (1959a). The kaolinite-mullite reaction series: I, A survey of outstanding problems, Journal of the American Ceramic Society 42, 311-314.

Brindley, G.W. and Nakahira, M. (1959b). The kaolinite-mullite reaction series: II, Metakaolin, Journal of the American Ceramic Society 42, 314-318.

Brough, A.R., Katz, A., Sun, G.K., Struble, L.J., Kirkpatrick, R.J. And Young, J.F. (2001). Adiabatically cured, alkali-activated cement-based wasteforms containing high levels of fly ash: Formation of zeolites and Al-substituted C-S-H, Cement and Concrete Research 31, 1437-1447.

Buhl, J.Ch. (1991a). Kinetics and mechanism of the intra-cage oxidation of nitrite sodalite, Reaction Kinetics and Catalysis Letters 43, 577-582.

Buhl, J.Ch. (1991b). Synthesis and characterization of the basic and non-basic members of the cancrinite-natrodavyne family, Thermochimica Acta 178, 19-31.

Buhl, J.Ch. and Löns, J. (1996). Synthesis and crystal structure of nitrate enclathrated sodalite $Na_8[AlSiO_4]_6(NO_3)_2$, Journal of Alloys and Compounds 235, 41-47.

Buhl, J.C., Hoffmann, W., Buckermann, W.A. and Muller-Warmuth, W. (2000a). The crystallization kinetics of sodalites grown by the hydrothermal transformation of kaolinite

studied by ^{29}Si MAS NMR, Solid State Nuclear Magnetic Resonance 9, 121-128.

Buhl, J.C., Stief, F., Fechtelkord, M., Gesing, T.M., Taphorn, U. and Taake, C. (2000b). Synthesis, X-ray diffraction and MAS NMR characteristics of nitrate cancrinite $Na_7.6[AlSiO_4]_6(NO_3)1.6(H_2O)_2$, Journal of Alloys and Compounds 305, 93-102.

Burkett, S.L. and Davis, M.E. (1993). Structure-directing effects in the crown ether-mediated syntheses of FAU and EMT zeolites, Microporous Materials 1, 265-282.

Cama, J., Ayora, C., Querol, X. and Ganor, J. (2005). Dissolution kinetics of synthetic zeolite NaP1 and its implication to zeolite treatment of contaminated waters, Environmental Science and Technology 39, 4871-4877.

Candela, S.A. and Quintero, J.A. (2004). Cartografía de las zonas de clinker en las áreas de minería del Complejo Carbonífero El Cerrejón (Guajira), Undergraduate Thesis, Universidad Industrial de Santander, Colombia, 90p.

Cañizares, P., Durán, A., Dorado, F. and Carmona, M. (2000). The role of sodium montmorillonite on bounded zeolite-type catalysts, Applied Clay Science 16, 273–287.

Carlson, L., Bigham, J.M., Schwertmann, U., Kyek, A. and Wagner, F. (2002). Scavenging of As from acid mine drainage byschwertmannite and ferrihydrite: a comparison with synthetic analogues, Environmental Science and Technology 36, 1712–1719.

Carroll, S.A. and Walther, J.V. (1988). A surface complex reaction model for the pH-dependence of corundum and kaolinite dissolution, Geochimica et Cosmochimica Acta 52, 2609--2623.

Carroll, S.A. and Walther, J.V. (1990). Kaolinite dissolution at 25 °, 60 ° and 80 °C, American Journal of Science 290, 797810.

Casiot, C., Morin, G., Juillot, F., Bruneel, O., Personné, J-Ch., Leblanc, M., Duquesne, K., Bonnefoy, V. and Elbaz-Poulichet, F. (2003). Bacterial immobilization and oxidation of arsenic in acid mine drainage (Carnoulès creek, France), Water Research 37, 2929-2936.

Catalfamo, P., Corigliano, F., Patrizia, P. and Di Pascuale, S. (1993). Study of the pre-crystallization stage of hydrothermally treated amorphous aluminosilicates through the

composition of the aqueous phase, Journal of the Chemical Society, Faraday Transactions 89, 171-175.

Catalfamo, P., di Pasquale, S., Corigliano, F. and Mavilia, L. (1997). Influence of the calcium content on the fly ash features in some innovative applications, Resources, Conservation and Recycling 20, 119–125.

Chakravorty, A.K. and Ghosh, D.K. (1991). Kaolinite-mullite reaction series: The development and significance of a binary aluminosilicate phase, Journal of the American Ceramic Society 74, 1401–1406.

Chandra, S. and Flodin, P. (1990). Interactions of polymers and organic admixtures on portland cement hydration, Cement and Concrete Research 17, 975-890.

Chandrasekhar, S. and Pramada, P.N. (1999). Investigation on the synthesis of zeolite NaX from Kerala kaolin, Journal of Porous Materials 6, 283-297.

Chang, H.L., Shih, W.H. (1998). A general method for the conversion of fly ash into zeolites as ion exchangers for cesium, Industrial and Engineering Chemistry Research 37, 71-78

Chartrand, M.M.G. and Bunce, N.J. (2003). Electrochemical remediation of acid mine drainage, Journal of Applied Electrochemistry 33, 259–264.

Chen, C-Y. and Tuan, W-H. (2002). Evolution of mullite texture on firing tape-cast kaolin bodies, Journal of the American Ceramic Society 85, 1121–1126.

Cho, H., Oh, D. and Kim, K. (2005). A study on removal characteristics of heavy metals from aqueous solution by fly ash, Journal of Hazardous Materials 127, 187-195.

Choi, S., Crosson, G., Mueller, K.T., Seraphin, S. and Chorover, J. (2005). Clay mineral weathering and contaminant dynamics in a caustic aqueous system. II. Mineral transformation and microscale partitioning, Geochimica et Cosmochimica Acta 69, 4437-4451.

Chorover, J., Choi, S., Amistadi, M.K., Karthikeyan, K.G., Crosson, G. and Mueller, K.T. (2003). Linking Cesium and Strontium uptake to kaolinite weathering in simulated tank waste leachate, Environmental Science Technology 37, 2200-2208.

Chou, M-I., Chou, S-F., Patel, V., Pickering, M.D. and Stucki, J.W. (2006). Manufacturing Fired Bricks With Class F Fly Ash From Illinois Basin Coals. Combustion Byproducts Recycling Consortium, Project Number: 02-CBRC-M12, Final Report.

Cincotti, A., Lai, N., Orrù, R. and Cao, G. (2001). Sardinian natural clinoptilolites for heavy metals and ammonium removal: experimental and modeling, Chemical Engineering Journal 84, 275-282.

Coleman, N.J. (2005). Synthesis, structure and ion exchange properties of 11 Å tobermorites from newsprint recycling residue, Bulletin of Material Science 40, 2000-2013.

Cosca, M., Essene, E., Geissman, J., Simmons, W. and Coates, D. (1989). Pyrometamorphic rocks associated with naturally burned coal beds, Powder River Basin, Wyoming, American Mineralogist 74, 85-100.

Covarrubias, C., Garcia, R., Arriagada, R., Yanez, J., and Garland, T. (2006). Cr(III) exchange on zeolites obtained from kaolin and natural mordenite, Microporous and Mesoporous Materials 88, 220-231.

Cui, H., Li, L.Y. and Grace, J.R. (2006). Exploration of remediation of acid rock drainage with clinoptilolite as sorbent in a slurry bubble column for both heavy metal capture and regeneration, Water Research 40, 3359-3366.

Davidovits, J. (1991). Geopolymers Inorganic polymeric new materials, Journal of Thermal Analysis 37, 1633-1656.

Davis, M.E. and Zones, S.I. (1997). A perspective on zeolite synthesis: How do you know what you'll get? In: Synthesis of Porous Materials: Zeolites, Clays and Nanostructures, M.L. Occelli and H. Kessler (Eds.), Marcel Dekker, Inc., New York, 1-34.

De Boer, C., Dekkers, M. and van Hoof, T. (2001). Rock-magnetic properties of TRM carrying baked and molten rocks straddling burnt coal seams, Physics of the Earth and Planetary Interiors 126, 93–108.

De vos Burchart, E., Jansen J.C., van Bekkum, H. (1989). Ordered overgrowth of zeolite X onto crystals of zeolite A, Zeolites 9, 432-435.

Demortier, A., Gobeltz, N., Lelieur, J.P. and Duhayon, C. (1999). Infrared evidence for the

formation of an intermediate compound during the synthesis of zeolite Na–A from metakaolin, International Journal of Inorganic Materials 1, 129-134.

Deng, Y., Harsh, J.B., Flury, M., Young, J.S. and Boyle, J.S. (2003). Mineral phase transformation in conditions mimic sediment solutions underlying leaked Hanford waste tanks. Abstracts, The Clay Minerals Society 40th Annual Meeting: June 7-12, Athens, pp. 50-51.

Deng, Y., Harsh, J.B., Flury, M., Young, J.S. and Boyle, J.S. (2006). Mineral formation during simulated leaks of Hanford waste tanks, Applied Geochemistry 21, 1392-1409.

Desbarats, A.J. and Dirom, G.C. (2007). Temporal variations in the chemistry of circum-neutral drainage from the 10-Level portal, Myra Mine, Vancouver Island, British Columbia, Applied Geochemistry 22, 415-435.

Dimitrijevic, R. and Dondur, V. (1995). Synthesis and Characterization of $KAlSiO_4$ Polymorphs on the SiO_2-$KAlO_2$ Join, Journal of Solid State Chemistry 115, 214-224.

Diz, H.R. and Novak, J.T. (1998). Fluidized bed for the removing of iron and acidity from acid mine drainage, Journal of Environment Engineering 124, 701-708.

Dougnier, F., Patarin, J., Guth, J.L. and Anglerot, D. (1992). Synthesis, characterization, and catalytic properties of silica-rich faujasite-type zeolite (FAU) and its hexagonal analog (EMT) prepared by using crown-ethers as templates, Zeolites 12, 160-166.

Dudzik, Z. and Kowalak, S. (1974). Preparation of zeolites of faujasite type from kaolinite, Przemys´l Chemiczny 53, 616-618.

Dweck, J., Buchler, P., Coelho, A. and Cartledge, F. (2000). Hydration of a Portland cement blended with calcium carbonate, Thermochimica Acta 346, 105-113.

Dyer, A. and Zubair, M. (1998). Ion-exchange in chabazite, Microporous and Mesoporous Materials 22, 135-150.

Eken-Saraçoğlu, N. and Çulfaz, M. (1999). Clinoptilolite zeolite as a builder in nonphosphated detergents, Journal of Environmental Science and Health - Part A Toxic/Hazardous Substances and Environmental Engineering 34, 1619-1626.

Ellyett, C. and Fleming, A. (1974). Thermal infrared imagery of the burning mountain coal fire, Remote Sensing Environment 11, 221-229.

Engelhardt, G. and Michel, D. (1987). High-resolution solid-state NMR of silicates and zeolites, Wiley, London.

Engelhardt, G., Luger, S., Buhl, J.Ch. and Felsche, J. (1989). ^{29}Si MAS N.M.R. of aluminosilicate sodalites: Correlations between chemical shifts and structure parameters, Zeolites 9, 182-186.

Evangelou, V.P. and Zhang, Y.L. (1995). A review: Pyrite oxidation mechanisms and acid mine drainage prevention, Critical Reviews in Environmental Science and Technology 25, 141-199.

Faucon, P., Charpentier, T., Nonat, A. and Petit, J.C. (1998). Triple-quantum two dimensional ^{27}Al magic angle nuclear magnetic resonance study of aluminum incorporation in calcium silicate hydrates, Journal of the American Chemical Society 120, 75-82.

Feng, D., Aldrich, C. and Tan, H. (2000). Treatment of acid mine water by use of heavy metal precipitation and ion exchange, Minerals Engineering 13, 623–642.

Fernández-Jiménez, A. and Palomo, A. (2005). Composition and microstructure of alkali activated fly ash binder: Effect of the activator, Cement and Concrete Research 35, 1984-1992.

Fernández-Jiménez, A., Palomo, A., Criado, M. (2005). Microstructure development of alkali-activated fly ash cement: a descriptive model, Cement and Concrete Research 32, 1204-1209.

Fernández-Jiménez, A., Palomo, A., Sobrados, I. and J. Sanz. (2006). The role played by the reactive alumina content in the alkaline activation of fly ashes, Microporous and Mesoporous Materials 91, 111-119.

Fernández-Jiménez, A., Monzó, M., Vicent, M., Barba, A. and Palomo, A. (2008). Alkaline activation of metakaolin–fly ash mixtures: Obtain of Zeoceramics and Zeocements, Microporous and Mesoporous Materials 108, 41-49.

Ficklin, W.H., Plumlee, G.S., Smith, K.S. and McHugh, J.B. (1992). Geochemical classification of

mine drainages and natural drainages in mineralized areas. In: Y.K. Kharaka and A.S. Maest (Eds.), Proceedings of the 7th International Symposium on Water Rock Interaction, Park City, Utah, pp. 381-384.

Fisher, G.L., Chang, D.P.Y. and Brummer, M. (1976). Fly ash collected from electrostatic precipitators: Microcrystalline structures and the mystery of the spheres, Science 192, 553-555.

Flanigen, E.M. (1973). Review and new perspectives in zeolite crystallization. In Advances in Chemistry, Ser. 121, 119-139.

Flanigen, E.M., Bennett, J.M., Crose, R.W., Cohen, J.P., Patton, R.L., Kirchner, R.M. and Smith, J.V. (1978). Silicalite, a new hydrophobic crystalline silica molecular sieve, Nature 271, 512-516.

Flanigen. E.M., Lok. B.M., Patton, R.L. and Wilson, S.T. (1986). Aluminophosphate molecular sieves and the periodic table, Pure and Applied Chemistry 58, 1351-1358.

Foit Jr., F.F., Hooper, R.L. and Rosenberg, P.E. (1987). An unusual pyroxene, melilite, and iron oxide mineral assemblage in a coal-fire buchite from Buffalo, Wyoming, American Mineralogist 72, 137-147.

Fordham, C.J. and Smalley, I.J. (1985). A simple thermogravimetric study of hydrated cement, Cement and Concrete Research 15, 141-144.

Fredlund, D.E. (1976). Fort Union porcellanite and fused glass: Distinctive lithic materials of coal burn origin on the northern Great Plains, Plains Anthropologist 21, 207-211.

Freyhardt, C.C., Tsapatsis, M., Lobo, R.F., Balkus Jr, K.J. and Davis, M.E. (1996). A high-silica zeolite with a 14-tetrahedral-atom pore opening, Nature 331, 295-298.

Frías, M. and Cabrera, J. (2002). The effect of temperature on the hydration rate and stability of the hydration phases of metakaolin-lime-water systems, Cement and Concrete Research 32, 133-138.

Frost, R.L., Mako, E., Krsitof, J. and Kloprogge, J.T. (2002). Modification of kaolinite surfaces through mechanochemical treatment - a mid-IR and near-IR spectroscopic study, Spectrochimica Acta Part A: Molecular and Biomolecular Spectroscopy 58, 2849-2859.

Frost, R.L., Horváth, E., Makóc, E., Kristóf, J. and Rédey, A. (2003). Slow transformation of mechanically dehydroxylated kaolinite to kaolinite - an aged mechanochemically activated formamide - intercalated kaolinite study, Thermochimica Acta 408, 103-113.

Fyfe, C.A., Brouwer, D.H., Lewis, A.R. and Chézeau, J-M. (2001). Location of the fluoride ion in tetrapropylammonium fluoride silicalite-1 determined by $^{1}H/^{19}F/^{29}Si$ triple resonance CP, REDOR and TEDOR MAS NMR Experiments, Journal of the American Chemical Society 123, 6882-6891.

García, J.E., González, M.M. and Notario, J.S. (1993). Phenol adsorption on natural phillipsite, Reactive Polymers 21, 171-176.

Genç-Fuhrman, H., Mikkelsen, P.S. and Ledin, A. (2007). Simultaneous removal of As, Cd, Cr, Cu, Ni and Zn from stormwater: Experimental comparison of 11 different Sorbents, Water Research 41, 591-602.

Gerson, A.R. and Zheng, K. (1997). Bayer process plant scale: Transformation of sodalite to cancrinite, Journal of Crystal Growth 171, 209-218.

Gibert, O., de Pablo, J., Cortina, J.L. and Ayora, C. (2005a). Municipal compost-based mixture for acid mine drainage bioremediation: Metal retention mechanisms, Applied Geochemistry 20, 1648–1657.

Gibert, O., de Pablo, J., Cortina, J.L. and Ayora, C. (2005b). Sorption studies of Zn(II) and Cu(II) onto vegetal compost used on reactive mixtures for *in situ* treatment of acid mine drainage, Water Research 39, 2827–2838.

Gitari, M.W., Petrik, L.F., Etchebers, O., Key, D.L., Iwuoha, E.I. and Okujeni, C. (2006). Treatment of acid mine drainage with fly ash: Removal of major contaminants and trace elements, Journal of Environmental Science and Health. Part A, Toxic/Hazardous Substances and Environmental Engineering 41, 1729-1747.

Gitari, W.M., Somerset, V.S., Petrik, L.F., Key, D., Iwuoha, E. and Okujeni, C. (2003). Treatment of acid mine drainage with fly ash: Removal of major, minor elements, SO_4 and utilization of the solid residues for wastewater treatment. International Ash Utilization Symposium, Center for Applied Energy Research, University of Kentucky, pp. 1-23.

Gode, A. and Pehlivan, E. (2003). A comparative study of two chelating ion exchange resins for the removal of chromium (III) from aqueous solution, Journal of Hazardous Materials B100, 231-243.

Gomes, S. and François, M. (2000). Characterization of mullite in silicoaluminous fly ash by XRD, TEM, and ^{29}Si MAS NMR, Cement and Concrete Research 30, 175-181.

Gora, L., Strelertzky, K., Thompson, R.W. and Phillies, G.D.J. (1997). Study of the crystallization of zeolite NaA by quasi-elastic light-scattering spectroscopy and electron microscopy, Zeolites 18, 119-131.

Gottardi, G. and Galli, E. (1985). Natural Zeolites, Springer-Verlag, Berlin, 409pp.

Govind, N., Andzelm, J., Reindel, K. and Fitzgerald, G. (2002). Zeolite-catalyzed hydrocarbon formation from methanol: density functional simulations, International Journal of Molecular Sciences 3, 423-434

Green, M., Mels, A., Lahav, O. and Tarre, S. (1996). Biological ion exchange process for ammonium removal from secondary effluent, Water science and technology 34, 449-458.

Grim, R.E. (1968). Clay Mineralogy, 2nd Ed., McGraw-Hill, New York, 596pp.

Grose, R.W and Flanigen, E.M. (1977). U.S. Patent No. 4 061 724.

Gualtieri, A., Norby, P., Artioli, G. and Hanson, J. (1997a). Kinetic study of hydroxysodalite formation from natural kaolinites by time-resolved synchrotron powder diffraction, Microporous Materials 9, 189-201.

Gualtieri, A., Norby, P., Artioli, G. and Hanson, J. (1997b). Kinetics of formation of zeolite Na-A [LTA] from natural kaolinites, Journal Physics and Chemistry of Minerals 24, 191-199.

Gualtieri, M. (2006). Synthesis and characterization of zeolite films and membranes, Luleå University of Technology, PhD thesis, 95p.

Guo, J., Wang, F. and Wang, F. (1997). Kaolinite-mullite reaction series: A ^{27}Al and ^{29}Si MAS NMR study, Acta Mineralogica Sinica 17, 250-259.

Haden, W.L. and Dzierzanowski, F.J. (1972). U.S. Patent Nos. 3 391 994 (1968), 3 503 900

(1972) and 3 657 154 (1972).

Hansen, S. and Fälth, L. (1982). X-ray study of the nepheline hydrate I structure, Zeolites 2, 162-166.

Hamdan, H. (2003). Design and molecular engineering of nanostructured zeolites and mesomorphous materials: Advancing through the pores, Penerbit Universiti Teknologi Malaysia, 44pp.

Hamdan, H., Kim, A.B. and Muhid, M.N.M. (2001). 25-P-12-Catalytic activity of secondary aluminated mesoporous molecular sieve ALMCM-41 in the Friedel-Crafts reaction of bulky aromatic compounds, Studies in Surface Science and Catalysis 135, 282.

Hamilton, E, Coker, E.W., Sacco, A., Dixon, A.G. and Thompson, R.W. (1993). The effects of the silica source on the crystallization of zeolite NaX, Zeolites 13, 645-653.

Hartmann, A., Buhl, J.Ch. and van Breugel, K. (2007). Structure and phase investigations on crystallization of 11 Å tobermorite in lime sand pellets, Cement and Concrete Research 37, 21-31.

Hayashi, S., Ueda, T., Hayamizu, K. and Akiba, E. (1992). NMR study of kaolinite. 1. ^{29}Si, ^{27}Al, and ^{1}H spectra, Journal of physical chemistry 96, 10922-10928.

He, H., Guo, J., Zhua, J., Yuan, P. and Hu, Ch. (2004). ^{29}Si and ^{27}Al MAS NMR spectra of mullites from different kaolinites, Spectrochimica Acta Part A 60, 1061-1064.

Healey, A.M., Johnson, G.M. and Weller, M.T. (2000a). The synthesis and characterisation of JBW-type zeolites. Part A: Sodium/potassium aluminosilicate, $Na_2K[Al_3Si_3O_{12}].0.5H_2O$, Microporous and Mesoporous Materials 37, 153–163.

Healey, A.M., Henry, P.F., Johnson, G.M., Weller, M.T., Webster, M.A. and Genge J. (2000b). The synthesis and characterisation of JBW-type zeolites. Part B: Sodium/rubidium aluminogermanate, $Na_2Rb[Al_3Ge_3O_{12}]\cdot H_2O$, Microporous and Mesoporous Materials 37, 165-174.

Heffern, E. and Coates, D. (1997). Clinker - its occurrence, uses, and effects on coal mining in the Powder River Basin. In: Proceedings of the 32nd Annual Forum on the Geology of Industrial Minerals, R.W. Jones and R.E. Harris (Eds.), Wyoming State Geological

Survey Public Information Circular No. 38, 151-165.

Heffern, E.L. (2006). Modern and ancient coal bed fires in the Powder River Basin, National Association of Abandoned Mined Land Programs of the 28th Annual Conference, Billings, Montana, 25-27 September; 2006

Heffern, E.L., Coates, D. and Naeser, C. (1983). Distribution and age of clinker in northern Powder River Basin, Montana (Abstract), American Association of Petroleum Geologist Bulletin 67, 1342.

Helfferrich, F. (1962). Ion exchange: McGraw-Hill Series in Advanced Chemistry. New York: McGraw-Hill Book Company, Inc, 322pp.

Henao, J.A., Carreño, A.M., Ramos, M.A., Quintero, J.A., Candela, S.A. and Ríos, C.A. (2005). Caracterización mineralógica y análisis cuantitativo del clinker del Complejo Carbonífero El Cerrejón (Guajira) por difracción de rayos-X de muestras policristalinas. In: Proceedings of VII Congreso Venezolano de Química. Merida; 6–10 November, 2005.

Hendricks, N.R. (2005). The application of high capacity ion exchange adsorbent material, synthesized from fly ash and acid mine drainage, for the removal of heavy and trace metals from secondary co-disposed process waters. Unpublished Master's thesis. Cape Town: University of the Western Cape, 287p.

Henmi, T. (1987). Increase in cation exchange of fly ash by alkali treatment, Clay Science 6, 277-282.

Hequet, V., Ricou, P., Lecuyer, I. and LeCloirec, P. (2000). Removal of Cu^{2+} and Zn^{2+} from aqueous solutions by sorption onto mixed fly ash, Fuel 80, 851-856.

Hidalgo, A., Petit, S., Domingo, C., Alonso, C., Andrade, C. (2007). Microstructural characterization of leaching effects in cement pastes due to neutralisation of their alkaline nature. Part I: Portland cement pastes, Cement and Concrete Research 37, 63–70.

Hlavay, J., Vigh, G., Olaszi, V. and Inczédy, J. (1982). Investigations on natural Hungarian zeolite for ammonia removal, Water Research 16, 417-420.

Hoch, M. and Bandara, A. (2005). Determination of the adsorption process of tributyltin (TBT)

and monobutyltin (MBT) onto kaolinite surface using Fourier transform infrared (FTIR) spectroscopy, Colloids and Surfaces A: Physicochemical and Engineering Aspects 253, 117-124.

Hoffman, G.K. (1996). Natural clinker: The red dog of aggregates in the Southwest. In: Proceedings of the 31st Forum on the Geology of Industrial Minerals-Borderland Forum, G.S. Austin, et al. (Eds.), New Mexico Bureau of Geology and Mineral Resources Bulletin 154, 187-196.

Höller, H. and Barth-Wirsching, U. (1985). Zeolite formation from fly ash, Fortschritte Der Mineralogie 63, 21-43.

Hollman, G.G., Steenbruggen, G. and Janssen-Jurkovičová, M. (1999). A two-step process for the synthesis of zeolites from fly ash, Fuel 78, 1225-1230.

Howell, P.A and Acara, N.A. (1964). U.S. Patent No.3 119 660.

Huang, W.L. (1993). The formation of illitic clays from kaolinite in KOH solution from 225 ^{o}C to 350^{o}C, Clays and Clay Minerals 41, 645654.

Ibrahim, K.M. and Akashah, T. (2004). Lead removal from wastewater using faujasite tuff, Environmental Geology 46, 865-870.

Ikhsan, J.; Johnson, I.B.B. and Wells, J.D. (1999). A comparative study of the adsorption of transition metals on kaolinite, Journal of Colloid and Interface Science 217, 403-410.

Inada, M., Eguchi, Y. Enomoto, N. Hojo, J. (2005). Synthesis of zeolite from coal ashes with different silica–alumina composition, Fuel 84, 299-304.

Inglezakis, V.J., Hadjiandreou, K.J., Loizidou, M.D. and Grigoropolou, H.P. (2001). Pretreatment of natural clinoptilolite in a laboratory scale ion exchange packed bed, Water Research 35, 2161-2166.

Inglezakis, V.J. and Grigoropoulou, H.P. (2003). Modeling of ion exchange of Pb^{2+} in fixed beds of clinoptilolite, Microporous and Mesoporous Materials 61, 273-282.

Inglezakis, V.J., Zorpas, A.A., Loizidou, M.D. and Grigoropoulou, H.P. (2003). Simultaneous removal of metals Cu^{2+}, Fe^{3+} and Cr^{3+} with anions SO_4^{2-} and HPO_4^{2-} using clinoptilolite,

Microporous and Mesoporous Materials 61, 167-171.

International Zeolite Association http: //www.iza-online.org (updated 23-April-2007)

Jacobs, P.A. and Martens, J.A. (1987). Synthesis of high-silica aluminosilicate zeolites, Elsevier Science, New York, 390pp.

Jacobsen, H.S., Norby, P., Bildsøe, H. and Jakobsen, H.J. (1989). 1:1 Correlation between ^{27}Al and ^{29}Si chemical shifts and correlations with lattice structures for some aluminosilicate sodalites, Zeolites 9, 491-495.

Jansen, J.C. (1991). The preparation of molecular sieves. In: Introduction to Zeolite Science and Practice, H. van Bekkum, E.M. Flanigen and J.C. Jansen (Eds.), Elsevier, Amsterdam, p.754.

Jiugao, G., Fuya, W. and Fuya, W. (1997). Kaolinite-mullite reaction series: A ^{27}Al and ^{29}Si MAS NMR study, Acta Mineralogica Sinica 17, 250-259.

Johnson, D.B. and Hallberg, K.B. (2005a). Acid mine drainage remediation options: a review, Science of the Total Environment 338, 3–14.

Johnson, D.B. and Hallberg, K.B. (2005b). Biochemistry of the compost bioreactor components of a composite acid mine drainage passive remediation system, Science of the Total Environment 338, 81-93.

Jones, A.H., Geissman, J.W. and Coates, D.A. (1984). Clinker deposits, Powder River Basin, Wyoming and Montana: A new source of highfidelity paleomagnetic data for the Quaternary, Geophysical Research Letters 2, 1231-1234.

Jorgensen, T.C. and Weatherley, L.R. (2003). Ammonia removal from wastewaters by ion exchange in the presence of organic contaminants, Water Research 37, 1723-1728.

Juan, R., Hernández, S., Andrés, J.M. and Ruiz, C. (2007). Synthesis of granular zeolitic materials with high cation exchange capacity from agglomerated fly ash, Fuel 86, 1811-1821.

Kakali, G., Perraki, T., Tsivilis, S. and Badogiannis, E. (2001). Thermal treatment of kaolin: the effect of mineralogy on the pozzolanic activity, Applied Clay Science 20, 73-80.

Kalin, M., Fyson, A. and Wheeler, W.N. (2006). The chemistry of conventional and alternative treatment systems for the neutralization of acid mine drainage, Science of the Total Environment 366, 395-408.

Kang, Sh-J., Egashira, K. and Yoshida, A. (1998). Transformation of a low-grade Korean natural zeolite to high cation exchanger by hydrothermal reaction with or without fusion with sodium hydroxide, Applied Clay Science 13, 117-135.

Kato, Y., Kakimoto, K., Ogawa, H. and Tomari, M. (1986). Application of hydrothermally crystallized coal ash for waste water treatment II, Kogyo Yosui 338, 37-45.

Kempa, P.B., Engelhardt, G., Buhl, J.Ch., Felsche, J., Harvey, G. and Baerlocher, Ch. (1991). X-ray powder diffraction crystal structure analysis and ^{29}Si, ^{23}Na MAS N.M.R. studies of nitrite sodalite, $Na_8[AlSiO_4]_6(NO_2)_2$, at 295 K, Zeolites 11, 558-562.

Kesraoui-Ouki, S. and Kavanagh, M. (1997). Performance of natural zeolites for the treatment of mixed metal-contaminated effluents, Waste Management and Research 15, 383-394.

Kesraoui-Ouki, S., Cheeseman, C.R. and Perry, R. (1994). Natural zeolite utilization in pollution control: a review of applications to metals' effluents, Journal of chemical technology and biotechnology 59, 121-126.

Kitchener, J.A. (1957). Ion-exchange Resins. Great Britain: Butler and Tanner Ltd.

Klimesch, D.S. and Ray, A. (1998). DTA-TGA of unstirred autoclaved metakaolin–lime–quartz slurries, The formation of hydrogarnet, Thermochimica Acta 316, 149-154.

Klimkiewicz, R. and Drąg, E.B. (2004). Catalytic activity of carbonaceous deposits in zeolite from halloysite in alcohol conversions, Journal of Physics and Chemistry of Solids 65, 459–464.

Klinowski, J. (1984). Nuclear magnetic resonance studies of zeolites, Progress in Nuclear Magnetic Resonance Spectroscopy 16, 237–309.

Kolousek, D., Seidl, V., Prochazkova, E., Obsasnikova, J., Kubelkova, L. and Svetlik, L. (1993). Ecological utilization of power-plant fly ashes by their alteration to phillipsite: Hydrothermal alteration, application, Acta Universitatis Carolinae Geologica 37, 167-178.

Komarneni, S., Roy, R., Roy, D.M., Fyfe, C.A., Kennedy, G.J., Bothner-By, A.A., Dadok, J. and Chesnick, A.S. (1985). ^{27}Al and ^{29}Si magic angle spinning nuclear magnetic resonance spectroscopy of Al-substituted tobermorites, Journal of Materials Science 20, 4209–4214.

Kristof, J., Mink, J., Horvath, E. and Gabor, M. (1993). Intercalation study of clay minerals by Fourier transform infrared spectrometry, Vibrational Spectroscopy 5, 61-67.

Kühl, G.H. (1970). In: 2nd International Conference on Molecular Sieve Zeolite, E.M. Flanigen and L.B. Sand (Eds.), American Chemical Society, Washington, D.C., 59.

La Rosa, J.L., Kwan, S., Grutzeck, M.W. (1992). Zeolite formation in Class F fly ash blended cement pastes, Journal of the American Ceramic Society 75, 1574-1580.

Langella, A., Pansini, M., Cappelletti, P., De Gennaro, B., De Gennaro, M. and Colella, C. (2000). NH_4^+, Cu^{2+}, Zn^{2+}, Cd^{2+} and Pb^{2+} exchange for Na^+ in a sedimentary clinoptilolite, North Sardinia, Italy, Microporous and Mesoporous Materials 37, 337-343.

Lambert, J.F., Minman, W.S. and Fripiat, J.J. (1989). Revisiting kaolinite dehydroxylation: A silicon-29 and aluminum-27 MAS NMR study, Journal of the American Chemical Society 111, 3517-3522.

Lapides, I. and Heller-Kallai, L. (2007). Reactions of metakaolinite with NaOH and colloidal silica - Comparison of different samples (Part 2), Applied Clay Sciences 35, 94-98.

Larosa-Thompson, J.L. and Grutzeck, M.W. (1996). C-S-H, tobermorite and coexisting phases in the system CaO-Al_2O_3-SiO_2-H_2O, World Cement 1, 69–74.

Le Blanc, R.J. (1991). Prehistoric clinker use on the Cape Bathurst Peninsula, Northwest Territories, Canada: The dynamics of formation and procurement, American Antiquity 56, 268-277.

Le Saoût, G., Lécolier, E., Rivereau, A. and Zanni, H. (2006). Chemical structure of cement aged at normal and elevated temperatures and pressures, Part II: Low permeability class G oilwell cement, Cement and Concrete Research 36, 428-433.

Lee, S., Kim, Y-J. and Moon, H-S. (2003). Energy-filtering electron microscopy (EF-TEM) study of a modulated structure in metakaolinite represented by a 14 modulation, Journal of the

American Ceramic Society 86, 174–176.

Lei, L., Li, X. and Zhang, X. (2008). Ammonium removal from aqueous solutions using microwave-treated natural Chinese zeolite, Separation and Purification Technology 58, 359-366.

Lenoble, V., Laclautre, Ch., Deluchat, V., Serpaud, B. and Bollinger, J-C. (2005). Arsenic removal by adsorption on iron(III) phosphate, Journal of Hazardous Materials 123, Pages 262-268.

Letaief, S., Elbokl, T.A. and Detellier, Ch. (2006). Reactivity of ionic liquids with kaolinite: Melt intersalation of ethyl pyridinium chloride in an urea-kaolinite pre-intercalate, Journal of Colloid and Interface Science 302, 254–258.

Li, Z., Burt, T. and Bowman, R.S. (2000). Sorption of ionizable organic solutes by surfactant-modified zeolite, Environmental Science and Technology 34, 3756-3760.

Li, L., Wang, S. and Zhu Z. (2006). Geopolymeric adsorbents from fly ash for dye removal from aqueous solution, Journal of Colloid and Interface Science 300, 52-59.

Lide, D.R. (2008). CRC Handbook of Chemistry and Physics, 89th Edition, CRC Press, 2688pp.

Lin, C.-F. and Hsi, H.-C. (1995). Resource recovery of waste fly ash: Synthesis of zeolite-like materials. Environmental Science and Technology 29, 1109-1117.

Lin, C.H., Wang, S.L. and Lii, K.H. (2001). $[Ga_2(DETA)(PO_4)_2]\cdot 2H_2O$ (DETA = Diethylenetriamine): A novel porous gallium phosphate containing 24-ring channels, Journal of the American Chemical Society 123, 4649-4650.

Lin, D.-Ch., Xu, X.-W., Zuo, F. Zuo and Long, Y.-C. (2004). Crystallization of JBW, CAN, SOD and ABW type zeolite from transformation of meta-kaolin, Microporous and Mesoporous Materials 70, 63-70.

Lindqvist, J., Hatherton, T. and Mumme, T. (1985). Magnetic anomalies resulting from baked sediments over burnt coal seams in southern New Zealand, Journal of Geology and Geophysics 28, 405-412.

Liu, Q., Spears, D.A. and Liu, Q. (2001). MAS NMR study of surface-modified calcined kaolin,

Applied Clay Science 19, 89-94.

Liu, X., Yan, Z., Wang, H. and Luo, Y. (2003). *In-situ* synthesis of NaY zeolite with coal-based kaolin, Journal of Natural Gas Chemistry 12, 63-70

Llenado, R.A. (1983). The use of sodium A zeolite in detergents. D. Olson and A. Bisio (Eds.), Proceedings of the 6th International Zeolite Conference, 940-956.

Lobo, R.F., Zones, S.I. and Davis, M.E. (1995). Structure-direction in zeolite synthesis, Journal of Inclusion Phenomena and Molecular Recognition in Chemistry 21, 47-78.

Loizidou, M., Haralambous, K., Loukatos, A. and Dimitrakopolou, D. (1992). Natural zeolites and their ion exchanger behavior towards chromium, Journal of Environment Science and Health, Part A Environmental Science 27, 1759-1769.

Lombi, E., Wenzel, W.W. and Sletten, R.S. (1999). Arsenic adsorption by soils and iron-oxide-coated sand: kinetics and reversibility, Journal of Plant Nutrition and Soil Science 162, 451–456.

Lussier, R. (1991). A novel clay-based catalytic material-preparation and properties, Journal of Catalysis 129, 225-237.

Lyman, R. and Volkmer, J. (2001). Pyrophoricity (spontaneous combustion) of Powder River Basin coals -considerations for coalbed methane development. Coal Report CR01-1, Wyoming State Geological Survey, Laramie, Wyoming, p. 12.

Mackenzie, K.J.D., Brown, I.W.M., Meinhold, R.H. and Bowden, M.E. (1985). Outstanding problems in the kaolinite-mullite reaction sequence investigated by ^{29}Si and ^{27}Al Solid-State Nuclear Magnetic Resonance: I. Metakaolinite, Journal of the American Ceramic Society 68, 293-297.

Mackenzie, R.C. (1970). Differential Thermal Analysis 1, Academic Press, London, 504-514.

Mackinnon, I., Millar, G. and Stolz, W. (2006). U.S. Patent No. 0 269 472.

Madani, A., Aznar, A., Sanza, J. and Serratosa, J.M. (1990). Si and Al MAS NMR study of zeolite formation from alkali-leached kaolinites. Influence of thermal activation, Journal of Physical Chemistry 94, 760-765.

Marañón, E., Ulmanu, M., Fernández, Y., Anger, I. and Castrillón, L. (2006). Removal of ammonium from aqueous solutions with volcanic tuff, Journal of Hazardous Materials 137, 1402-1409.

Marinin, D.V. and Brown, G.N. (2000). Studies of sorbent/ion-exchange materials for the removal of radioactive strontium from liquid radioactive waste and high hardness groundwaters, Waste Management 20, 545-553.

Maroto-Valer, M.M., Taulbee, D.N. and Hower, J.C. (1999). Novel separation of the differing forms of unburned carbon present in fly ash using density gradient centrifugation, Energy Fuels 13, 947–953.

Maruyama, N., Yamamoto, H. and Shibata, J. (2002). Mechanism of zeolite synthesis from fly ash by alkali hydrothermal reaction, International Journal of Mineral Processing 64, 1-17.

Mashal, K.Y., Harsh, J.B., Flury, M., Felmy, A.R. and Zhao, H. (2004). Colloid formation in Hanford sediments reacted with simulated tank waste, Environmental Science and Technology 38, 5750-5756.

Mashal, K.Y., Harsh, J.B., Flury, M. and Felmy, A.R. (2005). Analysis of precipitates from reactions of hyperalkaline solutions with soluble silica, Applied Geochemistry 20, 1357-1367.

McCusker, L.B. and Baerlocher, C. (2001). Zeolite structures. In: Introduction to zeolite science and practice, Van Bekkum, H., Flanigen, E.M., Jacobs, P.A. and Jansen, J.C. (Eds.), Studies in Surface Science and Catalysis 137, Elsevier, 37-65.

Meier, W.M. (1968). Zeolite structures. In: Molecular Sieves, Society of Chemical Industry, London, 10-27.

Meier, W.M., Olson, D.H. and Baerlocher, Ch. (1996). Atlas of zeolite structure types, 4th Ed., Elsevier, London, 230pp.

Meininghaus, C.K.W. and Prins, R. (2000). Sorption of volatile organic compounds on hydrophobic zeolites, Microporous and Mesoporous Materials 35-36, 349-365.

Meng, X., Korfiatis, G.P., Bang, S. and Bang, K.W.(2002). Combined effects of anions on arsenic removal by iron hydroxides, Toxicology Letters 133, 103-111.

Meor Yusoff, M.S., Masilana, M., Choo, T.F. and Julie, A.M. (2007). Production of high purity alumina and zeolite from low-grade kaolin, Advances in Materials Research 29-30, 187-190.

Mercer, B.W., Ames, L.L., Touhill, C.J., Van Slyke, W.J. and Dean, R.B. (1970). Ammonia removal from secondary effluents by selective ion exchange, Jouranl of the Water Pollution Control Federation. 42, 95–107.

Merwin, L.H., Sebald, A., Rager, H. and Schneider, H. (1991). ^{29}Si and ^{27}Al MAS NMR study of mullite, Physics and Chemistry of Minerals 18, 47-52.

Misak, N.Z. (2000). Some aspects of the application of adsorption isotherms to ion exchange reactions, Journal of Reactive and Functional Polymers 43, 153-164.

Mohan, D. and Chander, S. (2001). Single component and multi-component adsorption of metal ions by activated carbons, Colloids and Surfaces A 177, 183-196.

Mohan, D. and Chander, S. (2006). Removal and recovery of metal ions from acid mine drainage using lignite - A low cost sorbent, Journal of Hazardous Materials B137, 1545–1553.

Molina, A. and Poole, C. (2004). A comparative study using two methods to produce zeolites from fly ash, Minerals Engineering 17, 167-173.

Mon, J., Deng, Y., Flury, M. and Harsh, J.B. (2005). Cesium incorporation and diffusion in cancrinite, sodalite, zeolite,and allophone, Microporous and Mesoporous Materials 86, 277-286.

Mondale, K.D., Carland, R.M. and Aplan, F.F. (1995). The comparative ion exchange capacities of natural sedimentary and synthetic zeolites, Minerals Engineering 8, 535-548.

Mondragón, F., Rincón, F., Sierra, L., Escobar, J., Ramírez, J. and Fernández, J. (1990). New perspectives for coal ash utilization: Synthesis of zeolitic materials, Fuel 69, 263-266.

Moreno, N., Querol, X., Andrés, J.M., López-Soler, A., Janssen-Jurkovičová, M., Nugteren, H., Towler, M. Stanton, K. (2004). Determining suitability of a fly ash for silica extraction and zeolite synthesis, Journal of Chemical Technology and Biotechnology 79, 1009-1018.

Moreno, N., Querol, X., Andrés, J.M., Stanton, K., Towler, M., Janssen, M., Nugteren, H. and Jones, R. (2005). Physico-chemical characteristics of European pulverized coal combustion fly ashes, Fuel 84 1351-1363.

Moreno, N., Querol, X., Ayora, C., Pereira, C.F. and Janssen-Jurkovičová, M. (2001a). Utilization of zeolites synthesized from fly ash for the purification of acid mine waters, Environmental Sciences and Technology 35, 3526–3534.

Moreno, N., Querol, X., Ayora, C., Alastuey, A., Fernández-Pereira, C. and Janssen-Jurkovičová, M. (2001b). Potential environmental applications of pure zeolitic material synthesized from fly ash, Journal of Environment Engineering 127, 994-1002.

Moreno, N., Querol, X., Lopez-Soler, A., Andres, J.M., Janssen-Jurkovičová, M., Nugteren, H.W., Towler, M. and Stanton, K. (2004). Determining suitability of a fly ash for silica extraction and zeolite synthesis, Journal of Chemical Technology and Biotechnology 79, 1009-1018.

Moreno, N., Querol, X., Plana, F., Andres, J.M., Janssen, M. and Nugteren, H.W. (2002). Pure zeolite synthesis from silica extracted from fly ashes, Journal of Chemical Technology and Biotechnology 77, 274-279.

Mouhtaris, Th., Charistos, D., Kantiranis, N., Filippidis, A., Kassoli-Fournaraki, A. and Tsirambidis, A. (2003). GIS-type zeolite synthesis from Greek lignite sulphocalcic fly ash promoted by NaOH solutions, Microporous and Mesoporous Materials 61, 57-67.

Mundus, C., Mueller-Warmuth, W. and Buhl, J.Ch. (1996). Crystallisation of a basic sodalite under hydrothermal conditions studied by MAS-NMR, XRD and DTA/DTG, European Journal of Mineralogy 8, 231-239.

Murat, M., Amorkrane, A., Bastide, J.P. and Montanaro, L. (1992). Synthesis of zeolites from thermally activated kaolinite. Some observations on nucleation and growth, Clay Minerals 27, 119-130.

Ojha, K., Pradhan, N.C. and Samanta, A.N. (2004). Zeolite from fly ash: Synthesis and characterization, Bulletin of Material Science 27, 555-564.

Okada, Y., Sasaki, K., Zhong, B., Ishida, H. and Mitsuda, T. (1994). Formation processes of β-

C_2S by the decomposition of hydrothermally prepared C-S-H with $Ca(OH)_2$, Journal of the American Ceramic Society 77, 1319-1324.

Ollitrault-Fichet, R., Gauthier, C. Clamen, G. and Boch, P. (1998). Microstructural aspects in a polymer-modified cement, Cement and Concrete Research 28, 1687-1693.

Palomo, A., Alonso, S. Fernández-Jiménez, A., Sobrados, I. and Sanz, J. (2004). Alkaline activation of fly ashes. A ^{29}Si MAS NMR study of the reaction products, Journal of the American Ceramic Society 87, 1141-1145.

Panayotova, M.I. (2001). Kinetics and thermodynamics of copper ions removal from wastewater by use of zeolite, Waste Management 21, 671-676.

Panday, K.K., Parsed, G. and Singh, V.N. (1985). Copper (II) removal from aqueous solutions by fly ash, Water Research 19, 869-873.

Pansini, M. and Colella, C. (1991). Optimization of the process of Cr^{3+} removal from wastewaters by direct addition of natural zeolites. Proc. I Convegno Naz. di Scienza e Tecnologia delle zeoliti, C. Colella (Eds.), p 131-137. Napoles.

Park, M. and Choi, J. (1995). Synthesis of phillipsite from fly ash, Clay Science 9, 219-229.

Park, M., Choi, C.L., Lim, W.T., Kim, M.C., Choi, J. and Heo, N.H. (2000a). Molten-salt method for the synthesis of zeolitic materials: I. Zeolite formation in alkaline molten-salt system, Microporous and Mesoporous Materials 37, 81-89.

Park, M., Choi, C.L., Lim, W.T., Kim, M.C., Choi, J. and Heo, N.H. (2000b). Molten-salt method for the synthesis of zeolitic materials: II. Characterization of zeolitic maerials, Microporous and Mesoporous Materials 37, 91-98.

Pérez-López, R., Nieto, J.M. and Ruiz de Almodóvar, G. (2007a). Utilization of fly ash to improve the quality of the acid mine drainage generated by oxidation of a sulphide-rich mining waste: Column experiments, Chemosphere 67, 1637-1646.

Pérez-López, R., Cama, J., Nieto, J.M. and Ayora, C. (2007b). The iron-coating role on the oxidation kinetics of a pyritic sludge doped with fly ash, Geochimica et Cosmochimica Acta 71, 1921-1934.

Peric, J., Trigo, M. and Medvidović, N.V. (2004). Removal of zinc, copper and lead by natural zeolite – a comparison of adsorption isotherms, Journal of Water Research 38, 1893-1899.

Perissinotto, M., Storaro, L., Lenarda, M. and Ganzerla, R.J. (1997) Solid acid catalysts from clays: Acid leached metakaolin as isopropanol, Journal of Molecular Catalysis A: Chemical 121, 103-109.

Petrik, L.F., White, R.A., Klink, M.J., Somerset, V.S., Burgers, C.L. and Fey, M.V. (2003). Utilization of South African fly ash to treat acid coal mine drainage, and production of high quality zeolites from the residual solids. International Ash Utilization Symposium, Center for Applied Energy Research, University of Kentucky, 1-26.

Pitcher, S.K., Slade, R.C.T. and Wards, N.I. (2004). Heavy metal removal from motorway stormwater using zeolites, Science of the Total Environment 334-335, 161-166.

Plumlee, G.S., Smith, K.S., Mosier, E.L., Ficklin, W.H., Montour, M.R., Briggs, P. and Meier, A. (1995). Geochemical processes controlling acid-drainage generation and cyanide degradation at Summitville. In: H.H. Posey, J.A. Pendleton and D.J.A. van Zyl (Eds.), Proceedings of the Summitville Forum'95, Colorado Geol. Surv. Spec. Pub. 38, Colorado, 23–34.

Porcher, F., Dusausoy, Y., Souhassou, M. and Lecomte, C. (2000). Epitaxial growth of zeolite X on zeolite A and twinning in zeolite A: Structural and topological analysis, Mineralogical Magazine 64, 1-8.

Prakash, A., Gupta, R. and Saraf, A. (1997). A Landsat TM based comparative study of surface and subsurface fires in the Jharia coalfield, India, International Journal of Remote Sensing 18, 2463-2469.

Pushnyakova, V.A., Kotsupalo, N.P. and Berger, A.S. (1975). Journal of Applied Chemistry USSR 48, 1497.

Qafoku, N.P., Ainsworth, C.C., Szecsody, J.E., Bish, D.L., Young, J.S., McCready, D.E. and Qafoku, O.S. (2003). Aluminum effect on dissolution and precipitation under hyperalkaline conditions: II. Solid phase transformations, Journal of Environmental Quality 32, 2364–2372.

Qiu, G., Jiang, T., Li, G., Fan, X. and Huang, Z. (2004). Activation and removal of silicon in kaolinite by thermochemical process, Scandinavian Journal of Metallurgy 33, 121-128.

Querol, X., Plana, F., Alastuey, A., Fernández-Turiel, J.L. and Lopez-Soler, A. (1995). Synthesis of industrial minerals from fly ash, Coal Science Series 24, 1979-1982.

Querol, X., Plana, F., Alastuey, A. and Lopez-Soler, A. (1997a). Synthesis of Na-zeolites from fly ash, Fuel 76, 793-799.

Querol, X., Plana, F., Alastuey, A., Lopez-Soler, A., Andres, J.M., Juan, R., Ferrer, P., Ruiz, C.R. (1997b). A fast method of recycling fly ash: Microwave assisted zeolite synthesis, Environmental Sciences and Technology 31, 2527-2532.

Querol, X., Plana, F., Umaña, J., Alastuey, A., Andres, J.M., Juan, R. and Lopez-Soler, A. (1999). Industrial applications of coal combustion wastes: Zeolite synthesis and ceramic utilization, European Coal and Steel Community Contract 7220/ED/079. Final Report, 176pp.

Querol, X., Umaña, J.C., Plana, F., Alastuey, A., Lopez-Soler, A., Medinaceli, A., Valero, A., Domingo, M.J. and Gracia-Rojo, E. (2001). Synthesis of Na zeolites from fly ash in a pilot plant scale: Examples of potential environmental applications, Fuel 80, 857-865.

Querol, X., Moreno, N., Umaña, J.C., Alastuey, A., Hernández, E., López-Soler A. (2002a). Synthesis of zeolites from fly ash: An overview, International Journal of Mineral Processing 50, 413-423.

Querol, X., Moreno, N., Umaña, J.C., Juan, R., Hernández, S., Fernández-Pereira, C. Ayora, C., Janssen-Jurkovičová, M., García-Martínez, J., Linares-Solano, A. and Cazorla-Amoros, D. (2002b). Application of zeolitic material synthesized from fly ash to the decontamination of waste water and flue gas, Journal of Chemical Technology and Biotechnology 77, 292-298.

Querol, X., Alastuey, A., Moreno, N., Alvarez-Ayuso, E., García-Sánchez, A., Cama, J., Ayora , C. and Simón, M. (2006). Immobilization of heavy metals in polluted soils by the addition of zeolitic material synthesized from fly ash, Chemosphere 62, 171-180.

Râdan, S. and Râdan, M. (1998). Rock magnetism and paleomagnetism of porcelanites/clinkers

from the western Dacic Basin (Romania), Geologica Carpathica 49, 209-211.

Raghavendra, S.C., Khasim, S., Revanasiddappa, M., Ambika Prasad, M.V.N. and Kulkarni, A.B. (2003). Synthesis, characterization and low frequency a.c. conduction of polyaniline/ fly ash composites, Bulletin of Material Science 26, 733-739.

Rayalu, S., Meshram, S.U. and Hasan, M.Z. (2000). Highly crystalline faujasitic zeolites from fly ash, Journal of Hazardous Materials 77, 123-131.

Rayalu, S., Udhoji, J.S., Munshi, K.N and Hasan, M.Z. (2001). Highly crystalline zeolite-A from fly ash of bituminous and lignite coal combustion, Journal of Hazardous Materials 88, 107-121.

Rees, L.V.C. and Chandrasekhar, S. (1993). Hydrothermal reaction of kaolinite in presence of fluoride ions at pH less than 10, Zeolites 13, 534-541.

Rege, S.U. and Yang, R.T. (1997). Limits for air separation by adsorption with LiX zeolite, Industrial and Engineering Chemistry Research 36, 5358-5365.

Ríos, C.A. and Williams, C.D. (2008). Synthesis of zeolitic materials from natural clinker: A new alternative for recycling coal combustion by-products, Fuel 87, 2482-2492.

Ríos, C.A., Williams, C.D. and Castellanos, O.M. (2006). Synthesis and characterization of zeolites by activation of kaolinite and industrial by-products (fly ash and natural clinker) in alkaline solutions, Bistua 4, 60-71.

Ríos C.A., Williams, C.D. and Maple, M.J. (2007). Synthesis of zeolites and zeotypes by hydrothermal transformation of kaolinite and metakaolinite, Bistua 5, 15-26.

Ríos, C.A., Williams, C.D. and Roberts, C.L. (2008a). Removal of heavy metals from acid mine drainage (AMD) using fly ash, natural clinker and synthetic zeolites, Journal of Hazardous Materials 156, 23-35.

Ríos, C.A., Williams, C.D. and Fullen, M.A. (2008b). Nucleation and growth history of zeolite LTA synthesized from kaolinite by two different methods, Applied Clay Science, doi:10.1016/j.clay.2008.05.006

Rivas, J.M., Pena, P., De Aza, A.H., Turrillas, X., Sobrados, J. and Sanz, I. (2007). Solid-state

^{27}Al and ^{29}Si NMR investigations on Si-substituted hydrogarnets, Acta Materialia 55, 1183-1191.

Rocha, R. (1999). Single- and triple-quantum ^{27}Al MAS NMR study of the thermal transformation of kaolinite, Journal of Physics and Chemistry B 103, 9801-9804.

Rocha, J. and Klinowski, J. (1990). ^{29}Si and ^{27}Al magic-angle-spinning MAS NMR studies of the thermal transformation of kaolinite, Journal Physics and Chemistry of Minerals 17, 179-186.

Rocha, J., Klinowski J. and Adams, J.M. (1991). Synthesis of zeolite Na-A from metakaolinite revisited, Journal of the Chemical Society, Faraday Transactions 87, 3091-3097.

Roy, W.R. and Griffin, R.A. (1982). A proposed classification system for fly ash in multidisciplinary research, Journal of Environment Quality 11, 563-568.

Rozic, M., Cerjan-Stefanovic, S., Kurajica, S., Vancina, V. and Hodzic, E. (2000). Ammoniacal nitrogen removal from water by treatment with clays and zeolites, Water Research 34, 3675-3681.

Ruiz, R., Blanco, C., Pesquera, C., Gonzalez, F., Benito, I. and Lopez, J.L. (1997). Zeolitization of a bentonite and its application to the removal of ammonium ion from waste water, Applied Clay Science 12, 73-83.

Russell, J.D. and Fraser, A.R. (1994). Infrared methods. Chapter (2), In Clay Mineralogy: Spectroscopic and Chemical Determinative Methods, M.J. Wilson (Eds.), Chapman and Hall, London, Congress Catalogue card no. 93-74207, pp: 11-67.

Saikia, N.J., Bharali, D.J., Sengupta, P., Bordoloi, D., Goswamee, R.L., Saikia, P.C. and Bothakur, P.C. (2003). Characterization, beneficiation and utilization of a kaolinite clay from Assam, India, Applied Clay Science 24, 93–103.

Saltalı, K., Sarı, A. and Aydın, M. (2007). Removal of ammonium ion from aqueous solution by natural Turkish (Yıldızeli) zeolite for environmental quality, Journal of Hazardous Materials 141, 258-263.

Sand, L.B. (1980). Zeolite synthesis and crystallization, Pure and Applied Chemistry 52, 2105-2113.

Sanhueza, V., Kelm, U. and Cid, R. (1999). Synthesis of molecular sieves from Chilean kaolinites: 1. Synthesis of NaA type zeolites, Journal of Chemical Technology and Biotechnology 74, 358-363.

Santos, S., Machado, R. and Correia, M.J.N. (2004). Treatment of acid mining waters, Minerals Engineering 17, 225–232.

Schüth, Ch., Kummer, N-A., Weidenthaler, C. and Schad, H. (2004). Field application of a tailored catalyst for hydrodechlorinating chlorinated hydrocarbon contaminants in groundwater, Applied Catalysis B: Environmental 52, 197-203.

Seal, R.R., II, Foley, N.K. and Wanty, R.B. (2002). Introduction to geoenvironmental models of mineral deposits. In: R.R. Seal II and N.K. Foley (Eds.), Progress on Geoenvironmental Models for Selected Mineral Deposit Types, US Geol. Surv. Open File Rep. 02-195, pp. 1-7.

Semosa, L.J., Glasser, D. and Hildebradt, D. (2002). Industrial wastewater treatment using South African natural zeolite, Clinoptilolite. WISA. Durban, 19-23 May.

Shantz, D.F., Burton, A. and Lobo, R.F. (1999). Synthesis, structure solution, and characterization of the aluminosilicate MCM-61: the first aluminosilicate clathrate with 18-membered rings, Microporous and Mesoporous Materials 31, 61-73.

Sherman, J.D. (1999). Synthetic zeolites and other microporous oxide molecular sieves. Proceedings of the National Academy of Sciences of the United States of America 96, 3471-3478.

Shigemoto, M., Hayashi, H., Miyaura, K. (1993). Selective formation of Na-X zeolite from fly ash by fusion with sodium hydroxide prior to hydrothermal reaction, Journal of Materials Science 28, 4781-4786.

Shigemoto, N., Shirakami, S., Hirano, S., Hayashi, H. (1992). Preparation and characterisation of zeolites from coal ash, Nippon Kagaku Kaishi 5, 484-492.

Shigemoto, N., Sugiyama, S., Hayashi, H., Miyaura, K. (1995). Characterization of Na-X, Na-A, and fly ash zeolites and their amorphous precursors by IR, MAS NMR and XPS, Journal of Materials Science 30, 5777-5783.

Shih, W.H., Chang, H.L. (1996). Conversion of fly ash into zeolites for ion-exchange application, Materials Letters 28, 263-268.

Shih, W.H., Chang, H.L. and Shen, Z. (1995). Conversion of class-F fly ash to zeolites, Materials Research Society Symposium Proceedings 371, 39-44.

Siauciunas, R. and Baltusnikas, A. (2003). Influence of SiO_2 modification on hydrogarnet formation during hydrothermal synthesis, Cement and Concrete Research 33, 1789-1793.

Singer, A. and Berkgaut, V. (1995). Cation exchange properties of hydrothermally treated fly ash, Environmental Sciences and Technology 29, 1748-1753.

Singh, D.N. and Kolay, P.K. (2002). Simulation of ash–water interaction and its influence on ash characteristics, Progress in Energy and Combustion Science 28, 267-299.

Singh, G. and Prasad, B. (1997). Removal of ammonia from coke-plant wastewater by using synthetic zeolite, Water environment research 69, 157-161.

Sinha, P.K., Paniker, P.K. and Amalraj, R.V. (1995). Treatment of radioactive liquid waste containing caesium by indigenously available synthetic zeolites: A comparative study, Waste Management 15, 149-157.

Šiška, J. (2005). Extraction of heavy metals and ammonium from waters by unsaturated fatty acids and their soaps, Hydrometallurgy 76, 155-172.

Sitarz, M., Mozgawa, W., Handke, M. (1999). Rings in the structure of silicate glasses, Journal of Molecular Structure 281, 511-512.

Smith, J.V. and Blackwell, C.S. (1983). Nuclear magnetic resonance of silica polymorphs, Nature 303, 223-225.

Smith, T.R., Wilson, T.P. and Ineman, F.N. (1991). The relationship of iron bacteria geochemistry to trace metal distribution in an acid mine drainage system, NE Ohio, Geol. Soc. Am. Abstracts with Programs 23, p. 61.

Snoeyink, V.L. and Jenkis, D. (1980). Water Chemistry, John Wiley and Sons, Inc., New York.

Somerset, V.S., Petrik, L.F. and Iwuoha E.I. (2005a). Alkaline hydrothermal conversion of fly ash filtrates into zeolites 2: Utilization in wastewater treatment, Journal of Environmental Science and Health. Part A, Toxic/Hazardous Substances and Environmental Engineering 40, 1627-1636.

Somerset, V.S., Petrik, L.F., Klink, M.J., Etchebers, O., White, R.A., Key, D. and Iwuoha, E.I. (2005b). Acid mine drainage transformation of fly ash into zeolitic crystalline phases, Fresenius Environmental Bulletin 14, 1074-1076.

Somerset, V.S., Petrik, White, R.A., Klink, M.J., Key, D. and Iwuoha, E.I. (2005c). Alkaline hydrothermal zeolites synthesized from high SiO_2 and Al_2O_3 co-disposal fly ash filtrates, Fuel 84, 2324-2329.

Stathi, P., Litina, K., Gournis, D., Giannopoulos, T.S. and Deligiannakis, Y. (2007). Physicochemical study of novel organoclays as heavy metal ion adsorbents for environmental remediation, Journal of Colloid and Interface Science 316, 298-309.

Steveson, M. and Sagoe-Crentsil, K. (2005). Relationships between composition, structure and strength of inorganic polymers. Part 2 Fly ash-derived inorganic polymers, Journal of Materials Science 40, 4247-4259.

Stumm, W. and Lee, G.F. (1961). Oxygenation of ferrous iron, Industrial and Engineering Chemistry 53, 143-146.

Sulikowski, B., Rakoczy, J., Hamdan, H. and Klinowski, J. (1987). Structural and catalytic consequences of isomorphous substitution of silicon by aluminium and vice versa in the framework of pentasil zeolite, Journal of the Chemical Society, Chemical Communications 1542-1543.

Suraj, G., Lyer, G.S.P., Rugmini, S. and Llalithambika, M. (1997). The effect of micronization on kaolinites and their sorption behavior, Applied Clay Sciences 12, 111-130.

Swanepoel, J.C. and Strydom, C.A. (2002). Utilisation of fly ash in a geopolymeric material, Applied Geochemistry 17, 1143-1148.

Szoztak, R. (1998). Molecular sieves, Blackie Academic and Professional, London, 359pp.

Taylor, H.F.W. (1990). Cement Chemistry, Academic Press Ltd, London.

Taylor, H.F.W. (1992). Tobermorite, jennite and cement gel, Zeitschrift für Kristallograhie 202 (1992) 41-50.

Taylor, H.F.W. (1997). Cement Chemistry, 2nd ed., Thomas Telford Publishing, London.

Thompson, J.G. and Barron, P.F. (1987). Further consideration of the 29Si nuclear magnetic resonance spectrum of kaolinite, Clays and Clay Minerals 35, 38–42.

Tisivilis, S., Kakali, G., Chaniotakis, E. and Souravidou, A. (1998). A study on the hydration of Portland limestone cement by means of TG, Journal of Thermal Analysis 52, 863-870.

Traa, Y. and Thompson, R.W. (2002). Controlled co-crystallization of zeolites A and X, Journal of Materials Chemistry 12, 496-499.

U.S. Geological Survey and U.S. Bureau of Mines (1975). Status of mineral resource information for the Northern Cheyenne Indian Reservation, Montana. Administrative Report BIA-3, 60pp.

Uhlmann, W., Buttcher, H., Totsche, O. and Steinberg, C.E.W. (2004). Buffering of acidic mine lakes: The relevance of surface exchange and solid bound sulphate, Mine Water and the Environment 23, 20-27.

U.S. EPA (2001). National Primary Drinking Water Regulations: Arsenic and clarifications to compliance and new source contaminants monitoring - Final Rule. 40 CFR Parts 9, 141 and 142. U.S. Environmental Protection Agency, January 22.

Vaca, M., López, R., Gehr, R., Jiménez, B.E. and Alvarez, P.J.J. (2001). Heavy metal removal with mexican clinoptilolite: multi-component ionic exchange, Water Research 35, 373-378.

Valcke, E., Engels, B. and Cremers, A. (1997). The use of zeolites as amendments in radiocaesium- and radiostrontium-contaminated soils: A soil-chemical approach. Part II: Sr-Ca exchange in clinoptilolite, mordenite and zeolite A, Zeolites 18, 212-217.

Van der Marel, H.W. and Beutelspacher, H. (1976). Atlas of Infrared Spectroscopy of Clay Minerals and Their Admixtures, 1st Ed., Elsevier, Amsterdam, 396pp.

Van Jaarsveld, J.G.S., Van Deventer, J.S.J. and Lukey, G.C. (2003). The characterisation of

source materials in fly ash-based geopolymers, Materials Letters 57, 1272-1280.

Van Jaarsveld, J.G.S., Van Deventer, J.S.J. and Lorenzen, L. (1997). The potential use of geopolymeric materials to immobilise toxic metals: Part I. Theory and applications, Minerals Engineering 10, 659-669.

Vassilev, S.V. and Vassileva, C.G. (2007). A new approach for the classification of fly ashes based on their origin, composition, properties, and behaviour, Fuel 86, 1490-1512.

Wattena, B.J., Sibrella, P.L. and Schwartzb, M.F. (2005). Acid neutralization within limestone sand reactors receiving coal mine drainage, Environmental Pollution 137, 295-304.

Webster, J.G., Swedlund, P.J. and Webster, K.S. (1998). Trace metal adsorption onto an acid mine drainage iron (III) oxy hydroxy sulphate, Environmental Science and Technology 32, 1361-1368.

Wei, X., Viadero Jr., R.C. and Buzby, K.M. (2005). Recovery of iron and aluminium from acid mine drainage by selective precipitation, Environmental Engineering Science 22, 745–755.

Wei, B., Wang, Y., Xin, M.-H., Qiu, S.-L. (2007). Phenol solvothermal synthesis of JBW-type zeolites, Chemical Research in Chinese Universities 23, 511-513.

Weller, M.T. and Wong, G. (1988). New limits of silicon-29 solid-state N.M.R. chemical shifts, Journal of the Chemical Society, Chemical Communications, 1103-1104.

Wieker, W., Grimmer, A.R., Winkler, A., Magi, M., Tarmak, M. and Lippmaa, E. (1982). Solid-state high-resolution ^{29}Si MAS NMR spectroscopy of synthetic 14Å, 11Å and 9Å tobermorites, Cement and Concrete Research 12, 333–339.

Wilson, M.A. (1987). NMR techniques and applications in geochemistry and soil chemistry, Pergamon Press, Oxford.

Wingenfelder, U., Hansen, C., Furrer, G. and Schulin, R. (2005). Removal of heavy metals from mine waters by natural zeolites, Environmental Science and Technology 39, 4606–4613.

Xu, M., Cheng, M., Bao, X., Liu, X. and Tang, D. (1999). Growth of zeolite KSO1 on calcined kaolin microspheres, Journal of Materials Chemistry 9, 2965-2966.

Yoshikawa, M., Wagner, P., Lovallo, M., Tsuji, K., Takewaki, T., Chen, C-Y., Beck, L. W., Jones, Ch., Tsapatsis, M., Zones, S.I. and Davis M.E. (1998). Synthesis, characterization, and structure solution of CIT-5, a new, high-silica, extra-large-pore molecular sieve, Journal of Physical Chemistry B 102, 7139-7147.

Yu, P., Kirckpatrick, R.J., Poe, B., McMillan, P.F. and Cong, X. (1999). Structure of calcium silicate hydrate (C–S–H): Near-, mid-, and far-infrared spectroscopy, Journal of the American Ceramic Society 82, 742–748.

Zagury, G.J., Kulnieks, V.I. and Neculita, C.M. (2006). Characterization and reactivity assessment of organic substrates for sulphate-reducing bacteria in acid mine drainage treatment, Chemosphere 64, 944-954.

Zhang, X. (1998). Coal fires in Northwest China: Detection, monitoring, and prediction using remote sensing data, Ph.D. Thesis, Delft University of Technology, Delft, The Netherlands, 135pp.

Zhao, H., Deng, Y., Harsh, J.B., Flury, M. and Boyle, J.S. (2004). Alteration of kaolinite to cancrinite and sodalite by simulated hanford tank waste and its impact on cesium retention, Clays and Clay Minerals 52, 1-13.

Zhou, Y., Zhu, H., Chen, Z., Chen, M., Xu, Y., Zhang, H. and Zhao, D. (2001). A large 24-membered-ring germanate zeolite-type open-framework structure with three-dimensional intersecting channels, Angewandte Chemie International Edition 40, 2166-216.

Zubowa, H-L., Kosslick, H., Müller, D., Richter, M., Wilde, L. and Fricke, R. (2001). Crystallization of phase-pure zeolite NaP from MCM-22-type gel compositions under microwave radiation, Microporous and Mesoporous Materials 109, 542-548.

Appendices